2018

Role of a highly conserved region of the NF-kappaB essential modulator in its scaffolding function

BOSTON UNIVERSITY

GRADUATE SCHOOL OF ARTS AND SCIENCES

Dissertation

ROLE OF A HIGHLY CONSERVED REGION OF THE NF-kappaB ESSENTIAL MODULATOR IN ITS SCAFFOLDING FUNCTION

by

ROBERT ABRAHAM SHAFFER

B.S., Rensselaer Polytechnic Institute, 2012

Submitted in partial fulfillment of the

requirements for the degree of

Doctor of Philosophy

2018

Approved by

First Reader _____

Karen N. Allen, Ph.D.
Professor of Chemistry

Second Reader _____

Adrian Whitty, Ph.D.
Associate Professor of Chemistry

Third Reader _____

Dean R. Tolan, Ph.D.
Professor of Biology

Acknowledgments

I feel extremely fortunate to be where I am today. There is no doubt in my mind that without my teachers, professors, mentors, and especially family, I would not have been able to have such amazing opportunities. My high school biology teacher, Dr. Robert Langdon ("Doc" for short), was the best teacher I ever had; he is the reason I pursued a biology-related discipline. In college, I was lucky enough to land an internship at Pulmatrix, Inc., thanks to a family-friend connection. This internship was an amazing experience, perhaps was necessary for acceptance to grad school at Boston University, and definitely lit a fire in me to pursue an industrial career in the biotech world.

Patience and guidance are the most anyone could ask for from their graduate school PI. Adrian Whitty and Karen Allen, my co-advisors, epitomized these qualities. They always had suggestions to help, were patient when things were not going so well, and were remarkably always positive. This last point I cannot stress enough, how important this was to me. When anyone else complained to me about their boss, I always thought to myself how lucky I was to have Adrian and Karen, who always embodied precisely zero of the negative qualities being complained about. I have learned some great managerial and leadership skills from them, in addition to the scientific knowledge they have

imparted. In addition to my PI's, my labmates have been a constant source of support for me. Whether I need help with an experiment, finding a reagent, or just taking a moment to chat, they are there, and I cannot thank them enough. I must single out and wholeheartedly thank Dr. Shaun Cote, who was my mentor starting grad school and whose project I took over. He trained me on several assays and instruments, left behind lots of convenient aliquots of everything for me to use, and left me helpful protocols. He did his best to set me up to most efficiently continue the work he started, and I cannot thank him enough for that jumpstart.

There is no doubt that I would not be where I am today without the amazing support of the people closest to me. First and foremost, my parents Mark and Sharon Shaffer have been my rocks, supporting me in all of my major endeavors and shaping who I am today. I also need to thank my brothers Dan and Jason, especially for honing my competitiveness and drive to be the best. Finally, my wife Marlena is the reason I am not stressed out writing this thesis, is the reason I could handle the day-to-day challenges of being a science Ph.D. candidate, and is the reason I am intensely eager to see what my future holds. Thank you for all your love and support you have given me.

ROLE OF A HIGHLY CONSERVED REGION OF THE NF-kappaB ESSENTIAL MODULATOR IN ITS SCAFFOLDING FUNCTION

ROBERT ABRAHAM SHAFFER

Boston University Graduate School of Arts and Sciences, 2018

Major Professors: Karen N. Allen, Professor of Chemistry, and Adrian Whitty, Associate Professor of Chemistry

ABSTRACT

Scaffold proteins facilitate many aspects of intracellular signaling. These proteins can regulate two or more proteins in the same pathway, or coordinate signaling from multiple pathways. Scaffold proteins are therefore key control points for the flux of signaling and play essential roles in biological systems. There are four possible mechanisms by which scaffold proteins achieve activation and propagate signaling: 1) rigid protein binding between two or more proteins to co-localize binding partners, 2) ligand-induced activation such as may result from a conformational change, 3) disorder-to-order transition where the scaffold protein folds as a result of a protein-protein interaction, and 4) dynamic processes such as phosphorylation. The scaffold protein NF-κB essential modulator (NEMO) functions via ligand-induced activation and serves as the key control point for

canonical NF-κB signaling. The work described in this thesis investigates the role of a previously uncharacterized domain within NEMO that is required for function, which we term the Intervening Domain (IVD). Bioinformatic analysis reveals a high level of sequence conservation across species within this domain. Conformational changes following ligand binding are observed for NEMO and these changes require conserved sequences in the IVD. Additionally, a functional IVD is shown to increase the binding affinity of NEMO for IKKβ, enhance the thermal stability of NEMO, and is required to propagate NF-κB signaling in cells. A fluorescence-based assay is also developed to characterize the formation of a complex composed of NEMO, a zinc ion, and IκBα. A separate fluorescence-based assay is developed to measure IKK activity and is used to determine that NEMO alone or in the presence of linear tetraubiquitin does not enhance the rate of IKKβ phosphorylation of an IκBα-derived peptide. Furthermore, a number of organic small molecules and macrocycles are screened against the NEMO-IKKβ interaction. One small molecule was validated as an inhibitor and its biophysical properties and inhibition kinetics are described in this thesis. These analyses represent the first characterization of a highly conserved domain required for the function of the key control point in NF-κB signaling. The IVD domain of NEMO

could be targeted for development of an allosteric effector for therapeutic discovery.

Table of Contents

List of Tables

List of Figures

List of Abbreviations

Å	Angstroms
AES	Atomic Emission Spectroscopy
AUC	Analytical ultracentrifugation
BSA	Bovine serum albumin
CC1	Coiled Coil 1
CC2	Coiled Coil 2
CD	Circular dichroism
cLogP	Calculated log of the partition coefficient
CoZi	CC2-LZ region of NEMO
C-terminus	Carboxy terminus
Da	Daltons
DARPin	Designed-ankyrin repeat proteins
DMSO	Dimethyl sulfoxide
DTT	Dithiothreitol
ELISA	Enzyme-linked immunosorbent assay
ESI-MS	Electron spray ionization mass spectrometry
FA	Fluorescence anisotropy
FITC	Fluorescein isothiocyanate

FP	Fluorescence polarization
FPLC	Fast protein liquid chromatography
h	Hour(s)
HEPES	4-(2-hydroxyethyl)-1-piperazineethanesulfonic acid
HRP	Horseradish peroxidase
HTS	High-throughput screening
IC_{50}	Half-maximal inhibitory concentration
IκB	Inhibitor kappa B
IκBα	Inhibitor kappa B alpha
IκBβ	Inhibitor kappa B beta
IκBε	Inhibitor kappa B epsilon
IκBδ	Inhibitor kappa B delta
IKK complex	Inhibitor kappa B Kinase
IKKα	Inhibitor kappa B Kinase alpha
IKKβ	Inhibitor kappa B Kinase beta
IL-1R	Interleukin 1 receptor
IL-2	Interleukin 2
IL-2Rα	IL-2 receptor α chain
IPTG	Isopropyl β-D-1-thiogalactopyranoside

IRAK1	Interleukin-1 receptor-associated kinase 1
IVD	Intervening Domain
kcal	Kilocalories
K_D	Dissociation constant
K_I	Inhibition constant
LB	Luria broth
LUBAC	Linear ubiquitin chain assembly complex
LZ	Leucine zipper
m	Minute(s)
mol	Moles
MSA	Multiple Sequence Alignment
MST	Microscale Thermophoresis
NBD	NEMO binding domain
NEMO	NF-κB essential modulator
NF-κB	Nuclear factor kappa B
NTA	Nitrilotriacetic acid
N-terminus	Amino terminus
OD	Optical density
PARP1	Poly(ADP-ribose)-Polymerase 1

PIASγ	Protein inhibitor of activated STAT protein gamma
PEG	Polyethylene glycol
PIDD	p53-induced death domain-containing protein
PPI	Protein-protein interactions
RIP1	Receptor-interacting serine/threonine-protein kinase 1
RPC	Reversed phase chromatography
RPM	Revolutions per minute
s	Second(s)
S	Svedberg units
SAXS	Small angle x-ray scattering
SDS-PAGE	Sodium dodecyl sulfate polyacrylamide gel electrophoresis
SE-AUC	Sedimentation equilibrium analytical ultracentrifugation
SPR	Surface plasmon resonance
SV-AUC	Sedimentation velocity analytical ultracentrifugation
TAK	Transforming growth factor-β activated kinase 1
TCEP	Tris(2-carboxyethyl)phosphine
TLR	Toll-like receptor

TMB	3,3′,5,5′-Tetramethylbenzidine
TNFα	Tumor necrosis factor alpha
TNFR1	Tumor necrosis factor receptor 1
TRAF6	TNF receptor associated factor 6
v-FLIP	Viral FLICE inhibitory protein
ZF	Zinc finger

Chapter 1: Scaffold Proteins in Eukaryotic Signaling

1.1 Scaffold Proteins Provide Key Control Points for Intracellular Signaling

Signaling scaffold proteins are defined as molecules that bind two or more proteins[1], and facilitate the temporal, spatial, orientational, and contextual interactions between proteins involved in intracellular signaling. Classical scaffolds do not possess enzymatic activity; for the purpose of this dissertation, non-classical scaffold proteins that are catalysts (e.g., ATPases) are not discussed. Scaffold proteins may regulate two or more proteins of the same pathway, or coordinate signaling between different pathways[2]. The most basic function of scaffolds is to provide a binding platform to spatially and temporally co-localize kinases and/or phosphatases with their substrates, thereby directing and regulating phosphorylation events within signal transduction pathways[3,4] in either a positive or negative fashion. This spatial and temporal coordination affords greater specificity for pathway components, decreasing the likelihood of non-specific interactions and off-pathway effects[5]. Scaffolds can play a more active role than simple co-localization, however, for example by allosterically regulating the activity of their binding partners[6]. In some cases such as the yeast scaffold protein Ste5, scaffolds exert complex allosteric control to regulate the interactions between signaling components[7]. Because of their ubiquity and ability

to facilitate complex signaling events, scaffold proteins have been used in directed evolution to engineer signaling outcomes or efficiently generate desired products[7].

Scaffold proteins typically possess a modular domain structure. Each domain acts as a functional unit to impart a specific protein binding site or oligomerization interface, to contribute one or more overall scaffold protein roles. These domain modules can vary widely in both sequence and function. Scaffold proteins are found in all domains of life, such as YopM in bacteria and RACK1 in both prokaryotes and eukaryotes[8,9]. However, based on their substantial heterogeneity, it is likely that scaffold proteins evolved convergently. For instance, it is unlikely that the scaffold protein POSH, a multi-SH3 domain-containing protein, shares common ancestry with PSD-90, which is comprised of multiple PDZ domains. SH3 domains bind to proline and hydrophobic amino acids, whereas PDZ domains recognize short motifs at the C-termini of target proteins and are structurally distinct. Even MAPK scaffolds that organize the highly conserved set of MAPK cascade components into functional modules do not possess sequence similarity: Ste5, KSR, JIP, and β-arrestin family members all interact with MAPK proteins but are highly dissimilar[10]. This heterogeneity suggests that scaffolds have emerged several times independently during the

course of evolution. Another indication of convergent evolution is in the number of scaffolds identified in certain organisms. In primitive, unicellular eukaryotes and higher plants, the number of scaffold proteins is quite low[11,12]. Ste5 is the major MAPK scaffold protein in yeast, but is unrelated by sequence to the dozen or so MAPK scaffolds in mammals. Similarly, multi-PDZ domain proteins are abundant in animals but are rarely found in lower eukaryotes, fungi, or plants[13]. In contrast, tyrosine kinases likely evolved once during evolution due to their common sequence motifs and coincident emergence with multicellular organisms[12,14,15].

Scaffold proteins belong to many different and substantially distinct families. The most well-characterized scaffold families are the MAPK-participating scaffolds include the Kinase Suppressor of Ras (KSR) family[16], JNK-interacting protein (JIP) family[17], β-arrestins[18], and Ste5[19]. In addition to these well-known families, there are several examples of other similarly important but less often noted families. The following discussion is designed to illustrate the vast diversity in scaffold proteins, and highlight a few examples in lesser-known signaling pathways. Paxillins are scaffold proteins for adhesion of cells to the extracellular matrix and for focal adhesion of non-striated cells[20]. The Grb2-associated binder (Gab) family has been shown to play a central role in multiple

major signaling pathways through its Pleckstrin homology (PH) domain and binding sites for SH2 and SH3 domains[21]. The membrane-associated guanylate kinase (MAGUK) family contains PDZ (Psd-95 [Post Synaptic Density Protein], DlgA [Drosophila Disc Large Tumor Suppressor] and ZO1 [Zonula Occludens-1 Protein]), SH3 (Src Homology 3), and GUK domains, and participate in diverse processes including tissue development, cell-cell communication, and cell polarity control[22]. The Homer family of scaffolds contains an Ena/VASP homology 1 (EVH1) domain, coiled-coils, and leucine zippers, and maintains architecture in the post-synaptic density[23]. Notably, the MAGUK family contains PSD-95, a key scaffold at the post-synaptic density; this scaffold works alongside Homer proteins in a similar capacity, yet shares little sequence similarity, reinforcing the concept that scaffold proteins evolved convergently. A-kinase anchoring proteins (AKAPs) are structurally diverse scaffold proteins that typically bind protein kinase A (PKA) to localize it within the cell or to bring the kinase into close proximity to other proteins[24]. WD-repeat proteins typically have a circularized beta-propeller structure, but are involved in highly diverse functions including signal transduction and apoptosis[25]. The scaffold protein discussed herein does not belong to any of these classical families, but shares some domain structure similarity with the Homer family by the presence of both

coiled-coil domains and leucine zippers.

1.2 Mechanisms for Scaffold Activation and Function

Despite lack of sequence similarity and domain structure across scaffold proteins in general, two basic strategies are used for protein recognition and binding, and four strategies are used for activation of function. Some scaffolds bind one or more loops using a rigid protein structure, where these loops fit into a substantial but often shallow binding concavity on the surface of the scaffold protein. An example is the interaction of Adnectin binding to epidermal growth factor receptor (EGFR), where one loop of Adnectin fits into a flat pocket on EGFR[26]. The second strategy is by the interaction of surface-exposed side chains of secondary structure elements to form either hydrogen-bond networks or hydrophobic channels for structure; for example, a heterotetrameric coiled-coil of α-helices or leucine zippers[27–29]. The former strategy is more common for PPIs, the latter for oligomerization. These binding modes are illustrated in **Figure 1**; Fig. 1A illustrates a flat loop fitting into a shallow pocket[26], and Fig. 1B is an example of a leucine zipper where two α-helices come together forming a hydrophobic channel[29].

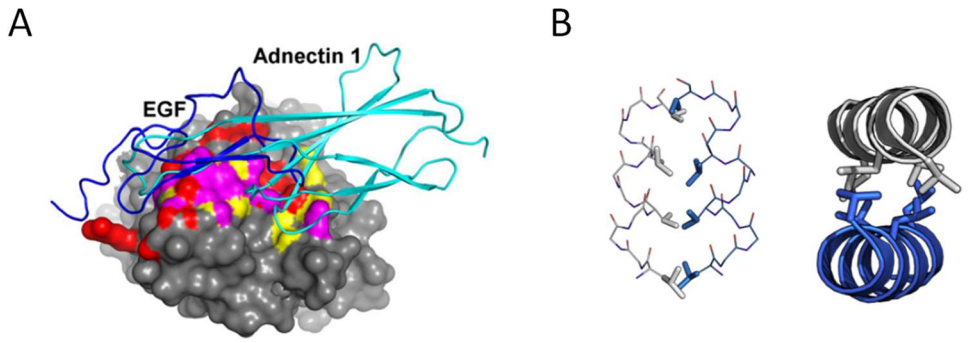

Figure 1: Strategies for scaffold protein recognition and binding. A: Fitting of loops into a substantial binding concavity. EGF (gray) contains a pocket for a loop of Adnectin (light blue) to bind between structure denoted as red space fill and dark blue loops. B: an example of a model leucine zipper creates a hydrophobic channel that facilitates PPIs.

To explore scaffold protein function beyond simple protein binding or requirement for signal propagation, recent studies analyzed four distinct scaffold protein activation mechanisms linked to downstream function. Specifically, these mechanisms may be accomplished by rigid protein binding, ligand-based activation, disorder-order transition, or dynamic processes such as pH change or phosphorylation (**Figure 2**). Often these strategies may be used in conjunction with each other.

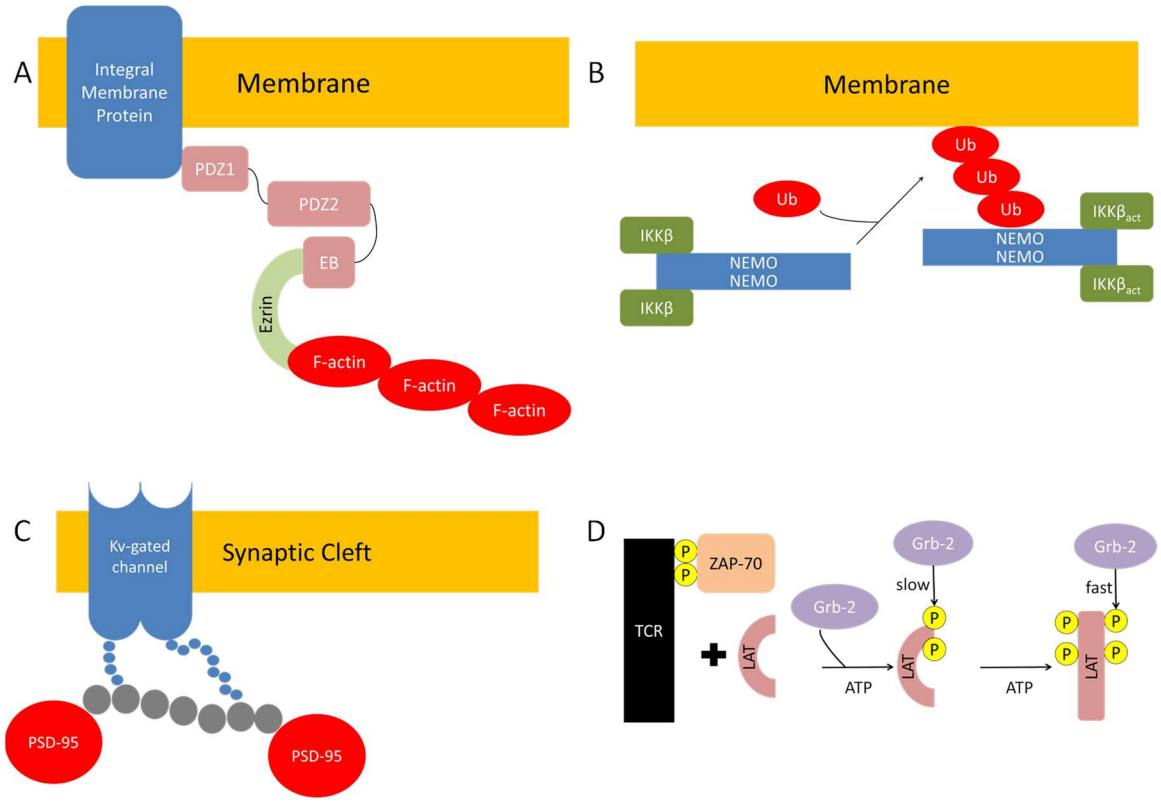

Figure 2: Mechanisms for scaffold activation. A: Rigid protein binding. EBP50 (pink) binds to integral membrane proteins through PDZ domains and cytoskeletal proteins through its EB domain to promote cytoskeletal formation. B: Ligand-based activation. NEMO and IKKβ are activated by membrane tethering by poly-ubiquitination, which enhances IKKβ binding and promotes NEMO-mediated complex activation. C: Disorder-to-order transition. Intrinsically disordered regions in Kv gated channels (small circles) bind PSD-95 weakly to promote ease-of-encounter complex formation once all complex components are available. D: Dynamic processes including phosphorylation. ZAP-70 phosphorylates LAT, which promotes Grb2 binding and subsequent activation.

Rigid protein binding (**Figure 2**A) is the classically accepted mechanism for scaffold activation[30]. Src-homology-2 and -3 (SH2 and SH3) domains comprise 50-100 amino acids that fold independently and recognize binding motifs ~5-10 residues in length[31]. PDZ domains bind to four C-terminal residues of a protein chain, and in some instances can bind internal recognition sequences[32]. Helical

repeats, including the Armadillo, HEAT, Ankyrin, and tetratricopeptide, are especially suited to bind longer linear motifs. These domains are bundles of repeated α-helices that are extended and conformationally rigid to create extensive surfaces for PPIs. They are commonly seen in proteins involved in translocation or sequestration events, such as in the nuclear transport shuttles, importins, that are comprised of Armadillo repeats[33], or Inhibitor of κB proteins that are comprised of Ankyrin repeats[34]. A simple exemplary role for rigid protein binding in scaffold activation is the assembly of signaling components for cytoskeletal formation. Co-immunoprecipitation assays demonstrated that NHERF1/EBP50 binds to integral membrane proteins via PDZ domains, and to actin filaments via an EB domain (ERM-binding domain, another such rigid protein binding domain), to link the cytoskeleton to the plasma membrane[5] (**Figure 2**A). Rigid protein binding, however, cannot account for the regulation of pathway branching and other complex signaling regulation events[30].

In ligand-based activation (**Figure 2**B), binding of a protein partner to the scaffold induces a conformational change or other allosteric regulation event to promote activity of a downstream molecule. In one example, crystallographic analysis and kinetics of phosphorylation show how KSR undergoes an allosteric transition upon B-Raf (BRAF) binding to stimulate phosphorylation of the

downstream signaling molecule MAPKK[35]. In another, homodimerization of AHNAK as determined by crystallography reveals a pocket for binding to a peptide thought to be important for downstream complex formation; however, the biological function of the complex has yet to be determined[32].

Disorder-to-order transition (**Figure 2**C) is a mechanism for scaffold proteins to achieve a multitude of functions with the same disordered domain. Here, high-specificity but low-affinity interactions are favored. For example, disorder-to-order transition is employed in ease of encounter complex formation in voltage-gated potassium channels: the disordered binding interface promotes weak non-specific interactions to keep binding partners such as PSD-95 in an encounter complex until subsequent spatial rearrangements result in the proper orientation for specific binding (**Figure 2**C). This type of intricate, step-wise complex formation is hypothesized to be a more general mechanism for large macromolecular complex formation, as opposed to rigid docking of several proteins into one complex[36]. Disorder-to-order transition may also achieve binding-site overlap. For example, co-immunoprecipitation was used to show that a 15-residue intrinsically disordered loop in glycogen synthase kinase 3β (GSK-3β) binds to frequently rearranged in activated T-cells (FRAT) in one context, and axin in another[2].

Dynamic processes that lead to scaffold activation (**Figure 2**D) include pH changes and phosphorylation events, among others. A pH-induced conformational change is observed by NMR in the scaffold protein IscU that is hypothesized to play an important physiological role in activation of iron-sulfur cluster biosynthesis[37]. The disordered protein linker for activation of T cells (LAT) is phosphorylated in a remote site by ZAP-70 to change the overall ensemble of conformational states. This equilibrium shift achieves an activated state that then modulates the accessibility of other phosphorylated sites to the binding partner Grb2 and promotes signaling activity[38] (**Figure 2**D). Dynamic processes such as conformational change can also affect simple rigid protein binding, as in the case of NHERF1. Here, a head-to-tail conformation masks NHERF1 association with PDZ domain-specific ligands PTEN and β-catenin. Association of the EB domain of NHERF1 with ezrin releases this auto-inhibitory state, allowing the scaffold to become activated and bind PDZ domain-specific ligands[39].

Table 1: Summary of activation mechanisms, with noted examples, key domains, and relevant pathways.

Activation Mechanism	Examples	Key Domain(s)	Pathways
Rigid protein binding	EBP50 Grb2 Importin	PDZ SH2 Armadillo	Cytoskeletal T cell activation Nuclear transport
Ligand-based activation	NEMO KSR AHNAK	CC[a], ZF[b] CC-SAM[c] PDZ	NF-κB MAPK Differentiation
Disorder-to-order	Kv channel GSK-3β	ID[d] ID	Axon potential Multiple
Dynamic processes	IscU LAT	NifU-like Transmembrane	Fe-S biosynthesis T cell activation

[a]CC, coiled-coil; [b]ZF, zinc finger; [c]CC-SAM, coiled-coil sterile α-motif; [d]ID, intrinsically disordered.

The above four mechanisms of scaffold activation are summarized in Table 1. However, this description would be incomplete if it neglected to discuss one of the most well-characterized scaffold proteins, Ste5. This protein organizes the yeast mating mitogen-activated protein kinase (MAPK) pathway. A model of auto-inhibition was generated by truncation mapping and a partial crystal structure. Here, a conformational change acts as a gate to present the binding surface for Fus3 to propagate a mating-specific signal upon α-factor binding[40]. Additionally, RING domain of Ste5 has been shown to undergo a major conformational transition upon Ste4/Ste18 binding, from a stable molten globule to a folded, more globular structure[41]. Four phosphorylation sites on Ste5 have been shown to regulate a switch-like dissociation of Fus3 that is necessary to

generate the switch-like mating response[19]. Therefore, Ste5 has been shown to exhibit the four above described scaffold protein activation mechanisms: ligand-based activation by α-factor binding, rigid binding of Fus3, disorder-to-order transition, and dynamic activation by phosphorylation. As exemplified by the most well studied scaffold protein, it is possible that most scaffold proteins employ multiple, if not all, such strategies. Widespread scaffold protein characterization would directly address this hypothesis.

1.3 NEMO as a Scaffold Protein and its Role in the NF-κB Pathway

The Nuclear Factor κB (NF-κB) pathway is a multi-component pathway that regulates the expression of hundreds of genes that are involved in diverse and key cellular and organismal processes, including cell proliferation, cell survival, the cellular stress response, innate immunity, and inflammation[42]. The NF-κB family contains five transcription factors that function as either homo- or heterodimers: NF-κB1, NF-κB2, RelA, RelB, and c-Rel[43,44]. These NF-κB proteins are typically sequestered in the cytoplasm by an Inhibitor κB (IκB) protein characterized by containing multiple Ankyrin repeat domains. There are multiple isoforms of IκB proteins: IκBα, IκBβ, IκBδ, IκBε, Bcl3, IκBζ, and IκBNS[44,45]. These IκB proteins are phosphorylated by IκB kinase α (IKKα) in the

non-canonical pathway, or IKKβ in the canonical pathway, which are homologous members of the IKK complex[46]. Phosphorylated IκB is degraded by the proteasome, which frees the previously sequestered NF-κB subunits to translocate into the nucleus. An essential regulatory element in the canonical pathway in the IKK complex is the scaffold protein IKKγ, or NF-κB Essential Modulator (NEMO). Upon pathway stimulation by tumor necrosis factor (TNF) α or other intercellular signaling molecules targeting TNF-receptor I, the IL-1R receptor, or TLRs[47], the IKK complex becomes poly-ubiquitinated and associates with effector proteins bound to the activating receptor. It is currently believed that there are three distinct mechanisms for activation of the IKK complex. One mechanism involves an E2/E3 ligase complex attaching linked ubiquitin chains onto the kinase Receptor Interacting Protein 1 (RIP1), which bind directly to NEMO and thereby recruit the IKK complex together with the kinase TAK1 into association with RIP1. TAK1 then phosphorylates IKKβ to activate the kinase. It has also been shown that IKKβ may be activated via trans-autophosphorylation, though in this activation mechanism TAK1 phosphorylation is the primary manner of IKKβ activation[48,49]. A second mechanism by which signaling can be activated is triggered by linear ubiquitin chain assembly complex (LUBAC) association with the TNFR1 receptor[50–52]. LUBAC can then directly link ubiquitin

chains to NEMO, which enables trans-autophosphorylation of IKKβ for complex activation[53]. A third mechanism for canonical NF-κB activation is dependent upon association of effector proteins with the IL-1R and TLR receptors. Ubc13 and TRAF6 proteins as part of an E2/E3 ligase complex are recruited to these receptors where they conjugate K63-linked ubiquitin chains to IRAK1 that is also associated with the receptors[48,54]. Similar to the first mechanism, binding of TAK1 and the IKK complex to the ubiquitin chains initiates phosphorylation of IKKβ to activate the complex[48]. Notably, GSK-3β has been shown to phosphorylate serines 8, 17, 31, and 43 within the disordered N-terminus of NEMO, which is hypothesized to be important for ordered canonical NF-κB signaling in each of the above activation cases[55–57]. These activation mechanisms classify NEMO in the first and fourth categories of scaffold activation as described above: ligand-based activation by poly-ubiquitin binding, and dynamic activation by phosphorylation events. Non-canonical NF-κB activation does not require NEMO, and is associated with organism development[47], which is not discussed in this thesis.

Within the IKK complex, NEMO binds IKKβ, an otherwise pleiotropic transducer[58]. They form a heterotetrameric complex involving a region close to the NEMO N-terminus encompassing residues 44-111 and a region close to the

IKKβ C-terminus encompassing residues 701-745[28]. IKKα may also bind NEMO in a similar functional complex[46,47], but has been shown to only function in canonical NF-κB signaling in IKKβ knockout models[59,60]. The minimal NEMO binding motif on IKKβ (NEMO-Binding Domain, NBD) comprises 11 residues (735-745)[28,61], though full binding affinity requires up to 45 residues[28]. NEMO dimerization is required for IKK activation[62], but phosphorylation of NEMO on S68 and within the IKKβ NBD disrupts the heterotetrameric complex, which may prove to be a negative feedback mechanism[45]. An additional negative feedback mechanism was postulated recently for residues 112-150, that the authors propose maintains NEMO in an autoinhibitory state prior to poly-ubiquitin (>4) binding[63]. In that work, the authors showed that inclusion of residues 112-150 prevents linear di-ubiquitin from binding to NEMO, despite ubiquitination occurring C-terminal to this region. Additionally, they argue that their SAXS model is too compact for NEMO to be fully extended (320 Å), and is likely in a conformation where the 112-150 region is folded back and in contact with the ubiquitin binding site.

The C-terminal zinc finger of NEMO, encompassing 25 residues from position 395 to 419, binds the Inhibitor of κB proteins; see Figure 3. The IκB protein most commonly studied in conjunction with NEMO is IκBα. A key

function of NEMO is therefore to direct IKKβ to phosphorylate IκBα[58]. This occurs on IκBα S32 and S36; IkBβ is phosphorylated on S19 and S23[45]. Phosphorylated IκBα is then released from the complex and is K48-linked polyubiquitinated by the E3 ubiquitin ligase SCF/βTRCP, releases the sequestered NF-κB subunits, and is degraded in the 26S proteasome[45,64]. The released NF-κB subunits are then free to translocate to the nucleus, and activate NF-κB responsive genes that regulate inflammation and other biological outcomes. This pathway is diagrammed in Figure 4.

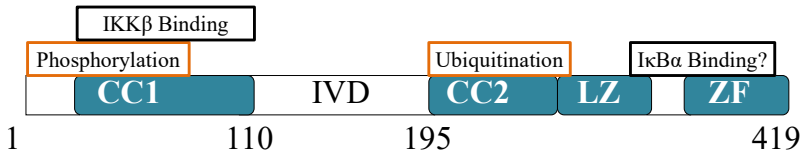

Figure 3: Schematic domain map of NEMO (domains in blue) with binding sites of major partners IKKβ and IκBα boxed in black, and sites of covalent modification boxed in orange.

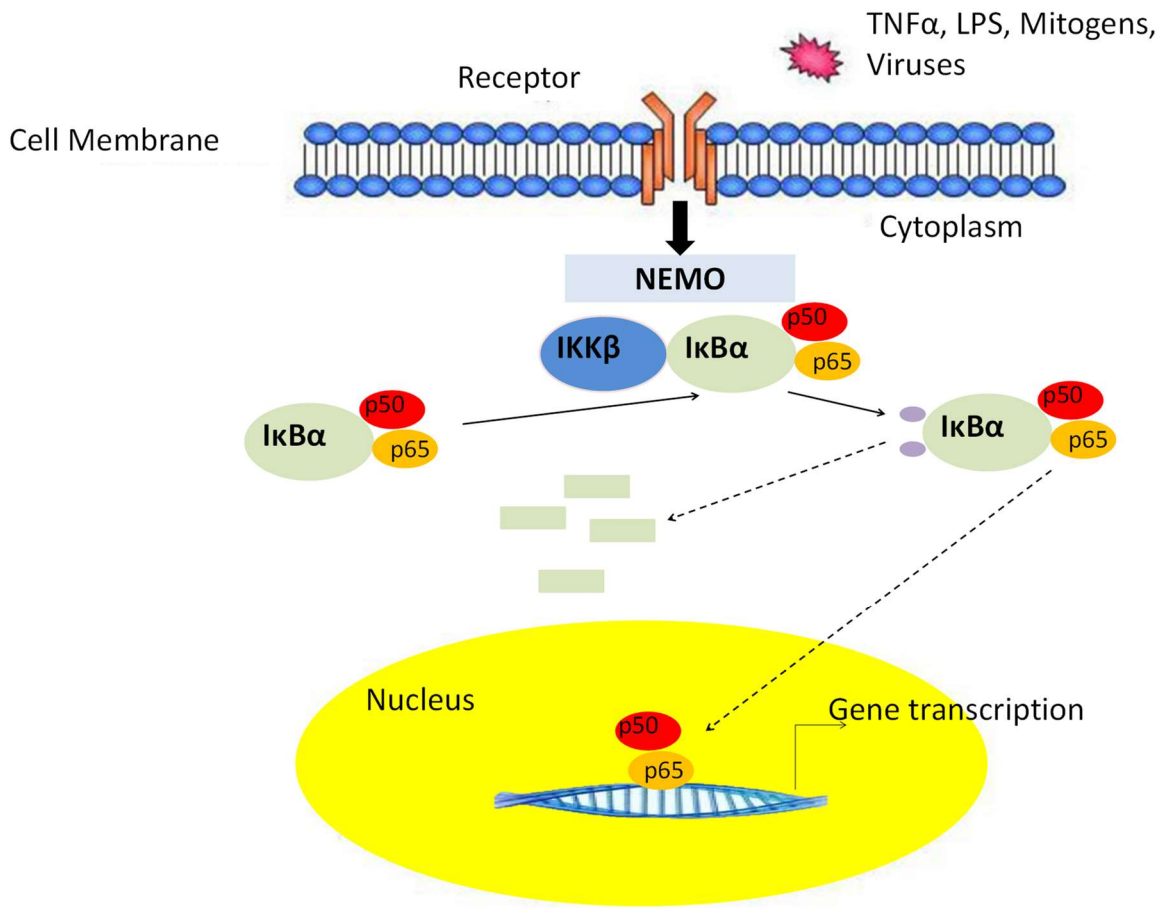

Figure 4: Schematic cartoon representation of canonical NF-κB signaling. Receptor representative of any receptor for listed stimuli. Solid lines denote single step in signaling. Dashed lines denote ultimate fates of components of IκBα:p50:p65 complex.

Additional binding partners have been reported for NEMO that affect NF-κB signaling. Poly ADP-ribose polymerase 1 (PARP1) and protein inhibitor of activated STAT γ (PIASγ) bind within the N-terminal 120 residues of NEMO, and activate the IKK complex in response to DNA damage[65]. Ataxia-telangiectasia mutated (ATM) is activated following DNA damage, which leads to binding and phosphorylation of NEMO at S85. NEMO is then mono-

ubiquitinated, and ATM-NEMO-Ub binds IKKβ to lead to IKK complex activation and induction of NK-kB signaling[66]. P53-induced death domain (PIDD) also activates NEMO in response to DNA damage, but the mechanism of activation is unknown[67]. Viral FLICE-like inhibitory protein (v-FLIP), a human herpes virus 8 protein, has been shown to bind between residues 150 and 272 of NEMO to activate the IKK complex in an Hsp90-dependent manner[68]. Interestingly, the chaperone Hsp90 has been shown to be physically associated with NEMO in a colonic malignant cell line, and contributes strongly to NF-κB signaling via this NEMO interaction. It is hypothesized that Hsp90 regulates the folding of NEMO and the IKK complex in another general regulation mechanism of canonical NF-κB signaling[69].

NEMO is essential for propagation of canonical NF-κB signaling. Several NEMO knockout studies have been performed that associate NEMO with a variety of diseases and therefore provide evidence for the essentiality of NEMO. Knockout of NEMO in a mouse model caused uncontrolled liver apoptosis arising from the absence of NF-κB-mediated proliferation signals, which led to fatal liver damage[70]. Thyroid-selective knockout of NEMO in a different mouse model led to the development of underweight mice with short lifespans[71]. Osteoporosis was induced following a knockout of NEMO in osteoclast and

myeloid progenitors in another mouse model[72]. Mice with a NEMO knockout in the pancreas developed caerulein pancreatitis[73]. In humans, because the NF-κB pathway is responsible for proliferation and differentiation outcomes, it has been shown to be significantly upregulated in certain cancers[74–77].

NEMO mutations abolishing its ability to dimerize have been shown to block NF-κB signaling[78,79]. An in-frame deletion mutation that eliminates residues Q134-R256 leads to Incontinentia Pigmenti (IP), likely through a lack of linear ubiquitination. IP is a genetic disease of the skin, hair, teeth and central nervous system[80]. The truncation mutation E391X in patients with inflammatory skin and intestinal disease in addition to ectodermal dysplasia with immunodeficiency (EDA-ID), has been correlated with abolition of the interaction with A20, a putative suppressor of NF-κB activity. EDA-ID is a group of conditions in which there is abnormal development of the skin, hair, nails, teeth, or sweat glands[81]. Even point mutations in NEMO are sufficient to bring about immune impairment diseases[42,82].

Because NEMO is an essential component of such an impactful pathway in human biology, there exists a strong therapeutic motive in studying and targeting this protein. A small-molecule inhibitor of the NEMO-Ubiquitin interaction was developed that selectively inhibits NF-κB activation in response

to TNFα, but not IL-1β, stimulation. This small molecule was shown to selectively kill lymphoma cells that were addicted to NF-κB signaling, providing strong evidence that NEMO is a potentially useful therapeutic target[83]. A different small-molecule inhibitor of the NEMO-IKKβ interaction was shown to inhibit cellular NF-κB signaling, and was computationally docked into the X-ray crystal structure of the NEMO-IKKβ binding interface[84]. However, no mechanistic studies were performed, so the precise target of the small molecule is unknown. A cell-permeant version of the NBD 11-mer peptide has been shown to disrupt the NEMO/IKKβ complex *in vivo*, and causes a specific biological outcome that attenuates activation of NF-κB but does not affect basal NF-κB function[85,86]. Quite surprisingly, the NBD peptide has been shown to prevent memory loss in a mouse model of Alzheimer's disease, a function with which NF-κB had not previously been directly linked[87]. The NBD peptide has also been shown to attenuate tumor proliferation and prolonged mouse survival in a malignant glioma mouse line[88]. A synthetic loop replacement version of the NBD, in which a conserved hydrogen bond was replaced with a covalent hydrocarbon bridge to enhance rigidity, has been shown to be 10-fold more potent in blocking NEMO-mediated NF-κB signaling than wild-type NBD peptide[89], and may prove to be a worthwhile strategy for further optimizing the NBD peptide for

therapeutic use. IKKβ knockout in a mouse model mimicked NEMO-knockout, but the fatal liver damage occurred at a later stage in embryonic development[90]. Notably, IKKβ inhibition through salicylate and its derivatives has been established but studied in models of vascular disorders and metabolic syndrome[91] in addition to immunomodulatory capacities[92,93]. These attempts to inhibit NF-κB signaling through IKKβ have not been shown to modulate NEMO-based NF-κB disease states.

1.4 Current State of Biochemical and Biophysical Characterization of NEMO

The full-length X-ray crystal structure of NEMO has yet to be determined, but a number of atomic resolution structures exist of individual domains (Figure 5). These include the X-ray crystallographic structure of IKKβ binding site in complex with a 45-mer of IKKβ in a 2:2 stoichiometry[28], the CC2 domain in complex with the viral FLICE inhibitory protein[94] (vFLIP), the CC2-LZ domain in

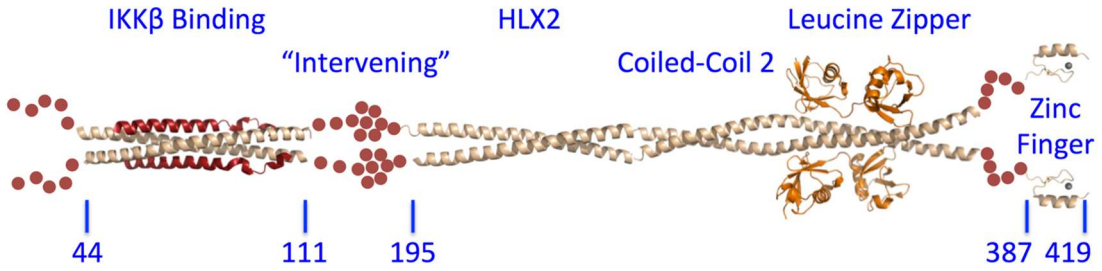

Figure 5: Domain map of NEMO and select complexes. The existing crystal structures of individual NEMO domains. NEMO in beige; IKKβ in red (PDB 3BRV); linear di-ubiquitin in orange (PDB 2ZVO); red spheres represent structurally uncharacterized regions. HLX2 from PDB 3CL3; ZF from PDB 2JVX.

complex with DARPin[95], the ubiquitin binding domain[96,97], and an NMR structure of the zinc-bound zinc finger[98]. These encompass the entirety of NEMO except for the first 44 residues, the 85 residues from 111 to 195, and the 48 residues from 345 to 393. Each of these structures, save the zinc finger, shows NEMO in an alpha-helical parallel dimer conformation. Many other oligomerization states of NEMO have been reported, including monomer[99–103], dimer[28,78,94–97,99–105], trimer[78,99–102], tetramer[79,104], and pentamer[102]. It is not known whether oligomeric states other than dimer are biologically relevant or exist as stable species; for instance, full-length NEMO is unlikely to exist as a trimer or pentamer given AUC and analytical gel filtration results from more recent studies[103,104].

Some of the challenge in studying NEMO biophysically has been attributed to the high aggregation, insolubility, and poor expression levels of the protein grown in *E. coli*. Due to these factors, determining oligomerization states has been complicated, and likely explains the variety of reported oligomerization states in literature. Up to seven of the cysteines outside of the NEMO zinc finger were mutated to alanine to avoid formation of unproductive disulfide bonds. Using this 7xAla construct, named for 7 Cys-to-Ala mutations, we determined NEMO to be a constitutive noncovalent dimer via analytical gel filtration and SDS-PAGE[103]. In NEMO-reconstituted cells, treatment with H_2O_2 to induce

oxidative stress formed covalent disulfide-linked dimers with wild-type NEMO and 5xAla NEMO, containing Cys54 and Cys347, but not 7xAla, with these two cysteines additionally mutated to alanines[99]. This demonstrated that Cys54 and Cys347 were sufficient for mediating interchain disulfide bonding. Most importantly, the 7xAla construct was shown to have an indistinguishable binding affinity for IKKβ(701-745) and ability to propagate TNFα-induced NF-κB signaling as compared to wild type NEMO[103]. For these reasons, 5xAla and 7xAla are used interchangeably throughout this thesis to serve as "wild-type" NEMO.

IκBα was shown by gel filtration to bind directly to the zinc finger of NEMO, encompassing residues 384-419; this is in addition to demonstrating that NEMO, IKKβ, and IκBα form a three-member heterologous complex that is stable enough for co-immunoprecipitation[58]. Perhaps most relevant to this thesis, Catici *et al.* (2015) demonstrated a conformational change undergone by NEMO in response to binding of IKKβ, IκBα, and both IKKβ and IκBα peptides by monitoring of intrinsic fluorescence and ANS dye binding. The conformational changes occur on the order of seconds, and the magnitude of the signal change is increased by polyubiquitin binding with a direct positive correlation to Ub chain length. Also importantly, the study demonstrated that IκBα binds to NEMO cooperatively at a ratio of 2:2[106]. From these studies, NEMO is emerging as a

dynamic regulator of the function or outcome of several components of a major signaling pathway, despite no apparent enzymatic activity.

As was discussed above, NEMO binds IKKα and IKKβ at the N-terminus, minimally requiring residues 47-80 of NEMO[61,62,107]. The affinity of NEMO binding to IKKβ(701-745) in a 2:2 stoichiometry has been measured to be 2.2 ± 0.8 nM in a fluorescence anisotropy assay[103], and similar values have been determined using surface plasmon resonance (D. Petrescu, unpublished). The binding affinity of NEMO for full-length IKKβ has not been reported. The binding interface has been tested via alanine-scanning mutagenesis along the NBD of IKKβ, and analyzed using computational hot-spot mapping[108]. These analyses have determined the location of a strong binding energy hot spot, specifically W739, W741, and L742, in addition to distal hot spots at L708/V709 and L719/I723. The top hot spot contains residues that are not only bulky but also reasonably close in space, forming a triangle with maximum dimensions of 6.6 x 5.5 x 3.6 Å. This may be a sufficiently large and hydrophobic pocket for a small molecule to bind, but may not be sufficient to allow design of a potent inhibitor; according to Kozakov *et al.*, a site is druggable if two strong hot spots have a center-to-center distance of less than 8 Å[109]. Because the major hot spot is farther away than 8 Å from the distal hot spots in NEMO, this protein-protein

interaction site may be difficult to target with more conventional drug-like molecules.

1.5 Overview of Thesis

In this thesis, I discuss the role of a previously uncharacterized domain, termed the IVD, within NEMO that is required for its function. Bioinformatic analysis illustrates a high level of sequence conservation across species within the IVD. Conformational dynamics and structural information have been elucidated for the IVD. Additionally, the contribution of this domain to the binding affinity to IKKβ and to the thermal stability of NEMO is described herein. Perhaps most significantly, the requirement of the IVD to propagate NF-κB signaling is also revealed in this thesis. In addition to the study of this previously uncharacterized domain, a fluorescence-based assay was developed to measure the binding affinity of NEMO and IκBα. Furthermore, a number of organic small molecules and macrocycles have been screened against the NEMO-IKKβ interaction, with the ultimate goal of finding the first non-peptide NEMO-targeted inhibitor. One small-molecule hit was validated and is described in this thesis. These data represent the first characterization of the IVD as a region required for the function of the key control point in NF-κB signaling, and may prove to be an allosteric target for NEMO drug discovery efforts.

Chapter 2: The Role of the Intervening Domain in NEMO Structure and Dynamics

2.1 Introduction

Scaffold proteins function by orienting their protein binding partners so as to enable or modulate their function. This orientation can occur by several distinct mechanisms, including rigid protein binding, ligand-based activation, disorder-to-order transition, and dynamic processes such as phosphorylation. Allosteric regulation of scaffold function appears to be implicit given these strategies, except for rigid protein binding, but the mechanism by which allostery occurs has yet to be elucidated. Evidence for such a mechanism shows that mutations outside of scaffold protein binding sites can affect binding[110,111]. For example, researchers were able to discover and characterize an allosteric inhibitor that binds an intrinsically disordered region of the Protein Tyrosine Phosphatase 1B (PTP1B)[112], and the same group showed unidentified allosteric sites outside of the canonical kinase interaction motif of striatal enriched protein tyrosine phosphatase contribute to ERK2 binding[113].

Recent work has suggested links between conformational dynamics and scaffold function. A pH-induced conformational change in the scaffold protein IscU has been suggested to play a role in iron-sulfur cluster biosynthesis[37].

Structural and kinetic studies have shown that Kinase Suppressor of Ras (KSR) undergoes an allosteric transition upon B-Raf binding, thereby stimulating phosphorylation of Mitogen-Activated Protein-Kinase Kinase (MAPKK)[35]. Truncation mapping and a partial crystal structure of the yeast scaffold Ste5 have been used to generate a model of autoinhibition, in which a conformational change in Ste5 acts as a gate to present the binding surface for Fus3, which then propagates a mating-specific signal[40]. In fact, Ste5 has been shown to employ all four scaffold protein functional strategies[19,41] (see Chapter 1 for discussion of strategies). It is possible that scaffold proteins commonly employ all or most of such strategies, and that we simply have not characterized them well enough to determine that this is the case.

NEMO is a good model for studying scaffold proteins because it has been extensively studied, but its underlying molecular mechanism of activation is unknown. NEMO has been shown to exist in multiple oligomeric states, particularly as a constitutive noncovalent dimer[28,104]. To date, four regions of NEMO have been crystallized[28,94,96,98], and binding interactions with some of its partners have also been well characterized[58,69,107,108]; refer to Figure 5 in Section 1.4. A number of mutations of NEMO have been shown to cause genetic immunodeficiencies[42,82,114,115]. This structural and functional information provides

a solid framework for the work presented in this and the following Chapter of this dissertation.

The region spanning residues 44 to 111 in NEMO is annotated as the IKKβ binding region, and has been extensively studied[28,116]. A domain of NEMO C-terminal to residue 195, referred to as CC2 for its coiled-coil structure, has also been extensively studied[28,94,104]. However, the region between these domains, which we term the Intervening Domain (IVD), has no known function or structure. This chapter discusses the IVD domain and these mutations in the context of sequence conservation. A high level of sequence conservation is generally correlated with strong evolutionary pressure to retain the same amino acid side chains; therefore, there likely is significant adaptive role of these particular side chains.

In addition to determining sequence conservation of NEMO, this chapter focuses on obtaining protein for, and subsequent structural characterization of, the IVD in the context of both NEMO(44-195) and full-length 7xAla NEMO. Protein purity is confirmed by SDS-PAGE, before secondary structure characterization by CD, conformational assessment by SAXS and AUC, and progress toward determining a high-resolution crystal structure of the construct

comprising the IKKβ binding domain with the previously uncharacterized IVD (NEMO(44-195)).

2.2 *Materials and Methods*

2.2.1 Multiple Sequence Alignment

Annotated NEMO sequences were obtained using BLASTp (National Center for Biotechnology Information). BLASTp takes an input protein sequence query, in this case WT-NEMO, and compares it through local, i.e. small sections of, alignments to all other protein sequences in NCBI-accessible databases. Local alignments with the top scores are extended to improve sequence cover, and top final scoring sequences are returned. Redundant sequences, splice variants, and hypothetical sequences were removed from the resulting 100 sequences, as were fragment sequences with fewer than 50 residues and the similar but functionally unrelated protein optineurin. These sequences were imported into Unipro UGENE[117] and exported as an MSA using the algorithm MUSCLE[118] with default settings. Iterative rounds of trimming, pruning, and re-aligning were performed to represent most accurately the conservation of NEMO sequences.

2.2.2 Vectors and Mutagenesis Strategies

Full-length NEMO constructs, NEMO(44-111), and NEMO(1-120) were

cloned as described previously[103,116]. NEMO(44-195) and NEMO(110-195) were cloned from 5xAla NEMO, a codon-optimized template (GenScript)[103], by PCR, and restriction digested and ligated into a SUMOstar vector (LifeSensors) via BsaI and XhoI sites and T4 DNA Ligase. These constructs were transformed into T7 Express competent cells (New England Biolabs) to take advantage of the codon optimization. The variants 9SG and L153R were generated from the 7xAla full-length NEMO template using the NEB Q5 Site-Directed Mutagenesis Kit (New England Biolabs), and transformed into Rosetta 2(DE3)pLysS competent cells (Novagen). This cell line allows for the expression of additional tRNAs to account for rare, i.e. eukaryotic-preferred, codons present in this NEMO clone. Point mutants E57K, L80P, D113N, and R123W were generated in a 7xAla template using QuickChange mutagenesis, and transformed into Rosetta 2(DE3)pLysS competent cells (Novagen). Full-length IκBα in a mammalian expression vector was graciously donated by Dr. Susan Kandarian. GST-tagged IκBα(1-55) in a mammalian expression vector was graciously donated by Dr. Thomas Gilmore. For bacterial protein expression, these IκBα sequences were PCR amplified and cloned into a pDEST-17 vector via Gateway Cloning (Invitrogen). The list of primers used to generate these constructs is listed in Appendix I. All constructs were confirmed by DNA sequencing by Genewiz

(South Plainfield, NJ) using universal T7 polymerase forward and terminator primers.

2.2.3 E. coli *Expression and Purification*

For each NEMO variant, cells transformed with a plasmid bearing the gene encoding NEMO were grown in LB broth shaking at 250 rpm at 37 °C overnight, to seed a new expression culture at a 1:200 dilution with 50 μg/mL kanamycin for antibiotic selection. This new culture was grown until OD_{600} reached between 0.4 and 0.6. Protein expression was induced by 1 mM isopropyl β-D-thiogalactoside (IPTG) and incubated for four more hours. Cells were pelleted by centrifugation and stored at -20 °C. The pellets were lysed using a microfluidizer, and incubated with 0.1 μL/mL Universal Nuclease (Pierce) and 10 μL/mL Halt Protease Inhibitor Cocktail (ThermoFisher) for 20 m. Urea (at 8 M) was then added to the lysate to prevent chaperones and other contaminating proteins from co-purifying with NEMO, and the solution incubated for 1 h. The lysate was then clarified by ultracentrifugation at 38,000 rpm for 30 m, sonicated to shear any remaining large DNA fragments, and filtered through a 0.8 μm filter.

The protein was initially purified from bacterial lysate as described previously, which includes a re-folding step on a nickel column to remove

urea[103,116]. Instead of the gel filtration step, NEMO(44-195) and NEMO(110-195) were concentrated to 1 mL and incubated with SUMOstar Protease 1 (LifeSensors) for 2 hours at room temperature, and then 4 °C overnight. To isolate untagged NEMO(44-195), this mixture was then applied to a 5 mL HisTrap HP column (GE Healthcare) for subtractive affinity chromatography; the six-His-tagged SUMOstar tag and SUMOstar Protease 1 bound the column, while the untagged NEMO(44-195) flowed through and was collected. Purified proteins were pooled and concentrated to < 3 mL, typically about 2 mg/mL for full-length NEMO and 10 mg/mL for the shorter NEMO constructs. Full-length NEMO protein concentrations were calculated from the absorbance at 280 nm (NanoDrop, Thermo Scientific) using an extinction coefficient of 14400 M^{-1} cm^{-1} as predicted by ExPASY ProtParam[119]. NEMO(44-195) and NEMO(110-195) contain no tryptophan residues, so protein concentration was calculated by densitometry via SDS-PAGE with protein standards. Aliquots of each prep were stored at -80 °C.

Expression and purification of full-length IκBα was performed similarly to that for full-length NEMO protein, except for the omission of the gel filtration step. Protein concentrations were calculated from the absorbance at 280 nm (NanoDrop, Thermo Scientific) using an extinction coefficient of 28000 M^{-1} cm^{-1} as

predicted by ExPASY ProtParam[119]. Purity was assessed by SDS-PAGE.

2.2.4 SDS-PAGE Analysis

All SDS-PAGE experiments were performed using 12% polyacrylamide Tris-HEPES gels. Gels were stained using a solution of 40% methanol, 10% acetic acid, and 0.3% Coomassie R-250. To oxidize or reduce the protein, NEMO constructs were pre-treated with 5% H_2O_2 or 5 mM DTT for 1 h. After pre-treatment, the protein was incubated in SDS sample buffer (4% [w/v] SDS, 20% [v/v] glycerol, 0.01% [w/v] Bromophenol Blue, 125 mM Tris, pH 6.8) for 5 m and/or boiled in SDS sample buffer with 100 mM DTT prior to analysis.

2.2.5 Circular Dichroism Spectroscopy

NEMO constructs were diluted to 0.25 mg/mL in a buffer containing 20 mM sodium phosphate and 500 mM NaCl at pH 7.4. Spectra were obtained using a 1 mm 300 μL quartz cuvette in an Applied Photophysics Chirascan CD spectrometer. Buffer-subtracted spectra from 180 to 260 nm with a step of 1 nm were measured at 10 °C. Mean molar residual ellipticity (in units of degrees square centimeters per decimole) was calculated from the raw signal (in units of millidegrees) to normalize for differences in concentration and number of residues[120]. For thermal denaturation experiments[121], mean molar residual ellipticity was calculated from the signal at 222 nm, and traced as the sample

temperature was ramped at 1 °C /m from 10 °C to 70 °C. Slowing the ramping rate to 0.5 °C /m had no effect on the T_M. T_M values were determined as the maximum of a plot of the first derivative of the thermal denaturation curve, ($\delta\Theta/\delta T$). For 2,2,2-trifluoroethanol (TFE) inclusion to determine maximum level of α-helicity, NEMO was concentrated to 2.5 mg/mL before 10-fold dilution with TFE to yield a 90% TFE solution. Spectra were then obtained as described above. Percentage α-helix is calculated as a ratio described previously by Zhou and colleagues[116], between Θ_{222} in aqueous buffer and that in TFE-containing buffer according to Equation 1 below:

$$\alpha\ helix\ (\%) = \frac{\theta_{222}(aqueous)}{\theta_{222}(TFE)} * 100 \quad (1)$$

2.2.6 Small-Angle X-ray Scattering

5xAla-NEMO SAXS data were collected on beamline X9 of the National Synchrotron Light Source, and all other sample data were collected on beamline 16-ID-LIX of the National Synchrotron Light Source II, at Brookhaven National Laboratories (Upton, NY). Samples were transported frozen and filtered with a 0.22 μm filter after thawing, and centrifuged to remove any particulates. The protein concentrations were ~1.6 mg/mL and ~0.8 mg/mL for each component in 20 mM sodium phosphate, 500 mM NaCl, pH 7.4. Samples were loaded into 8-tube strips at ambient temperature and aspirated into a thin-walled 1.5-mm

diameter sample tube using an automated system as described previously[122]. At X9, scattered intensities were determined from q = 0.005 to 1.99 $Å^{-1}$ using an X-ray wavelength of 0.9184 Å and detected via a Mar 165 CCD detector 3.4 m from the sample. At LiX, scattered intensities were determined from q = 0.005 to 2.47 $Å^{-1}$ using an X-ray wavelength of 0.9184 Å and detected via a Pilatus3 1M SAXS detector and two Pilatus3 300K WAXS detectors. Three replicates were collected and data processing was performed using the X9 or LIX software packages to produce radially averaged intensity profiles extending over the entire scattering range. The data from the two concentrations were checked for consistency at low q and merged using PRIMUS[123]. For data collection and processing software comparison, 5XAla-NEMO datasets were obtained at both sites: the R_g for data collected and processed at X9 was 90 Å; at LIX R_g was 94 Å.

X-ray scattering patterns were initially checked for aggregation using the ATSAS suite[123]. The radius of gyration (R_g) and P(r) function were calculated using GNOM[124] with the data range indicated in Table 2. Following P(r) function determination by GNOM, this information was used in DAMMIN[125] to generate 10 *ab initio* models of the shape of each construct of NEMO using default parameters. The 10 models were averaged using DAMAVER[126]. The final output of DAMAVER was then re-run through DAMMIN for final refinement, using

default parameters. The goodness of fit of this final model was determined by FoXS[127,128] in CHIMERA by χ-value calculation[129]. The volume envelope of the model was generated using the "Fit in Map" feature of CHIMERA[129]. CHIMERA was also used to align the NEMO(44-195) volume envelope with that of the full-length NEMO model for direct comparison. Superposition of the envelope with previously solved X-ray crystal structures of individual NEMO domains IBD, HLX2, and CoZi was accomplished by using BUNCH[130]. This atomistic modeling fits the original scattering data well (χ = 0.74 theoretical scattering versus experimental), but should be considered provisional due to SAXS resolution limits.

2.2.7 *Analytical Ultracentrifugation*

Sedimentation velocity experiments were performed in a Beckman XL-I analytical ultracentrifuge[131], using aluminum double-sector sapphire cells in an An-50 Ti rotor (located at the MIT Biophysical Instrumentation Facility, Cambridge, MA). The rotor speed was 3,000 rpm for temperature equilibration (10 °C throughout the run), and then 42,000 rpm during the sedimentation run. Prior to centrifugation, protein samples were buffer exchanged against the buffer blank (20 mM sodium phosphate, 500 mM NaCl, pH 7.4). The protein concentration was at 0.7 mg/mL and 0.3 mg/mL; when included, IKKβ(701-745)

was in 10-fold molar excess. Interference images were collected every 60 s during the sedimentation run. The data recorded from moving boundaries was automatically buffer subtracted by the Beckman XL-I software and processed using SedAnal[132].

Sedimentation equilibrium experiments with the same instrument and rotor as for equilibrium velocity experiments were performed, except using aluminum six-sector sapphire cells. The spin speeds were 11,200, 14,000, and 21,000 rpm. The temperature was maintained at 10 °C. Prior to centrifugation, protein samples were buffer exchanged against what would be used as the buffer blank (20 mM sodium phosphate, 500 mM NaCl, pH 7.4). The protein concentration was at 0.7 mg/mL and 0.3 mg/mL; when included, IKKβ(701-745) was in 10-fold molar excess.

2.2.8 Crystallography of NEMO(44-195)

For selenomethionine (SeMet)-labeling for phase solution[133], NEMO(44-195) was expressed in T7 Express cells (New England Biolabs, Ipswich, MA) as was also done for the native protein. A 15 mL overnight culture was grown with shaking at 250 RPM at 37 °C in LB broth with 50 μg/mL kanamycin (GoldBio). A portion of the overnight culture (3 mL) was used to inoculate 1 L of fresh M9 minimal media supplemented with 50 μg/mL kanamycin, glucose, vitamins,

$MgSO_4$, and $CaCl_2$. Cultures grown with shaking at 250 rpm at 37 °C until OD_{600} reached 0.8-1.0. Amino acids were then added to the media to stop the natural methionine biosynthesis pathway: threonine, lysine, phenylalanine, leucine, isoleucine, valine, and selenomethionine, and were allowed to incubate for 15 m. IPTG was then used to induce expression of NEMO(44-195) overnight. Cells were pelleted at 5000 RPM and stored frozen at -20 °C until purification. Purification of SeMet NEMO(44-195) was identical to native protein except for inclusion of 5 mM DTT throughout until dialysis with the crystallization buffer (containing 10 mM Tris, 100 mM NaCl, 2.5 mM TCEP, at pH 7).

Dilute protein sample at ~0.001 mg/mL in the crystallization buffer was incubated with equimolar NBD peptide dissolved in water at 37 °C for 30 m, and subsequently concentrated to <200 μL. Crystals were grown using vapor-diffusion hanging-drop geometry at 17 °C using a 0.5:2 μL volume ratio of concentrated protein to crystallization solution of 100 mM HEPES pH 7.5, 5 mM DTT, and 19% PEG 3350. Two rounds of microseeding were accomplished by centrifuging crystals using Seed Beads (Hampton Research) in 100 mM HEPES pH 7.5, 5 mM DTT, and 25% PEG-3350, diluting the microseed solution 1:10, and adding 0.5 μL of this dilution to each drop that had been equilibrating for at least 24 h. The final crystals were cryoprotected in 100 mM HEPES, 5 mM DTT, 26%

PEG 3350, and 30% glycerol and transferred into liquid nitrogen. The I71M mutant was cloned using the NEB Q5 Mutagenesis Kit (New England Biolabs, Ipswich, MA), and protein was expressed, purified, and crystallized identically to the selenomethionine-incorporated WT version of the protein.

Multiple anomalous dispersion (MAD) data for SeMet NEMO(44-195) were collected at BL9-2 at Stanford Synchrotron Radiation Lightsource (Menlo Park, CA) at wavelengths 0.979 (peak), 0.91162 (remote), and 0.97934 (inflection). Data processing to 2.11 Å was performed with the HKL2000[134] program package. The attempt to solve the structure of the NEMO/NBD peptide complex by MAD phasing used AutoSol[135], which identified two selenium sites per asymmetric unit and produced phases with a figure of merit of 0.481 to 2.2 Å. AutoBuild[136] was used to attempt model building into electron density output by AutoSol, with several different attempts with different parameter selections, including but not limited to Quick Mode, simulated annealing, and a lower resolution cutoff. SHELX[137] was also used to attempt to solve phases using a different method; heavy atom sites from SHELXC/D were fed into the Phenix pipeline starting with AutoSol for subsequent attempts at model building.

One crystal was observed for SeMet NEMO(44-195) I71M under identical conditions to those that produced the above crystal, except no seeding was used.

This crystal was cryo-protected in 50% well solution and 50% glycerol and transferred into liquid nitrogen. Data collection was attempted at beamline NE CAT 24-ID-C at Advanced Photon Source (Lemont, IL), but no diffraction was observed for this crystal.

2.3 Results and Discussion

2.3.1 The IVD is Highly Conserved and Contains Human Disease-Associated Mutations

The error rate for DNA replication is between 10^{-8} and 10^{-10} for eukaryotic DNA polymerases after repair mechanisms are taken into account[138]. In the entire human genome of over $3x10^{9}$ base pairs, errors occur on average less than once per replication event. If an error is made in a gene that does not affect function significantly, it can be safely passed down to the subsequent generations. Mutations can be beneficial, i.e. gain of function, but they can also be detrimental, and can either result in disease or be lethal *in utero*. For residues directly involved in function and/or structural stability, there is little to no tolerance for mutation. By analyzing sequence variation for orthologs, residues under evolutionary pressure can be determined. Residues important for function are not as free to change, and are thus more highly conserved; residues

unimportant for function are freer to change to other residues. To analyze this sequence variation, a Multiple Sequence Alignment (MSA) was performed on the sequences obtained from BLASTp. This procedure may be performed in multiple ways; the most common, and the one used in this thesis, is progressive alignment construction as implemented by MUSCLE[118]. In brief, the technique aligns the most similar sequences first, progressively, until the most distantly related is aligned.

To determine whether the sequence of the IVD is conserved across species, we performed an MSA using annotated NEMO sequences obtained from BLASTp (National Center for Biotechnology Information). Of the 38 unique NEMO sequences after removing redundant sequences etc., 27 were from mammals, 10 from fish or amphibians, and 1 from *Drosophila*. The results suggest that NEMO appeared no more than 780 million years ago[139], as the most evolutionarily distant homolog for which sequence information is available is an arthropod (*Drosophila melanogaster*). Among all these species, NEMO is highly conserved (Appendix V). The alignment showed that, in the core regions of functionally important domains such as the IBD (IKKβ binding), the HLX2 domain (LUBAC binding), the CC2-LZ domains (ubiquitin binding), and the zinc finger (IκBα binding), the NEMO sequence is highly conserved even among the

non-mammalian orthologs. However, conservation is significantly lower towards the borders of these domains, and in the segments linking them (Appendix V). The alignment of the central portion of IVD is shown in **Figure 6**. Within the IVD, encompassing residues 112-195, there was high sequence conservation. Specifically, there is a highly conserved segment (residues 134-161), which includes a stretch of nine amino acids (QV/ATSLLGEL; aa 145-153) that is strictly conserved across all mammalian and non-mammalian vertebrate species, with the exception of a conservative Val/Ala polymorphism at position 146 in some non-mammalian species (Figure 6). Several residues in or near this region of the IVD sequence are conserved, even in *Drosophila*. Thus, the core of the IVD shows sequence conservation that is as high as or higher than any of the other functional regions of NEMO (Appendix V). The high sequence conservation observed in this region is consistent with the hypothesis that the IVD plays an important role in NEMO function. This hypothesis is further strengthened by the observation that several mutations associated with genetic immunodeficiency diseases are located in or near the IVD, including D113N, R123W, L153R, R173G, R175P and Q183H[42,82]. These IVD disease mutations do not significantly reduce NEMO expression[140–144], and thus likely exert their effects by altering NEMO protein function. From this information, it is interesting to note that the more

highly conserved center of the IVD appears to play a role in ectodermal dysplasia with immunodeficiency (EDA-ID), while the periphery of this domain is associated with incontinentia pigmenti (IP) (**Table 2**).

Table 2: Disease-associated mutations within the IVD.

Mutation	Disease	% Identity
D113N	IP	55.3
R123W*	IP	26.3
L153R	EDA-ID	97.4
Q157P	OL-EDA-ID	97.4
A169P**	EDA-ID	55.3
L170P	IP	92.1
R173G	IP	76.3
R175P	EDA-ID	78.9
R182P	IP	76.3
Q183H	IP	73.7

*42.1% Q; **18.4% T. IP: Incontinentia Pigmenti. OL-EDA-ID: osteopetrosis, lymphedema, anhidrotic ectodermal dysplasia, and immunodeficiency. % Identity: percent conservation of noted residue among sequences in NEMO MSA (Appendix V).

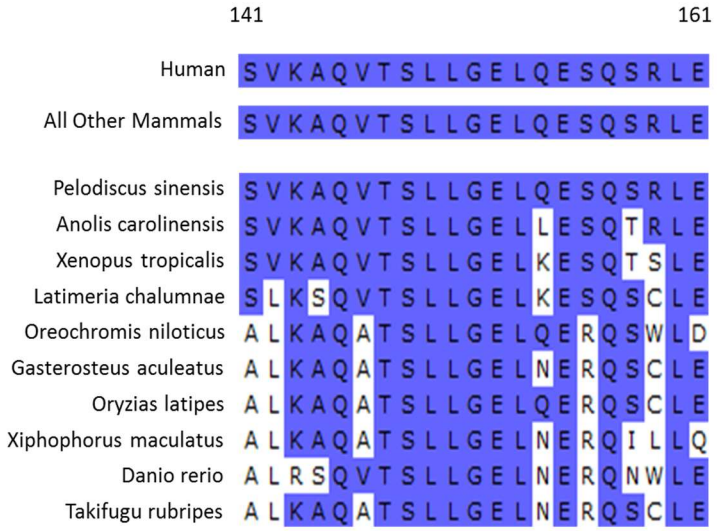

Figure 6: Multiple sequence alignment of full-length NEMO reveals a high level of sequence conservation in the IVD region. Shown is the region that spans residues 141-161. 9SG substitution is 145-QVTSLLGEL-153. Residues in blue indicate consensus.

2.3.2 *Design and Production of IVD Constructs for Bacterial Expression*

To assess the biochemical and biophysical properties of the IVD *in vitro*, bacterial expression vectors were created for a variety of NEMO constructs. These are shown in Figure 7. The boundaries of the construct NEMO(44-195) were selected to encompass both the entire IKKβ binding site and the IVD. A construct NEMO(44-111), which does not include the IVD, had been crystallized previously bound to the IKKβ(701-745)[28], and the structure determined. This NEMO(44-195) construct was made along with NEMO(110-195), which contains only the IVD. Both constructs were cloned from a previously codon-optimized 5xAla template[103] into a SUMOstar vector (LifeSensors) that contained a six-His tag N-terminal to a SUMOstar tag, which is N-terminal to the gene of interest.

This construction allowed for initial purification via nickel-NTA affinity chromatography, followed by proteolytic cleavage of the SUMOstar tag with subtractive nickel-NTA chromatography, to purify away the SUMOstar tags from the protein of interest. The SUMOstar tag has been optimized for increased bacterial expression, and additionally was included to increase solubility of newly expressed protein to avoid inclusion bodies which is a known obstacle in NEMO(1-120) purification[116].

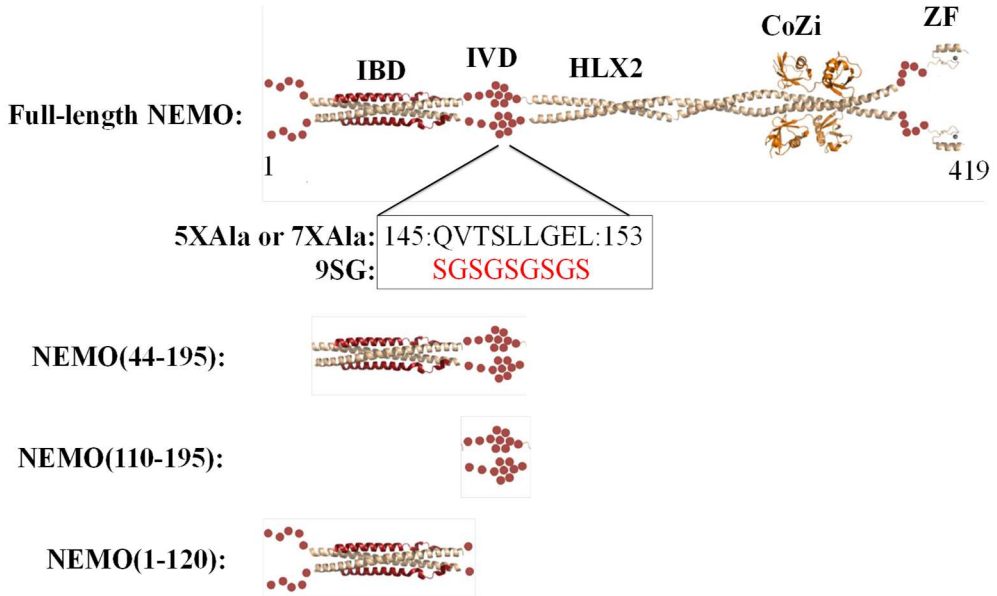

Figure 7: Full-length NEMO, L153R, 9SG, and NEMO(44-195) indicated on NEMO domain map with indicated mutations and fusions. NEMO(110-195) comprises the IVD, and 1-120 comprises residues 1 through the CC1 or IKKβ binding site.

Recombinant full-length 7xAla NEMO protein was developed previously and purified according to the original purification scheme[103]. 9SG NEMO, which contains a nine amino acid substitution in a core conserved region of NEMO

(Figure 7), was constructed in the same background, and is expressed and purified identically. Recombinant 5xAla-, 7xAla-, and 9SG-NEMO include an uncleaved six-His tag at the C-terminus as a result of inclusion in the pET24b vector (Appendix I). NEMO variants E57K, L80P, D113N, and R123W were generated successfully but were not used in any of the following experiments.

2.3.3 IVD Mutations Negatively Affect NEMO Stability

To determine whether the IVD is a significant structural component, the effect of the presence or absence of the IVD on thermal stability of the IBD was measured using circular dichroism spectroscopy (CD) to monitor thermal unfolding through the associated loss of secondary structure. FL-NEMO had a melting temperature of 41 ± 3 °C (n = 3) (Figure 8A), while it was previously shown that covalently dimeric NEMO(1-120) is less stable, melting at a temperature of 33 ± 2 °C[116]. Notably, NEMO(44-195) showed a single cooperative melting transition, with T_M = 45 ± 2 °C (n = 3), comparable to the T_M of FL-NEMO (41 ± 3 °C, n = 3). The NEMO(1-120) and NEMO(44-195) each contain a single inter-chain disulfide through Cys54; therefore, the difference in thermal stability can be attributed directly to the effect of the presence or absence of the IVD. The result that inclusion of the IVD substantially stabilized the protein to form a single, cooperatively unfolding unit therefore indicates that the IBD and IVD are

intimately structurally interconnected. The 9SG-NEMO variant had reduced structural stability, melting with T_M 34 ± 2 °C (n = 2), comparable to the value seen for the IBD only construct (Figure 8A). This result and the results from the IKKβ binding experiments show that the 9SG variant of the IVD disrupts the structure and function of the IBD-IVD region of NEMO.

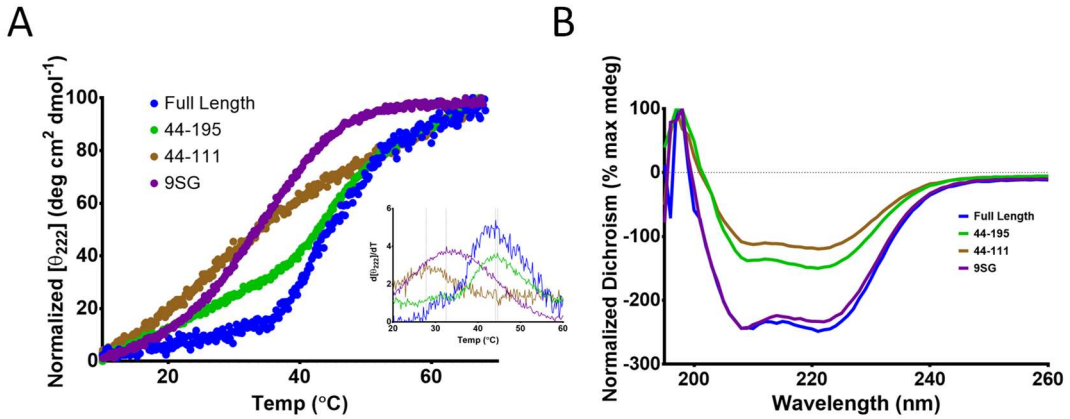

Figure 8: Influence of IVD on NEMO thermal stability. A: Thermal denaturation of NEMO monitored by CD. An increase in signal at Θ= 222 nm corresponds to loss of secondary structure. Curves are normalized to each other and are representative of n≥2 experiments. Inset: first derivative of melting curve used to identify T_M value. B: CD spectra of NEMO constructs determined at 10 °C and normalized. Normalization was performed, rather than calculating mean molar residual ellipticity, because the error in concentration determination of the tryptophan-less NEMO(44-195) and NEMO(44-111) may have confounded direct comparison. Negative peaks at 208 and 222 nm indicative of alpha-helical content.

To determine whether the 9SG mutation disrupts protein secondary structure, we characterized 9SG-NEMO and NEMO(44-195) by CD. Helical content was quantified by comparing the CD spectra measured in aqueous buffer with that in 90% 2,2,2-trifluoroethanol (TFE), a solvent that induces adoption of α-helical structure regardless of the protein primary structure[145,146]. Taking the

spectrum obtained in 90% TFE as representative of a 100% α-helical structure, the ratio of the molar ellipticity at 222 nm measured in aqueous buffer to the corresponding value in 90% TFE gives an estimate of the α-helix content of the protein in aqueous conditions. The results of these measurements showed that, in aqueous buffer, 9SG-NEMO was 65% α-helix, approximately the same as FL-NEMO. This finding suggests that the 9SG mutations do not cause overall disruption of the protein secondary structure. Using the same approach, NEMO(44-195) was found to be 83% α-helix. To verify that 90% TFE was sufficient to induce full α-helicity, NEMO(44-195) was also evaluated in 97% TFE, giving an result which does not differ significantly (81% α-helix). This high helical content suggests that the bulk of the IVD domain is folded and α-helical in secondary structure.

2.3.4 Structure of the IVD in the Context of Full-Length NEMO

Small-angle X-ray scattering (SAXS) has been used to reveal information about macromolecular structure and dynamics in solution. In SAXS, the raw x-ray scattering data are radially averaged about the beam center, and then buffer-subtracted to obtain the specific scattering intensity of the protein as a function of scattering angle. This information can be analyzed to reveal features of the protein structure, including generating a three-dimensional shape reconstruction

with a resolution on the order of 10- 50 Å[147]. The solution structure of full-length NEMO in complex with MBP-tagged herpesvirus FLICE inhibitory protein (vFLIP) has recently been determined by SAXS[63]. To probe the structure of unliganded full-length NEMO, we analyzed 5XAla-NEMO using SAXS. The scattering data are shown in Figure 9A as scattering intensity (I) against inverse scattering angle (q, $Å^{-1}$). Although the Guinier plot ($\ln(I)$ versus q^2, where I is the scattering intensity and q is a function of the scattering angle) for this data (Figure 9B) is not linear below $q^2 = 0.0006$ $Å^{-2}$, extended macromolecules are not expected to be linear in this region[147]. The key SAXS results for all constructs discussed in this dissertation are summarized in Table 3.

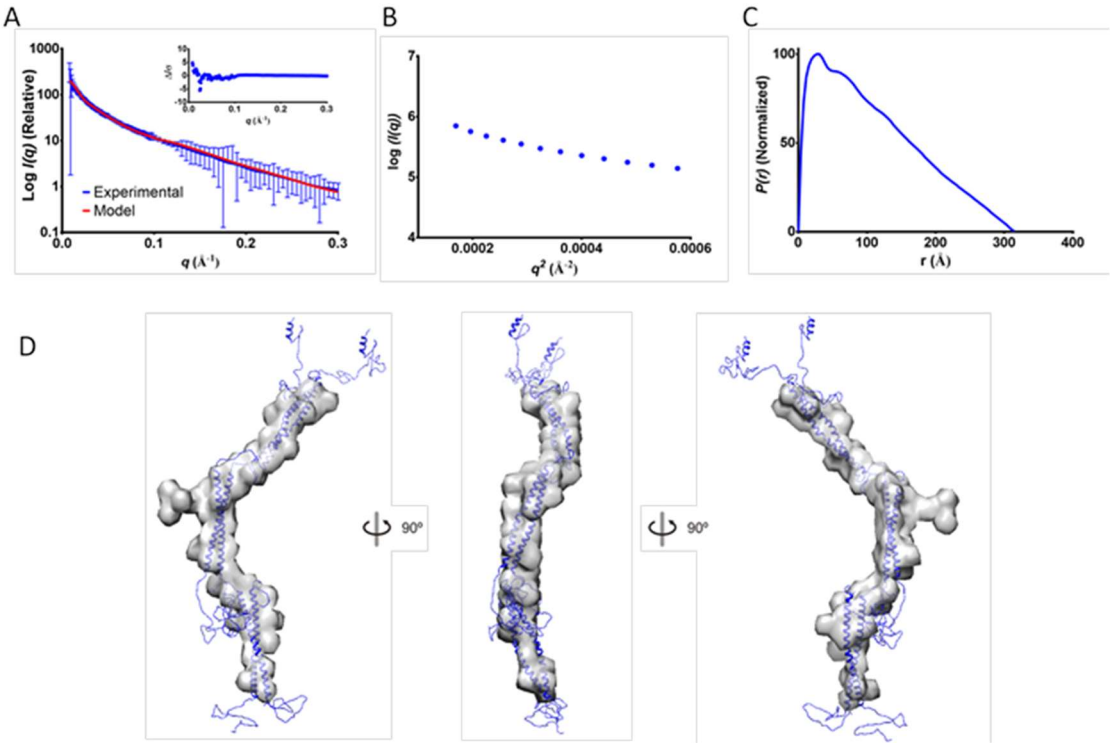

Figure 9: 5XAla-NEMO SAXS analysis. A: scattering curve for 5XAla-NEMO (blue), with theoretical scattering (red) calculated from model shown in panel D. B: Guinier plot. Nonlinearity at low *q* is expected for a partially flexible, extended protein. C: Distance-distribution function generated by GNOM. D: Shape reconstruction generated by DAMMIN (gray envelope) with superposed NEMO model (blue) generated by BUNCH.

The initial scattering curve can be used to calculate a distance-distribution function P(r), a histogram of all possible pairwise atom distances. The form of the P(r) plot is characteristic of the three-dimensional shape of the molecule and the maximum x-value equal to the maximum dimension of the scattering particle[147]. The P(r) plot for 5XAla-NEMO is shown in Figure 9C. The scoring function of GNOM is similar to χ^2 analysis[124]; a theoretical, extended model with a SAXS curve calculated by FoXS resulted in a χ^2 value of 0.601; 5XAla-NEMO resulted

in χ^2 = 0.583. This plot indicates that full-length NEMO has a highly extended structure, with a maximum at short interatomic distances and a long tail extending to the maximum particle dimension, D_{max}, of 315 Å. This is similar to the NEMO-MBP-vFLIP complex (320 Å) reported previously[63]. Fragments of NEMO encompassing residues 44-111 (IBD)[28], 197-249 (HLX2)[94], and 269-336 (CC2-LZ; unpublished PDB ID 4BWN), have been crystallized and shown to be dimeric coiled coils (Figure 4). The structure of the ZF of NEMO (residues 391-419) has been determined by NMR and adopts a fold typical of CCHC zinc fingers (PDB ID 2JVX)[98], but is not resolved in our SAXS model. The three ordered segments that fit in our model sum to 186 residues, corresponding to ~280 Å of extended α-helical structure. Therefore, our value of 315 Å indicates that the remaining 233 residues cannot all be in an extended coiled-coil conformation, and must be disordered or assume more tightly folded forms. It is possible, but unlikely, that the subdomains adopt a different conformation in the context of full-length NEMO.

The SAXS data were further analyzed to allow *ab initio* structure modeling. Specifically, the software package DAMMIN[125] was used to generate low resolution structures of each sample based on the P(r) data, modeling the protein by using dummy beads on a fixed lattice[125]. Ten models were generated,

averaged, and refined; prior to averaging, their average normalized spatial discrepancy is 0.58 ± 0.3. This unitless value reflects variability among DAMMIN models, with values < 1 indicating acceptable convergence on a final structure. The final highest scoring model was fit into a volume map using UCSF CHIMERA[129] revealing the shape of the average volume in solution.

The quality of the resulting model for 5XAla-NEMO was evaluated in three ways. First, FoXS was used to calculate a theoretical scattering curve from the final DAMMIN model[127,128], demonstrating how well each model represents the original scattering data (Figure 9A). The quality of the fit of the 5XAla-NEMO model was assessed using FoXS to calculate χ. The value of $\chi = 0.6$ indicates that the model fit well to the original experimental scattering data. As a further test of robustness, a NEMO model was generated using AllosMOD-FoXS[127,128] ($\chi = 0.6$), which calculates a model differently than DAMMIN. There is a high degree of similarity between the DAMMIN and AllosMOD-FoXS; R_g is 94 Å from the ATSAS suite, and 88 Å from AllosMOD-FoXS.

The structural model for 5XAla-NEMO (Figure 9D), reveals an extended structure containing several kinks. Superposing the extended, coil-coil segments of the published X-ray crystal structures of the IBD, HLX2 and CC2-LZ fragments of NEMO were modeled together using BUNCH[130]. The results also

indicate that the C-terminal ZF domains of NEMO are not visible in the SAXS structure, suggesting that the ZF domains are not fixed in position relative to the remainder of NEMO. Similarly, N-terminal residues 1-43 are absent from the SAXS surface envelope, consistent with previous results indicating that this region is structurally disordered[28,116]. It is notable that this disordered region is well conserved among mammalian sequences of NEMO, but not in more evolutionarily distant species, suggesting a recently evolved function, perhaps related to phosphorylation events[57]. The small projection visible at the center of the extended structure likely reflects residual electron density resulting from a small fraction of dimer-dimer contacts involving this region of the molecule, as has been proposed[79,104], but may also be an artifact from DAMMIN. The apparent compact, globular, nature of the residues between the IBD and HLX2 (i.e. the region containing the IVD) is notable given the extended nature of the individual NEMO X-ray crystal structures and previous lack of characterization of this region. Further evidence supporting the observation that this region is folded and compact include the circular dichroism experiments in Section 2.3.3.

To probe the structure of NEMO(44-195) in solution, SAXS was employed as for 5XAla-NEMO (*vide supra*). The experimental scattering was overlaid with theoretical scattering from the shape reconstruction model (Figure 10A), showing

a reasonable fit with χ = 0.7. The Guinier plot (Figure 10B) indicates no significant aggregation, as it is linear up to q^2 = 0.0006 $Å^{-2}$. The P(r) function for NEMO(44-195) is shown in Figure 10C (χ^2 = 0.507), and the shape reconstruction in Figure 10D. The notable consistency between the shape reconstruction of the fragment and that of FL-NEMO is shown by superposition in Figure 10E. This is direct evidence that the conformation and oligomerization state of the IBD plus IVD within FL-NEMO is to that of the shorter construct NEMO(44-195). Therefore, NEMO(44-195) is a good surrogate for FL-NEMO for probing NEMO functionality.

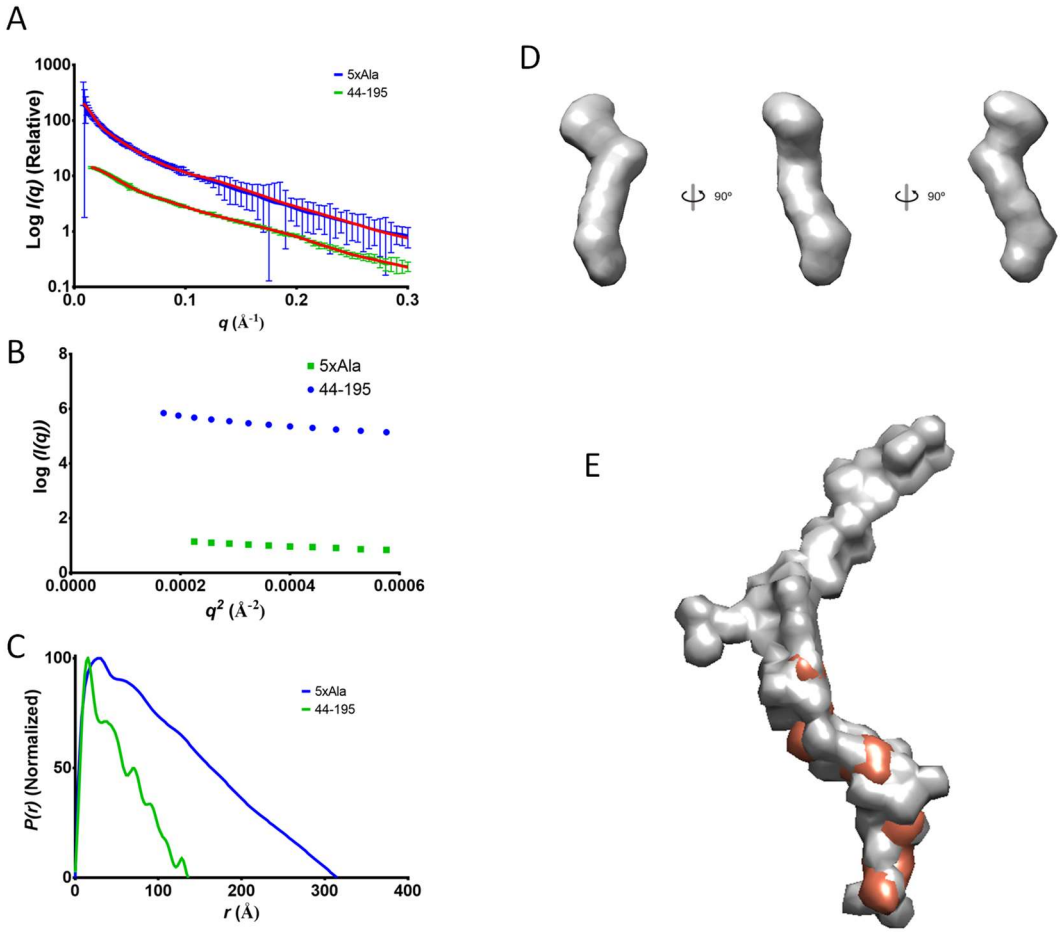

Figure 10: Solution structure of full length 5XAla-NEMO and NEMO(44-195). A: Scattering curves for 5XAla-NEMO and NEMO(44-195). Theoretical scattering for curve fits of models overlaid in red. B: Guinier plots. C: Distance-distribution functions generated by GNOM. D: Shape reconstruction for NEMO(44-195) generated by DAMMIN. E: Shape reconstruction for NEMO(44-195) in orange superposed on shape reconstruction for full length 5XAla-NEMO (gray).

2.3.5 *Structural Dynamics of NEMO in Response to IKKβ Binding*

To further probe the impact of the 9SG substitution, we analyzed the structural dynamics of 5XAla-NEMO and NEMO(44-195) versus 9SG-NEMO in response to IKKβ(701-745) binding. This IKKβ peptide, and all IKKβ peptides used throughout this thesis, contain a mutation of the only endogenous cysteine

to an alanine to prevent disulfide-mediated aggregation. The scattering curves, Guinier plots, and P(r) plots for these conditions are shown in Figure 11A-C. Notably, the P(r) functions for both NEMO(44-195) (with IKKβ, χ^2 = 0.843) and 5XAla-NEMO (with IKKβ, χ^2 = 0.580) indicate that, upon IKKβ binding, NEMO appears to fold in on itself. Specifically, D_{max} for 5XAla-NEMO decreases from 315 to 255 Å, and for NEMO(44-195) D_{max} decreases from 138 to 93 Å. It is important to note why we have chosen to discuss D_{max} here, as opposed to R_g. Because D_{max} is the maximum distance present in the scattering mass, it will not change upon addition of a smaller peptide. On the other hand, R_g is the square root of the average squared distance of each scatterer to its center, so it would be expected to change with addition of a smaller species such as a peptide as that average distance shrinks[147]. These solution scattering results indicate that binding of IKKβ peptide causes NEMO to adopt a conformation that is more compact than that seen for unbound NEMO as demonstrated by a reduction in the length of the maximum distance vector in the scattering mass. Unlike the case for wild-type IVD-containing NEMO constructs 5XAla-NEMO and NEMO(44-195), 9SG-NEMO solution scattering is not consistent with a more compact form upon IKKβ binding as illustrated by the P(r) functions (χ^2 = 0.529 and 0.620, respectively). In fact, 9SG-NEMO appears to elongate upon IKKβ binding, from

250 to 280 Å. This may be due to an overall rigidification of 9SG-NEMO upon IKKβ binding. Key SAXS results are summarized in Table 3. Taken together, these results suggest that the wild-type IVD sequence is required for ligand-induced conformational change to occur in NEMO, and that this change is required for downstream signal-induced activation of IKKβ.

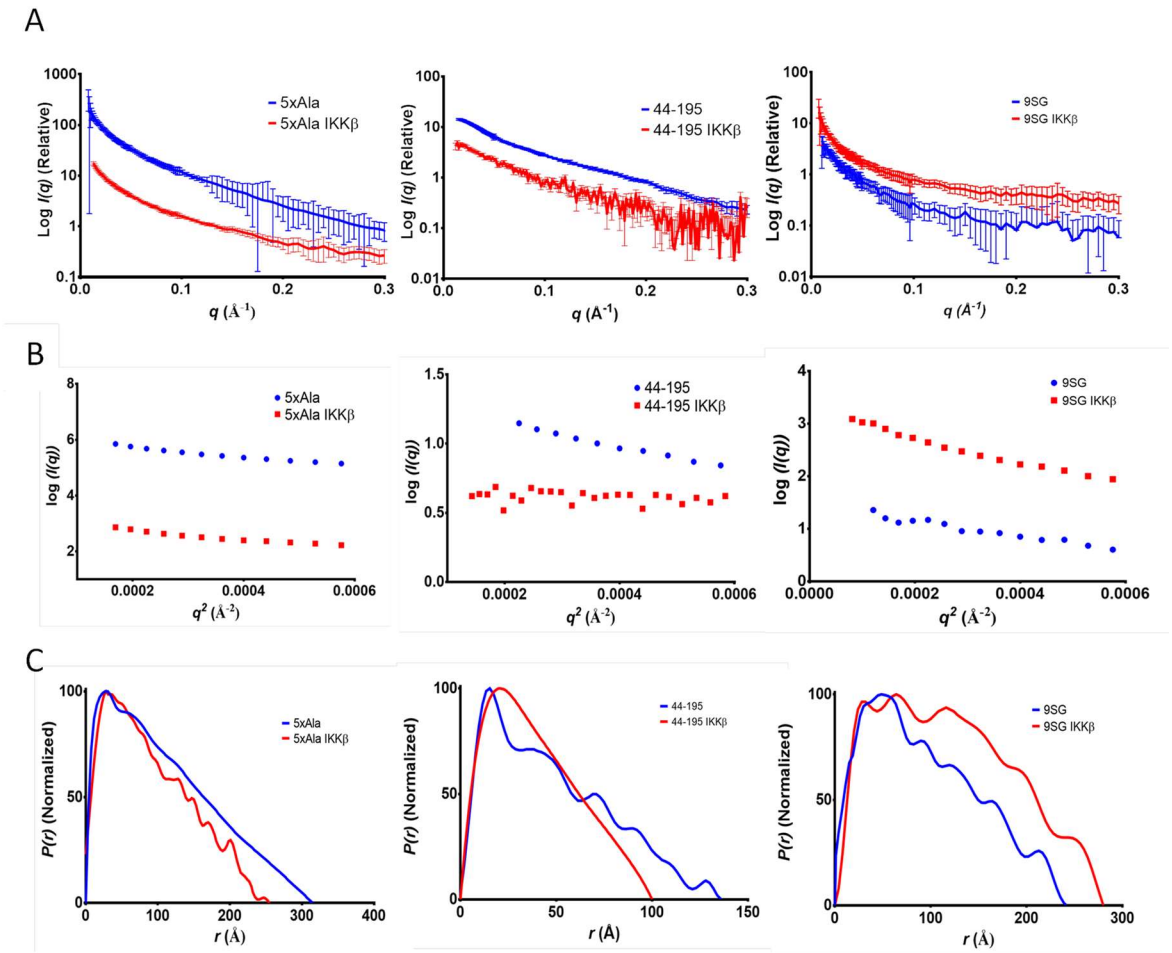

Figure 11: SAXS analysis of each NEMO construct with and without IKKβ(701-745). A: scattering curves with (red) and without (blue) IKKβ(701-745) in 10-fold molar excess. Error bars are SEM of three independent measurements. Protein concentrations were ~1.6 mg/mL and ~0.8 mg/mL for each component in 20 mM sodium phosphate, 500 mM NaCl, pH 7.4. Data are merged scattering intensities from the two concentrations after data quality confirmation in PRIMUS. B: Guinier plots calculated from squaring x-axis in scattering curves in panel A. Data range from scattering plots in panel A used to generate Guinier plots (in $Å^{-1}$): 44-195, 0.015-0.325; 44-195 with IKKβ(701-745), 0.012-0.3128; 5xAla, 0.008-0.26; 5xAla with IKKβ(701-745), 0.013-0.56; 9SG, 0.011-0.79; 9SG with IKKβ(701-745), 0.009-0.255. C: Normalized distance-distribution functions generated by GNOM calculated from scattering curves in panel A, where x-intercept indicates maximum dimension of the scattering mass (D_{max}).

Table 3: Summary of key SAXS parameters.

Protein	R_g (Å)[a]	D_{max} (Å)[a]	Max D_{max} (Å)[b]	Data Range (Å^{-1})	GNOM χ^2 [c]	Model χ value[d]	DAMMIN Models NSD[e]
44-195	38.8 ± 1.8	138	226.5	0.015 – 0.325	0.507	0.6	0.55 ± 0.2
44-195 plus IKKβ	31.6 ± 0.33	100	226.5	0.012 – 0.3128	0.843	n.d.	N/A
5xAla	94.2 ± 1.5	315	628.5	0.008 – 0.26	0.583	0.3	0.58 ± 0.3
5xAla plus IKKβ	79.6 ± 9.0	255	628.5	0.013 – 0.56	0.580	n.d.	N/A
9SG	77.4 ± 17.6	250	628.5	0.011 – 0.79	0.529	n.d.	N/A
9SG plus IKKβ	89.9 ± 10.5	280	628.5	0.009 – 0.255	0.620	n.d.	N/A
Theoretical Extended	76.2	270	270	0.000 – 0.499	0.601	n.d.	N/A
Theoretical Bent	46.7	129	270	0.000 – 0.499	0.754	n.d.	N/A

[a]R_g and D_{max} values calculated by GNOM. Standard deviation for D_{max} not reported because it is a user input; D_{max} is best fit by optimizing GNOM χ^2. [b]Max D_{max} refers to the maximum possible dimension if the same number of residues adopted a purely extended α-helix (1.5 Å x n residues). [c]GNOM χ^2 refers to scoring function from P(r) calculation; above 0.5 is reasonable. [d]Model χ-value calculated by FoXS. [e]NSD (unitless) is normalized spatial discrepancy average ± standard deviation for each DAMMIN model during averaging; n.d. not determined; N/A not applicable.

To corroborate these findings, we performed analytical ultracentrifugation (AUC). AUC works on the principle that proteins sediment along a centrifuge cell ultimately according to their size and shape[131]. Sedimentation velocity experiments were performed with NEMO(44-195) in the presence and absence of IKKβ(701-745). Results can be shown by a distribution function, G(s), versus sedimentation coefficient (s) plot. It is therefore related directly to the distribution of macromolecules as a function of signal intensity[131]. This plot for

unliganded NEMO(44-195) shows two peaks, corresponding to two different species in solution, likely monomer and dimer (**Figure 12**). Note the presence of 2.5 mM TCEP may be sufficient for some measurable fraction of NEMO to be reduced and monomeric. The plot for NEMO(44-195) in the presence of 10-fold molar excess of IKKβ(701-745), on the other hand, displays a single peak that is right-shifted, indicating an increase in mass (**Figure 12**). Peaks correspond to s = 1.1 and 1.7 for NEMO(44-195), and s = 2.2 for NEMO(44-195) in complex with IKKβ(701-745). The data are not of sufficient quality to draw more meaningful conclusions, but we can conclude the basic facts that the presence of IKKβ induces a homogenous population in solution, where each particle is larger by mass than any particle in the unliganded sample. Further analysis is required with 7XAla-NEMO and NEMO(44-111) to establish the direct relationship between the IVD and IKKβ-induced hydrodynamic changes.

Sedimentation equilibrium experiments were also performed with NEMO(44-195) in the presence and absence of IKKβ(701-745). However, unlike SV experiments, protein aggregation was sufficient to prevent processing of the SE data. Future attempts at running SE experiments will require optimization of sample prep. Fresh protein, purified within one week of experimentation, may be required.

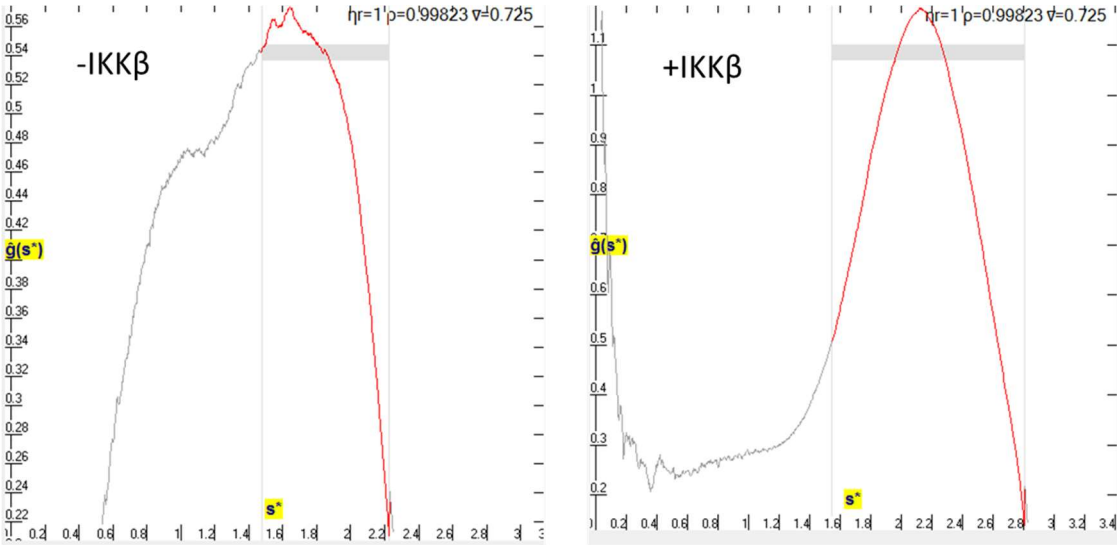

Figure 12: IKKβ promotes NEMO hydrodynamic changes. This preliminary data screenshot from SedAnal showing G(s) versus s indicates a clear difference in the hydrodynamic behavior of NEMO(44-195) before (left) versus after (right) addition of IKKβ(701-745). Further analysis is required with 7XAla-NEMO and NEMO(44-111) to establish the direct relationship between the IVD and IKKβ-induced hydrodynamic changes. G(s) is distribution of s values.

2.3.6 *Crystallography of NEMO(44-195)*

Attempts to crystallize NEMO were based on success with NEMO(44-111) construct[28] and previous positive results from Dr. Andrew Lynch. Briefly, crystallization conditions were optimized to co-crystallization with equimolar NBD peptide, 0.1 M HEPES pH 7.5 and 17-22% PEG-3350, following three rounds of microseeding using quasi-crystals. Additional attempts to refine crystallization conditions for the NEMO(44-195) construct included use of the Silver Bullet additive screen (Hampton), finer grid screening, seeding in dioxane to poison new nucleation, and replacing the NBD peptide with a longer 45mer

peptide, IKKβ(701-745), to attempt to increase rigidity. None of these additional attempts produced crystals.

One crystal, shown in **Figure 13**A, diffracted, and its diffraction pattern is shown in **Figure 13**B. Basic structure solution was attempted as described in section 2.2.8 above. Data were collected to 2.11Å, and the unit cell was observed with the following dimensions: a=41.659Å, b=40.059Å, c=58.01Å, α=90°, β=98.446°, γ=90°. Additionally, attempts to solve the structure were performed using the CCP4 suite, specifically the SHELXC/D/E pipeline. Output from these programs yielded some contiguous electron density, but attempts to build protein models within the density consistently failed as before in Phenix.

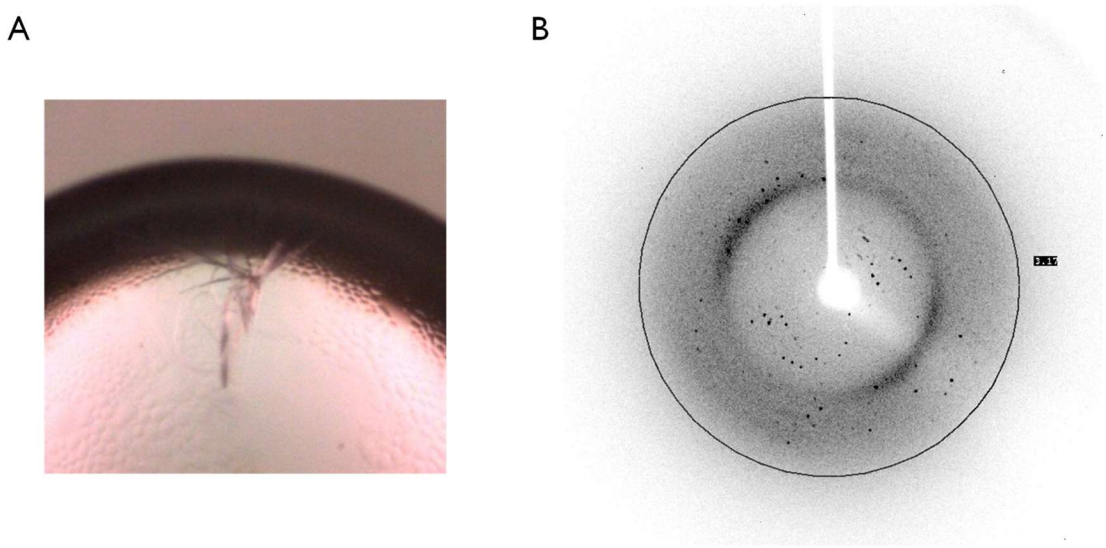

Figure 13: Crystallography of NEMO(44-195). A: Crystal that diffracted to 2.11 Å grown in 0.1 M HEPES pH 7.5 and 20% PEG-3350 after three rounds of microseeding. B: Resulting diffraction pattern.

To attempt to manually add information to aid structure solution, molecular replacement and manual model building were attempted. For molecular replacement, Phaser-MR[148] was used with various model inputs: PDB 3BRV, 3BRV modified to truncate IKKβ to NBD peptide, 3BRV with truncated IKKβ with symmetry data trimmed from the file, 3BRV with truncated IKKβ with symmetry mates generated by Coot[149], and 3BRV with truncated IKKβ docked into best electron density map from AutoSol using Coot. When molecular replacement would not generate a reasonable model, sulfur sites from the molecular replacement solutions were used as heavy atom sites for selenium in subsequent AutoSol runs for phasing attempts. These were unsuccessful as well.

Manual model building was attempted using Coot in two different ways. First, results from AutoBuild that were poor solutions were altered with 1) correct amino acid side chains based on heavy atom sites assuming there are selenomethionine residues, and 2) rotamer selection and fitting to best occupy the electron density. Subsequent refinement in AutoBuild using these models never generated results with R free better than 0.5. The second model building procedure involved using Coot to generate *de novo* an extended alpha-helix of the N-terminus of the IVD (LKRAQQQMAEDKASV) to be used in addition to modified 3BRV described above. This procedure also failed to generate models

with R free better than 0.5.

2.4 Conclusions and Future Directions

Scaffold proteins have been shown to employ a small variety of strategies to perform their function; however, the underlying molecular mechanisms by which these functions are accomplished are unknown. Herein, we have shown that the central IVD region of NEMO is highly conserved, has a defined structure, confers thermal stability, and is required for IKKβ-induced conformational change to occur. We hypothesize that the IVD is highly conserved because it plays a role in conformational change that is required for downstream signaling to NF-κB. This would indicate that NEMO is an allosterically regulated scaffold protein. The functional importance of this region is further explored in Chapter 3. Of note, the last residue of the targeted region in the 9SG variant (i.e., L153) is the site of an EDA-ID-associated mutant (L153R), which is defective for NF-κB signaling[141]. This hypothesis is further tested in the following chapter of this dissertation.

In addition to L153R, there are several disease-associated mutations within this highly conserved region, between residues 110-195. D113N, R123W, L170P, R173G, R182P and Q183H are associated with IP, Q157P with anhidrotic

ectodermal dysplasia with immunodeficiency, osteopetrosis, and lymphedema (OL-EDA-ID), and A169P and R175P with EDA-ID[82]. From this information, it is interesting that the more highly conserved central segment of the IVD appears to play a role in EDA-ID, whereas the periphery of this domain is associated with IP (Table 2).

The 9SG substitution in the IVD impacts thermal stability. Despite the lower thermal stability in the 9SG variant, the IVD is structured, given that the 9SG and 7XAla NEMO variants both have 65% α-helix, as measured by TFE experiments using CD. The 9SG substitution therefore does not disrupt the overall fold of NEMO. It is notable that NEMO(44-195) has a higher percent α-helix than FL-NEMO at 82%; this is likely due to substantially disordered regions of NEMO, including the first 43 residues and perhaps residues 336-387[28,95]. With higher quality data, Kratky plots from SAXS data may be useful to further probe the folded-ness of each of these NEMO constructs in solution. Additionally, AUC experiments would be ideal to corroborate SAXS findings, especially with respect to molecular shape.

A recent study[106] demonstrated, by both intrinsic tryptophan fluorescence and ANS fluorescence in the presence of either the IKKβ(735-745) NBD peptide or a 13mer peptide of IκBα, that NEMO undergoes a ligand-induced

conformational change. Importantly, this established that NEMO alters its structure once bound to its canonical NF-κB signaling binding partners. In view of our SAXS data on molecular dimensions and previous evidence of conformational change, we favor a model where the IVD is required for a conformational change in NEMO that is necessary for directed phosphorylation of IκBα by IKKβ. We propose that other scaffold proteins may function similarly, and a similar approach to the one taken herein may be useful to determine their major regulatory regions. The study of undruggable targets may benefit from this approach, in identifying regions that may be targeted with small molecules to modulate function by impacting the target's ability to undergo an essential conformational change. SAXS is a powerful tool to probe these ligand-induced conformational changes. A high-throughput application of SAXS would be useful in identifying potential therapeutics that alter either apo- or liganded-conformational states of a target protein. Scaffold proteins are a specific class that would benefit most directly from this approach, as functional assays are more difficult to develop due to the lack of intrinsic catalytic activity.

We have attempted to crystallize NEMO(44-195) in complex with IKKβ(701-745). Previously, the structure of NEMO(44-111) was solved[28], leaving the IVD structurally uncharacterized. Despite obtaining high resolution (2.21 Å)

data sets for a selenomethionine-incorporated version of NEMO(44-195), with phase figure of merit of 0.481, we were unable to solve the structure. This may be due to the difficulty placing α-helices along long, tube-like electron density; rotation and translation functions likely cannot distinguish productive from nonproductive helix placement. To attempt to address this, an I71M variant of NEMO(44-195) was cloned and used to increase the phasing power by incorporation of an additional methionine. Unfortunately, diffracting crystals were not produced from the variant. Future experiments include additional crystallization conditions for this variant to obtain diffracting crystals, co-crystallization with IKKβ(701-745) for increased rigidity, and optimization of cryo-protection conditions, as the introduced mutation may have altered the requirements for stable freezing, resulting in a loss of diffraction.

Chapter 3: The Intervening Domain is Required for NEMO Function in Canonical NF-κB Signaling

3.1 Introduction

NEMO function has been extensively studied: protein binding interactions have been mapped, individual domains have been crystallized, a number of disease-associated mutations have been annotated, and its oligomerization state has been debated[28,42,58,69,82,94,96,98,104,107,108,114,115]. Additions to this endeavor are described above in Chapter 2. However, beyond rigid-protein binding[28,58], the mechanism of action of NEMO is poorly understood. In the previous chapter, the structural, thermal stability, and dynamical contributions of the IVD to NEMO overall were described. Given this dynamic nature, it is unlikely that NEMO only serves as a rigid docking site for protein binding. In this chapter, the functional attributes of the IVD will be explored, to determine a link between biophysical traits and biologically relevant functionality.

To probe IVD function, WT-NEMO activity is compared to that of 9SG-NEMO, where the central site of highest conservation in the IVD has been mutated to serines and glycines. Given the lack of ability to undergo IKKβ-induced conformational change as determined by SAXS, we expect the 9SG mutant to be less capable of propagating NF-κB signaling. This idea is not

unprecedented: it has been shown that mutations outside of binding sites can affect function. In one example, two mutant versions of mouse transcription factor c-Rel were generated: R266H and SPW (insertion of proline and tryptophan between aa 266 and 267). These mutations occur outside of the dimer interface, yet prevent dimerization and thus efficient transcriptional activity from occurring[110]. In another example, the most common mutation (A149P) in aldolase B associated with hereditary fructose intolerance (HFI) was generated in recombinantly expressed protein. The crystal structure was solved, and it was determined that the proline substitution disrupts quaternary structure and thermal stability. Interestingly, this disruption is propagated to a loop region comprising residues 110-129, which is the subunit-subunit interface, and explains the loss of quaternary structure and enzymatic activity resulting in HFI[111].

NEMO(1-120) is a fragment of NEMO containing the disordered N-terminal tail and the entire IKKβ-binding site, yet binds to IKKβ with an affinity approximately 10-fold lower than full-length NEMO[116]. Therefore, there must exist some allosteric contribution from another domain of NEMO. This might be accomplished by either of two mechanisms: pre-ordering, where the entropic cost of the formation of the final protein-protein complex is lowered by rigidification of the binding site; or by additional physical interactions, where

another part of NEMO folds around or onto the IKKβ protein to make additional contacts, increasing affinity. The rod-like, extended nature of all existing crystal structures of NEMO domains and the crystal structure of NEMO(44-111) in complex with IKKβ(701-745) suggest that additional NEMO contacts to IKKβ would be limited at best due to the "seal" of residues around the hydrophobic binding interface[28]. It is therefore more likely that the IVD allosterically regulates NEMO by pre-ordering rather than additional physical interactions with IKKβ. Another part of NEMO likely pre-orders the IKKβ binding site for a lower entropic cost upon binding. This hypothesis is also supported by the contributions of the IVD to thermal stability and conformational rigidity described above in Chapter 2. A recent paper introduces the hypothesis that additional physical interactions drive negative regulation[63]. The CC1 of NEMO (residues 120-150) is postulated to interact with the UBAN domain to block the ability of NEMO to adopt an active conformation, until poly-ubiquitin (at least Ub_4) disrupts the CC1-UBAN interaction, opening up NEMO. The plausibility of this model is discussed later in this chapter.

In this chapter, the development of a NEMO-IκBα FA assay is described to establish the first quantitative analysis of this interaction. The zinc requirement and kinetics of the interaction are also described. Using a peptide

similar to that in the FA assay as a substrate, an *in vitro* assay to measure the contribution of NEMO to IKK activity will be discussed. This assay is also used to explore the effect of linear tetra-ubiquitin on NEMO-mediated IKK activity, which has been postulated to be required for activation of NEMO[63]. The IVD is the most logical domain to investigate for allosteric control due to the findings in Chapter 2, especially the high level of sequence conservation that must be due to evolutionarily important function. Simply put, the IVD confers pre-ordering, stability, and contributes to the conformational dynamics of NEMO, so it likely plays a key role in the function of the protein. To this end, this chapter also explores the contribution of the IVD in NEMO binding to IKKβ by use of a FA assay developed previously[103]. To relate all of the above findings to a biologically relevant context, cellular studies conducted by the Gilmore group at Boston University are also described. Specifically, the ability of 9SG-NEMO and L153R-NEMO to propagate NF-κB signaling and co-immunoprecipitate IKKβ and IκB*α* are tested. One way NEMO may signal is *in trans*, where a head-to-tail dimer brings the terminally-bound ligands into close proximity, negating the requirement for a conformational change in function. This hypothesis was tested and is described using co-transfected ΔN and ΔC truncated versions of NEMO.

3.2 *Materials and Methods*

3.2.1 Materials

All NEMO constructs used in this chapter were generated and prepared as described in Sections 2.2.2 and 2.2.3. NEMO cDNAs used in mammalian cell-based experiments were cloned identically, except into mammalian vectors pBABE and/or pcDNA-FLAG, and are described below. FITC-IKKβ(701-PAKKSEELVAEAHNLCTLLENAIQDTVREQDSFTALDWSWLQTE-745), unlabeled IKKβ(701-745), FITC-IκBα(20-LKKERLLDDRHDSGLDSMKDEEY-42), and unlabeled IκBα(20-42) were purchased from Genscript (Piscataway, NJ). The IKKβ sequence has been highly characterized in terms of its structure and interactions with NEMO[28,102,103,108,150], and the IκBα sequences is based on the site shown to interact with NEMO[58,106]. Each FITC conjugation was at the N-terminus of the peptide via a flexible aminohexanoic acid moiety. Unlabeled peptides contain an N-terminal acetylation and a C-terminal amidation. The Sox-based[151] kinase assay described herein was developed by AssayQuant (Marlborough, MA), and reagents specific to that assay were graciously provided by the company.

GST-tagged IκBα(1-55) was provided by the Gilmore group at Boston University. Transformed BL21 DE3 cells were grown in LB broth shaking at 250

rpm at 37 °C overnight, to seed a new expression culture at a 1:200 dilution with ampicillin antibiotic selection. This new culture was grown until OD_{600} reached between 0.4 and 0.6. Protein expression was induced by 1 mM IPTG and incubated at 37 °C for 4 more hours. Cells were pelleted by centrifugation and stored at -20 °C. The pellets were lysed by microfluidizer, and incubated with 0.1 μL/mL Universal Nuclease (Pierce) and 10 μL/mL Halt Protease Inhibitor Cocktail (Thermo) for 20 m. 8 M urea was then added to the lysate to prevent chaperones and other contaminating proteins from co-purifying with the protein, and incubated for 1 h. The lysate was then clarified by ultracentrifugation at 38,000 rpm for 30 m, sonicated to shear any remaining large DNA fragments, and filtered through a 0.8 μm filter. This lysate was then incubated with GST resin overnight at 4 °C. The resin-lysate solution was then centrifuged to collect non-bound flow-through, washed twice with 20 mM sodium phosphate, 500 mM NaCl, pH 7.4 buffer, and GST-tagged IκB*α*(1-55) was eluted with 20 mM sodium phosphate, 500 mM NaCl, 10 mM reduced glutathione at pH 7.4 following a 30 m incubation.

3.2.2 Fluorescence Anisotropy Binding Studies

The NEMO-IKKβ FA assay used herein has been described previously[103]; the NEMO-IκB*α* FA assay is based on that protocol. Briefly, assays were run in

black 96-well polypropylene plates with a total assay volume of 200 μL. The assay buffer contained 50 mM Tris, 200 mM NaCl, and 0.01% Triton X-100, at pH 7.4. Assays with FITC-IκBα included 1 mM $ZnCl_2$ and no DTT, unless otherwise indicated. NEMO concentrations were varied from 10 pM to 1 μM while keeping FITC-IKKβ(701-745) peptide or FITC-IκBα(20-42) peptide (tracer probe) constant at 15 nM. Plates were incubated at 25 °C for 1 h prior to reading for FITC-IKKβ experiments, or 15 m for FITC-IκBα experiments. Fluorescence anisotropy was read using a SpectraMax M5 plate reader using λ = 488/520 ex/em and 100 reads per well. Anisotropy was calculated as described previously according to Equation 2 below, where r is anisotropy and I is the measured intensity in either the parallel (∥) or perpendicular directions (⊥)[103].

$$r = 1000 * \left(\frac{I_{\parallel} - I_{\perp}}{I_{\parallel} + 2I_{\perp}}\right) \quad (2)$$

Briefly, raw anisotropy was calculated using the SpectraMax plate reader software and multiplied by 1000 as in Equation 2. These values were then exported to Microsoft Excel for averaging and calculation of standard deviation. These results were then plotted and fitted to a relevant binding equation in GraphPad Prism. Data were either plotted as averages ± standard deviation with no background subtraction or were normalized to high (NEMO + tracer probe) or low (tracer probe alone) controls.

3.2.3 *Dynamic Light Scattering*

Size distribution experiments using dynamic light scattering were performed with a DynaPro NanoStar DLS instrument (Wyatt Technology Corporation, Santa Barbara, CA, US) in the presence of 15 nM FITC-IκBα, 10 mM Tris, 500 mM NaCl, 5 mM DTT, at pH 7.4. Exogenous addition of metal ion (Mg^{2+} or Zn^{2+}) was accomplished by additional inclusion of buffer containing 50 mM Tris, 200 mM NaCl, and 0.02% Triton X-100 at pH 7.4 containing metal and concentration as indicated in Section 3.2.2. Tris was included in the buffer as a weak zinc chelator to improve its solubility at such high concentrations. DTT was included to minimize disulfide-mediated protein aggregation. The presence of both Tris and DTT likely lowered the free zinc concentration available to NEMO, but did not prevent a zinc-specific effect from being observed. Final volumes were 10 μL. Measurements were taken with a 100 mW He-Ne laser with λ = 633 nm at a scattering angle of Θ = 90° at ambient room temperature in a microcuvette. For data analysis, particle type was assumed to be globular (as opposed to a type of large polymer), and 10 acquisitions were collected and averaged for final scattering determination.

3.2.4 *Surface Plasmon Resonance Binding Studies*

7xAla NEMO was immobilized on a GLH sensor chip in a Bio-Rad

ProteOn XPR36 SPR system (Hercules, CA) using either amine coupling (resulting in 12,880 RU) or thiol coupling (6,600 RU) as indicated. Amine coupling was accomplished through N-hydroxysuccinimide ethyl(dimethylaminopropyl) carbodiimide (NHS-EDC) chemistry, where an EDC cross-linker forms an amine-reactive sulfo-NHS ester on the chip. The primary amine (from lysine) can then attack the original carbonyl from the chip to form an amide bond. Thiol coupling was accomplished using NHS-EDC reagents also, but with subsequent addition of 2-(pyridinyldithio)ethane amine (PDEA) prior to protein addition. PDEA generates a disulfide bonded leaving group, which once dissociated allows protein to come in and link through a free cysteine. Blocking was performed with water for amine-coupled lanes, and L-cysteine for thiol-coupled lanes. Binding to FITC-IκBα(20-42) or GST-tagged IκBα(1-55) was performed twice: once in 50 mM Tris, 200 mM NaCl, 0.01% Triton X-100, pH 7.4 buffer, and again in the same buffer but with 1 mM $ZnCl_2$. 200 nM each IκBα protein was serially diluted 2-fold for a concentration series. The flow rate was 50 μL/min, contact time 120 s, and dissociation time 300 s. Sensor data were processed using the Bio-Rad ProteOn Manager software and plotted in GraphPad Prism.

3.2.5 *Microscale Thermophoresis*

To determine the affinity of NEMO binding to zinc by MST, all measurements were performed on a NanoTemper Monolith NT.115 instrument (Munich, Germany) according to previously published protocols[152]. 7xAla NEMO was kept unlabeled at 500 μM, and therefore heat-induced diffusion was monitored by absorbance at 280 nm. $ZnCl_2$ was serially diluted 2-fold from an initial concentration of 1 mM. Data were processed using the NanoTemper Software, and plotted and fit to a quadratic binding equation in GraphPad Prism.

3.2.6 *Atomic Emission Spectroscopy*

To determine the metal content of NEMO (i.e., what metal is bound and in what concentration relative to protein), all measurements were performed on an Agilent 4200 MP-AES instrument with an SPS 4 Autosampler (Santa Clara, California, US). ZnAc and/or $NiCl_2$ standards were prepared at 5, 10, and 15 μM concentrations. NEMO samples were either desalted or not, and diluted to 5 μM in dH_2O. The system was equilibrated with nitrogen gas prior to and during data collection. Autosampler uptake time was set to 75 s, and stabilization time set to 10 s. Zinc concentration was measured at 213.857 nm, and nickel concentration was measured at 352.454 nm, both by averaging three readings and subtracting averaged background reading from water-only blank. Data were processed using

the Agilent software, and a linear fit of the standard data was performed with GraphPad Prism to interpret sample concentration.

3.2.7 *Development of an* in vitro *Assay to Measure IKKβ Phosphorylation of IκBα*

An assay to determine Michaelis-Menton parameters for IKK complex function, and effect of mutation of NEMO thereof, was developed by Assay Quant Technologies Inc. (Marlborough, MA, US) and is based on Sox peptide phosphorylation detection[151]. Reactions include 50 mM HEPES pH 7.5, 1 mM ATP, 1 mM DTT, 0.01% Brij-35, 1% glycerol, 0.2 mg/mL BSA, 0.5 mM EGTA, 10 mM $MgCl_2$, 10 μM IκB-based Sox substrate (AQT0220, Assay Quant Technologies), 5 nM or varied full-length IKKβ, 100 nM or varied NEMO, and 30 μM or varied zinc. To allow sufficient equilibration time for NEMO to bind IKKβ, all assay components including NEMO and IKKβ were incubated for 10 m at 30 °C prior to addition of ATP to begin the reaction. Note the NEMO-IKKβ FA assay equilibrates for 1 h, which implies a $t_{1/2}$ of at most 3.75 m. Reactions are run at 30 °C for 120 m, with ex/em 360/485 nm readings taken every 2 m in Corning half-area 96-well, white flat-bottom polystyrene NBS microplates (Corning, NY). Background signal from IKKβ(-) wells is subtracted from IKKβ(+) wells.

3.2.8 *Design and Cloning of IVD Constructs for Mammalian Expression*

WT NEMO, 5xAla, 7xAla, and R123W were previously prepared for

mammalian expression by the Gilmore group[103,153,154]. 9SG and L153R NEMO were cloned into both pBABE-7xAla and pcDNA-FLAG-7xAla vectors by Q5 Mutagenesis Kit (New England Biolabs, Ipswich, MA) or standard QuickChange mutagenesis, respectively. Primers used in this regard are listed in Appendix I. The decision for use of these constructs is explained above in section 2.2.2.

3.2.9 In Cellulo *Characterization of Disease-Associated Mutations within the IVD*

The following procedure was performed by Professor Thomas Gilmore and members of his lab; it is briefly described here for convenience. NEMO-deficient mouse fibroblasts (NIH3T3), 293 cells and NEMO-deficient 293T cells were grown in Dulbecco's modified Eagle's medium (DMEM) (Thermo Fisher, Waltham, MA) supplemented with 10% heat-inactivated fetal bovine serum (FBS) (Biologos, Montgomery, IL) as described previously[103,153,154]. NEMO-deficient 293T-cells were generated by CRISPR/Cas9 disruption of a short sequence in the 5′-UTR of the NEMO gene. The creation of pcDNA-FLAG and pBABE-puro vectors for the expression of WT NEMO and 7XAlaNEMO have been described previously[103,153]. The 9SG mutation in NEMO was created using the NEB Q5 Site-Directed Mutagenesis Kit (New England Biolabs). The pDNA-FLAG and pBABE vectors for the 9SG mutant were created by standard recombinant DNA techniques. Transfections of 293 cells and retroviral

transduction of mouse NEMO knockout cells were performed as described previously[103]. Virally transduced NEMO-knockout fibroblasts were selected using 2.5 μg/mL puromycin (Sigma, St. Louis, MO) for approximately 1–2 weeks[110].

Western blotting was performed as described previously[153]. For analyzing phosphorylation of IκBα, cells were first treated with 20 ng/mL TNFα (R&D Systems, Minneapolis, MN) for 10 m, 2 ng/mL of IL-1 for 6 m, or 100 ng/mL of LPS for 12 m. Cells were then lysed directly in 2X SDS sample buffer. In all cases, samples containing approximately equal amounts of protein were separated on SDS–polyacrylamide gels, proteins were transferred to nitrocellulose membranes, and filters were incubated overnight at 4 °C with anti-NEMO antiserum (catalog no. 2685, Cell Signaling Technology, Danvers, MA; 1:1000 dilution) or anti-phospho-IκBα (catalog no. 9246, Cell Signaling Technology; 1:1000 dilution). Horseradish peroxidase-labeled secondary antiserum was added, and immunoreactive proteins were detected by Supersignal Dura West chemiluminescence (Thermo Scientific). For co-immunoprecipitation experiments, transfected 293 cells in subconfluent 100-mm tissue culture dishes were lysed in 500 μL of AT buffer [20 mM HEPES (pH 7.9), 1 mM EDTA, 1 mM EGTA, 20 mM $Na_4P_2O_7$, 1 mM DTT, 1% (v/v) Triton X-100,

20% (w/v) glycerol, 1 mM Na_3VO_4, 1 μg/mL PMSF, 1 μg/mL leupeptin, and 1 μg/mL pepstatin]. An aliquot (20 μL) was saved as the input sample. To the remainder of the lysate was added 30 μL of anti-FLAG agarose beads (Sigma cat #A2220; Sigma, St. Louis, MO), and samples were incubated overnight with rocking at 4 °C. The beads were washed several times with AT buffer, and then bound proteins were removed by heating the samples at 90 °C in SDS sample buffer containing β-mercaptoethanol. Samples (input or immunoprecipitates) were then analyzed by reducing SDS–PAGE followed by Western blotting with the anti-IKKβ antibody (sc-7607, Santa Cruz Biotechnology), anti-NEMO antiserum (catalog no. 2685, Cell Signaling Technology), or anti-FLAG antiserum (Cell Signaling Technology car #2368; Cell Signaling Technology, Danvers, MA) as described previously[103].

3.3 Results and Discussion

3.3.1 Development of a NEMO-IκBα Fluorescence Anisotropy Assay

An FA assay was developed to measure the binding affinity of the NEMO-IκBα interaction. This interaction has been qualitatively demonstrated *in vitro* to require the ZF of NEMO by gel filtration chromatography[58] and by inducing change in ANS binding to NEMO[106]. Therefore, the exact binding affinity, zinc

requirements, and kinetics remain unknown. The assay was designed based on the FA assay for measuring NEMO-IKKβ binding, developed previously[103]. The fluorescein moiety for fluorescence detection was used due to its fluorescence lifetime of 4 ns, near the ideal 10 ns calculated previously for the NEMO-IKKβ interaction[155]. The region of IκBα that was selected encompasses residues 20-42. This selection is based on the IκB responsive region highlighted by Schröfelbauer and colleagues (2012)[58] plus additional residues C-terminal to S36 including Y42 for quantitation purposes using UV spectroscopy. Of note, the IκB responsive region contains two Asp residues that are important for co-immunorecipitation with NEMO, as compared to a construct with substitution of the aspartates for argininies.

Holding FITC-IκBα constant at 15 nM, 5XAla-NEMO was titrated from 10 μM down to 0.78 nM in the presence of 1 mM $ZnCl_2$ and equilibrated for 15 m. Zinc was included because 1) preliminary experiments showed no measurable binding in the absence of zinc (for example, see results from inclusion of EDTA in Figure 14), 2) it has previously been shown that the ZF is required for interaction with IκBα, and 3) it was unknown whether the ZF was occupied with zinc. It was observed that the signal remains constant over the first 15 m. The kinetics are further explored below in Section 3.3.2. The data were fit to the

quadratic binding equation and the apparent binding affinity was measured to be 2.0 μM (1.5 and 2.5 μM, n = 2). A control experiment with no Zn^{2+} and 100 μM EDTA showed that no binding is measured in the absence of zinc. The results from both experiments are shown in Figure 14. To determine if the interaction between NEMO-Zn and FITC-IκB*α*(20-42) had reached equilibrium after 15 m, the binding was measured after assay incubation for times of 1, 5, 15, 30, or 60 m. The data remained unchanged over the first 15 m after reading, indicating that the complex reaches equilibrium rather quickly. Notably, the signal appears to degrade at high [NEMO] after 15 m; this is likely due to NEMO instability in such high concentrations of zinc, as such signal decreases are not seen in experiments without added zinc. A binding curve measured after 15, 30, and 60 m is shown in Figure 15.

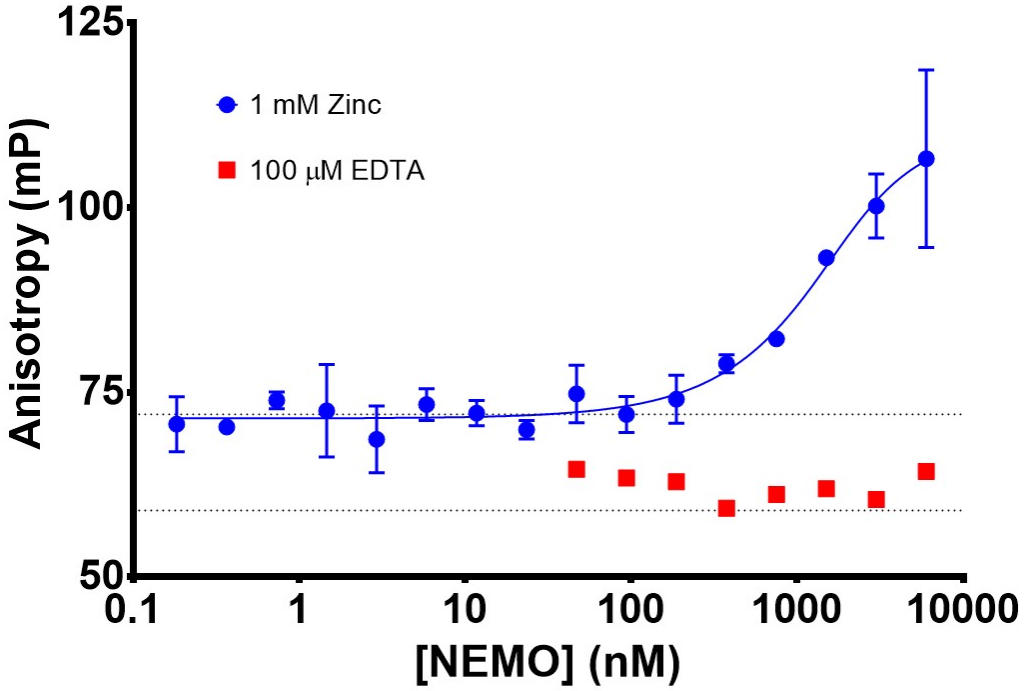

Figure 14: Fluorescence anisotropy binding assay to determine affinity of NEMO binding to FITC-IκBα, either with 1 mM Zn^{2+} (blue) or 100 μM EDTA (red). Error bars are standard deviation of three technical replicates. The dashed horizontal lines indicate IκBα controls in either zinc or EDTA. The solid line is the best fit of the data to a quadratic binding equation, showing that NEMO binds FITC-IκBα with an apparent affinity of 2 μM in the presence of 1 mM zinc. In the presence of 100 μM EDTA, no binding was observed.

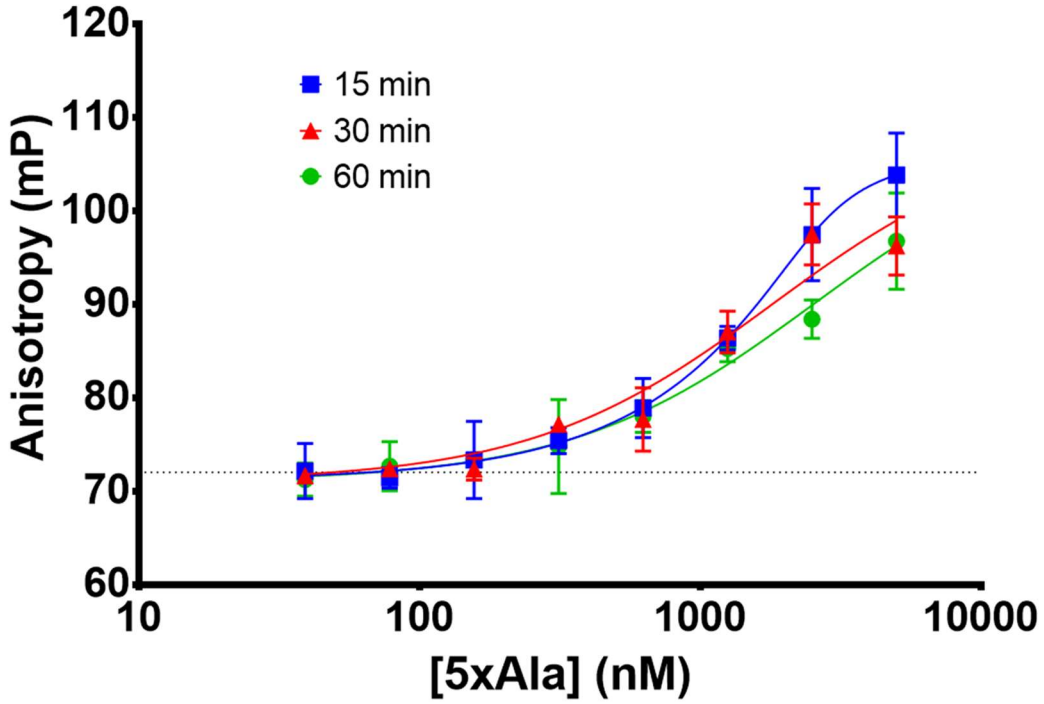

Figure 15: NEMO-IκBα binding curve measured after 15 (blue), 30 (red), or 60 minutes (green) in the presence of 1 mM zinc. Signal degrades at high NEMO concentration after 15 minutes. Error bars are standard deviation of three technical replicates. The dashed horizontal line indicates the IκBα alone control. The solid line is the fit of the data to a quadratic binding equation.

An unlabeled IκBα(20-42) peptide was used as a positive control competitive inhibitor of the interaction of NEMO-Zn with FITC-IκBα(20-42) (Figure 16). The primary motivation for this assay was to 1) determine the affinity of the IκBα-derived peptide without a fluorescein label, and 2) ensure that the increase in anisotropy signal from NEMO titration is due to specific binding, and is not nonspecific or otherwise artefactual. Holding FITC-IκBα constant at 15 nM and NEMO constant at 500 nM, the unlabeled peptide was

titrated from 250 μM in the presence of 1 or 10 mM $ZnCl_2$ and equilibrated for 15 m. An inhibition curve was observed, indicating that the unlabeled peptide was able to compete off the FITC-labeled peptide. IC_{50} values were determined to be 33.7 ± 5.6 μM (n = 2) for the 1 mM zinc condition, and 45.5 μM for the 10 mM zinc condition. Because the IC_{50} values are materially similar for the two zinc conditions, they were averaged for determination of the binding affinity of the unlabeled peptide. The Cheng-Prusoff relationship allows for this calculation, when the labeled peptide is in competition with a titrated and otherwise identical unlabeled species. The apparent binding constant of the unlabeled IκBα(20-42) peptide was thus determined to be 50 ± 40 μM (n = 3). This affinity is an order of magnitude above that of the labeled peptide. There are two potential explanations for the large difference. The unlabeled peptide has an additional tryptophan at the N-terminus for quantification purposes, and the labeled peptide has a large fluorescein moiety; it is possible that one or both have a detrimental effect on binding affinity, and explains this order of magnitude difference.

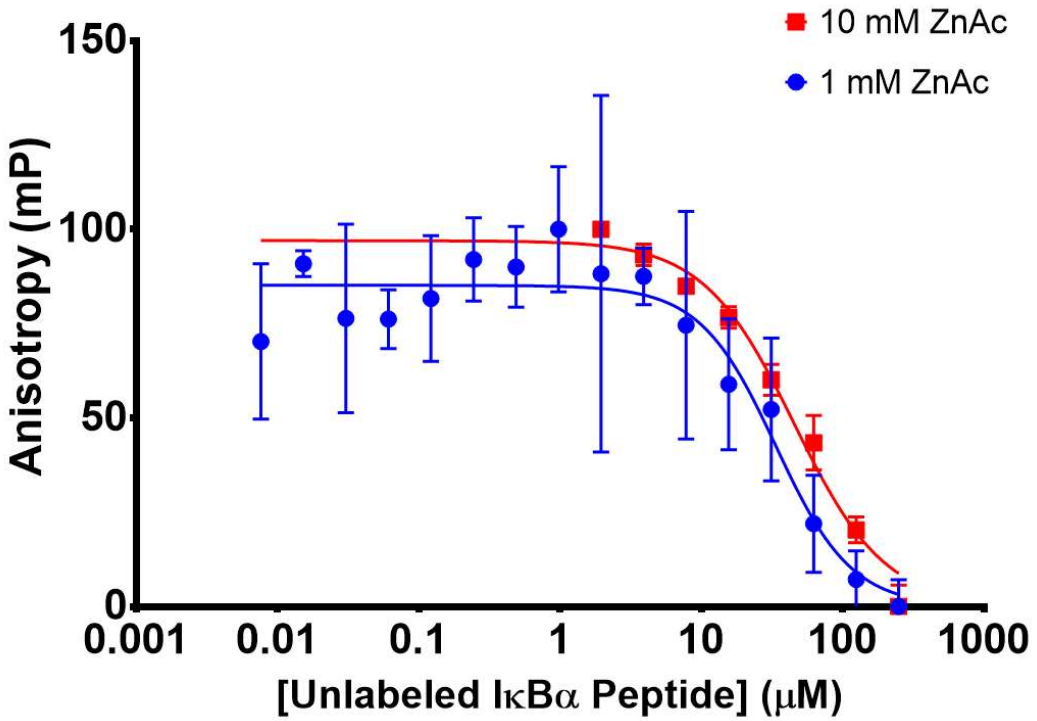

Figure 16: Unlabeled IκB*α* competition assay. FITC-IκB*α* at 15 nM was competed off 500 nM NEMO by an unlabeled version of the peptide in the indicated concentration of zinc acetate. Error bars are standard error of the mean of two technical replicates. Anisotropy was normalized to high (NEMO + FITC-IκB*α*) and low (IκB*α* alone) controls. The solid line is the best fit of the data to the four-parameter inhibition equation.

A previous study reported a significant effect of polyubiquitin on the rate of ligand-induced conformational change in NEMO. To determine whether linear di-ubiquitin, previously shown to bind directly to NEMO with an affinity in the low single-digit μM range[83], affects the binding affinity of NEMO for IκB*α*, linear di-ubiquitin was titrated in the FA assay from 1 μM down to 7.8 nM. 1 μM was the highest concentration possible given the stock from Enzo Life Sciences, which is equivalent to the affinity of NEMO for linear di-ubiquitin[83]. No

measurable effect on the assay was observed. Therefore, at these concentrations the presence of linear di-ubiquitin likely does not impact the binding affinity of NEMO for IκBα. Similar experiments were performed with FITC-IKKβ and are shown in Appendix III. No effect was observed for the presence of linear di-ubiquitin on IKKβ binding to NEMO either.

3.3.2 Validation of Zinc Addition Requirement for NEMO to bind IκBα

To corroborate the finding that zinc must be added exogenously for NEMO to bind IκBα, SPR experiments were performed. Two protocols for coupling of NEMO to the surface of a chip were developed by Dan Petrescu. First, homogenous coupling of 7XAla-NEMO was achieved via thiol coupling of its single solvent exposed cysteine at the C-terminus. The second strategy was through random amine coupling. For these experiments, both strategies were used, but because IκBα is thought to bind to the NEMO C-terminus, which is precluded by thiol coupling, only the data from the random amine coupling strategy was chosen for subsequent analysis. A total of 12,880 response units (RUs) of NEMO were immobilized on a GLH chip (BioRad). These chips are better suited for amine coupling of protein than others. NEMO was chosen for immobilization due to potential avidity effects, because NEMO is known to dimerize, and it is unlikely that IκBα peptide dimerizes. The mass ratio of

NEMO and IκBα is 50 kDa to 2.5 kDa, or approximately 20x. Given this mass ratio we can estimate that, given the RUs of immobilized NEMO, saturated binding should yield 644 RU. FITC-IκBα(20-42), the same ligand as that used in the FA assays, was flowed over as the analyte in a concentration series from 200 nM diluted two-fold down to 6.25 nM. In the running buffer, zinc was either not included, or included at 1 mM. As the analyte is injected, the signal (RU) increases when binding occurs, until an equilibrium point where the on-rate is equal to the off-rate. Once the analyte injection is terminated, the signal decreases as the analytes dissociate from the immobilized protein. As shown in Figure 17A, there is no measurable binding in the absence of zinc. In Figure 17B, in the presence of 1 mM zinc, a binding signal is seen. This is less than the 613 RU estimated for saturation of binding, indicating saturation has not been reached, but direct binding to NEMO had occurred. A sub-saturating signal is not surprising, given the concentrations of IκBα were limited to those below the apparent affinity from FA experiments. These data are informative about the zinc requirement for NEMO binding to IκBα.

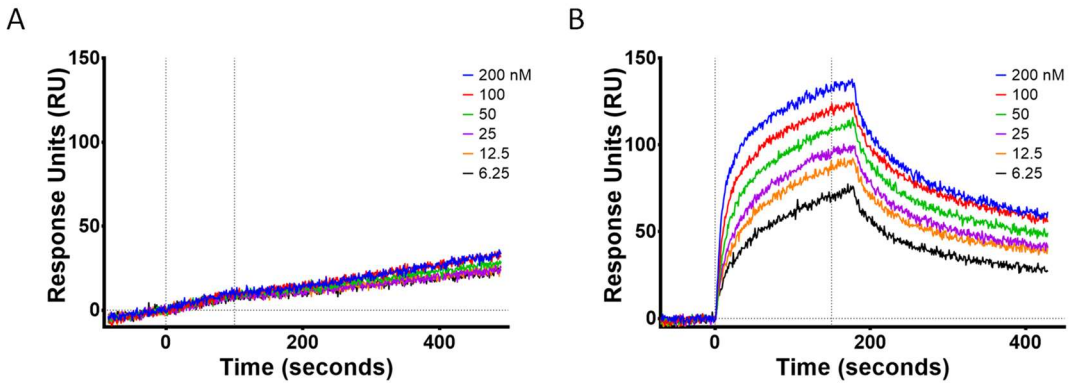

Figure 17: SPR results for IκBα(20-42) flowed over random-amine coupled NEMO. In panel A analyte is flowed without zinc in the running buffer; in panel B analyte is flowed in presence of 1 mM zinc in buffer. Vertical lines indicate time of analyte injection (left line) and switch back to running buffer (right line). Analyte concentrations are listed in the legend.

All previous experiments with FITC-IκBα were performed with a single concentration of zinc at 1 mM. However, it is unknown if this concentration of zinc is saturating, or if it is only enough to just detect NEMO binding to IκBα. To determine a full titration curve for zinc in the FA assay, NEMO was kept constant at 500 nM, zinc was titrated from 1 mM down to 7.8 μM, and magnesium was counter-titrated to maintain a constant concentration of divalent cation. Despite this high concentration of zinc, the anisotropy signal does not plateau at 1 mM, but rather appears to be increasing substantially. In order to achieve saturation, the titration was repeated starting with zinc at 10 mM. As shown in Figure 18, this higher concentration of zinc allowed for saturation at 375 mP (milli-polarization units). The largest anisotropy value possible is 400 mP, which would indicate a complex large enough that the absorption and

emission dipoles are collinear, so there is no re-orientation resulting in depolarization[156]. Therefore, the NEMO-IκBα-zinc complex must be rather large. An EC_{50} for the zinc requirement in the FA assay was calculated to be 4 mM. If this large signal were due to simple protein aggregation, there would be a substantial increase in the absorbance at 600 nm, as proteins do not absorb at such long wavelengths unless there are large particulates blocking the transmission of light. These experiments appeared to be unaffected by large amounts of zinc, decreasing the likelihood of large-scale aggregation. To determine whether the signal from this large zinc addition is nonspecific, the experiment was repeated with a FITC-IL-2 peptide, which is not expected to bind to NEMO. **Figure 18** shows that these anisotropy levels are unaffected by titration of zinc, indicating that the zinc effect seen before was specific to the NEMO-IκBα interaction and is not due to nonspecific effects such as protein aggregation. The NEMO-IKKβ interaction was probed similarly; constant 500 nM NEMO and 15 nM FITC-IKKβ were included in the same zinc titration. FITC-IKKβ alone was not affected by increasing concentrations of zinc, but the signal in the presence of NEMO increases by about 70 units with an EC_{50} near 1 mM. This is potentially due to large complexes of NEMO formed in high concentrations of zinc.

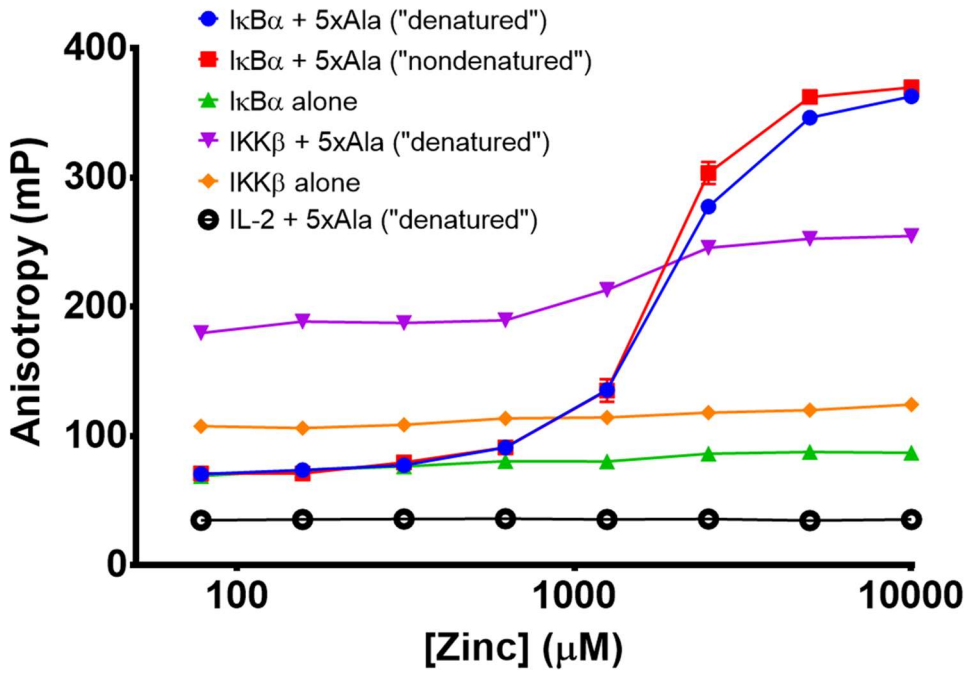

Figure 18: NEMO-IκBα FA assay control experiments in saturating concentrations of zinc. "Denatured" and "nondenatured" refer to denaturation, or not, of NEMO during purification procedure, and are further discussed in Section 3.3.3. All FITC-tagged peptides kept constant at 15 nM, NEMO at 500 nM. Zinc titrated from 10 mM down to 78 μM. Solid lines connect points.

To provide evidence that the large anisotropy signal in the presence of a large excess of zinc was in fact due to large complex formation and nonspecific aggregation, dynamic light scattering was used. This technique determines the size of particles in solution in a nondestructive manner. It is sensitive to transient and low affinity interactions, and allows for higher-throughput optimization. First, 5XAla-NEMO was analyzed on its own to establish a baseline (top plot

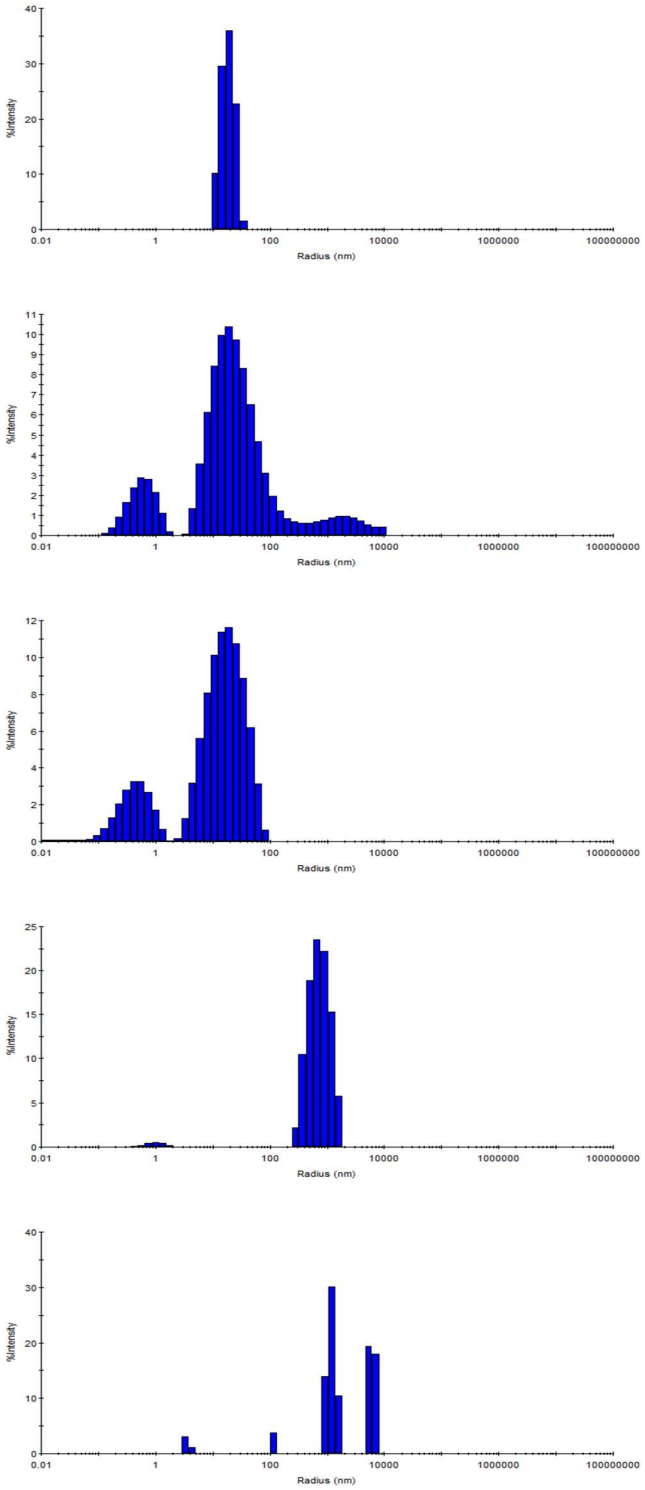

Figure 19: NEMO-IκBα-Zn complex size determination by DLS. From top to bottom: 5XAla-NEMO at 10 μM; with FA assay buffer; with 1 mM Mg; with 1 mM Zn; and with 10 mM Zn. Blue bars indicate signal intensity for a given particle radius in nm. Clusters of blue bars are indicative of a single species relative to instrument precision.

Figure 19). Then, a series of samples were prepared identically as in the FA assay shown in Figure 15, except 5XAla-NEMO was at 10 μM, and the concentration of metal additive varied: no metal, 1 mM magnesium, 1 mM zinc, and 10 mM zinc. This experiment was done to analyze the NEMO-IκBα-zinc complex in a manner as close as possible to the anisotropy assay for direct comparison. The concentration of NEMO was increased to 10 μM to ensure enough signal. Tris was included in the buffer as a weak zinc chelator to improve its solubility at such high concentrations. DTT was included to minimize disulfide-mediated protein aggregation. The presence of both Tris and DTT likely lowered the free zinc concentration available to NEMO, but did not prevent a zinc-specific effect from being observed. Figure 19 shows the distribution of the intensity of light scatter as a function of particle diameter for each condition. For 5XAla-NEMO alone, the major species particle radius of 38.6 nm, or 386 Å, is slightly larger than that seen by SAXS (315 Å), but is important to note the difference in buffers used (sodium phosphate for SAXS, Tris with DTT for DLS). For 5XAla-NEMO as in the FA assay with either no metal additives or the addition of 1 mM magnesium, this peak broadens, but as expected, no noteworthy size increase is observed. In the FA assay, the addition of 1 mM zinc is where the sigmoidal curve starts its exponential phase; this is corroborated by a right shift in particle

radius to 1605 nm as measured by DLS and is shown in Figure 19. Finally, the curve from the FA assay has plateaued around 10 mM zinc, the magnitude of which indicates the presence of very large complexes. In DLS, this condition shows a sharpening of the radius distribution around the right-shifted peak, with the addition of an even larger peak at 12560 nm. Therefore, these DLS experiments provide key evidence corroborating the large complex formation seen in the zinc titration in the FA assay.

To attempt to determine kinetics of IκBα binding to NEMO-Zn, the NEMO-IκBα FA assay was used as previously. The binding was initially measured at t = -1 m, to determine the starting, equilibrium anisotropy level. At t = 0 m, EDTA was spiked in a stoichiometric excess (5 mM) and the plate was read immediately to attempt to measure an off rate. As is shown in Figure 20, binding was no longer detected within the time it took to spike EDTA and read the plate, likely indicating zinc was no longer available in sufficient amount to activate the ZF of NEMO. The quickness of the apparent k_{off} corroborates the previous finding that the NEMO-IκBα binding affinity is rather weak, and indicates that the NEMO-Zn binding affinity is rather weak as it can be displaced by EDTA rapidly.

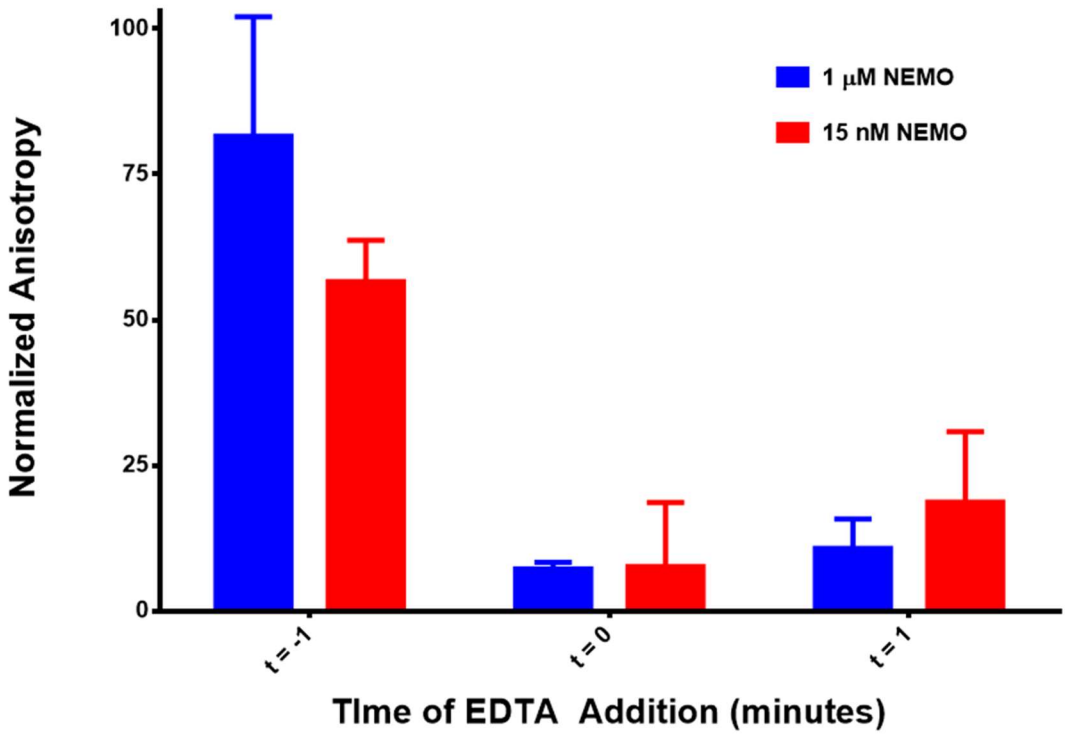

Figure 20: NEMO-IκBα complex dissociates rapidly following addition of to the assay at indicated times, and anisotropy was measured within 15 seconds. Error bars (SD) representative of three technical replicates. Anisotropy normalized to high (NEMO with IκBα and 1 mM zinc) and low (IκBα alone with 1 mM zinc) controls.

The NEMO-IκBα complex is dependent on the presence of exogenously added zinc and dissociates rapidly. If zinc binds to NEMO prior to IκBα, then the EC_{50} of zinc titration will be independent of IκBα concentration. However, if the EC_{50} of zinc titration varies with IκBα concentration, then IκBα may bind to NEMO first. To determine the order of binding, zinc titrations were performed from 1 mM down to 7.8 μM in the presence of varying concentrations of IκBα. As shown in **Figure 21**, there is no effect on the EC_{50} of zinc titration for IκBα

concentrations up to 135 nM. The highest concentration of IκBα, 135 nM, was chosen because of solubility issues of the peptide at concentrations above this level. Because the zinc titration EC_{50} was not affected my increasing concentrations of IκBα, zinc binding to NEMO is independent of IκBα concentration, so zinc must bind to NEMO before IκBα can.

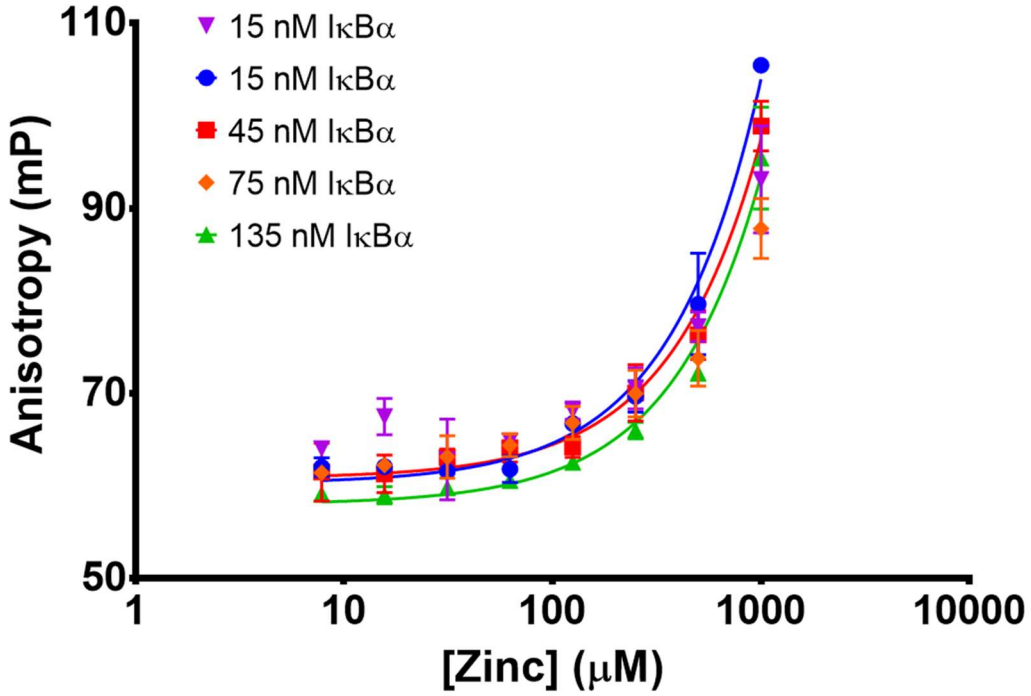

Figure 21: NEMO-IκBα FA assay zinc titration in the presence of varying concentrations of FITC-IκBα. NEMO kept constant at 500 nM. Zinc titrated from 1 mM down to 7.8 μM. Data fit to a quadratic binding equation. 15 nM FITC-IκBα experiments are independent replicates.

3.3.3 NEMO Binds Zinc with Low Affinity

To explore this potentially weak interaction between NEMO and zinc, the affinity was determined by Microscale Thermophoresis (MST). Briefly, MST

works on the principle that proteins or complexes of different sizes or hydration shells diffuse at different rates away from a heat source. If a protein is bound to a ligand, its diffusion characteristics change, which can be determined by monitoring the intensity of protein fluorescence in a specific location as a result of heating at that location[152]. Holding NEMO constant at 500 nM, and titrating zinc from 1 mM down to 0.78 μM, the affinity of zinc binding was determined to be 14 μM (**Figure 22**). Previous studies have determined the NEMO ZF affinity for zinc to be 0.3 ± 0.1 μM[98], or approximately 50 times higher than determined here. The discrepancy may be due to several factors discussed below in this Section. The affinity of various zinc finger peptides for Zn^{2+} ranges over nearly 7 orders of magnitude (6.3 nM to 2 fM) at pH 7.0. The NEMO ZF is type CCHC; for these specifically, K_{app} at pH 7.0 was reported to be around 1 fM[157]. Regardless of this large range, according to our results and previous results from Cordier and colleagues[98], the NEMO ZF affinity for zinc ion appears to be substantially weaker than expected.

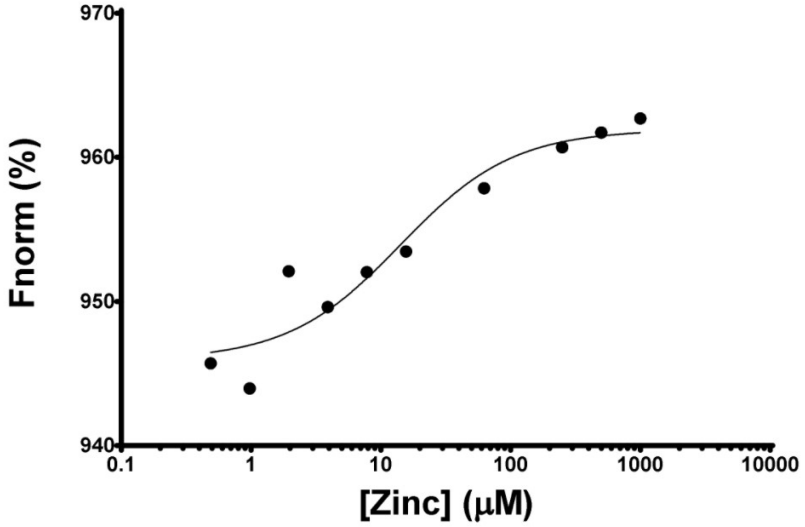

Figure 22: Determination of the binding affinity of zinc to NEMO using MST. Fnorm (%) is change in signal, F, normalized out of 1000, using the NanoTemper software. Solid line is curve fit to quadratic equation to determine EC_{50}.

One potential explanation for the weak binding of zinc to NEMO is that there is another metal bound, that must be competed away for zinc to occupy its binding site. The most likely other metal is nickel. Because NEMO is purified on a nickel column, an unoccupied ZF may pull nickel off the column as it is refolded (see purification protocol in section 2.2.2). To test for the presence of nickel, we used atomic emission spectroscopy (AES). AES works on the principle that incinerated metal will emit at a precise wavelength. The comparison of this emission to standards of known concentration allows for determination of concentration of that metal. The results for AES metal determination in NEMO are shown in Figure 23: the plot above shows the standard curve, and table

below is a table of results. Nickel concentrations were below the limit of detection, so nickel is not bound in the ZF of NEMO. Important buffer controls are listed in the table of results. In two separate experiments, it was determined that WT-NEMO is zinc-occupied. In the first, 5 μM of protein was shown to contain 5.5 μM zinc; in the second, 10 μM protein contains 8 μM zinc. Interestingly, 5xAla-NEMO only contains 1 μM of zinc for 5 μM of protein. This was not an equilibrium experiment, so it is not possible to determine from these data whether WT-NEMO has a higher affinity for zinc than 5xAla-NEMO.

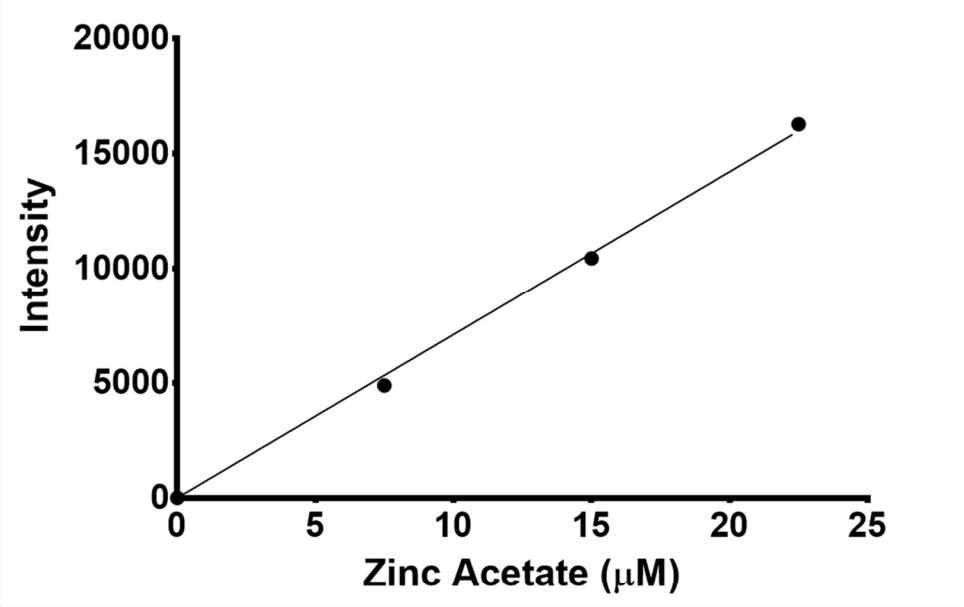

Sample ID	[Zn] (μM)	[NEMO] (μM)	[Ni] (μM)
NaPO4 Buffer	0.255	N/A	<=0.009
Water	0.14	N/A	<=0.009
WT-NEMO	5.475	5	<=0.009
WT-NEMO (repeat)	8.66	10	n.d.

Figure 23: Atomic Emission Spectroscopy results for WT-NEMO. Above plot is the standard curve to determine zinc concentration. Table at bottom displays concentrations of zinc interpolated from standard curve. Each concentration is the average of three technical replicates.

Another potential explanation for weak zinc binding is that during purification, the ZF is irreparably misfolded during the denaturation step and therefore only a small fraction of NEMO ZF's can bind zinc following this harsh treatment. To test this hypothesis, 5xAla-NEMO was purified without denaturation and subjected to AES. Two peaks were collected from the nickel affinity purification, whereas inclusion of urea earlier in the purification process

yields a single peak. The first peak contained zinc in a roughly 1:1 ratio to NEMO protein, while the second did not contain zinc. Notably, this zinc-containing protein behaved identically in requiring zinc to bind to IκBα as its purification-denatured counterpart.

In summary, WT-NEMO appears to co-purify with zinc, whereas 5XAla-NEMO co-purifies with zinc only when purified under non-denaturing conditions. 5XAla-NEMO is therefore not zinc-loaded when purified under denaturing conditions. In the IκBα FA assay, 5XAla-NEMO that was not denatured during purification behaved identically to that which was denatured during purification, and only the former co-purifies with zinc. The requirement of addition of a large amount of zinc suggests either the presence of a secondary binding site for zinc, or that zinc in some way induces multimerization of NEMO. It is unlikely that there exists a second zinc-binding site required for binding to IκBα, as concentrations of zinc used in these assays are far above the μM concentrations seen in living cells. Therefore, it is likely that there is a large complex formation induced by the presence of large quantities of zinc that is competent and required to bind IκBα, irrespective of the zinc occupancy of the ZF.

3.3.4 *Development of an* in vitro *assay to measure IKKβ phosphorylation of IκBα*

At this point, the interactions of NEMO with IκBα, zinc, IKKβ[103], and linear di-ubiquitin[83] have been characterized. To study how these individual components contribute to an active IKK signaling complex, a fluorescence-based assay using Sox peptide technology was developed in collaboration with Assay Quant Technologies (Marlborough, MA)[151]. Briefly, the assay requires a peptide with four modules: a phosphorylation site, a β-turn sequence, a recognition site for the kinase, and a Sox amino acid. The side chain of the Sox amino acid is a fluorophore that, once the peptide is phosphorylated, forms a complex with a magnesium ion and the phosphorylated residue. The complex is diagramed in **Figure 24**. This complex is excited at 360 nm and emits at 485 nm, with an intensity 3-5 fold brighter following phosphorylation. This complex is then stable on the scale of hours, allowing for low concentrations of enzyme for easily observable rates. Results will be shown as plots of time versus RFU (relative fluorescence units), where an increase in RFU is proportional to an increase in amount of phosphorylated peptide.

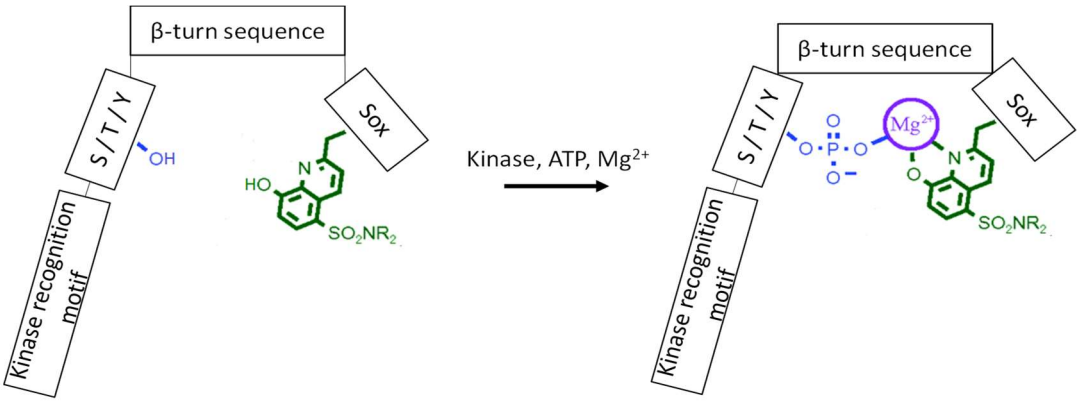

Figure 24: Scheme representing Sox peptide fluorescent probe construction. Sox amino acid side chain chemical structure shown in box in lower right. Upon phosphorylation of S/T/Y, a magnesium ion is chelated by the phosphate and the Sox peptide, which emits at 485 nm after excitation at 360 nm. Figure adapted from Shults and colleagues (2003)[151].

First, a fluorescence anisotropy competition assay was performed to demonstrate that the Sox peptide used here is capable of binding to NEMO similarly to the IκBα peptide used previously (see Figure 16). As shown in the top panel of **Figure 25**, the Sox peptide binds almost identically to NEMO as the unlabeled IκBα peptide. That is, the IC_{50} values are 1.5 ± 0.4 and 2.3 ± 0.4 μM for the unlabeled IκBα peptide and Sox peptide, respectively. This was expected, given the high degree of sequence overlap as shown at the bottom of **Figure 25**. It should be noted that the arrangement of the Sox peptide modules is crucial. The Sox amino acid is best located in the middle of the IKKβ recognition sequence of IκBα (31-DSGLDSMKD-38) in terms of the most IKKβ phosphorylation as screened by Assay Quant. The Sox amino acid replaces L34. It is unclear which

phosphorylation site is responsible for the Sox signal.

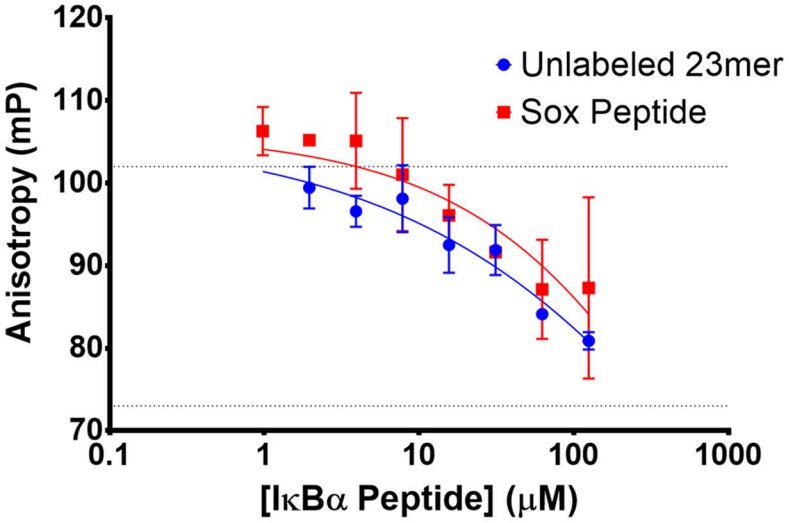

FITC-Ahx-LKKERLLDDRHDSG--------LDSMKDEEY-amide
Ac-KKERLLDDRHDSG-C(Sx)-DSMKDEE-amide

Figure 25: FA competition assay comparing the affinity of the Sox peptide (red) used in this section to the unlabeled IκBα peptide (blue) used in Section 3.3.2. Phosphorylation sites are S32 and S36 and are underlined above; C(Sx) replaces L34. IC_{50} values are 2.3 and 1.5 μM for the unlabeled IκBα peptide and Sox peptide, respectively. Error bars represent standard deviation. Dotted lines indicate anisotropy level of high (NEMO plus IκBα) control and low (IκBα alone) control. Concentrations were NEMO at 500 nM, FITC-IκBα at 15 nM, and zinc at 1 mM.

First, a titration of the enzyme, IKKβ, was performed to demonstrate linearity in rate versus enzyme concentration. **Figure 26**A-B show the course of the reaction (change in RFU) over time. Initial rates were determined by calculating the slope over the first 20 m. Plots of rate versus enzyme concentration are shown on the right side in **Figure 26**.

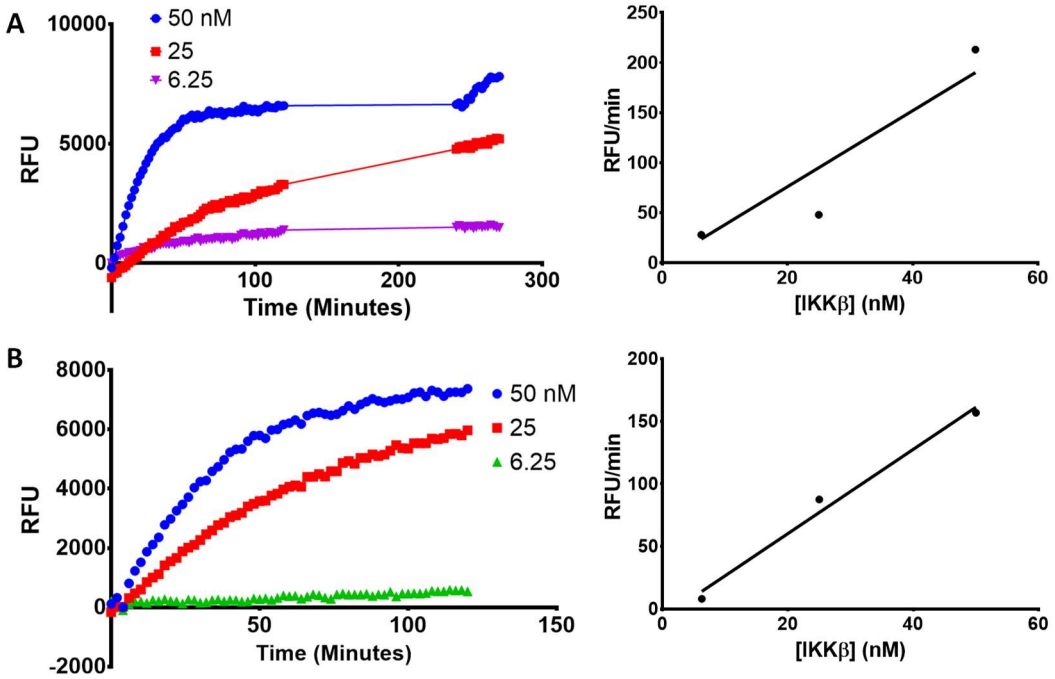

Figure 26: IKKβ titrations. A, left: Titration of IKKβ from 50 nM with additional substrate spike at 4 h. Right: Plot of initial rate of reaction versus enzyme concentration. Solid line is linear fit. B, left: Titration of IKKβ from 50 nM. Right: Plot of initial rate of reaction versus enzyme concentration. Solid line is linear fit.

Overall, the reaction rate appears to be linear with respect to enzyme concentration. Additional tests of the assay were designed to determine whether the equilibrium reached with higher concentrations of IKKβ is due to inactive enzyme or exhaustion of substrate. In Figure 26A, the peptide substrate was spiked at 4 h. In the 50 nM IKKβ case, the signal that had plateaued began increasing again, indicating that the enzyme was still active prior to substrate spiking and an equilibrium was reached for maximal phosphorylation of the Sox-IκBα peptide.

To determine the IκBα peptide substrate K_M value and a saturable V_{max}, a substrate titration was performed. Here, IKKβ was kept constant at 25 nM, NEMO at 100 nM, and zinc at 62.5 μM. As shown in **Figure 27**, the plot of rate versus substrate concentration is hyperbolic and shows saturation. A Michaelis-Menten fit of this curve together with an independent replicate yields a K_M value of 29 μM (22.8 – 35.2 μM, n = 2). This K_M value is approximately 29 times the reported value by Kishore *et al.* (2002) of 1 μM using a similar peptide of IκBα[158]. The difference may be caused by the presence of the Sox amino acid, reducing the affinity of the peptide for IKKβ.

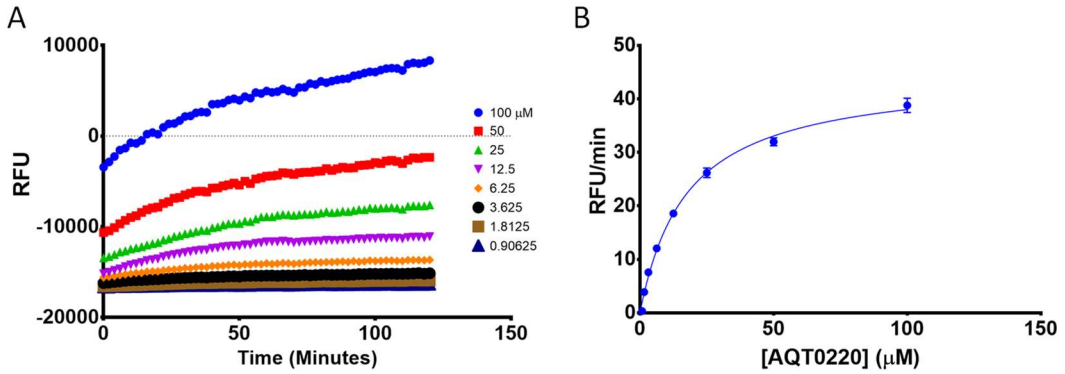

Figure 27: Substrate titration shows saturable V_{max} with K_M = 29 ± 6.2 μM. Substrate AQT0220 titrated from 100 μM down to 78 nM, and IKKβ at 25 nM. A: Timecourse from which initial slopes were determined. B: Plot of initial slopes of the reactions versus substrate (AQT0220) concentration. Blue line is fit to Michaelis-Menten equation to determine K_M and V_{max}.

Next, the effect on IKKβ phosphorylation rate from the titration of zinc, NEMO, and/or linear poly-ubiquitin was assessed. Zinc addition was shown to be required for IκBα binding to NEMO, so it was included. Linear poly-ubiquitin

has been shown to be required for IKK activation[50,105] and was hypothesized to be required to activate NEMO[63], so it is hypothesized to enhance or be required for NEMO-mediated IKK activity. In these experiments, IKKβ was kept at 6.25 nM, substrate at 10 μM, and additive was titrated from 125 μM, 1 μM, and 1 μM, for zinc, NEMO, and linear poly-ubiquitin, respectively. From FA results in Figure 24, the addition of zinc is required for NEMO to bind IκB*α*; therefore, it is hypothesized that NEMO would not have an effect on the Sox assay without the addition of zinc. To determine the concentration of zinc to use, two independent zinc titration replicates indicated that IKK activity is steady at concentrations lower than 125 μM (**Figure 28**A). Zinc is known to compete with magnesium for binding to the Sox peptide for fluorescence emission to occur[151], so it is important to show concentrations of zinc in excess of NEMO do not adversely affect the reaction. Moving forward, the concentration 62.5 μM zinc was used, which is in great excess over NEMO. For NEMO addition (**Figure 28**B), it appears that higher concentrations of NEMO have little, if any, effect on IKKβ activity. The magnitude of change from highest to lowest concentration of NEMO is no more than 4 RFU/min, which is a rather modest change and more replicates would be needed to establish if the minor apparent inhibition is of statistical significance.

To compare the effect of M1-2Ub and M1-4Ub on IKKβ phosphorylation

rate in the presence of 100 nM NEMO, these ubiquitin proteins were titrated while keeping other assay conditions identical. Results are shown in **Figure 28**C. The only difference was that for the M1-2Ub experiment, the IKKβ used was older and had been kept frozen for approximately two months longer than the IKKβ used in the M1-4Ub experiment. Therefore, it is difficult to compare directly the magnitude of the rates for each experiment, as the older IKKβ may not have been as active. There is no dose-dependent effect for M1-2Ub on IKK activity. There appears to be a peak for M1-4Ub at lower concentrations (91.25 and 45.6 nM). However, it is unlikely that this is mechanistically relevant given that this is not dose-dependent. An additional replicate for M1-4Ub titration is shown in **Figure 28**D; again, there is no dose-dependence, supporting the conclusion that M1-4Ub has no effect on NEMO-mediated IKKβ activity.

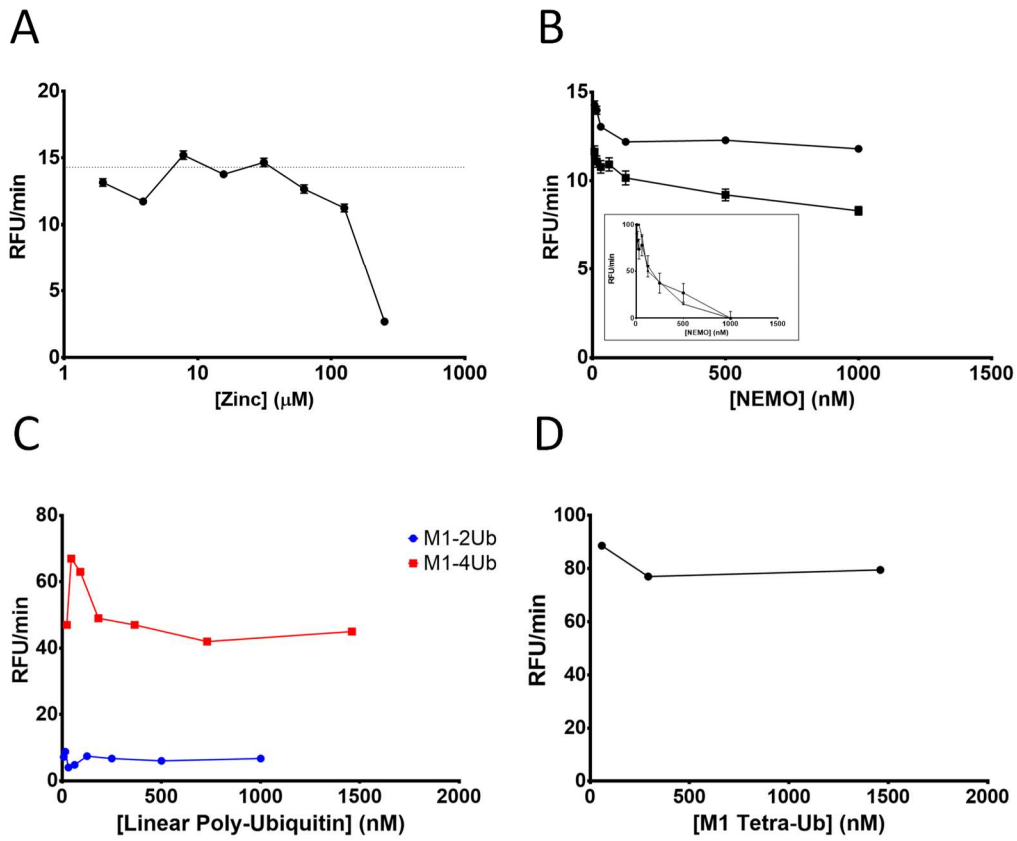

Figure 28: Effect of addition of various relevant signaling components on IKKβ phosphorylation of IκBα. A: Representative zinc titration from 250 μM down to 38 nM. Dashed horizontal line indicates activity in the absence of zinc. B: Two independent replicates of NEMO titration from 1000 nM down to 7.8 nM. Inset: curves were normalized to show reproducible behavior. C: Titration of either M1-2Ub or M1-4Ub with 100 nM NEMO and 62.5 μM zinc present. D: Replicate of M1-4Ub titration at 1500, 300, and 60 nM.

To validate the result that NEMO plus M1-4Ub has no effect on IKKβ phosphorylation rate, which is surprising given recent findings[63], substrate titrations were performed with the addition of one or more of these components. First, the effect of NEMO on IKKβ activity was determined and is shown in **Figure 29**A. Notably, NEMO appears to inhibit the reaction, as the observed rates

are slower in the presence of 100 nM NEMO. Specifically, the K_M roughly doubles in the presence of NEMO from 18 ± 1.5 to 37 ± 5.9 μM, while V_{max} remains unchanged.

To determine whether M1-4Ub can overcome this NEMO-dependent inhibition, a similar substrate titration was performed in the presence of 100 nM NEMO and 1 μM M1-4Ub. In this experiment, shown in **Figure 29**B, there was no difference in observed rate between the conditions with M1-4Ub versus without. K_M values are similar to previous findings, at 21 ± 2.6 and 25 ± 6.3 μM, while V_{max} remains unchanged, indicating again no substantial effect of NEMO with M1-4Ub on IKKβ activity. An expanded experiment was performed to add in a key control, M1-4Ub without NEMO, to determine whether M1-4Ub inhibits IKKβ activity on its own. Results are shown in **Figure 29**C. There is no substantial difference in activity in the presence of NEMO and M1-4Ub together versus each component added individually. A further expanded experiment with an additional key control, IKKβ alone, was then performed. Results are shown in **Figure 29**D. As had been seen in most previous experiments, there appeared to be no effect of any combination of added component in this experiment, as all observed rates were comparable to that seen in the IKKβ alone case.

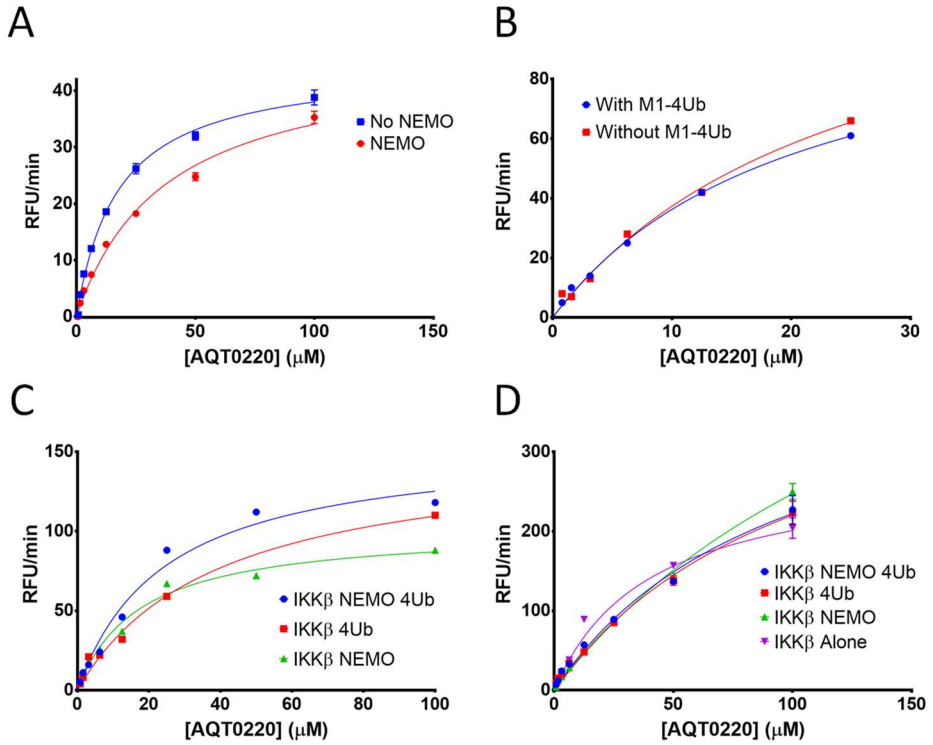

Figure 29: Substrate titration results. A: The presence of NEMO at 100 nM appears to slow IKKβ activity. B: 1 μM M1-4Ub with 100 nM NEMO has no effect on IKKβ activity except at the highest concentration of substrate, which is difficult to explain mechanistically. C: Substrate titration to determine the activity of the indicated combinations of components. D: Same experiment as in C except additional condition, IKKβ alone. All curve fits performed using Michaelis-Menten fit.

The above results show that the Sox amino acid-based phosphorylation assay to measure the rate of IKKβ phosphorylation of IκB*α* appears to be working, in that the rate versus enzyme concentration is linear, and the rate versus substrate concentration is hyperbolic. These results are reproducible. A dose-dependent slowing of reaction rate in two independent NEMO titration experiments (Figure 28A), and a comparison of the presence versus absence of

NEMO in a substrate titration (Figure 29A), indicates that rather than increasing the reaction rate between IKKβ and IκBα, NEMO appears to slightly inhibit IKKβ activity under the conditions used. At the indicated concentrations of NEMO (100 nM) and IKKβ (25 nM), which are above K_D, it is possible that two NEMO molecules may bind to one IKKβ, preventing IKKβ dimerization which has been shown in solution and may be important for activity[159]. Based on a hypothesis from Hauenstein *et al.*[63] and discussed above in Section 3.1, the addition of M1-4Ub was thought to increase NEMO-mediated IKKβ activity. However, NEMO and M1-4Ub together appear to have no effect on the rate of IKKβ phosphorylation of the IκBα peptide; there is a lack of a dose-response in 2 independent M1-4Ub titrations (one is shown in Figure 28C, the two are averaged in Figure 29D), and no effect in a substrate titration (Figure 29B).

There are at least five ways to explain these results. First, the affinity of M1-4Ub for NEMO has not been reported, so it is unknown if we were using concentrations below K_D which would lead to fewer than 50% of NEMO molecules bound to M1-4Ub. Additionally, it is not known whether M1-4Ub does anything other than facilitate ligand-induced conformational changes by IKKβ and IκBα[106]. These conformational changes may or may not contribute significantly to activity. Second, it has been shown previously[57] that NEMO is

phosphorylated on N-terminal residues, which may be important for enhancing IKKβ activity. Without phosphorylation, as is the case in these experiments, NEMO may not be competent to enhance IKKβ activity. Third, previous assays[58] that showed NEMO can enhance IKKβ activity were performed with full-length IκB*α*; perhaps the peptide we are using is missing important residues for interactions with NEMO. Fourth, it has been shown that 5xAla-NEMO can restore canonical NF-κB signaling in NEMO knockout cells; though unlikely, perhaps it is through a manner other than enhancing IKKβ activity that this construct accomplishes this task. It would therefore be interesting to test WT-NEMO in this Sox assay to answer this question. Fifth, it has been demonstrated above using fluorescence anisotropy that NEMO requires a large excess of zinc, at least 1 mM, to show measurable binding to almost the same IκB*α* peptide. In these assays, concentrations of zinc above 62.5 μM inhibited the reaction, so this was the concentration used. According to the FA assay results, this concentration of zinc is insufficient to observe binding of NEMO to IκB*α*, and perhaps NEMO is not binding to IκB*α* in these assays. However, it is possible that the NEMO-IκB*α* interaction only need to be transient for efficient directed phosphorylation by IKKβ to occur, whereas stable binding is required for observation by FA. Finally, IKKβ may need to be phosphorylated by another protein such as TAK1,

to become fully active.

A fluorescence-based assay has been developed to quantitatively characterize the phosphorylation of IκBα by IKKβ. Given results from a previous study[58], NEMO was thought to enhance IKKβ activity; however, it was shown here to not affect it, possibly due to one or more of the reasons stated above. Hauenstein and colleagues[63] hypothesized that NEMO exists in an auto-inhibitory state prior to poly-ubiquitin binding. Therefore, we assessed the ability of tetra-ubiquitin to activate NEMO by means of enhancing IKKβ activity. Tetra-ubiquitin was shown to have no effect on this activity, discounting this hypothesis.

3.3.5 The Intervening Domain Confers Full Binding Affinity to NEMO for IKKβ

Previously, an FA assay to characterize the NEMO-IKKβ interaction was published by our group[103]; here, we used that assay to assess the contribution of the IVD to the interaction of NEMO and IKKβ. First, the ability of NEMO(44-195) to bind to a 45-mer peptide derived from the C-terminal sequence of IKKβ[61] was explored. Previous studies have shown that covalently dimeric NEMO(1-120) and NEMO(44-111) constructs, which contain the IBD but not the IVD, bind IKKβ with an affinity of 70-310 nM and 210-560 nM, respectively[116]. Similarly,

IBD constructs comprising residues 44-111, rendered dimeric by fusion at the N- and/or C-terminus to a constitutively dimeric α-helical coiled-coil, binds the same IKKβ peptide with an affinity of 100-1000 nM, and likewise, when expressed as a dimeric fusion protein with glutathione-S-transferase (GST) binds with K_D = 170 nM[160]. Full-length NEMO, on the other hand, binds this IKKβ peptide with the substantially higher affinity of 2.2 ± 0.8 nM[103]. These differences in affinity for IKKβ between fragments of NEMO up to residue 120 and full-length NEMO have previously been assumed to derive from subtle differences in the structure or flexibility of constructs containing the IBD alone compared to full-length NEMO[116]. To determine whether the IVD affects the binding affinity of the IBD for IKKβ, we tested the binding of NEMO(44-195) and 9SG-NEMO to the same IKKβ-derived peptide using a FA binding assay described previously[103,108]. **Figure 30** shows that, consistent with previous results, FL-NEMO bound the IKKβ peptide with K_D = 4.9 ± 0.6 nM (n = 3), although the IBD-only NEMO(1-120) construct displayed a lower affinity of K_D = 95 ± 25 nM (n = 3)[116] (inset table). NEMO(44-195), which contains both the IBD and IVD region, bound the IKKβ peptide with an affinity of 7.4 ± 2.2 nM (n = 4). This result shows that the presence of the IVD affords IKKβ binding affinity to truncated NEMO similar to that of full-length NEMO. Notably, 9SG-NEMO bound the IKKβ

peptide with K_D = 67 ± 17 nM (n = 3) (**Figure 30**), i.e., 10-fold more weakly than FL-NEMO, and similar to the value obtained for NEMO(1-120) (inset table). The NEMO(110-195) construct comprising the IVD alone showed no detectable binding to the IKKβ peptide (**Figure 30**), ruling out the possibility that the peptide could be binding directly to a site in the IVD itself. Thus, mutation of the nine highly conserved residues at the core of the IVD abolishes the ability of the IVD to confer high IKKβ binding affinity to the adjacent IBD.

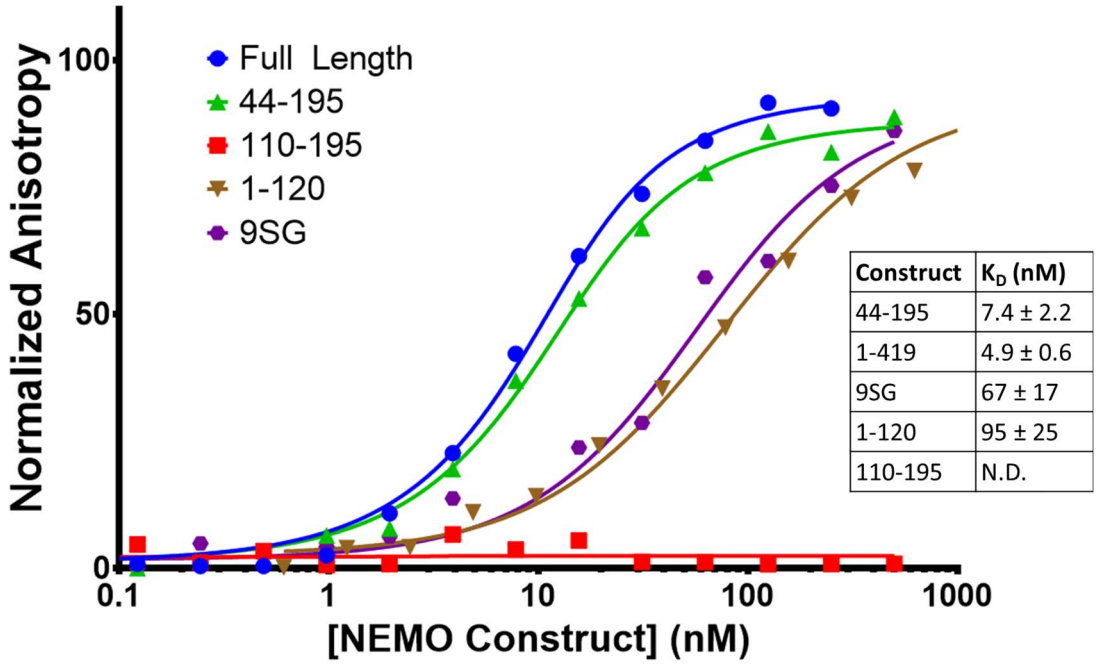

Construct	K_D (nM)
44-195	7.4 ± 2.2
1-419	4.9 ± 0.6
9SG	67 ± 17
1-120	95 ± 25
110-195	N.D.

Figure 30: Fluorescence anisotropy binding assay results for various NEMO constructs. Results are representative of three independent experiments. Inset: table of mean affinities of each NEMO construct for FITC-IKKβ(701-745) after three independent replicates. Refer to text for standard deviations.

3.3.6 *Mutation of Highly Conserved Residues in the IVD Abolishes Canonical NF-κB Signaling*

All cellular assays were performed by members of the Gilmore group. As a first test of whether the IVD plays a role in the ability of NEMO ability to mediate NF-κB pathway signaling, the ability of 9SG-NEMO to restore TNFα-induced phosphorylation of IκBα was tested in a 293T cell line in which NEMO expression had been disrupted by CRISPR/Cas9 targeting (Figure 31, left). These NEMO-deficient cells displayed TNFα-dependent phosphorylation of IκBα after transfection with FLAG-NEMO, but expression of equivalent levels of 9SG-NEMO gave a substantially weaker response (Figure 31, right).

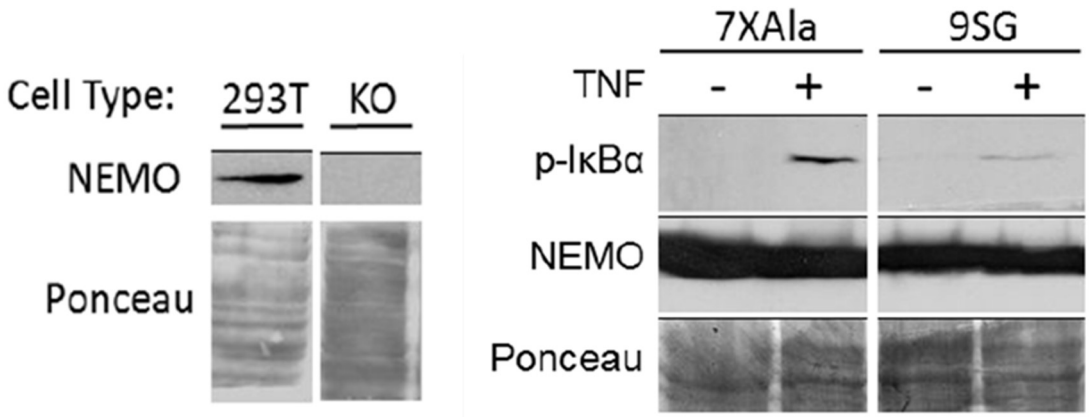

Figure 31: 7XAla-NEMO rescues IKK function in NEMO knockout cells, but 9SG-NEMO does not. Left, Whole cell extracts from WT- and NEMO-knockout 293T cells were analyzed by anti-NEMO Western blotting (top) or Ponceau staining for total protein (bottom). Right, 293T NEMO knockout cells were transfected with plasmids for the expression of 7XAla- or 9SG-NEMO. Cells that were either untreated (-) or treated with TNFα (+) were analyzed by Western blotting for phospho-IκBα or NEMO or by Ponceau staining. These experiments were performed by Yuekun Liu of the Gilmore group.

As a more extensive test of 9SG-NEMO function, retroviral transduction

was used to reconstitute mouse NEMO knockout cells with FL-NEMO or the 9SG mutant. Previously, this method has been shown to express biologically relevant levels of NEMO protein and can be used to test NEMO activity[103,153]. Mouse knockout cells reconstituted with FL-NEMO showed phosphorylation of IκBα upon treatment with the known NF-κB pathway activators TNFα, LPS or IL-1β (Figure 32). In contrast, there was little to no induction of IκBα phosphorylation in cells reconstituted with 9SG-NEMO or the empty vector control. Similar levels of NEMO protein were expressed in all cells. To ensure that the lack of activity of the 9SG mutant was not due to the 7X-Ala background, we also created the 9SG mutation in the wild-type NEMO background. The 9SG variant in the wild-type NEMO background was also defective for TNFα-induced phosphorylation of IκBα when expressed in mouse NEMO knockout cells, whereas expression of WT NEMO restored TNFα-induced phosphorylation of IκBα in these cells.

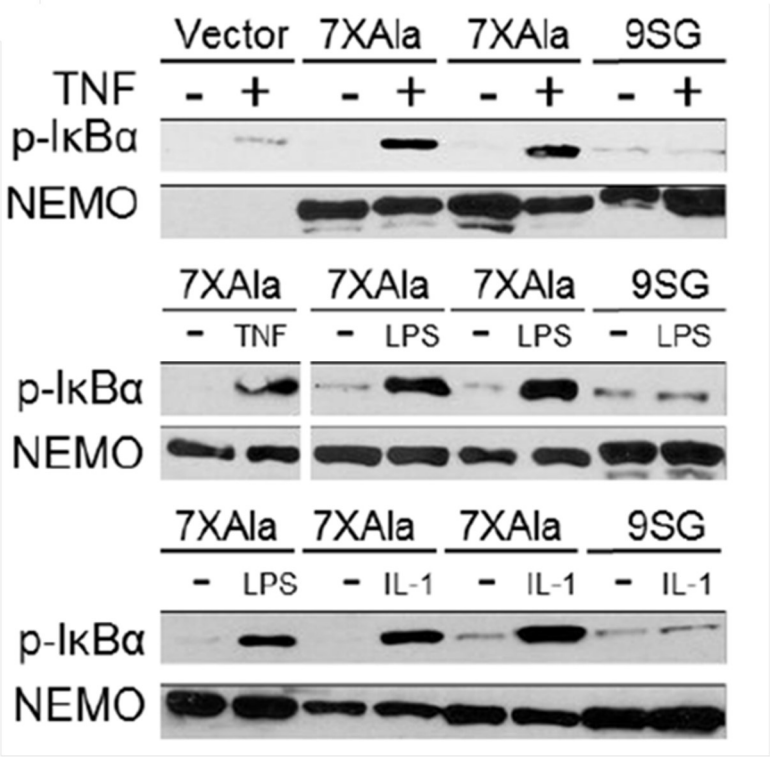

Figure 32: 7XAla-NEMO can propagate TNF-mediated signaling but 9SG-NEMO cannot. Mouse NEMO knockout fibroblasts were stably transduced with retroviral vectors for the indicated NEMO proteins. Stable cell lines were then untreated (-) or treated (+) with the indicated compounds. Extracts were then analyzed by Western blotting for the indicated proteins. These experiments were performed by Larisa Kagermazova of the Gilmore group.

Taken together, these results show that disruption of the highly conserved core IVD sequence by the 9SG mutation disrupts the ability of NEMO to support activation of IKK in human and mouse cells in response to a variety of upstream inducers of NF κB activity.

3.3.7 IVD Mutations do not Affect NEMO Ability to Co-Immunoprecipitate IKKβ or IκBα

To determine whether this loss of signaling ability is due to a loss of

interaction with IKKβ, the ability of wild-type and 9SG-NEMO to co-immunoprecipitate IKKβ in cells was compared. Human 293 cells were transfected with overexpression vectors for FLAG-NEMO or FLAG-9SG-NEMO, and binding to endogenous IKKβ was evaluated in anti-FLAG co-immunoprecipitation assays. As shown in Figure 33, similar amounts of IKKβ were co-precipitated with FLAG-NEMO and FLAG-9SG. No IKKβ was co-precipitated in extracts from cells transfected with the empty vector control. The ability of 9SG-NEMO to pull down IKKβ similarly to wild-type NEMO suggests that a 10-fold loss of NEMO binding affinity to the 45-mer IKKβ peptide as measured in vitro may not be apparent by Western blotting of co-immunoprecipitates from cells for two reasons: full-length IKKβ dimerizes[159] whereas the IKKβ peptide used *in vitro* does not, and likely imparts an avidity effect, and NEMO was highly overexpressed in the 293T cells used for the co-immunoprecipitation experiments.

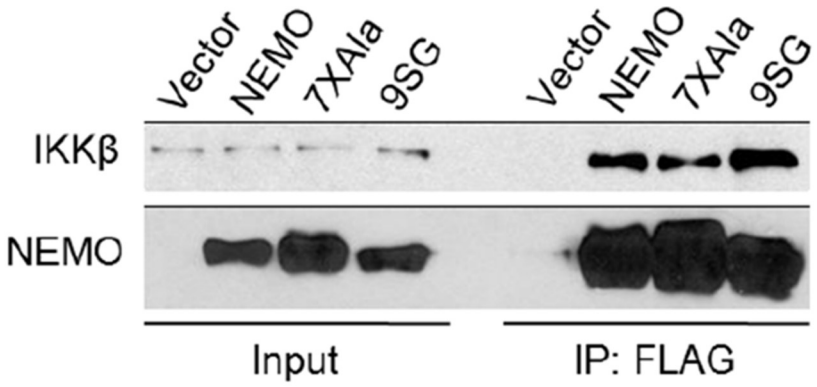

Figure 33: The indicated FLAG-tagged NEMO constructs were transfected into 293T cells, and extracts were immunoprecipitated (IP) with anti-FLAG beads. Immunoprecipitates were then analyzed by anti-FLAG (bottom) and anti-IKKβ (top) Western blotting. In the Input lanes, 4% of the extract used in the immunoprecipitations was analyzed by Western blotting. These experiments were performed by Larisa Kagermazova of the Gilmore group.

3.3.8 NEMO Cannot Undergo in Trans *Signaling*

A crucial test for the hypothesis that a ligand-induced conformational change is required for signal propagation, is that NEMO must not be able to propagate signaling *in trans*. In other words, if head-to-tail signaling is possible and NEMO can associate in an anti-parallel fashion, then there is no reason to expect conformational change to be necessary to actively bring protein ligands together for signaling to occur. To determine whether NEMO is capable of such *in trans* signaling, ΔN- and ΔC-NEMO were cloned into pcDNA-FLAG vectors by deletion using standard subcloning with primers listed in Appendix I. *In vivo* experiments were performed by the Gilmore group and results are shown in **Figure 34**. Human 293 cells with disrupted *NEMO* gene (see Figure 31) were

transfected with indicated NEMO constructs. Upon 10 m of TNF stimulation, WT-NEMO allows phosphorylation of IκBα as has been demonstrated previously[103]. Notably, co-transfection of ΔN- and ΔC-NEMO does not increase the phosphorylation of IκBα seen with ΔC-NEMO alone. Interestingly, transfection of only the ΔC-NEMO construct did allow some TNF-induced phosphorylation of IκBα, as was seen previously[161].

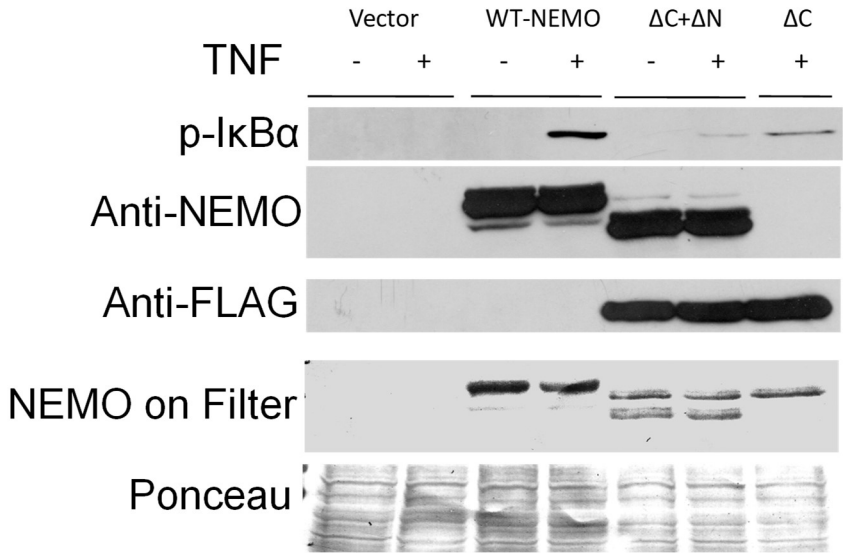

Figure 34: ΔN- and ΔC-NEMO cannot reconstitute TNF-induced phosphorylation of IκBα, whereas ΔC-NEMO on its own shows partial activity. Note NEMO truncation constructs FLAG-tagged. These experiments were performed by Yuekun Liu of the Gilmore group.

From these results, a hypothesis may be formed to explain the pairwise roles within the IKK complex. NEMO may sequester either IKKβ (ΔC-NEMO, IKKβ bound at N-terminus) or IκBα (ΔN-NEMO, IκBα bound at C-terminus) as has been postulated previously[58]; binding of NEMO to IKKβ activates IKKβ,

whereas IκBα binding to NEMO contributes to signaling but is not required for propagation to occur.

3.4 Conclusions and Future Directions

In this chapter, the protein-protein interaction between NEMO and IκBα was quantitatively characterized for the first time. This interaction has been shown previously to be direct by co-elution from size exclusion chromatography and to require the ZF of NEMO[58], and that a short peptide of IκBα induces a conformational change in NEMO[106]. However, the binding affinity and zinc requirement of the NEMO-IκBα interaction was previously unknown. Here, we showed that the NEMO-IκBα interaction is fast on/off, and requires a large amount of zinc to achieve a stable complex for such equilibrium measurements.

A binding scheme for the formation of the NEMO-zinc-IκBα complex is shown in **Figure 35**. As shown in **Figure 21**, zinc binding to NEMO is independent of IκBα concentration, so the first step in complex formation must be the association of NEMO and zinc. From MST experiments, the NEMO-zinc binding affinity, denoted as K_1 in the scheme below, was determined to be 14 μM in Section 3.3.3. However, even zinc concentrations ~ 8-fold above this K_D at 100 μM were not sufficient to achieve measurable binding of NEMO to IκBα.

Therefore, there must be an additional zinc-dependent event to induce an IκBα-binding competent form of NEMO, denoted here as N*, upon the addition of even more zinc. This event may either be zinc binding to a secondary site, or zinc inducing multimerization of NEMO in some other fashion. It is unlikely that there exists a second zinc-binding site on NEMO required for binding to IκBα, as concentrations of zinc used in these assays are far above the μM concentrations of zinc seen in living cells. However, it is also unlikely that this zinc affinity represents the binding of zinc ion to the ZF because NEMO can co-purify with zinc under non-denaturing conditions and this is substantially weaker than other reported ZF-zinc binding[162].

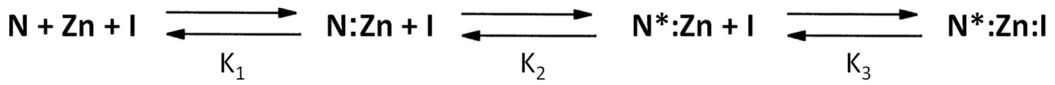

Figure 35: Binding scheme for the NEMO-zinc-IκBα interaction. N denotes NEMO; N* denotes the large complex formed in the presence of excess zinc; Zn denotes zinc; I denotes IκBα. Zinc binding to NEMO is independent of IκBα concentration, so zinc must bind to NEMO before IκBα.

The EC_{50} for the formation of N*:Zn from zinc titration in the FA assay in Section 3.3.2, or K_1*K_2, is 2.5 ± 0.3 mM (n = 2). Once these competent complexes are formed, IκBα can then bind with dissociation constant K_3. This was shown to be 2.0 ± 0.5 μM (n = 2) in Section 3.3.1. This complex formation is substantially weaker than that of the NEMO-IKKβ interaction. This can be rationalized by

thinking about possible IKK signaling mechanisms. There are two such possible mechanisms: single turnover, where the complex forms, one IκBα molecule is phosphorylated, and the complex dissociates; or multiple turnover, where NEMO and IKKβ form a stable complex, turning over multiple IκBα phosphorylation events. The 1000-fold difference in binding affinity between IKKβ and IκBα binding to NEMO favors the latter scenario, of a stable IKK complex turning over many IκBα substrates. If NEMO had identical affinity for both IKKβ and IκBα, it would suggest that the two ligands bind NEMO an equal number of times per activation event. A key test of this hypothesis would be to perform SPR experiments to determine the on/off rates of IKKβ and IκBα binding to NEMO to calculate residence time. Additionally, relation of these *in vitro* findings to a more biologically relevant situation, tracking IKKβ and IκBα localization within the cell during NF-κB activation would be strong evidence for or against this hypothesis. We do not know for a fact that the binding affinity measured with the IκBα peptide is representative of that that would be seen with full-length IκBα. It is also possible that a NEMO-IKKβ complex binds IκBα more tightly than NEMO alone does. In any event, NEMO-IκBα peptide complex formation requires exogenous zinc, is substantially weaker than that of NEMO-IKKβ, and NEMO-zinc-IκBα peptide complexes are large as demonstrated by

DLS experiments.

In collaboration with Assay Quant Technologies, Inc. (Marlborough, MA), we developed an *in vitro* kinase assay based on Sox peptide technology[151] to quantitatively characterize IKK activity towards an IκBα peptide, and specifically the contribution of NEMO thereof. We demonstrated that the IκBα-derived peptide substrate binds to NEMO similarly to an unmodified version of IκBα peptide discussed above in the presence of large molar excess of zinc. Given previous results from Schröfelbauer *et al.*, we expected NEMO to increase IKKβ phosphorylation activity towards IκBα. However, this was not the case, and in fact NEMO appeared to inhibit the IKK activity in our assays. Notably, we have also demonstrated that linear tetra-ubiquitin does not enhance NEMO-mediated IKK activity in this context, contrary to the hypothesis from Hauenstein and colleagues[63]. Many possible explanations exist as discussed above, including the possibility that NEMO requires an additional modification to be competent to function with these binding partners in this context. In summary, there must be some additional required aspect to NEMO-mediated IKK activity, or full-length IκBα is required for NEMO to elicit an effect on activity. Establishment of conditions where NEMO enhances the rate of IKKβ activity in the Sox assay is perhaps most important to quantitatively assess the effect on activity of disease-

associated mutations and other components such as TAK1.

Additionally, we analyzed the contribution of the IVD to NEMO binding of IKKβ. 5xAla-NEMO binds IKKβ(701-745) with an affinity of 4.9 ± 0.6 nM, whereas 9SG-NEMO binds with an affinity of 67 ± 17 nM. Clearly, the SG substitution at the sequence of highest conservation in the IVD impacts IKKβ binding, despite being outside of the interaction site. To further support this conclusion, NEMO(44-195), which includes the IBD and the IVD, binds similarly to FL-NEMO (7.4 ± 2.2 nM), whereas a construct without the IVD, NEMO(1-120), binds similarly to 9SG-NEMO (95 ± 25 nM). NEMO(110-195) showed no measureable binding, suggesting that IKKβ makes no contacts with the IVD. We previously showed that an IKKβ-induced conformational change occurs in 5xAla-NEMO and NEMO(44-195) but not in 9SG-NEMO. It is possible that this conformational change effectively "locks" IKKβ in to NEMO, raising the apparent binding affinity by slowing the off rate. If this mechanism were to be true, it would have to be distinct from the stabilization demonstrated by Zhou and colleagues[116] achieved via disulfide bonds, because the binding affinity of disulfide-stabilized, IVD-less NEMO constructs to IKKβ is lower than that of IVD-included constructs. Another possibility is that the IVD pre-orders the IBD for IKKβ binding, lowering the entropic cost of binding. Either way, at the very

least, the IVD allosterically regulates NEMO interactions.

Previous studies have tested the ability of NEMO bearing various disease-associated mutations to propagate NF-κB signaling[114,115,163]. However, disease-associated NEMO mutants are typically still functional in response to at least one stimulus of canonical NF-κB signaling. For instance, in patients with an E315A mutation in NEMO, LPS induction of NF-κB was diminished, while TNF and IL-1β were able to stimulate NF-κB as normal[163]. Additional evidence for differential signaling effects of NEMO mutations lies in the distinct ubiquitin requirements for activating the IKK complex by TNFα and IL-1β as demonstrated by IKK complex formation seen by confocal microcopy of GFP-tagged NEMO[83,164], and a differential signaling response to LPS compared to IL-1β and TNFα as demonstrated by mutagenesis of ubiquitination sites on the NEMO UBAN domain[165]. In this thesis, we have shown that the 9SG substitution abolishes the ability of NEMO to function in canonical signaling in response to TNF, LPS or IL-1β. It is almost certainly not due to diminished affinity for IKKβ, as a 10-fold loss of binding affinity is modest, and it was measured using a 45-mer peptide surrogate for the full-length protein that may or may not retain full binding affinity. Therefore, it is likely that the SG mutation disrupts the ability of NEMO to perform some other required function for downstream signaling, aside from

binding IKKβ. This could be explained by several scenarios. Given the results of Chapter 2, we hypothesize that this loss of function with 9SG-NEMO is due to a loss of ability to undergo a productive ligand-induced conformational change. If NEMO does require a conformational change to occur to activate IKKβ, then efficiently signaling *in trans* would be dispensable. This idea can be tested by disrupting the ability of NEMO to undergo a conformational change. If *in trans* signaling can occur, then abolishing the conformational change would allow some level of signaling to continue by the *in trans* mechanism. Indeed, co-transfection of ΔN- and ΔC-NEMO does not reconstitute WT-NEMO activity, providing crucial evidence for the requirement of conformational change in signal propagation.

From these data, we can learn a great deal more about the mechanism by which the IKK complex propagates NF-κB signaling. An expanded model of these signaling events is shown in **Figure 36**.

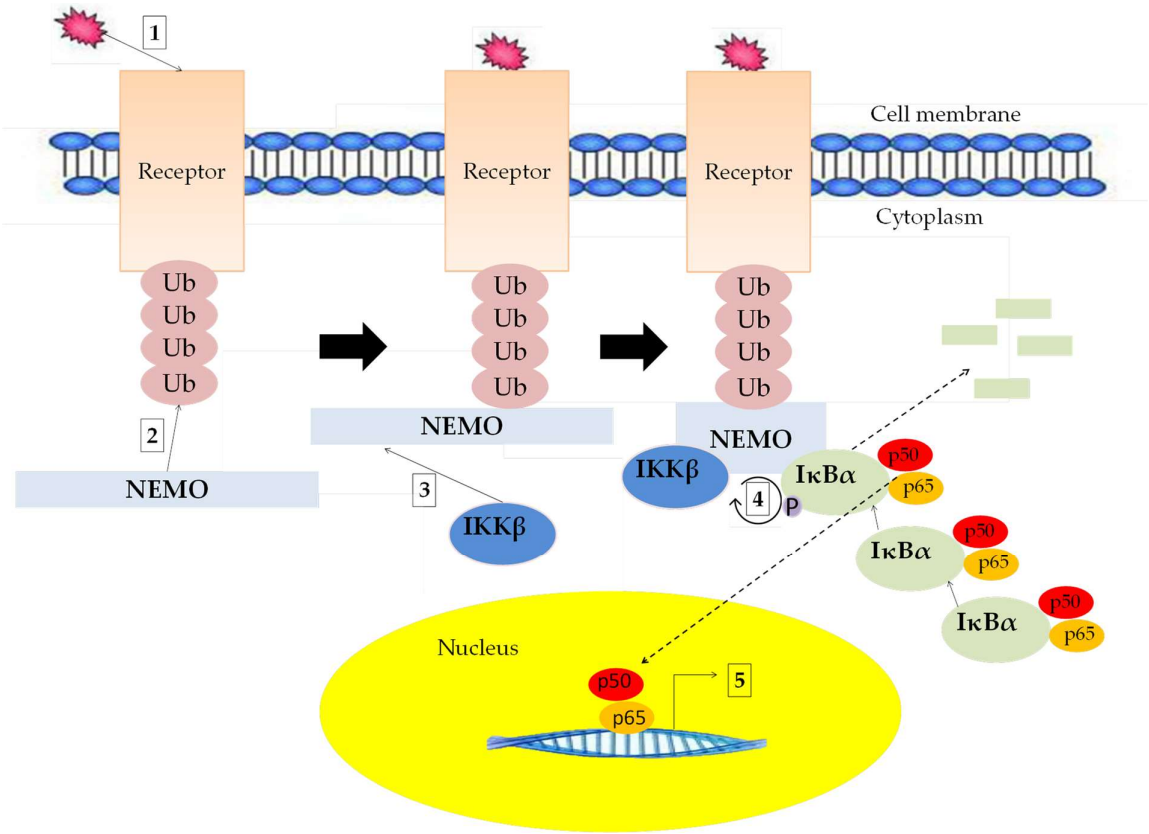

Figure 36: Schematic of NF-κB expanded with findings from this dissertation. 1: The pathway can be turned on by several extracellular stimuli including LPS, TNF, and IL-1β. 2: An activated receptor associates with effector proteins such as RIP that become poly-ubiquitinated. NEMO is then attached to these poly-ubiquitin chains and localized to the membrane. 3: IKKβ binds to NEMO and induces a conformational change as determined by SAXS that we believe is required for subsequent signal propagation. The IVD is required for this change to occur, and for full binding affinity to IKKβ. 4: NEMO-bound IKKβ phosphorylates multiple IκBα molecules, as suggested by the 1000-fold weaker apparent affinity of NEMO-Zn for IκBα than IKKβ. IκBα is then degraded in the proteasome, which releases the previously sequestered NF-κB subunits (here, p50 and p65) to 5: translocate into the nucleus and upregulate NF-κB target gene transcription.

The pathway can be turned on by multiple external stimuli including LPS, TNF, and IL-1β. Their respective receptors are subsequently activated, which associate with effector proteins such as RIP. RIP is then poly-ubiquitinated by E2/E3 ligases. This poly-ubiquitin chain is then attached to NEMO, localizing it

to the cell membrane. IKKβ then binds to NEMO and induces a conformational change that requires an intact IVD region, as determined by SAXS (see Section 2.3.5). The IVD is highly conserved, as shown in the MSA in Section 2.3.1, which highlights its importance in NEMO function. The IVD also contributes to the thermal stability of NEMO (Section 2.3.4), and the binding affinity of NEMO to IKKβ (Section 3.3.5), but neither is sufficient to substantially impact binding to IKKβ or signaling capability in cells (Sections 3.3.6 and 3.3.7). Therefore, a deficit in conformational change is likely the reason for the inability of the IVD mutant 9SG-NEMO to propagate NF-κB signaling. Additional evidence for this is shown by the inability of co-transfected ΔN- and ΔC-NEMO constructs to activate IKKβ (Section 3.3.8): if NEMO can signal *in trans*, conformational change would be dispensable for NF-κB signaling. We have shown that this is not the case. It is important to note that because the addition of NEMO to the Sox assay did not enhance the rate of IKKβ phosphorylation of IκBα, despite IKKβ inducing a conformational change in NEMO under somewhat similar conditions, this conformational change may not be sufficient for signal propagation to occur. More likely, there are additional co-factors such as poly-ubiquitin that are required for signaling to be activated.

For instance, a study by Catici and colleagues[106] provided evidence that

poly-ubiquitin allosterically drives molecular interactions of NEMO with IKKβ and IκBα. The presence of IKKβ and IκBα on their own or in concert induced a conformational change in NEMO as measured by ANS fluorescence changes and the change in intrinsic fluorescence of W6. This ligand-induced conformational change concept is illustrated in **Figure 37**C. A conformational change in NEMO upon IKKβ binding was also demonstrated in Section 2.3.5 of this dissertation. The addition of deca-ubiquitin changed the kinetics of these conformational changes from zero-order with respect to the concentration of IKKβ and IκBα, to first-order. Therefore, ubiquitin binding is likely eliminating a rate-limiting step to make NEMO more competent to either bind IKKβ and IκBα or undergo a conformational change. Using SAXS to probe the effect of poly-ubiquitin on NEMO conformational change, as has been demonstrated in this dissertation, would allow more detailed exploration of this allosteric mechanism by which ubiquitin drives NEMO interactions. While the evidence of Catici *et al.* is clear that IκBα induces a conformational change in NEMO, it is unlikely that this relatively slow event is a mechanistically important occurrence because NEMO-IKKβ likely phosphorylate multiple IκBα molecules per complex formation, as discussed above and is diagrammed in **Figure 37**D.

An alternative model was recently proposed by Hauenstein and

colleagues[63] where NEMO is in an auto-inhibited state prior to binding of ubiquitin chains longer than four units. The region spanning amino acids 120-150 in NEMO was hypothesized to be required for maintenance of this auto-inhibited state, as its presence precludes binding of a more C-terminal region of NEMO to linear di-ubiquitin, but not linear tetra-ubiquitin. This model is illustrated in **Figure 37**B. If it were true, mutation of highly conserved residues 145-153 as in the 9SG-NEMO construct, as well as the disease-associated mutation R123W, would likely prevent auto-inhibition from occurring, resulting in a constitutively active NEMO. Section 3.3.6 and a study by Fusco and colleagues[140] provide evidence contrary to the Hauenstein *et al.* hypothesis, as 9SG-NEMO is inactive in propagating signaling and R123W behaves as WT. Additionally, these authors argue, based on SAXS analysis, that vFLIP activates NEMO by opening it up, overcoming auto-inhibition. vFLIP has been previously shown to induce NF-κB signal activation by binding to NEMO[68]. This MBP-vFLIP-NEMO SAXS model is highly similar to that shown above in Section 2.3.3 which is unliganded (D_{max} 320 versus 315 Å, respectively), despite the perhaps misinterpreted presence of MBP-vFLIP. Therefore, it is unlikely that their SAXS model reflects a vFLIP-induced "opening" of NEMO, but rather reflects the "open" natural conformation of NEMO on its own. Given all of the above, the opposite of the Hauenstein *et al.*

hypothesis is more likely to be true: NEMO is extended and inactive prior to IKKβ binding (Section 2.3.5) and poly-ubiquitin binding[106], rather than folded inward and inactive prior to poly-ubiquitin binding "opening up" NEMO.

Once a stable ubiquitin-NEMO-IKKβ complex is formed at the membrane, it is likely that this complex phosphorylates many IκB*α* molecules, as opposed to the complex turning over one molecule per complex formation. Evidence for this is from the apparent affinity of NEMO-zinc for IκB*α*, which is approximately 1000-fold weaker than the binding affinity of NEMO for IKKβ as discussed in Section 3.3.3. A single turnover for the formed complex would likely require an affinity of NEMO for IκB*α* similar to that of IKKβ, and would likely be energetically costly to assemble such a complex for a single phosphorylation event. **Figure 37**D illustrates the hypothesis that a stable NEMO-IKKβ complex turns over multiple IκB*α* molecules. It should be noted that this inference from *in vitro* experiments might or might not be true *in vivo* for a few possible reasons, rendering single turnover IKK complex formation to be more energetically efficient and plausible: perhaps other binding partners enhance IKK complex formation; the IKK complex members are localized to the membrane so dissociated complexes may reform much more rapidly than *in vitro*; and there may be additional post-translational modifications that alter complex formation

and turnover. Once phosphorylation is complete, IκBα is subsequently degraded in the proteasome, releasing the previously sequestered NF-κB subunits to translocate into the nucleus and upregulate NF-κB gene transcription.

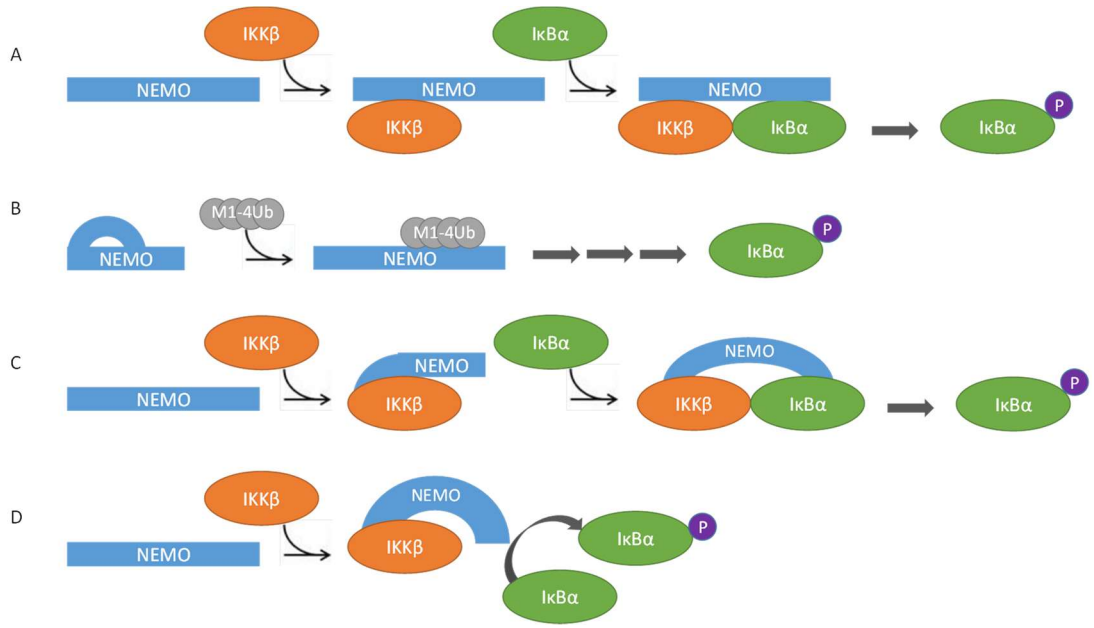

Figure 37: Possible mechanisms of NEMO activation. A: IKKβ and IκBα bind to NEMO through simple rigid protein binding. IKKβ and IκBα are close enough to produce a phosphorylation event. B: Model proposed by Hauenstein and colleagues[63], where NEMO exists in an auto-inhibitory state with binding sites inaccessible or occluded prior to linear tetra-ubiquitin (M1-4Ub) binding. Subsequent steps occur in some fashion, perhaps according to schemes A, C, or D, in which phosphorylated IκBα is produced. C: IKKβ and IκBα each induce a conformational change in NEMO that leads to a final productive complex formation. This model, combined with linear poly-ubiquitin binding, is consistent with findings from Catici and colleagues[106]. D: IKKβ binds to NEMO and induces a conformational change to a catalytically competent complex, where the stable complex can phosphorylate multiple sequential IκBα molecules.

Chapter 4: Screening for NEMO-IKKβ Interaction Inhibitors

4.1 Introduction

Scaffold proteins typically do not have so-called active sites for chemistry to occur; instead, they function by binding their target protein(s), which in turn elicits a response. These protein-protein interaction sites, or PPIs, are often lacking concavities with binding energy hot spots more dispersed than typically seen in a small binding pocket, and are often considered undruggable. This is because small molecule libraries have been refined based on likeness to existing drugs[166], most of which may have difficulty selectively bridging multiple binding hot spots on a potentially featureless surface[167]. Also, many PPIs share common binding interface characteristics, such as similar electrostatics and shape. This greatly increases the challenge in finding a selective PPI inhibitor. It is estimated that of the approximately 30,000 proteins in the human proteome, there are between 40,000 and 200,000 PPIs in the human interactome[168,169]. To rationally exploit this large number of potential drug targets and overcome the challenge of "undruggability," we need to better understand PPIs beyond simple protein binding. Because of this current limited knowledge and other technical difficulties, investment of resources in PPI targets by pharmaceutical companies is rare. Despite this, some progress has been made regarding types of PPIs that

can be inhibited[109,170] and individual PPIs have been successfully targeted with drug-like compounds[171–178]. Notably and conversely, progress has also been shown using small molecules that promote stabilization of PPIs[179].

Binding energy hot spots are sites on a protein where specific interatomic interactions contribute significantly to $\Delta\Delta G$ of a binding event. Docking algorithms such as FTMap[180] have been designed to robustly identify such hot spots, and have been validated experimentally[108]. Because PPIs typically have larger, flatter binding surfaces, the identification of hot spots may help facilitate the design of inhibitors that, while substantially smaller than their protein competitors, bind efficiently to these sites, competing for surface. On one hand, classical small molecules may be screened for inhibition, with structure-activity relationship studies performed on hits to improve potency and other relevant parameters. However, they are less likely to occupy multiple hot spots to provide sufficient potency[181]. Additionally, there is the issue of macromolecular crowding in cells that can lead to reduction in inhibitory activity *in vivo*. For example 1), the observation of reduction of inhibition activity of a capsid-binding peptide and a small capsid protein domain that interfere with assembly of the human immunodeficiency virus capsid *in cellulo* versus *ex cellulo*, and 2), similarly that of a RGD-containing peptide blocking the interaction between foot-and-mouth

disease virus and receptor molecules on the host cell membrane[182,183]. Therefore, for an inhibitor to elicit a therapeutically relevant response in cells, it must be highly potent to overcome these potential crowding issues.

A potentially advantageous strategy is to screen molecules more likely to occupy multiple hot spots to begin with, thus increasing potency. Macrocycles are such molecules, which are large organic molecules often above 500 Da that frequently bind to proteins to modulate their function[184]. Additionally, stabilization of the molecule by having a rigid ring structure lowers the entropic cost of binding, and may enhance cell permeability[185,186]. Because of these potential advantages, macrocycles are a good class of potential inhibitors to screen for PPI inhibition. Importantly, there have been successes with non-classical drug-like, FDA-approved macrocycles for treatment of disease, primarily from natural product analogs such as Torisel (temsirolimus, mTOR inhibitor)[187], Ixempra (ixabepilone, a microtubule stabilizer)[188], and 17-allylamino-geldanamycin (Hsp90 inhibitor)[189].

Because NEMO is an essential component of a major signaling pathway in human biology, there exists a strong therapeutic motive in studying and targeting this protein. A small-molecule inhibitor of the NEMO-Ubiquitin interaction was developed that selectively inhibits NF-κB activation in response

to TNFα, but not IL-1β, stimulation. This small molecule was shown to selectively kill lymphoma cells that were addicted to NF-κB signaling, providing strong evidence that NEMO is a potentially useful therapeutic target[83]. A different small-molecule inhibitor of the NEMO-IKKβ interaction was shown to inhibit cellular NF-κB signaling, and was computationally docked into the X-ray crystal structure of the NEMO-IKKβ binding interface[84]. However, no mechanistic studies were performed, so the precise target of the small molecule is unknown. A cell-permeant version of the NBD 11-mer peptide has been shown to disrupt the NEMO/IKKβ complex *in vivo*, and causes a specific biological outcome that attenuates activation of NF-κB but does not affect basal NF-κB function[85,86]. Quite surprisingly, the NBD peptide has been shown to prevent memory loss in a mouse model of Alzheimer's disease, a function with which NF-κB had not previously been directly linked[87]. The NBD peptide has also been shown to attenuate tumor proliferation and prolonged mouse survival in a malignant glioma mouse line[88]. A synthetic loop replacement version of the NBD, in which a conserved hydrogen bond was replaced with a covalent hydrocarbon bridge to enhance rigidity, has been shown to be 10-fold more potent in blocking NEMO-mediated NF-κB signaling than wild-type NBD peptide[89], and may prove to be a worthwhile strategy for further optimizing the NBD peptide for

therapeutic use. IKKβ knockout in a mouse model mimicked NEMO-knockout, but the fatal liver damage occurred at a later stage in embryonic development[90]. Notably, IKKβ inhibition through salicylate and its derivatives has been established but studied in models of vascular disorders and metabolic syndrome[91] in addition to immunomodulatory capacities[92,93]. These attempts to inhibit NF-κB signaling through IKKβ have not been shown to modulate NEMO-based NF-κB disease states.

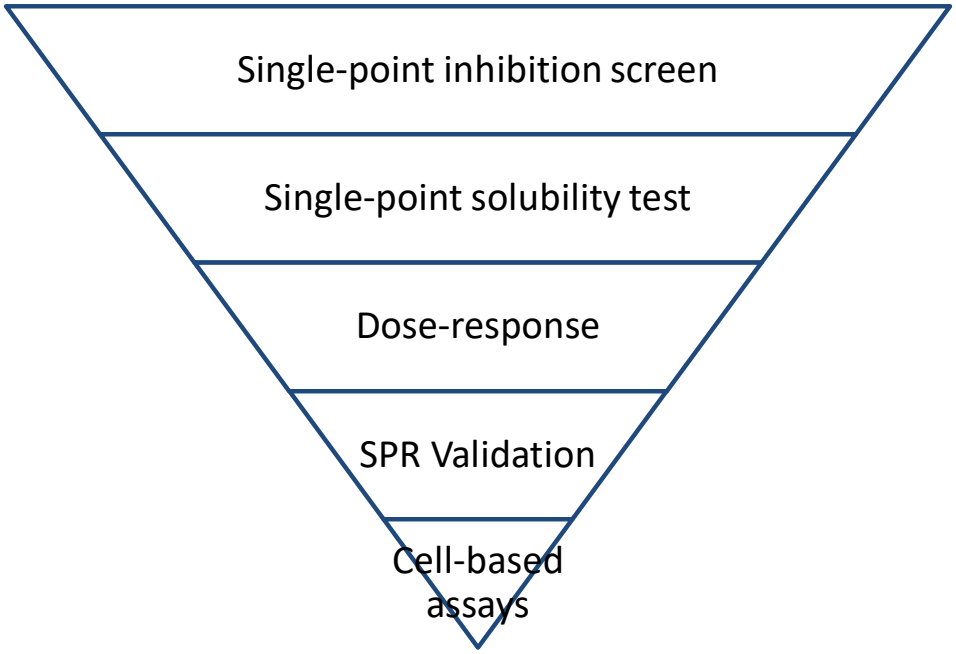

Figure 38: Inhibitor discovery work flow. Pyramid indicates that each step should narrow down the number of compounds by eliminating those with no activity or that were false hits.

This chapter describes attempts to develop a non-peptide small molecule or macrocycle inhibitor of NEMO. The work flow is illustrated as a funnel in

Figure 38 in order to draw attention to the fact that each step in the process is designed to eliminate false hits from previous steps and verify true NEMO inhibitors. First, compounds were screened for inhibition and solubility in an aqueous environment at a single concentration. Determining solubility at this step is important to reduce the likelihood of false positives; additionally, organic small molecules tend to have poor solubility in an aqueous environment; these are less likely to become therapeutically relevant given the aqueous nature of cells. Second, the concentration dependence of inhibition of the initial hits is measured to eliminate false positives due to, for example, microaggregates nonspecifically segregating or inactivating one or both of the binding partners[190]. A true inhibitor should go from 10% inhibition to 90% inhibition over two log units of concentration; microaggregates typically have a steeper slope over this inhibition range, corresponding to its solubility[190]. Third, fluorescence-based assays are prone to inhibition for a number of reasons[156,190,191], so a secondary validation assay is important. Here, SPR is employed to show that the compound binds to NEMO in a simple stoichiometric fashion, with an affinity relatable to that measured in a dose-response FA assay. Finally, the ability of the compound to inhibit NEMO in a cellular context is evaluated by two means: stimulating NF-κB signaling and measuring the ability of NEMO to direct IκBα phosphorylation;

and determining whether NEMO can co-immunoprecipitate with IKKβ. This demonstrates whether the compound is cell permeable and whether it may be potent enough for further studies as a therapeutic.

In silico analysis can strengthen or weaken the case for a compound to inhibit its target. This is accomplished by docking the molecule into the 3D structure of the target; this often illuminates possible binding modes, which can yield invaluable information for subsequent SAR work to improve potency and/or PK/PD profiles. Occasionally, however, docking identifies no meaningful binding pose. If no meaningful binding pose is found despite clear *in vitro* inhibition, either the molecule is inhibiting by some allosteric mechanism, i.e. binding to a region outside of the 3D structure used for docking, or the molecule is likely to be a false positive. Because these two possibilities are often extremely difficult to distinguish, computational docking is not considered a "filtering" step. Nevertheless, docking analysis for a small-molecule hit is presented here, and shows an interesting binding pose that may be valuable for SAR follow-up work.

In this chapter, the described discovery pipeline is presented for inhibitor discovery for the NEMO-IKKβ interaction. Both classical drug-like small-molecule and non-classical macrocycle libraries were screened. One hit from the

CMD collection is described in terms of its physicochemical properties, and validated by an orthogonal FA assay, SPR, and in a cell lysate Co-IP. However, no macrocycles passed the first validation step.

4.2 Materials and Methods

4.2.1 Materials

All small-molecule compounds and Set 5 macrocycles were provided by the Boston University Center for Molecular Discovery (BU-CMD) from their library of compounds. From an initial library of 80,000 macrocycles from Asinex Corporation (Winston-Salem, NC), the BU-CMD selected 800 of which had predicted good aqueous solubility and structural diversity. The remaining reagents were identical to those used in Chapter 3 (Section 3.2.2). A list of the screened compound sets is provided in Table 4, and the structures for all hits are shown in Appendix VI.

Table 4: List of screened compound sets.

	Type	Origin	# screened	# initial hits	# validated by D-R[a]	# for further study
Set 1	Small-molecule	CMLD	869	26	4	1
Set 2	Small-molecule	CMLD	12	5	2	2
Set 3	Small-molecule	CMLD	45	2	1	0
Set 4	Diverse	CMLD	2457	35	--	--
Set 5	Macrocycle	CMLD	28	0	--	--
Set 6	Macrocycle	Asinex	800	7	0	--

[a]D-R: dose-response

4.2.2 *Initial Screen using Fluorescence Anisotropy and UV/Vis Spectroscopy*

Screened compounds were provided either as a stock solution in 100% DMSO at 20 mM, 100% DMSO at 0.3 mM, or 200 nmol dry powder. Compounds were provided dried in 96-well plate format, and were re-dissolved with 10 μL of 100% DMSO to achieve a concentration of 20 mM. For initial screening of compounds provided at 20 mM, the compounds were diluted to 400 μM in 50 μL of 10% (v/v) DMSO, so that addition of this solution into the 200 μL final assay volume results in a final concentration of 100 μM compound and 2.5% (v/v) DMSO. For initial screening of compounds provided at 0.3 mM, the compounds were diluted to 120 μM in 25 μL in 60% (v/v) DMSO, so that addition into the 100 μL final assay volume results in a final concentration of 30 μM in 15% (v/v) DMSO. Prior to screening, the UV spectra from 220-750 nm of the compounds in final assay solution was measured in a 96-well UV-transparent microtiter plate.

The turbidity at 700 nm relative to a blank containing all assay components except compound was used to determine solubility; small organic molecules, which are not green in color, should not absorb at long wavelengths such as 700 nm, so any "absorbance" is due to optical interference by insoluble particles. Compounds with absorbance values > 20% above the baseline were deemed insoluble.

Regardless of solubility at this stage, compounds were then transferred to black opaque 96-well plates for performance of the FA assay. These assays were performed as described previously (Section 3.2.2). Briefly, 50 μL assay buffer (200 mM Tris, pH 7.4, 800 mM NaCl, 0.04% (v/v) Triton X-100, 4 mM DTT, stock concentration) was added to each well. Both NEMO and FITC-IKKβ were diluted from a concentrated stock to 60 nM in water and then added to the wells at 50 μL each. Columns 1 and 12 of each assay plate were reserved for controls: wells A, B, and C contained the high control, NEMO plus FITC-IKKβ; wells D, E, and F contained the low control, FITC-IKKβ alone; and wells G and H contained only buffer. The assay plate was then covered with opaque adhesive to prevent fluorophore bleaching and incubated at 25 °C for 1 h before the fluorescence was measured.

The anisotropy signals were calculated based on the method used in

Section 3.2.2 and converted to % Max FA signal using Equation 3:

$$\% \, Max \, FA = \left(\frac{S - S_{min}}{S_{max} - S_{min}}\right) * 100 \quad (3)$$

For each well, the assay signal (S) was normalized to the assay range of each plate (S_{max} and S_{min} determined by high [NEMO plus FITC-IKKβ] and low [FITC-IKKβ alone] controls, respectively), and multiplied by 100 to give the percentage of tracer probe binding at the indicated compound concentration. Normalization corrects for plate-to-plate variability. Compounds that showed both (a) < 50% Max FA Signal, i.e. > 50% inhibition, and (b) an absorbance at 700 nm less than 20% above baseline were deemed hits from this initial screen. These strict cutoffs were chosen to achieve < 5% hit rate for follow-up.

4.2.3 Dose-Response Fluorescence Anisotropy Assay

Hits from the initial single-point screen were then further characterized using the FA assay in a dose-response format. The assay was identical to the initial screen with one difference: working concentrations were 400 μM in 50 μL (for 200 μL assay volume) or 120 μM in 25 μL (for 100 μL assay volume) prior to two-fold serial dilution in 10% or 40% (v/v) DMSO respectively. The assay was performed and data were normalized as in Section 4.2.2. If dose-dependent inhibition was observed for a compound, the data were fit to the four-parameter Equation 4 below to determine the IC_{50}, where L is IC_{50}, and F is a scaling factor:

$$Y = (Y_{max} - Y_{min}) * \left(\frac{1}{1+\left(\frac{L}{x}\right)^{F}}\right) + Y_{min} \quad (4)$$

Occasionally compounds may pass initial screening tests despite being false positives[190]. For compounds showing any unusual signs, such as a steep slope (typically defined as greater than 1.5) between 10% and 90% inhibition, total fluorescence intensity was examined to confirm dose-dependent inhibition in this assay. Aggregation of the compounds would be a primary cause of inconsistency in total fluorescence. The fluorescence intensity of each compound was determined by examining the raw fluorescence data from the plate reader. None of the validated hits showed dose-dependent fluorescence intensity changes above or below the minus-compound controls.

4.2.4 Hit Validation

Compounds that passed the follow-up dose-response assay with an IC_{50} < 50 μM and no unusual features in solubility or dose-response were then subjected to three validation tests to rule out false positive inhibition as a result of an assay artifact. The first test was an orthogonal dose-response inhibition screen against the Keap1-Nrf2 interaction developed by Mengqi Zhong of the Whitty group (M. Zhong, unpublished). A specific inhibitor should not inhibit an unrelated PPI. Compounds were tested identically as in the NEMO/IKKβ assay,

except the final concentration of Keap1 was 10 nM and FITC-Nrf2 was 5 nM.

The second validation test was surface plasmon resonance (SPR) to measure direct binding and signs of compound aggregation. SPR was run identically as described in Section 3.2.3, except the 7xAla-NEMO protein coupled to the surface was only thiol-coupled, with NEMO(44-195) and BSA as negative controls random amine coupled to the chip. Compounds were initially tested at 200 μM and serially diluted from 100 μM to 12.5 μM for a dose-response format. A true hit should show reversible binding (i.e. signal decreases to baseline after stoppage of compound injection) and a signal in response units (RU) proportional to that expected for its mass.

The third validation test was co-immunoprecipitation (Co-IP), performed by the Gilmore group, to test for inhibition in a more biologically-relevant environment. Briefly, Mouse Embryonic Fibroblasts (MEFs) that express FLAG-NEMO and IKKβ were harvested and lysed. Varying concentrations of the inhibitor were then added to the lysate, or DMSO alone as a negative control. Agarose beads displaying anti-FLAG antibodies were then used to immunoprecipitate the FLAG-NEMO from the cell lysate. These samples were analyzed by Western blot to determine whether the compound blocked the co-immunoprecipitation of IKKβ with the NEMO.

4.3 Results and Discussion

4.3.1 Small-Molecule Library Screening and Validation

A set of 869 small organic compounds (Set 1) were provided by the BU-CMD for screening. These compounds were screened for solubility and inhibition of the NEMO- IKKβ peptide interaction at a single concentration, 100 μM in 10% DMSO v/v. Out of this set, 26 compounds emerged as hits (Appendix VI), having better than 50% inhibition and absorbance at 700 nm below 0.1. This corresponds to a hit rate of 3% (Figure 39).

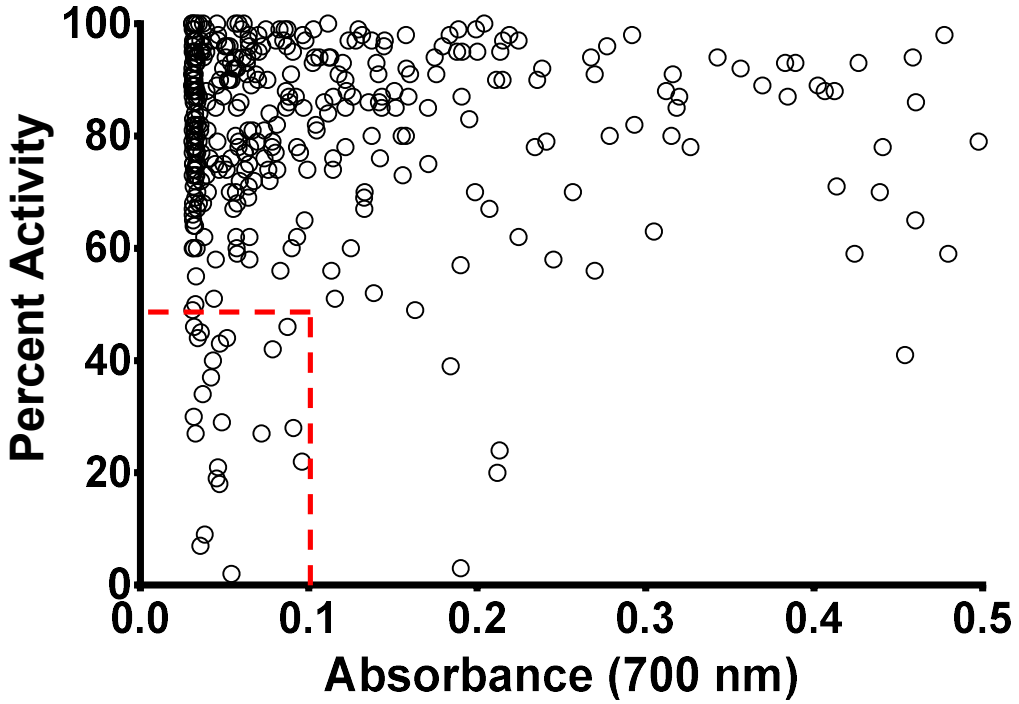

Figure 39: Results of inhibition and solubility screens of Set 1. Compounds that showed better than 50% inhibition (lower than 50% max FA signal) and an absorbance at 700 nm < 0.1 were selected for dose-response analysis and are within the box delineated by red dashed lines.

Each of the 26 hits was then analyzed in an eight-point dose-response assay titrated from a concentration of 100 μM to 0.78 μM. Eight of the 26 hits showed a dose-response. Of these, four were deemed too weak (IC_{50} > 100 μM) to continue, and four were then subjected to a repeat dose-response assay performed in triplicate. The final results of initial % max FA signal at 100 μM, Abs at 700 nm, and IC_{50} are shown in Table 5, and the selected dose-response profiles of the top two hits are shown in Figure 40. The compound that showed the best inhibition was 10190, which gave IC_{50} values in the two independent

experiments of 17 ± 1.8 μM and 32 ± 1.6 μM.

Table 5: Statistics for 8 hits from Set 1 that passed dose-response validation.

CMD Code	% Max FA Signal	Abs_{700}	IC_{50}
9571	34	0.04	≥100 μM
9574	21	0.05	≥100 μM
9576	19	0.05	≥100 μM
9578	37	0.04	≥100 μM
9725	30	0.03	≥100 μM
9744	46	0.04	≥100 μM
10190	-18	0.05	16 μM
10197	7.5	0.04	70 μM

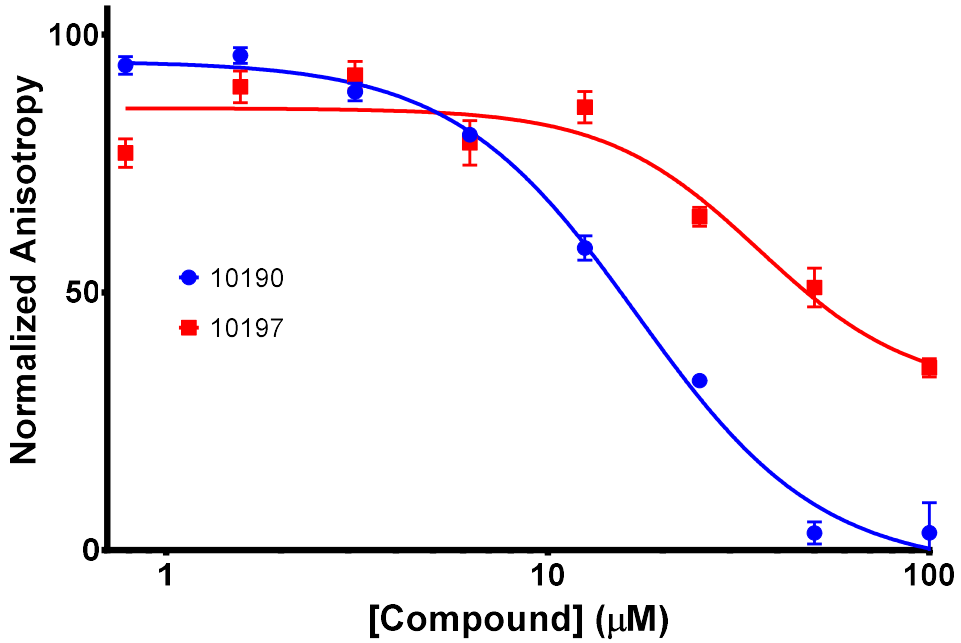

Figure 40: Dose-response data for top two compound hits from Set 1. Assay was normalized to high (NEMO+IKKβ) and low controls (IKKβ alone). Data were fit to the four-parameter equation shown in Equation 2.

Additional analogs of 10190, designed for improved solubility, were obtained from the CMD-BU and were tested in the NEMO FA assay in a dose-response format. These compounds are referred to as Set 2. Of the twelve compounds in

Set 2, five showed IC_{50} values < 50 μM, but only two showed acceptable solubility as well ($Abs_{700\ nm}$ < 0.1) (Figure 41). These compounds were 10487 and 10557; both showed IC_{50} values of 8 μM, and were selected for further validation as described below in Section 4.3.3.

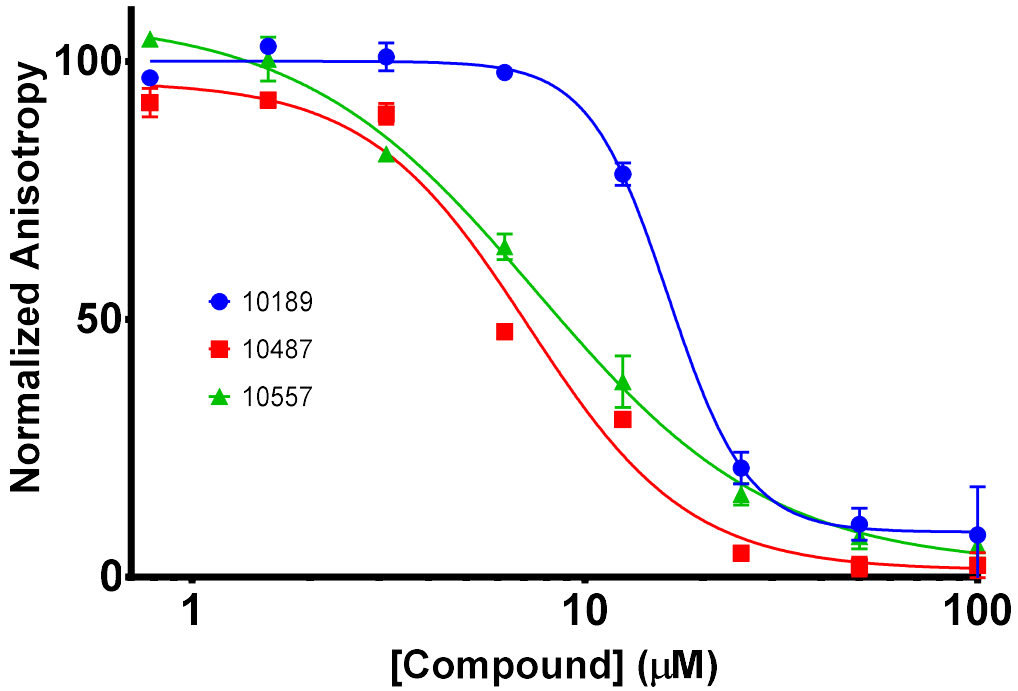

Figure 41: Dose-response of top two hits from Set 2, soluble analogs of initial hit 10190. 10189 is a free base form of 10190; its IC_{50} is comparable. Assay normalized to high (NEMO+IKKβ) and low controls (IKKβ alone). Data were fitted to the four-parameter equation shown in Equation 4.

Next, 45 structurally similar analogs of 10190 were screened (Set 3) as an expanded version of Set 2. In this set, two compounds showed significant inhibition following screening at 30 μM in 10% (v/v) DMSO: 10197 (previously identified as a weak hit in Set 1) was the only one to also show acceptable

solubility, below the typical Abs_{700} cutoff of 0.1 (Figure 42). Compounds 10557 (from Set 2) and 10190 (from Set 1) were included in this screen but, unexpectedly, did not show significant inhibition, despite multiple previous demonstrations of inhibition. Nevertheless, it was notable that 10197 showed signs of inhibition, because it was not pursued following weak inhibition from the screen in Set 1. These discrepancies may be a result of screening at a four-fold higher concentration of DMSO than previously, despite previous evidence suggesting that the assay can tolerate such concentrations (Shaun Cote, unpublished).

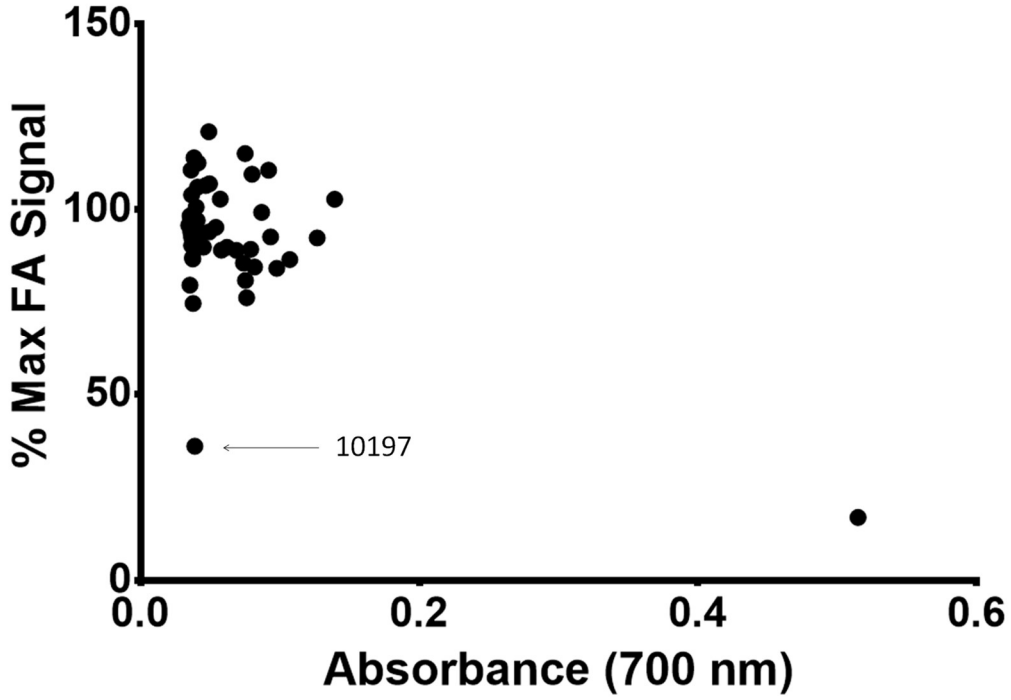

Figure 42: Results from initial inhibition and solubility screen for Set 3. Compound 10197 was the only compound to show acceptable inhibition (<50% max FA signal) and solubility (Abs_{700} below 0.042, baseline).

The availability of an updated and greatly-expanded CMD library yielded an opportunity to screen a larger and more diverse set of 2457 compounds (Set 4). These compounds were screened at 30 μM in 10% DMSO v/v, and 35 hits were selected that showed better than 50% inhibition and an Abs_{700} below 0.042 (Figure 43). The resulting hit rate of this set meeting these criteria is 1.4%.

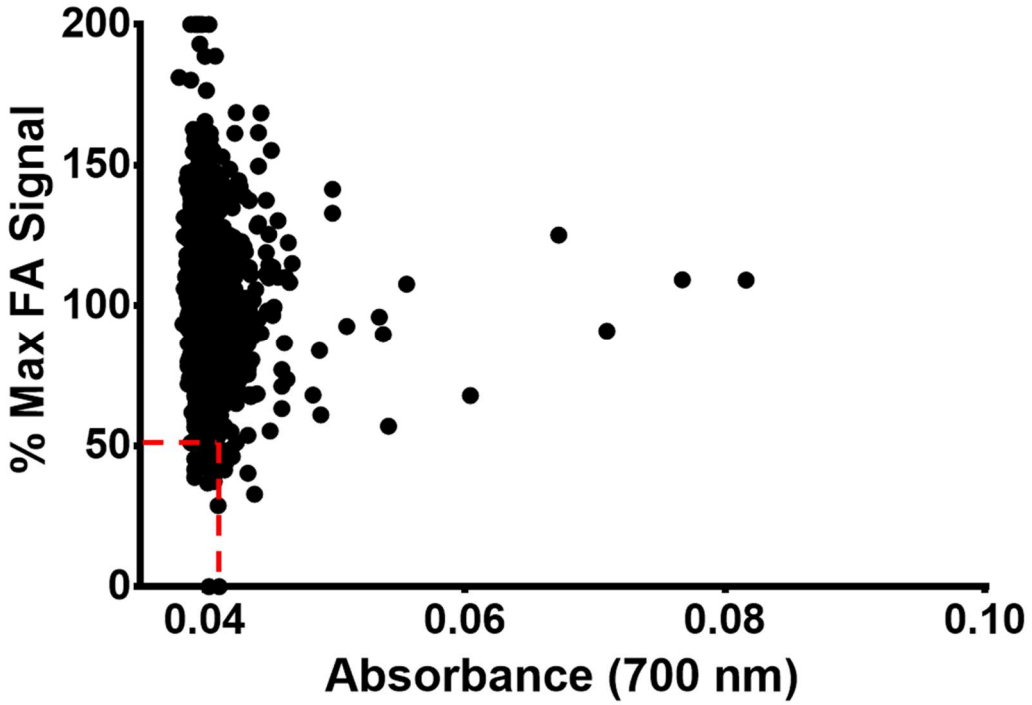

Figure 43: Results from initial inhibition and solubility screen for Set 4. A total of 35 compounds out of 2457 showed acceptable inhibition (<50% max FA signal) and solubility ($Abs_{700\ nm} < 0.042$, baseline).

4.3.2 *Macrocyclic Compound Screening*

In addition to the small molecules assayed above, synthetic macrocycles were explored as potential NEMO inhibitors. First, a set of 18 compounds (Set 5) was provided by the CMD. Fifteen were macrocycles, and three were multimeric analogs of a previous compound of interest, 9644. The three multimeric analogs of 9644 were include here because they are similar to macrocycles in that they are not considered classically drug-like. Each of these compounds was screened in a dose-response format, starting at 500 μM, and serially diluted to 3.9 μM in 2.5%

v/v DMSO. The resulting anisotropy values for each compound were normalized to the controls as above. The data from this assay are shown in Figure 44. None of these compounds showed signs of inhibition, even at concentrations up to 500 μM. In fact, some of the compounds showed an increase in anisotropy at these high concentrations; this is likely due to nonspecific hydrophobic interactions between fluorescein and aggregated compound, resulting in a slower tumbling rate for the FITC-IKKβ tracer probe than when bound to NEMO.

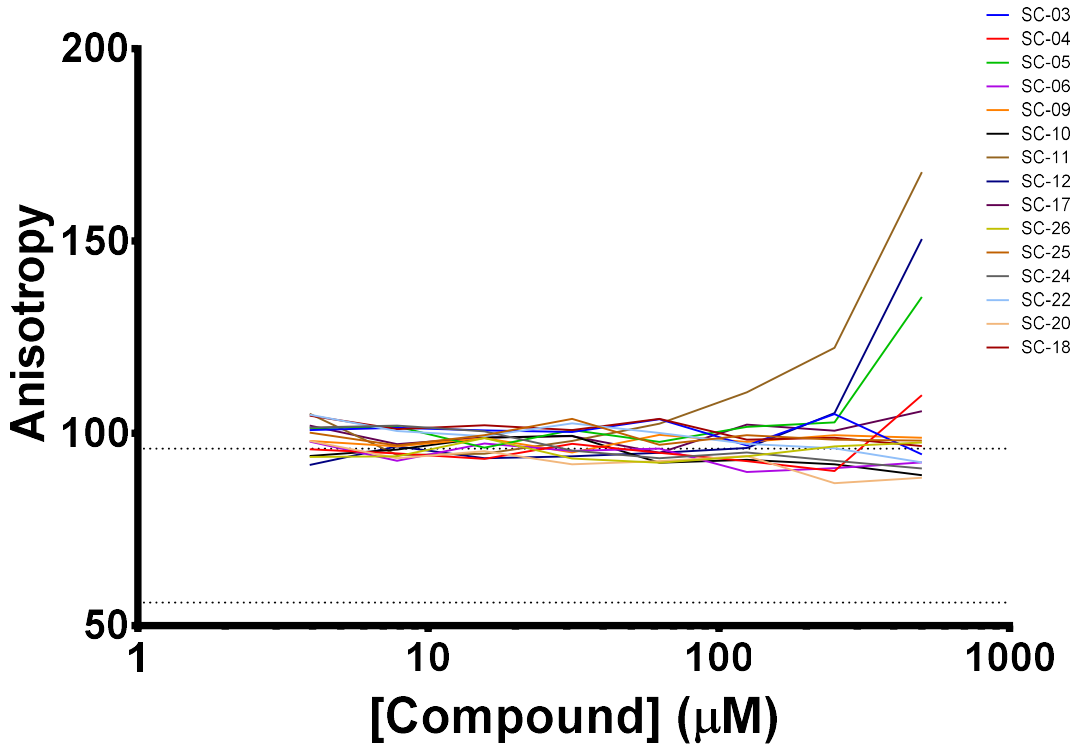

Figure 44: Dose response results for Set 5. None of the compounds exhibited significant inhibition. Some showed an increase in anisotropy signal at high concentrations; this is likely due to insolubility artifacts. Dashed lines indicate high (NEMO + IKKβ) and low (IKKβ alone) controls.

In addition to this set, the natural product version of 9644, Calafianin, as well as a

mono-ketal protected version, were analyzed in a dose-response format. Only the mono-ketal protected version showed significant inhibition, at 20 μM (Figure 45).

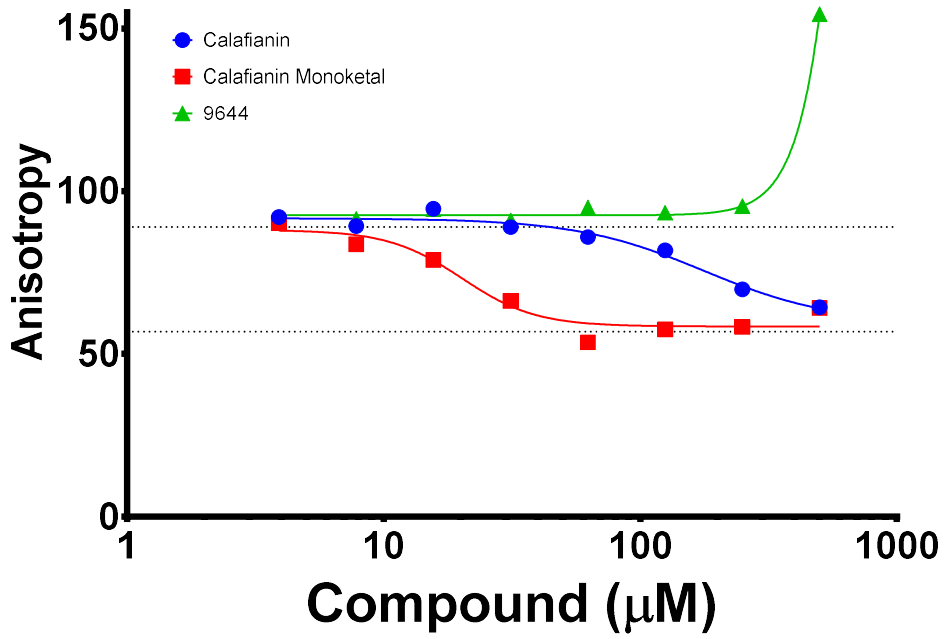

Figure 45: Dose response results for 9644 and precursors. The natural product precursor to 9644, Calafianin, as well as a mono-ketal protected version, showed dose-dependent inhibition of NEMO-IKKβ binding, whereas 9644 showed an increase in anisotropy that is likely the result of insolubility. Dashed lines indicate high (NEMO + IKKβ) and low (IKKβ alone) controls.

A set of 800 macrocycles from Asinex Corporation were selected by the CMD out of 80,000 for structural diversity and predicted aqueous solubility, and were screened in the NEMO-IKKβ FA assay (Set 6) at 30 μM in 10% v/v DMSO. Seven hits showed greater than 50% inhibition with acceptable solubility, but none replicated in a dose-response assay at concentrations up to 100 μM (Figure 46).

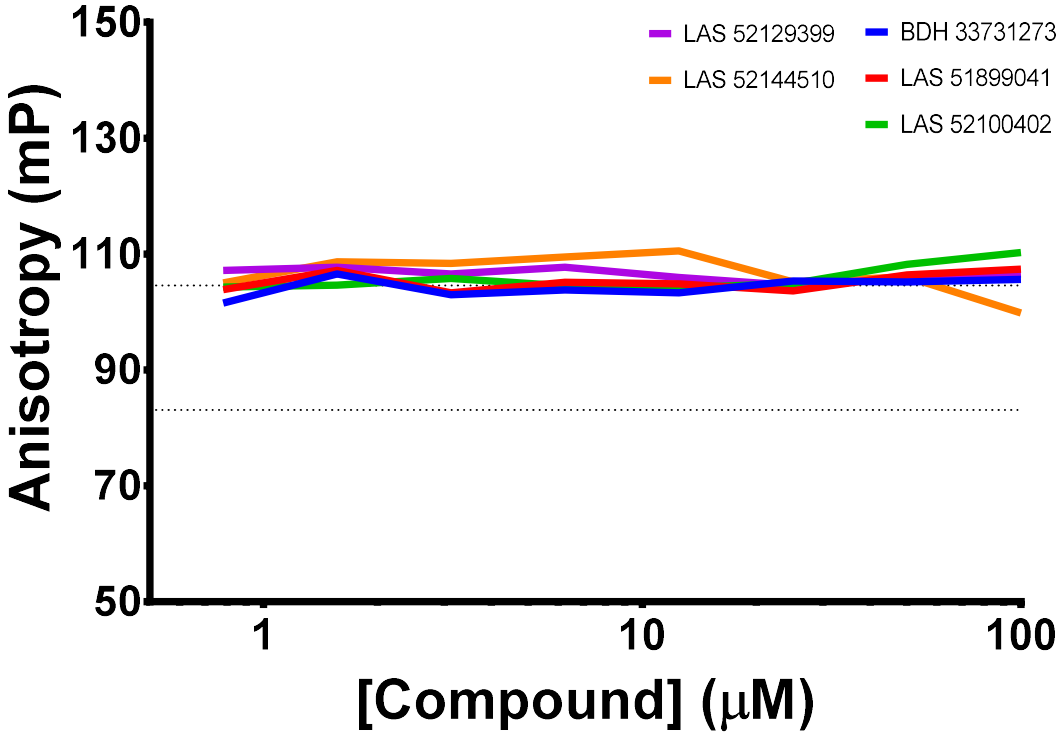

Figure 46: Dose response results of Asinex macrocycle hits. None showed significant inhibition up to 100 μM. Dashed lines indicate high (NEMO + IKKβ) and low (IKKβ alone) controls.

4.3.3 Secondary Validation of Small-Molecule Hits

Attempts were made to validate 10190 first because of its promising IC_{50} and solubility. To determine inhibition specificity, the Keap1-Nrf2 FA assay was used in a dose-response format. No significant inhibition was observed at concentrations of 10190 up to 100 μM. However, 10190 then failed the next two validation tests. SPR was used to test for direct binding of 10190 to NEMO (assay performed by Dan Petrescu). However, superstoichiometric binding was

observed, indicating large nonspecific aggregates of the compound bound to the surface of the chip, causing a large increase in signal disproportionate to the mass of the protein and compound. The second test was a co-immunoprecipitation assay performed by the Gilmore group. The goal was to determine whether 10190 could block Co-IP of NEMO and IKKβ from 293 cells following treatment with DMSO or varying concentrations of 10190. Not only was there no sign of inhibition of binding, but there were seemingly no effects on the cells; this led to the conclusion that 10190 is likely not cell permeable. It is also possible that 10190 has insufficient affinity for NEMO to overcome macromolecular crowding effects, which would be manifested in a lack of activity in cells.

To seek a variant of this chemotype that has activity in the cellular assays, the focus turned to the more-potent compounds 10487 and 10557 described above from Set 2. First, the compounds were analyzed for direct binding to NEMO in SPR. Compound 10557 shows direct binding to NEMO as determined by reversible binding and signal (RU) proportional to the mass of the compound (10557 shown in Figure 47). However, 10487 appeared to have a higher than expected signal, with signs of possible reversible covalent binding or otherwise unexpectedly slow dissociation kinetics. This is evident by linear binding

behavior with a sharp slope during the association phase and shallow slope during the dissociation phase. Because of these potential complications, and the fact that 10557 showed reversible stoichiometric binding, 10557 alone was continued for further validation.

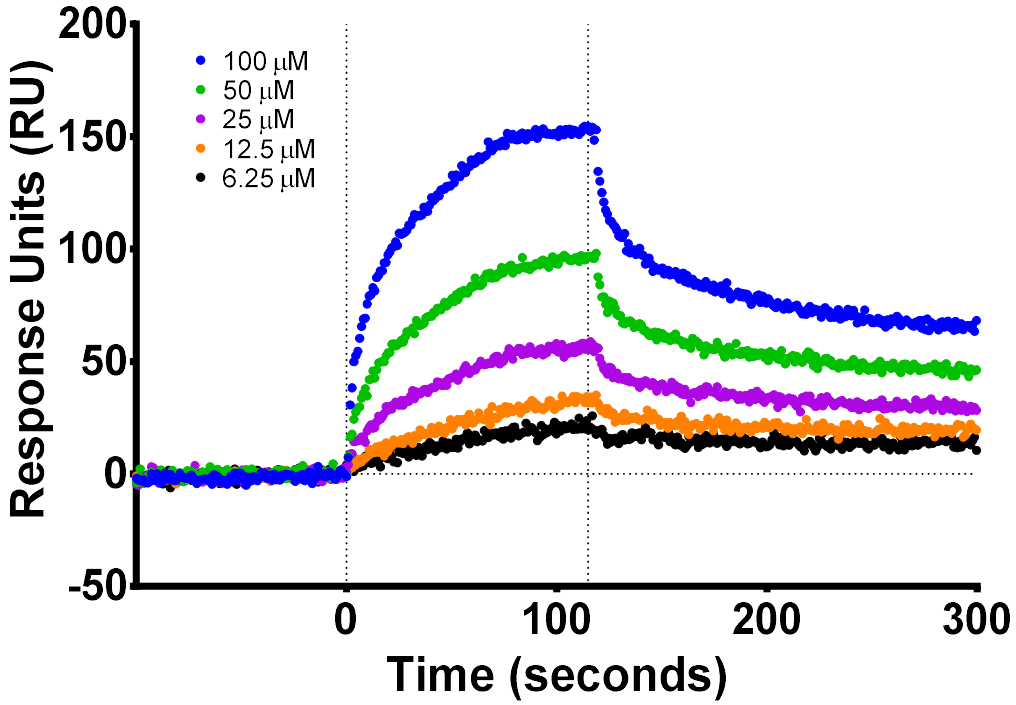

Figure 47: SPR results for 10557 binding to 7xAla-NEMO. 7xAla was thiol-coupled to the surface of the chip and two-fold serial dilutions of 10557 were flowed over the surface. Vertical lines indicate start (left) and end (right) of 10557 injection. Concentration of 10557 shown in legend in upper left corner of plot.

The second validation test for 10557 was for inhibition of the NEMO-IKKβ interaction in cell lysate, performed by the Gilmore group. Here, cells were treated with either 10557 or DMSO, and lysed. NEMO was then immunoprecipitated from the lysate, and a Western blot was used to probe for

co-immunoprecipitated IKKβ. As shown in Figure 48, the resultant Western blot appears to show decreasing IKKβ pull down with increasing concentrations of 10557, a sign of inhibition. However, there is a faint band detected by the anti-IKKβ antibody at a higher-than-expected molecular weight that appears in the presence of 10557. The faint band is not high enough to indicate an oligomer, but may instead be indicative of formation of a covalent adduct between 10557 and IKKβ. However, the formation of a covalent adduct is inconsistent with the SPR data that showed reversible noncovalent interaction between 10557 and NEMO. Thus, the only plausible mechanism for covalent adduct formation is through a specific interaction between 10557 and IKKβ, which seems unlikely.

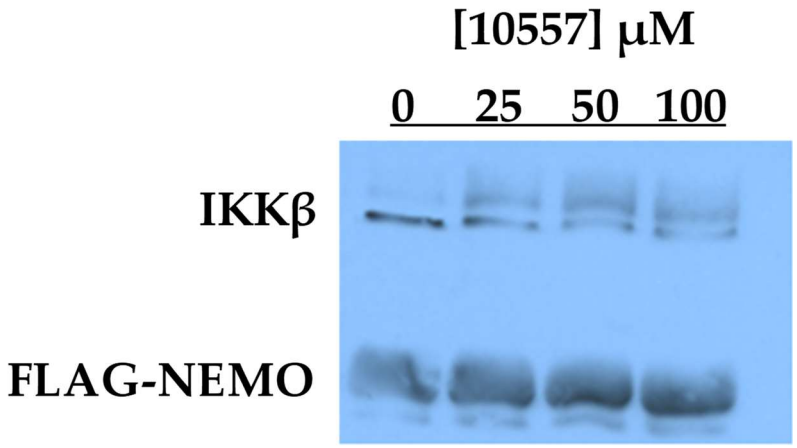

Figure 48: Cells that express IKKβ and FLAG-NEMO were lysed and treated with indicated concentrations of 10557. Beads were then added that were coated with an anti-FLAG antibody, and were pelleted by centrifugation. The pellets were resuspended and denatured with SDS running buffer to dissociate bound protein, and run on SDS-PAGE before Western blotting. Detection was with an anti-IKKβ antibody (IKKβ) or anti-FLAG antibody (NEMO).

4.3.4 *Properties of Hit: CMLD10557*

To determine a theoretical binding pose, 10557 was computationally docked into the crystal structure of NEMO(44-111)[28] using AutoDock Vina[192]. The resulting pose is displayed in Figure 49, which was created using UCSF Chimera[129]. In the docking procedure, the IKKβ chains in the structure were removed, leaving the IKKβ-binding site in the NEMO dimer open for ligand binding. The binding pose shown suggests that the bulk of the compound occupies a hydrophobic pocket that, in the liganded complex, accommodates hot spot residues W739 and W741 of IKKβ. Therefore, 10557 is likely a competitive inhibitor of IKKβ, competing for the same binding site. Notably, and perhaps predictably, AutoDock Vina docked 10557 into the top binding energy hot spot as determined by FTMap and alanine-scanning mutagenesis[104].

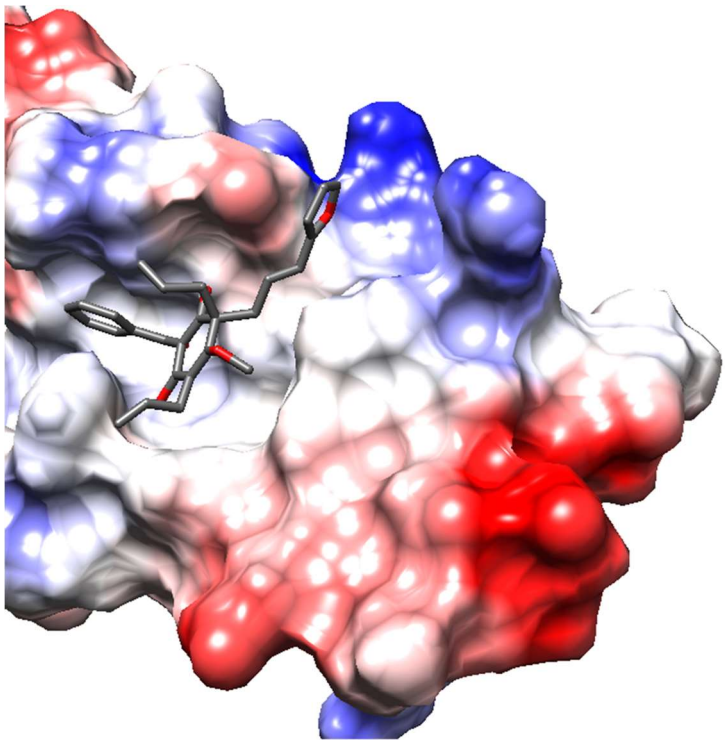

Figure 49: Compound 10557 was computationally docked into the NEMO(44-111) structure with ligand removed using AutoDock Vina and displayed in UCSF Chimera. The surface of NEMO is colored as an electrostatic map; red indicates negatively charged surface, blue positively charged surface. White indicates neutral or

Table 6: Key properties of compound 10557.

Property	**Value**
cLogP[a]	3.67
TPSA[b]	76.74
MW[c]	430.5
H-bond[d] acceptors	5
H-bond donors	1
# rotatable bonds	10

[a]cLogP, octanol-water partition coefficient; [b]TPSA, topological polar surface area; [c]MW, molecular weight; [d]H-bond, hydrogen bond.

Drug-like properties were determined for 10557 for further

characterization. Solubility has been addressed in Section 4.3.2; in an aqueous environment, an inhibitor should be soluble at > 100 μM, > 10-times above IC_{50}. Physicochemical properties have classically been indicative of drug-likeness, despite numerous exceptions and extensions to this idea[166,193–196]. These key properties are outlined in Table 6 and were calculated using Molinspiration[193,195,197].

Compound 10557 falls within each tenet of Lipinski's Rule of 5[193], which would be remarkable for a therapeutic PPI inhibitor given the aforementioned difficulties in blocking a large interaction interface. Notably, the ligand efficiency (LE), or binding energy contribution from each heavy atom, is 0.23 kcal/mol. A typical Lipinski-compliant[193] small molecule target for LE is 0.3 kcal/mol[168]; it is expected that 10557 is below this target value with μM affinity, versus drug-like affinities typically in the lower, single-digit nM range. Additionally, 10557 is predicted to have good oral bioavailability due to the number of rotatable bonds being <10 and the polar surface area being <140 $Å^2$ [195]. Due to the theoretical binding pose at the major IKKβ binding energy hot spot and the acceptable physicochemical properties, 10557 appears to be a practical candidate for further study as a NEMO-IKKβ interaction inhibitor.

4.4 Conclusions and Future Directions

A previous study showed that small-molecule inhibitor of the NEMO-IKKβ interaction inhibits cellular NF-κB signaling, and was computationally docked into the X-ray crystal structure of the NEMO-IKKβ binding interface[84]. However, no mechanistic studies were performed, so the precise target of the small molecule is unknown. A cell-permeant version of the NBD 11-mer peptide has been shown to disrupt the NEMO/IKKβ complex *in vivo*, and causes a specific biological outcome that attenuates activation of NF-κB but does not affect basal NF-κB function[85,86]. The NBD peptide has also been shown to attenuate tumor proliferation and prolonged mouse survival in a malignant glioma mouse line[88]. A synthetic loop replacement version of the NBD, in which a conserved hydrogen bond was replaced with a covalent hydrocarbon bridge to enhance rigidity, has been shown to be 10-fold more potent in blocking NEMO-mediated NF-κB signaling than wild-type NBD peptide[89], and may prove to be a worthwhile strategy for further optimizing the NBD peptide for therapeutic use. Other than the synthetic loop replacement strategy for utilization of the NBD peptide for NEMO inhibition, the literature has not shown any mechanistic studies of a small molecule or stable (i.e., non-peptide) potential therapeutic to treat NEMO-related human disease. The work performed in this chapter was

aimed at addressing this shortcoming.

A small number of the macrocyclic compounds tested showed initial activity as inhibitors of NEMO-IKKβ binding. The initial hit rate was similar to that of typical small molecule inhibitor screens, <5%, but none were validated in a dose-response assay. Improvements in computational screening will allow for selection of macrocycles with a higher chance of success in the future. This, coupled with improvements in macrocycle synthesis methods, will allow for better rational macrocycle library design for inhibition of protein-protein interactions. Additionally, an increased knowledge of how macrocycles bind in grooves, such as the groove in NEMO to which IKKβ binds, will afford a better chance of success in these endeavors.

Compound 10190 was identified as a hit from an initial screen of the CMD collection after it passed dose-response validation and an initial solubility screen. The compound failed in an SPR orthogonal assay, however, that clearly showed signs of superstoichiometric binding typically observed with aggregation-prone compounds. Additionally, it did not show any signs of inhibition or toxicity in cells, so it may not have been cell-permeable. It is also possible that the compound has insufficient affinity for NEMO to overcome the effects of macromolecular crowding that decreases the apparent inhibition activity in a

crowded environment, which would also explain the lack of activity in cells.

More soluble analogs of 10190 were subsequently assayed for dose response, and one compound emerged as both highly soluble and displayed a better IC_{50} than its parent compound. This compound, 10557, was verified by SPR to bind directly to NEMO in a stoichiometric manner, and appeared to block NEMO-IKKβ co-IP in cell lysate, though there are some technical concerns with that result due to the faint bands at slightly higher molecular weight that cannot be due to oligomerization. Physicochemical properties of this compound fall within Lipinski's Rule of 5, and a reasonable docked pose on the NEMO 44-111 structure are shown above in section 4.3.4.

Further tests are necessary to determine whether the molecule 10557 represents a useful starting point for a potential therapeutic NEMO inhibitor. Orthogonal FA assays would be useful to determine inhibition specificity. Cell permeability assays, such as PAMPA[198] or Caco-2[199], would determine whether this compound is able to cross the cell membrane to block NF-κB signaling in the cytoplasm. In parallel artificial membrane permeability (PAMPA) assays, mass spectroscopy is used to determine whether the analyte has crossed from a donor compartment to an acceptor compartment through an artificial membrane that simulates a cell membrane. The Caco-2 cell line is a contiguous layer of

heterogenous human epithelial colorectal adenocarcinoma cells commonly used as an *in vitro* model to predict absorption of oral drugs. It is becoming less commonly used than PAMPA due to divergent characteristics of the cells following different passage protocols. Signaling assays *in vivo* such as whether the compound can block propagation of NF-κB signaling as discussed above would be the most direct way of assessing the potential of this hit for disrupting biological function. Similar assays have been performed by the Gilmore group (i.e. for 10190). Direct binding has been shown by SPR, but 2D NMR experiments would allow mapping of the binding site on NEMO. Such an approach could be useful to elucidate the structural determinants for binding, which would aid SAR studies to improve the potency of the compound.

From these results and previous work in the lab[155], the NEMO-IKKβ binding site can likely be targeted with small molecule inhibitors. One group reported a NEMO-IKKβ inhibitor, but did not provide evidence that the molecule actually targeted this interaction. It remains to be seen whether macrocycles can be used as well, but there exists a starting point for rational inhibitor design that has strong therapeutic potential.

Appendices

Appendix I) Primers Used for Cloning

Construct	Use	Direction	Sequence
9SG NEMO	Mutation	Forward	TGGGTCTGGGTCTCAGGAGAGCCAGAGTCGC
	pET24b(+)	Reverse	GACCCAGACCCAGAGGCTTTCACAGAGGCCTTG
L153R NEMO	Mutation	Forward	CTCGGGGAGCGGCAGGAGAGC
	pET24b(+)	Reverse	CAAGGACGTCACCTGGGC
44-195 NEMO	Cloning	Forward	TATACATATGCAGGGTGCACCGG
	SUMOstar	Reverse	GTGCTCGAGATGCTGCTGCTG
44-195 I71M	Mutation	Forward	GTAATCAGATGCTGCGTGAAC
	SUMOstar	Reverse	TCTGGCGAATCGCATCAC
110-195 NEMO	Cloning	Forward	TATACATATGGAAAAACTGGATCTGAAAC
	SUMOstar	Reverse	GTGCTCGAGATGCTGCTGCTG
ΔN NEMO	Cloning	Forward	ATGGCCAAGTTCCAGGAG
	Del 1-100	Reverse	ATGTATATCTCCTTCTTAAAGTTAAAC
ΔC NEMO	Cloning	Forward	CACCACCACCACCACCACTG
	Del 384-419	Reverse	AGGTGGCTCCTCGGG
E57K NEMO	Mutation	Forward	CAGCGCGCCCTGGAGAAAAATCAAGAGCTCCGA
	E57K	Reverse	TCGGAGCTCTTGATTTTTCTCCAGGGCGCGCTG
L80P NEMO	Mutation	Forward	GCCGAGGAGCTTCCGCATTTCCAAGCCA
	L80P	Reverse	TGGCTTGGAAATGCGGAAGCTCCTCGGC
D113N NEMO	Mutation	Forward	GGGTCTGGAAAAACTGAATCTGAAACGTCAG
	D113N	Reverse	CTGACGTTTCAGATTCAGTTTTTCCAGACCC
R123W NEMO	Mutation	Forward	AGCAGGCTCTGTGGGAGGTGGAGCA
	R123W	Reverse	TGCTCCACCTCCCACAGAGCCTGCT
IκBα	Cloning	Forward	GAGAACCTGTACTTTCAGGGTAGCGGTATGTTCCAGGCGGCCGAG
	pDEST-42	Reverse	CTCTTGGACATGAAAGCCCACGCCTTATCATAACGTCAGACGCTGGCC

Appendix II) Protein Sequences of NEMO Constructs

```
CLUSTAL W 2.0 multiple sequence alignment

WT_NEMO         MNRHLWKSQLCEMVQPSGGPAADQDVLGEESPLGKPAMLHLPSEQGAPETLQRCLEENQE 60
7xAla           MNRHLWKSQLAEMVQPSGGPAADQDVLGEESPLGKPAMLHLPSEQGAPETLQRALEENQE 60
5xAla           MNRHLWKSQLAEMVQPSGGPAADQDVLGEESPLGKPAMLHLPSEQGAPETLQRCLEENQE 60
9SG             MNRHLWKSQLAEMVQPSGGPAADQDVLGEESPLGKPAMLHLPSEQGAPETLQRALEENQE 60
E57K            MNRHLWKSQLAEMVQPSGGPAADQDVLGEESPLGKPAMLHLPSEQGAPETLQRALEKNQE 60
L80P            MNRHLWKSQLAEMVQPSGGPAADQDVLGEESPLGKPAMLHLPSEQGAPETLQRALEENQE 60
D113N           MNRHLWKSQLAEMVQPSGGPAADQDVLGEESPLGKPAMLHLPSEQGAPETLQRALEENQE 60
R123W           MNRHLWKSQLAEMVQPSGGPAADQDVLGEESPLGKPAMLHLPSEQGAPETLQRALEENQE 60
L153R           MNRHLWKSQLAEMVQPSGGPAADQDVLGEESPLGKPAMLHLPSEQGAPETLQRALEENQE 60
dC25            MNRHLWKSQLAEMVQPSGGPAADQDVLGEESPLGKPAMLHLPSEQGAPETLQRALEENQE 60
dN100           ------------------------------------------------------------ 60
44-195          ---------------------------------------------QGAPETLQRCLEENQE 60
44-195_I71M     ---------------------------------------------QGAPETLQRCLEENQE 60
44-111          ---------------------------------------------QGAPETLQRCLEENQE 60


WT_NEMO         LRDAIRQSNQILRERCEELLHFQASQREEKEFLMCKFQEARKLVERLGLEKLDLKRQKEQ 120
7xAla           LRDAIRQSNQILRERAEELLHFQASQREEKEFLMAKFQEARKLVERLGLEKLDLKRQKEQ 120
5xAla           LRDAIRQSNQILRERAEELLHFQASQREEKEFLMAKFQEARKLVERLGLEKLDLKRQKEQ 120
9SG             LRDAIRQSNQILRERAEELLHFQASQREEKEFLMAKFQEARKLVERLGLEKLDLKRQKEQ 120
E57K            LRDAIRQSNQILRERAEELLHFQASQREEKEFLMAKFQEARKLVERLGLEKLDLKRQKEQ 120
L80P            LRDAIRQSNQILRERAEELPHFQASQREEKEFLMAKFQEARKLVERLGLEKLDLKRQKEQ 120
D113N           LRDAIRQSNQILRERAEELLHFQASQREEKEFLMAKFQEARKLVERLGLEKLNLKRQKEQ 120
R123W           LRDAIRQSNQILRERAEELLHFQASQREEKEFLMAKFQEARKLVERLGLEKLDLKRQKEQ 120
L153R           LRDAIRQSNQILRERAEELLHFQASQREEKEFLMAKFQEARKLVERLGLEKLDLKRQKEQ 120
dC25            LRDAIRQSNQILRERAEELLHFQASQREEKEFLMAKFQEARKLVERLGLEKLDLKRQKEQ 120
dN100           ---------------------------------------ARKLVERLGLEKLDLKRQKEQ 120
44-195          LRDAIRQSNQILRERAEELLHFQASQREEKEFLMAKFQEARKLVERLGLEKLDLKRQKEQ 120
44-195_I71M     LRDAIRQSNQMLRERAEELLHFQASQREEKEFLMAKFQEARKLVERLGLEKLDLKRQKEQ 120
44-111          LRDAIRQSNQILRERAEELLHFQASQREEKEFLMAKFQEARKLVERLGLE---------- 120
                                                   ***********

WT_NEMO         ALREVEHLKRCQQQMAEDKASVKAQVTSLLGELQESQSRLEAATKECQALEGRARAASEQ 180
7xAla           ALREVEHLKRAQQQMAEDKASVKAQVTSLLGELQESQSRLEAATKEAQALEGRARAASEQ 180
5xAla           ALREVEHLKRAQQQMAEDKASVKAQVTSLLGELQESQSRLEAATKEAQALEGRARAASEQ 180
9SG             ALREVEHLKRAQQQMAEDKASVKASGSGSGSGSQESQSRLEAATKEAQALEGRARAASEQ 180
E57K            ALREVEHLKRAQQQMAEDKASVKAQVTSLLGELQESQSRLEAATKEAQALEGRARAASEQ 180
L80P            ALREVEHLKRAQQQMAEDKASVKAQVTSLLGELQESQSRLEAATKEAQALEGRARAASEQ 180
D113N           ALREVEHLKRAQQQMAEDKASVKAQVTSLLGELQESQSRLEAATKEAQALEGRARAASEQ 180
R123W           ALWEVEHLKRAQQQMAEDKASVKAQVTSLLGELQESQSRLEAATKEAQALEGRARAASEQ 180
L153R           ALREVEHLKRAQQQMAEDKASVKAQVTSLLGERQESQSRLEAATKEAQALEGRARAASEQ 180
dC25            ALREVEHLKRAQQQMAEDKASVKAQVTSLLGELQESQSRLEAATKEAQALEGRARAASEQ 180
dN100           ALREVEHLKRAQQQMAEDKASVKAQVTSLLGELQESQSRLEAATKEAQALEGRARAASEQ 180
44-195          ALREVEHLKRAQQQMAEDKASVKAQVTSLLGELQESQSRLEAATKEAQALEGRARAASEQ 180
44-195_I71M     ALREVEHLKRAQQQMAEDKASVKAQVTSLLGELQESQSRLEAATKEAQALEGRARAASEQ 180
44-111          ------------------------------------------------------------ 180


WT_NEMO         ARQLESEREALQQQHSVQVDQLRMQGQSVEAALRMERQAASEEKRKLAQLQVAYHQLFQE 240
7xAla           ARQLESEREALQQQHSVQVDQLRMQGQSVEAALRMERQAASEEKRKLAQLQVAYHQLFQE 240
5xAla           ARQLESEREALQQQHSVQVDQLRMQGQSVEAALRMERQAASEEKRKLAQLQVAYHQLFQE 240
9SG             ARQLESEREALQQQHSVQVDQLRMQGQSVEAALRMERQAASEEKRKLAQLQVAYHQLFQE 240
E57K            ARQLESEREALQQQHSVQVDQLRMQGQSVEAALRMERQAASEEKRKLAQLQVAYHQLFQE 240
L80P            ARQLESEREALQQQHSVQVDQLRMQGQSVEAALRMERQAASEEKRKLAQLQVAYHQLFQE 240
D113N           ARQLESEREALQQQHSVQVDQLRMQGQSVEAALRMERQAASEEKRKLAQLQVAYHQLFQE 240
```

```
R123W          ARQLESEREALQQQHSVQVDQLRMQGQSVEAALRMERQAASEEKRKLAQLQVAYHQLFQE 240
L153R          ARQLESEREALQQQHSVQVDQLRMQGQSVEAALRMERQAASEEKRKLAQLQVAYHQLFQE 240
dC25           ARQLESEREALQQQHSVQVDQLRMQGQSVEAALRMERQAASEEKRKLAQLQVAYHQLFQE 240
dN100          ARQLESEREALQQQHSVQVDQLRMQGQSVEAALRMERQAASEEKRKLAQLQVAYHQLFQE 240
44-195         ARQLESEREALQQQH--------------------------------------------- 240
44-195_I71M    ARQLESEREALQQQH--------------------------------------------- 240
44-111         ------------------------------------------------------------ 240

WT_NEMO        YDNHIKSSVVGSERKRGMQLEDLKQQLQQAEEALVAKQEVIDKLKEEAEQHKIVMETVPV 300
7xAla          YDNHIKSSVVGSERKRGMQLEDLKQQLQQAEEALVAKQEVIDKLKEEAEQHKIVMETVPV 300
5xAla          YDNHIKSSVVGSERKRGMQLEDLKQQLQQAEEALVAKQEVIDKLKEEAEQHKIVMETVPV 300
9SG            YDNHIKSSVVGSERKRGMQLEDLKQQLQQAEEALVAKQEVIDKLKEEAEQHKIVMETVPV 300
E57K           YDNHIKSSVVGSERKRGMQLEDLKQQLQQAEEALVAKQEVIDKLKEEAEQHKIVMETVPV 300
L80P           YDNHIKSSVVGSERKRGMQLEDLKQQLQQAEEALVAKQEVIDKLKEEAEQHKIVMETVPV 300
D113N          YDNHIKSSVVGSERKRGMQLEDLKQQLQQAEEALVAKQEVIDKLKEEAEQHKIVMETVPV 300
R123W          YDNHIKSSVVGSERKRGMQLEDLKQQLQQAEEALVAKQEVIDKLKEEAEQHKIVMETVPV 300
L153R          YDNHIKSSVVGSERKRGMQLEDLKQQLQQAEEALVAKQEVIDKLKEEAEQHKIVMETVPV 300
dC25           YDNHIKSSVVGSERKRGMQLEDLKQQLQQAEEALVAKQEVIDKLKEEAEQHKIVMETVPV 300
dN100          YDNHIKSSVVGSERKRGMQLEDLKQQLQQAEEALVAKQEVIDKLKEEAEQHKIVMETVPV 300
44-195         ------------------------------------------------------------ 300
44-195_I71M    ------------------------------------------------------------ 300
44-111         ------------------------------------------------------------ 300

WT_NEMO        LKAQADIYKADFQAERQAREKLAEKKELLQEQLEQLQREYSKLKASCQESARIEDMRKRH 360
7xAla          LKAQADIYKADFQAERQAREKLAEKKELLQEQLEQLQREYSKLKASAQESARIEDMRKRH 360
5xAla          LKAQADIYKADFQAERQAREKLAEKKELLQEQLEQLQREYSKLKASCQESARIEDMRKRH 360
9SG            LKAQADIYKADFQAERQAREKLAEKKELLQEQLEQLQREYSKLKASAQESARIEDMRKRH 360
E57K           LKAQADIYKADFQAERQAREKLAEKKELLQEQLEQLQREYSKLKASAQESARIEDMRKRH 360
L80P           LKAQADIYKADFQAERQAREKLAEKKELLQEQLEQLQREYSKLKASAQESARIEDMRKRH 360
D113N          LKAQADIYKADFQAERQAREKLAEKKELLQEQLEQLQREYSKLKASAQESARIEDMRKRH 360
R123W          LKAQADIYKADFQAERQAREKLAEKKELLQEQLEQLQREYSKLKASAQESARIEDMRKRH 360
L153R          LKAQADIYKADFQAERQAREKLAEKKELLQEQLEQLQREYSKLKASAQESARIEDMRKRH 360
dC25           LKAQADIYKADFQAERQAREKLAEKKELLQEQLEQLQREYSKLKASAQESARIEDMRKRH 360
dN100          LKAQADIYKADFQAERQAREKLAEKKELLQEQLEQLQREYSKLKASAQESARIEDMRKRH 360
44-195         ------------------------------------------------------------ 360
44-195_I71M    ------------------------------------------------------------ 360
44-111         ------------------------------------------------------------ 360

WT_NEMO        VEVSQAPLPPAPAYLSSPLALPSQRRSPPEESSDFCCPKCQYQAPDMDTLQIHVMECIE 419
7xAla          VEVSQAPLPPAPAYLSSPLALPSQRRSPPEESSDFCCPKCQYQAPDMDTLQIHVMECIE 419
5xAla          VEVSQAPLPPAPAYLSSPLALPSQRRSPPEESSDFCCPKCQYQAPDMDTLQIHVMECIE 419
9SG            VEVSQAPLPPAPAYLSSPLALPSQRRSPPEESSDFCCPKCQYQAPDMDTLQIHVMECIE 419
E57K           VEVSQAPLPPAPAYLSSPLALPSQRRSPPEESSDFCCPKCQYQAPDMDTLQIHVMECIE 419
L80P           VEVSQAPLPPAPAYLSSPLALPSQRRSPPEESSDFCCPKCQYQAPDMDTLQIHVMECIE 419
D113N          VEVSQAPLPPAPAYLSSPLALPSQRRSPPEESSDFCCPKCQYQAPDMDTLQIHVMECIE 419
R123W          VEVSQAPLPPAPAYLSSPLALPSQRRSPPEESSDFCCPKCQYQAPDMDTLQIHVMECIE 419
L153R          VEVSQAPLPPAPAYLSSPLALPSQRRSPPEESSDFCCPKCQYQAPDMDTLQIHVMECIE 419
dC25           VEVSQAPLPPAPAYLSSPLALPSQRRSPPEESSD-------------------------- 419
dN100          VEVSQAPLPPAPAYLSSPLALPSQRRSPPEESSDFCCPKCQYQAPDMDTLQIHVMECIE 419
44-195         ------------------------------------------------------------ 419
44-195_I71M    ------------------------------------------------------------ 419
44-111         ------------------------------------------------------------ 419
```

Appendix III) Linear Di-Ubiquitin has no Effect on 5xAla-IKKβ Binding in Fluorescence Anisotropy

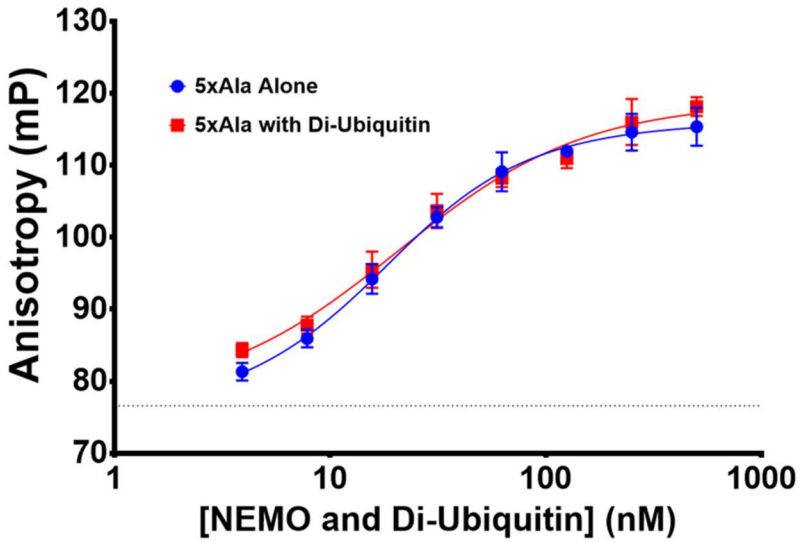

Appendix Figure 1: Titration of 5xAla and 10-fold molar excess of M1-linked di-ubiquitin with constant 15 nM FITC-IKKβ has no significant effect on fluorescence anisotropy compared to 5xAla alone with FITC-IKKβ (n=3 each).

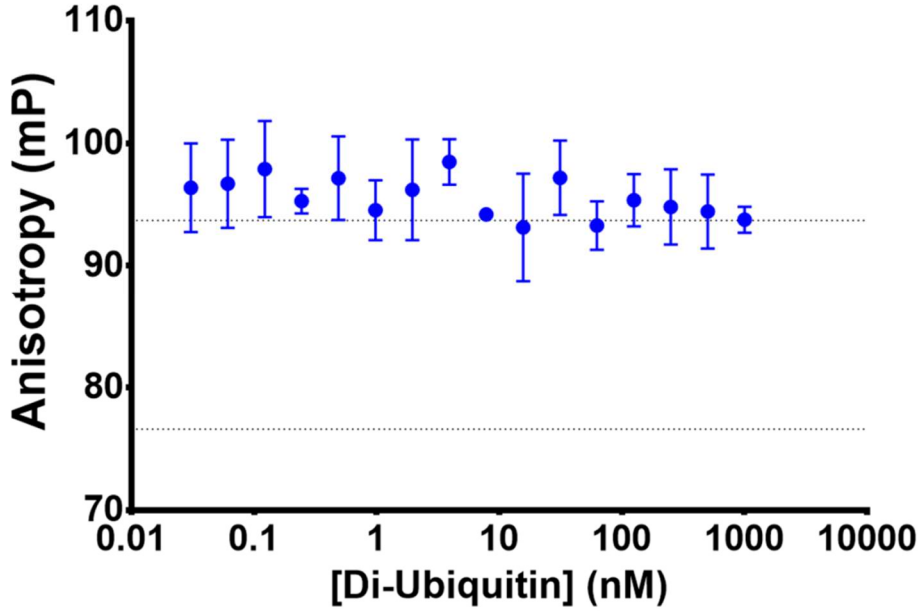

Appendix Figure 2: Titration of M1-linked di-ubiquitin with constant 15 nM each 5xAla and FITC-IKKβ has no significant effect on fluorescence anisotropy (n=3 each).

Appendix IV) Redox CD and SDS-PAGE Experiments with 5xAla, 7xAla, and WT NEMO

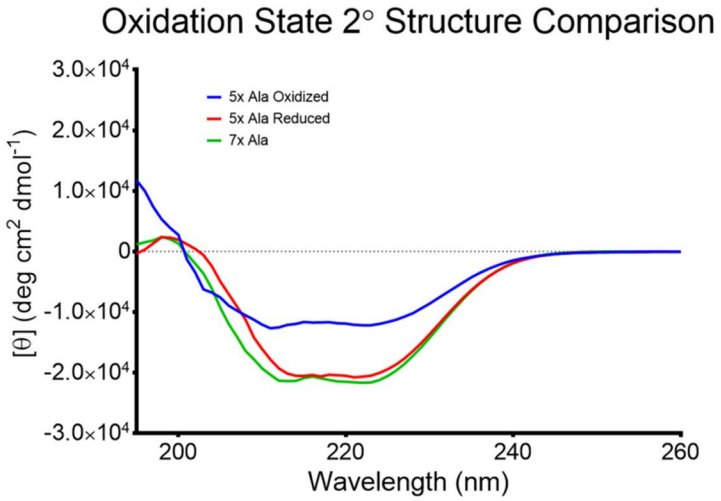

Appendix Figure 3: Comparison of CD spectra for 5xAla oxidized, reduced, and 7xAla to compare effect of disulfide bond formation on secondary structure.

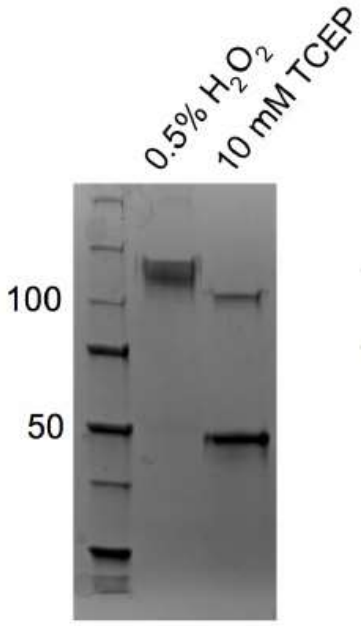

Appendix Figure 4: SDS-PAGE of oxidized (0.5% H_2O_2) versus reduced (10 mM TCEP) 5xAla protein. MW standards on left side are in units of kDa.

Appendix V) NEMO MSA and IκBα MSA

NEMO MSA:

```
                                        1         10        20            30
Heterocephalus_glaber        ...............MSRHPWKSQLCEMVQPSGGPAGDQDVLG...EESSLG...
Cavia_porcellus              ...............MSKHPWKSQLCEMVQPGSGPAGDQDMLG...EESPLG...
Mesocricetus_auratus         ...............MSRHLWKNQLSEMVQPSGGPAGDQDMQG...EESSLG...
Mus_musculus                 ...............MNKHPWKNQLSEMVQPSGGPAEDQDMLG...EESSLG...
Rattus_norvegicus            ...............MSRHLWKNQLSEMVQPSGGPAEDQDMLG...EESSLG...
Bos_taurus                   ...............MSRPPWKSPLCEMVQPSGSPAGDQDMLG...EESSLG...
Tarsius_syrichta             ...............MSRHPWKSRPCEMVQPSGGPAADQDDLG...EESSPG...
Oryctolagus_cuniculus        ...............MSRQPWKNQLCEMVQPSGGPAGDQDVLP...EESSLG...
Lipotes_vexillifer           ...............MSRPPWKSPLYEMVQPSGGPAGDQDVLG...EESSLG...
Otolemur_garnettii           ...............MNRLLWKNQLCDMVQPSCGLAGEQDMLG...EESSLG...
Sus_scrofa                   ...............MSRTPWKSQPCEMVQPSGGPAGDQDVLG...EESSLG...
Rhinolophus_ferrumequinum    ...............MSGPPWKSQLCEMVQPSGGPAGDQDVLG...EESSLG...
Saimiri_boliviensis          KARASWKRAPWPCCRSRHLWKSQSCEMVQPSGGPAAGHDVLR...EESPLG...
Homo_Sapiens                 ...............MNRHLWKSQLCEMVQPSGGPAADQDVLG...EESPLG...
Pongo_abelii                 ...............MSRHLWKSQLCEMVQPSGGPAADQDVLG...EDSPLG...
Macaca_mulatta               ...............MSRHLWKSQLCEMVQPSGGPAADQDVLG...EESPLG...
Macaca_fascicularis          KARAFWKGAPLPCWMSRHLWKSQLCEMVQPSGGPAADQDVLG...EESPLG...
Chlorocebus_sabaeus          .........PLPCWMSRHLWKSQLCEMVQPSGGPAADQDVLG...EESPLG...
Papio_anubis                 ...............MSRHLWKSQLCEMVQPSGGPAADQDVLG...EESPLG...
Callithrix_jacchus           ...............MSRHLWKSQLCEMVQPSGGPAADQDVLG...EESPLG...
Callicebus_moloch            ...............MSRHLWKSQLCEMVQPGGGPAADQDVLG...EESPVG...
Canis_lupus_familiaris       ...............MSRAPWKSQPSEMVQPSGGPAGDQDVLG...EESSLG...
Equus_caballus               ...............MSRPPWKSQLCEMVQPSGGPAGDQDVLG...EESSLG...
Felis_catus                  ...............MSRPPWKSQLCEMVQPSGGPAGDQDVLG...EESSLG...
Ailuropoda_melanoleuca       ...............MSRPPWKSQLCEMVQPSGGPAGDQDVLG...EESSLG...
Odobenus_rosmarus_divergens  ...............MSRPSWKSQPCEMVQPSGGPAGDQDVLG...EESSLG...
Leptonychotes_weddellii      ...............MSRPPWKSQPCEMVQPSGGPAGDQDVLG...EEPSLG...
Drosophila_melanogaster      ..........MSDEESFVILGSSPCSSLMPDS..SLRSDVCG...NAQEAKETV
Pelodiscus_sinensis          ................MNGTRQRRSCEMVQPGGCPGSDCSALG...EDSSLG...
Anolis_carolinensis          ..............................................MMG...DDSSLG...
Xenopus_tropicalis           ...........................MVQPKESSAAEYNPCEGGPGDTSLG...
Latimeria_chalumnae          ................MSLDRATPIHKMVQPSGSLRNECDMNS...GGSSLG...
Oreochromis_niloticus        ...........................MVQPQPDG..PMQWEMSG...EESGAT...
Gasterosteus_aculeatus       ..............................................................
Oryzias_latipes              ..............................................................
Xiphophorus_maculatus        ...........................MVQPQPDG..PMQWDMSG...EDSGGT...
Danio_rerio                  ...........................MVQPQPSGGCTLQYELNG...EETAGSEGQ
Takifugu_rubripes            ...........................MVQPQPEG..PMQWDMSA...DESG.....
```

```
                                         40        50        60        70        80
Heterocephalus_glaber          ......KPAMLQLRAEQGSPEALQRCLEENHELRDAIRQSNQMLRERCEELLHF
Cavia_porcellus                ......KPAMLQLQVEQGSPEALQHCLEENHELRDAIRQNNQMLRERCEELLHF
Mesocricetus_auratus           ......KPAMLQLPSEQGTPETFQRCLEENQELRDAIRQSNQMLRERCKELLHF
Mus_musculus                   ......KPAMLHLPSEQGTPETLQRCLEENQELRDAIRQSNQMLRERCEELLHF
Rattus_norvegicus              ......KPAMLHLPSEQGTPETLQRCLEENQELRDAIRQSNQMLRERCEELLHF
Bos_taurus                     ......KPAMLHVPSEQGTPETFQRCLEENQELRDAIRQSNQMLRERCEELQHF
Tarsius_syrichta               ......KPAMLHLPSEQGTPDTLQRSLEENQELRDAIRQSNQMLRERCEELRRF
Oryctolagus_cuniculus          ......KPAMLHLPAEQGAPDALQRCLEENQELRDAIRQSNQMLRERCEELLRF
Lipotes_vexillifer             ......KPAMLHLPSEQAAPETFQRCLEENQELRDAIRQSNQMLRERCEELQRF
Otolemur_garnettii             ......KPAMLHLPSEQGTPETLQRCVEENQELRDAIRQSNQMLRERCEELLHF
Sus_scrofa                     ......KPTMLHLPSEQGAPETFQRCLEENQELRDAIRQSNQMLRERCEELQRF
Rhinolophus_ferrumequinum      ......KPTMLHLPSEQGAPETFQRCLEENQELRDAIRQSNQMLRECCEELQRF
Saimiri_boliviensis            ......KPAMLHLPSEQAAPETLQRCLEENQELRDAIRQSNQMLRERCEELLHF
Homo_Sapiens                   ......KPAMLHLPSEQGAPETLQRCLEENQELRDAIRQSNQILRERCEELLHF
Pongo_abelii                   ......KPAMLHLPSEQGAPETLQRCLEENQELRDAIRQSNQMLRERCEELLHF
Macaca_mulatta                 ......KPAMLHLPSEQGTPETLQRCLEENQELRDAIRQSNQMLRERCEELLHF
Macaca_fascicularis            ......KPAMLHLPSEQGAPETLQRCLEENQELRDAIRQSNQMLRERCEELLHF
Chlorocebus_sabaeus            ......KPAMLHLPSEQGAPETLQRCLEENQELRDAIRQSNQMLRERCEELLHF
Papio_anubis                   ......KPAMLHLPSEQGAPETLQRCLEENQELRDAIRQSNQMLRERCEELLHF
Callithrix_jacchus             ......KQAMLHLPSEQGAPETLQRCLEENQELRDAIRQSNQMLRERCEELLHF
Callicebus_moloch              ......KPAMLHLPSEQGAPETLQRCLEENQELRDAIRQSNQMLRERCEELLHF
Canis_lupus_familiaris         ......KPAMLHLPSEQGTPETYQRCLEENQELRDAIRQSNQMLRERCEELQRF
Equus_caballus                 ......KPAMLHLPSEQGTPETFQRCLEENQELRDAIRQSNQMLRERCEELQHF
Felis_catus                    ......KPAMPHLPSEQGTPETFQRCVEENQELRDAIRQSNQMLRERCEELQRF
Ailuropoda_melanoleuca         ......KPAMLHLPSEQGTPETFQRCLEENQELRDAIRQSNQMLRERCEELQRF
Odobenus_rosmarus_divergens    ......KPAMLHLPSEQGTPESFQRCLEENQELRDAIRQSNQMLRERCEELQRF
Leptonychotes_weddellii        ......KPAMLHVPSEQGTPESFQRCLEENQELRDAIRQSNQMLRERCEELQRF
Drosophila_melanogaster        ASTSTQPPTVNCIPVSITASQQQHKSLDSGSSQQQSLATSFIM.....GEIQSD
Pelodiscus_sinensis            ......KVAAWQLPPELAGHEALQRFLLENQDLKEAIRQSNQMLRQRYQEFVGF
Anolis_carolinensis            ......RDGPLHLPAELAGHEAVQHVLAENRDLKEAIQRSNHMLRERYREFLQF
Xenopus_tropicalis             ......KPEV..LPPELTSNEAFQRIWAENHDLRAALEQSNMMLRKGHGDMLEF
Latimeria_chalumnae            .......SRRPDLPLELNSQEALQRLQAENYDLREAMRQSNLALRERYDELLAF
Oreochromis_niloticus          ..........LRVPPELAANEVVTRLLSDNQQLREALRRSNLALRQRCEEMEGW
Gasterosteus_aculeatus         ..............................................
Oryzias_latipes                ..........MFAPPE.............ALRRSNQALRLRCEEMEGW
Xiphophorus_maculatus          ..........LRVPPELAGNEVVTRLLGDNQQLREALRRSNQALRQRCEEMEGW
Danio_rerio                    VSLMASSQGSLRVPADLAGNEIVQKLITDNHQLREALKRSNDALKERCEEMEGW
Takifugu_rubripes              .......GVLRVPPELAANEVFTRLLSDNQQLRETLRRSNLALRQRCEEMEGW

                                         90        100       110       120
Heterocephalus_glaber          QASQREEKEFIM.CKFQEARKLVERLSL...EKLELRKQKEQAV..........
Cavia_porcellus                QASQKEEREFLM.CKFQEARKLVERLSL...EKLELRRQKEQAL..........
Mesocricetus_auratus           QVSQRKEKEFLM.CKFQEARKLVERLSL...EKLDLQRQREQVL..........
Mus_musculus                   QVSQREEKEFLM.CKFQEARKLVERLSL...EKLDLRSQREQAL..........
Rattus_norvegicus              QVSQREEKEFLM.CKFQEARKLVERLSL...EKLDLRRQREQAL..........
Bos_taurus                     QGNQREEKAFLM.QKFQEARDLVVRLSL...EKRELRQQREQAL..........
Tarsius_syrichta               QDSQREEREFLV.CKFQEARKLVERLSL...EKLDLKRQREQAL..........
Oryctolagus_cuniculus          QVSQREEKEFLL.CKFQEARKLVERLNL...EKLDLKRQREQAL..........
Lipotes_vexillifer             QGSQREEKAFLM.QKFQEARDLVERLSL...ERRELHRQREQAL..........
Otolemur_garnettii             QVSQREEKAFLT.HKFQEARKLVERLSL...EKLDLKRQREQAL..........
Sus_scrofa                     QGSQREEKEFLM.QKFCEARRLVERLSL...EKLELRRQREQAL..........
Rhinolophus_ferrumequinum      QGNQREEKEFLM.QRFQEARSLVERLSL...EKVDLRRQREQAL..........
Saimiri_boliviensis            QASQREEKEFLM.CKFQEARKLVERLSL...EKLNLKRQKEQAV..........
Homo_Sapiens                   QASQREEKEFLM.CKFQEARKLVERLGL...EKLDLKRQKEQAL..........
Pongo_abelii                   QASQREEKEFLM.CKFQEARKLVERLSL...EKLDLKRQKEQAL..........
Macaca_mulatta                 QASQREEKEFLM.CKFQEARKLVERLSL...EKLDLKRQKEQAL..........
Macaca_fascicularis            QASQREEKEFLM.CKFQEARKLVERLSL...EKLDLKRQKEQAL..........
Chlorocebus_sabaeus            QASQREEKEFLM.CKFQEARKLVERLSL...EKLDLKRQKEQAL..........
Papio_anubis                   QASQREEKEFLM.CKFQEARKLVERLSL...EKLDLKRQKEQAL..........
Callithrix_jacchus             QASQREEKEFLM.CKFQEARKLVERLSL...EKLDLKRQKEQAL..........
Callicebus_moloch              QASQREEKEFLM.CKFQEARKLVERLSL...EKLDLKRQKEQAL..........
Canis_lupus_familiaris         QGSQRKEKEFLM.QKFQEARKLVERLSL...EKLDLRTQREQAL..........
Equus_caballus                 QSSQREEKEFLM.QKFQEARKLVERLSL...EKLDLRRQREQAL..........
Felis_catus                    QGSQRKEKEFLM.QKFQEARKLVERLSL...EKLDLRRQREQAL..........
Ailuropoda_melanoleuca         QGSQRKEKEFLM.QKFQEARKLVERLSL...EKLDLRRQREQAL..........
Odobenus_rosmarus_divergens    QGSQRKEKEFLM.QKFQEARKLVERLNL...EKLDLRRQREQAL..........
Leptonychotes_weddellii        QGSQRKEKEFLM.QKFQEARKLVERLNL...EKLDLRRQREQAL..........
Drosophila_melanogaster        VLKNSVYSQFPSLCSLQGSAEEVVKLQNMMTEYLALKSTLDKVN..........
Pelodiscus_sinensis            QAVQREEKDFLL.LRFREARDVVQKLNA...ERAEMKRQLEQAL..........
Anolis_carolinensis            QASHKQEKEFLF.CKFQEARLLVENLQL...ERTGLKKKLEKTA..........
Xenopus_tropicalis             QDSQRKEREFIT.YKFGEARDLVLRLTN...ERNSLQAQLEEAM..........
Latimeria_chalumnae            RARNKEEKDFML.ERFKEARCLVEKLSQ...EKVEIQHQLEEAY..........
Oreochromis_niloticus          QRRTKEEREFLS.CRFQEARSLVERLAQ...ENHSLQSMVNGPGSSNTSSNHCC
Gasterosteus_aculeatus         ..RTRDEREFLS.CRFQEARALVERLAQ...ENHSLQSLVNEPAS.....DHCC
Oryzias_latipes                QQRTRDEREFLS.CRFQEARALVERLAQ...ENHSLKVTANGPGSSPSS.GLSC
Xiphophorus_maculatus          QRRTREEREFLS.CRFQEARALVERLAQ...ENHSLQSMVNGPGSSS...NRSY
Danio_rerio                    QRRSREEREFLS.CRFREARELVQRLAQ...ENQSLLGQLNLSVSQAGSLGISK
Takifugu_rubripes              QRRSREDREFLS.CRFQEARALVERLAE...ENHSLRGVVNGPASSSSP.....
```

```
                                   130
Heterocephalus_glaber        ...QEVEQLKRCQQ.........................................
Cavia_porcellus              ...QEAEQLKRCQQ.........................................
Mesocricetus_auratus         ...KDLEHLKKCQQ.........................................
Mus_musculus                 ...KELEQLKKCQQ.........................................
Rattus_norvegicus            ...EDLEHLKKCQQ.........................................
Bos_taurus                   ...KEVERLKTCQQ.........................................
Tarsius_syrichta             ...QEVEHLKRCQQ.........................................
Oryctolagus_cuniculus        ...QEVEHLKRCQQ.........................................
Lipotes_vexillifer           ...QEVERLKTCQQ.........................................
Otolemur_garnettii           ...QEVEHLKRCQQ.........................................
Sus_scrofa                   ...QEVELLKTCQQ.........................................
Rhinolophus_ferrumequinum    ...QEVEHLKRCQQ.........................................
Saimiri_boliviensis          ...REVEHLKRCQQ.........................................
Homo_Sapiens                 ...REVEHLKRCQQ.........................................
Pongo_abelii                 ...REVEHLKRCQQ.........................................
Macaca_mulatta               ...REVEHLKRCQQ.........................................
Macaca_fascicularis          ...REVEHLKRCQQ.........................................
Chlorocebus_sabaeus          ...REVEHLKRCQQ.........................................
Papio_anubis                 ...REVEHLKRCQQ.........................................
Callithrix_jacchus           ...REVEHLKRCQQ.........................................
Callicebus_moloch            ...REAEHLKRCQQ.........................................
Canis_lupus_familiaris       ...QEVEHLKRCQQ.........................................
Equus_caballus               ...KEVEHLKRCQQ.........................................
Felis_catus                  ...QEVEHLKRCQK.........................................
Ailuropoda_melanoleuca       ...QEVEHLKRCQQ.........................................
Odobenus_rosmarus_divergens  ...QEVEHLKRCQQ.........................................
Leptonychotes_weddellii      ...QEVEHLKRCQQ.........................................
Drosophila_melanogaster      ...QTMLNYHNLTQ.............QWRQEAADRE...................
Pelodiscus_sinensis          ...QEVEQLKGSQK.....VSGELPATSPRGSRASGLGHLLSDMQKEIPEP...
Anolis_carolinensis          ...QELEQLKRQLA.....ASHPCPSEKEASGAQEDQDTVTLTQEENIF.....
Xenopus_tropicalis           ...KQLAEVREVKS.........RGSTENEQGRLEDTILTDRRSPRKAY.....
Latimeria_chalumnae          ...RDMEQLRTGNK.........HTTEDGEEAAAQGGLSKMLEDPPNNHNMDNS
Oreochromis_niloticus        SS.SQTEDPQLRPA.RNGPVDGPQTLDQREKKRVEDTEQCTQTSPPRSLDNTSA
Gasterosteus_aculeatus       RS.SQTEDLQGPPA.RSRALEGPQTLHPREKTRVEETDRHTQTTPPRSL.....
Oryzias_latipes              SS.SQTEDLQGRPA.VNGPTDGQQTLDQWERKRADETEQRTQTTPPRSL.....
Xiphophorus_maculatus        SS.AQMEASPGLPA.RNGPLDEPKTLDQWERKRVEETEQQTQTTPLRSL.....
Danio_rerio                  ETGSQDQELKCTNAEKNVLIDSPEVLNAAVLTECAEGDTDRHTMP.QSL.....
Takifugu_rubripes            PS.SQAEDLQGPPP.PKGPVDGAQTLEQRDGTRLEEADQCTQTTPPRSL.....

                                                   140       150       160
Heterocephalus_glaber        ...................QMAEDKASVKAQVTSLLGELQESQSRLESATKERQ
Cavia_porcellus              ...................QMAEDKASVKAQVTSLLGELQESQSRLEAATKERQ
Mesocricetus_auratus         ...................QMAEDKASVKAQVTSLLGELQESQSRLEAATKERQ
Mus_musculus                 ...................QMAEDKASVKAQVTSLLGELQESQSRLEAATKDRQ
Rattus_norvegicus            ...................QMAEDKASVKAQVTSLLGELQESQSRLEAATKERQ
Bos_taurus                   ...................QMAEDKASVKAQVTSLLGELQESQSRLEAATKERQ
Tarsius_syrichta             ...................QMAEDKASVKAQVTSLLGELQESQSRLEAATKERQ
Oryctolagus_cuniculus        ...................QMAEDKASVKAQVTSLLGELQESQSRLEAATKERE
Lipotes_vexillifer           ...................QMAEDKASVKAQVTSLLGELQESQSRLEATTKERQ
Otolemur_garnettii           ...................QMAEDKASVKAQVTSLLGELQESQSRLEAATKERQ
Sus_scrofa                   ...................QMAEDKASVKAQVTSLLGELQESQSRLEAATKERQ
Rhinolophus_ferrumequinum    ...................QMAEDKASVKAQVTSLLGELQESQSRLEAATKERQ
Saimiri_boliviensis          ...................QMAEDKASVKAQVTSLLGELQESQSRLEAATKECQ
Homo_Sapiens                 ...................QMAEDKASVKAQVTSLLGELQESQSRLEAATKECQ
Pongo_abelii                 ...................QMAEDKASVKAQVTSLLGELQESQSRLEAATKECQ
Macaca_mulatta               ...................QMAEDKASVKAQVTSLLGELQESQSRLEAATKECQ
Macaca_fascicularis          ...................QMAEDKASVKAQVTSLLGELQESQSRLEAATKECQ
Chlorocebus_sabaeus          ...................QMAEDKASVKAQVTSLLGELQESQSRLEAATKECQ
Papio_anubis                 ...................QMAEDKASVKAQVTSLLGELQESQSRLEAATKECQ
Callithrix_jacchus           ...................QMAEDKASVKAQVTSLLGELQESQSRLEAATKECQ
Callicebus_moloch            ...................QMAEDKASVKAQVTSLLGELQESQSRLEAATKECQ
Canis_lupus_familiaris       ...................QMAEDKASVKAQVTSLLGELQESQSRLEAATKERQ
Equus_caballus               ...................QMAEDKASVKAQVTSLLGELQESQSRLEAATKERQ
Felis_catus                  ...................QLAEDKASVKAQVTSLLGELQESQSRLEAAIKERQ
Ailuropoda_melanoleuca       ...................QMAEDKASVKAQVTSLLGELQESQSRLEAATKERQ
Odobenus_rosmarus_divergens  ...................QMAEDKASVKAQVTSLLGELQESQSRLEAATKERQ
Leptonychotes_weddellii      ...................QMAEDKASVKAQVTSLLGELQESQSRLEAATKERQ
Drosophila_melanogaster      ..................HQYKEHVKECQAQIAILRVENQELKRDLETKIEQIE
Pelodiscus_sinensis          QD....AEQQVQALRKQLEQMTEDRASVKAQVTSLLGELQESQSRLEACVLEKK
Anolis_carolinensis          QE....TQQQLQTLNKQLEQFGEDRASVKAQVTSLLGELLESQTRLETSTKEKK
Xenopus_tropicalis           VEKGEESQKQLQSLQLQMEQLSEERNSVKAQVTSLLGELKESQTSLEICLQEKR
Latimeria_chalumnae          KEVEWTNEQKLQTLSKQIEQLTEDKASLKSQVTSLLGELKESQSCLENCMKEKT
Oreochromis_niloticus        ......TEALLKQKDKDCAQLAKDCEALKAQATSLLGELQERQSWLDKSEHERV
Gasterosteus_aculeatus       ......TEAVLKQKDKDCVQLAKDCEALKAQATSLLGELNERQSCLEKSERERK
Oryzias_latipes              ......TEALLKQKEKDCVQLAKDCEALKAQATSLLGELQERQSCLEKSEHERK
Xiphophorus_maculatus        ......TEALLKQKDKDCAQLAKDCEALKAQATSLLGELNERQILLQKSDDERK
Danio_rerio                  ......TEALLKQKEKEFVQVQKDSEALRSQVTSLLGELNERQNWLEKSEAEKR
Takifugu_rubripes            ......TETLLKQKEKDCAQLAKDCEALKAQATSLLGELNERQSCLEKSEHERK
```

```
                                170       180       190       200       210       220
Heterocephalus_glaber           ALEARARVASEQVRQLEKEREVLQQQHSVQVDQLRMQNQSMEAALRMERQAASE
Cavia_porcellus                 ALEARARAASEQARQLEKEREVLQQQHSVQVDQLRMQNQSVEAALRMERQAASE
Mesocricetus_auratus            TLEGRMRAVSEQVRQLESEREVLQQQHSVQVDQLRMQNQSVEAALRMERQAASE
Mus_musculus                    ALEGRIRAVSEQVRQLESEREVLQQQHSVQVDQLRMQNQSVEAALRMERQAASE
Rattus_norvegicus               TLEGRIRAVSEQVRQLESEREVLQQQHSVQVDQLRMQNQSVEAALRMERQAASE
Bos_taurus                      ALESRARVASEKARQLESEREALEQRHSVQVDQLVLQNESMEAALRMERQAASE
Tarsius_syrichta                ALEGRARAASEQARQLESEREALQQQHSVQVDQLRMQSQSMEAALRMERQAASE
Oryctolagus_cuniculus           ALEGRARAASEQARQLESEREALQQQHSVQVDQLRMQSQSVEAALRMERQAASE
Lipotes_vexillifer              ALEGRVRAASEQARQLENEREALQQQHSVQVDQLRLQNQSMDAALRMERQAASE
Otolemur_garnettii              ALEGRARAASEQARQLESEREALQQQHSVQVDQLRMQSQSVEAALRMERQAASE
Sus_scrofa                      ALESRVRATSEQVRQLENEREALQQQHSVQVDQLRLQSQSMEAALRMERQAASE
Rhinolophus_ferrumequinum       ALESRARVASEQARQLESEREALQQQHSVQVDQLRMQTQSMEAALRMERQAASE
Saimiri_boliviensis             ALEGRAREASEQVRQLESEREALQQQHSVQVDQLRMQAQSVEAALRMERQAASE
Homo_Sapiens                    ALEGRARAASEQARQLESEREALQQQHSVQVDQLRMQGQSVEAALRMERQAASE
Pongo_abelii                    ALEGRARAASEQARQLESEREALQQQHSVQVDQLRMQGQSVEAALRMERQAASE
Macaca_mulatta                  TLEGRARAASEQARQLESEREALQQQHSVQVDQLRMQGQSVEAALRMERQAASE
Macaca_fascicularis             TLEGRARAASEQARQLESEREALQQQHSVQVDQLRMQGQSVEAALRMERQAASE
Chlorocebus_sabaeus             TLEGRARAASEQARQLESEREALQQQHSVQVDQLRMQGQSVEAALRMERQAASE
Papio_anubis                    TLEGRARAASEQARQLESEREALQQQHSVQVDQLRMQGQSVEAALRMERQAASE
Callithrix_jacchus              ALEGRARAASEQVRQLESEREALQQQHSVQVDQLRMQGQSVEAALRMERQAASE
Callicebus_moloch               ALEGRARAASEQVRQLESEREALQQQHSVQVDQLRMQGQSVEAALRMERQAASE
Canis_lupus_familiaris          ALEGRARAASEQARQLESEREALQQQHSVQVDQLRMQSQSVEAALRMERQAASE
Equus_caballus                  ALEGRARAASEQARQLESEREALQQQHNVQVDQLRMQTQSMEAALRMERQAASE
Felis_catus                     ALEGRARAASEQARQLESEREALQQQHSVQVDQLRMQSQSVEAALRMERQAASE
Ailuropoda_melanoleuca          ALEGRARAASEQARQLESEREALQQQHSVQVDQLRMQSQSVEAALRMERQAASE
Odobenus_rosmarus_divergens     ALEGRARAASEQARQLESERETLQQQHSVQVDQLRMQSQSVEAALRMERQAASE
Leptonychotes_weddellii         ALEGRARAASEQARQLESEREALQQQHSVQVDQLRMQSQSVEAALRMERQAASE
Drosophila_melanogaster         GVHTIRLKEQDELRKSVSEKQSLIDNMRVEIDKLK...................
Pelodiscus_sinensis             DLEGKAQAAAEQGRRLAGEAEALHKQHSVQVDQLRMQAQNLEAALRVERQSATE
Anolis_carolinensis             ELEERIRGTAEQLHQFEREADARTKQHSVQVDQLRLQVQNLESALRVERQSASE
Xenopus_tropicalis              KVEDSLRSALEE....KKGWEAQVKQQVVQLDQRMMQVQNLETALKMERQNATD
Latimeria_chalumnae             QLDERYRATSESLKTQEREYETQKRQHNVLVDQLRMQVQNLEPALKLERQNASE
Oreochromis_niloticus           LLEDKLSSKIKALQVAERELEQQKKQHHVAMDKLLLQTQSLEQALKSERHVVTE
Gasterosteus_aculeatus          VSEEKLCSKTKALQVAEQELEQQRKQHHVAMDKLLLQTQSLEQALKTERHVVTE
Oryzias_latipes                 MLEEKLGSKVKALQAAERELEQQRKQHHVAVDKLMLQSQSLEQALKVERHVVTE
Xiphophorus_maculatus           MLEEKLVSKVKALQAAERELEQQRKQHHVANDKLLLQVQSLESALKSERHVVTE
Danio_rerio                     TLEDKLVTKSERLQTVEREMEQQKKQHSVTVDNLLLKTQNLEAALKNERLVIVE
Takifugu_rubripes               LLEEKLCSKTKALQGAERELEQQRKQHHVAMDELLLQSQNLEQALKTERHVVTE

                                    230       240       250       260
Heterocephalus_glaber           EKRKLAQLQVAYHQLFQDYDNHIKSSVVSGERKRGMQ...LEDLKQQL......
Cavia_porcellus                 EKRKLAQLQVAYHQLFQDYDNHIKSSMVSGERKRGMQ...LEDLKQQL......
Mesocricetus_auratus            EKRKLAQLQAAYHQLFQDYDSHIKSSKVSEEHKLGMQ...LEDLRQQL......
Mus_musculus                    EKRKLAQLQAAYHQLFQDYDSHIKSS.......KGMQ...LEDLRQQL......
Rattus_norvegicus               EKRKLAQLQAAYHQLFQDYDSHIKSS.......KGMQ...LEDLRQQL......
Bos_taurus                      EKRKLAQLQVAYHQLFQEYDNHMKSSMVSSERNRGLQ...LEDLKQQL......
Tarsius_syrichta                EKRKLAQLQVAYHQLFQDYDNHIKNSMGSSERKRGMQ...LEDLKQQL......
Oryctolagus_cuniculus           EKRKLAQLQVAYHQLFQDYDNHIKNSMVSGERKRGMQ...LEDLKQQL......
Lipotes_vexillifer              EKRKLAQLQVAYHQLFQEYDSHIKSSM.......GLQ...LEDLKQQL......
Otolemur_garnettii              EKRKLAQLQVAYHQLFQEYDNHIKSSMVSSERKRGMQ...LDDLKQQL......
Sus_scrofa                      EKRKLAQLQVAYHQLFQEYDNHIKSSVVSSERNRGLQ...LEDLKQQL......
Rhinolophus_ferrumequinum       EKRKLAQLQVAYHQLFQDYDNHIKSSVMSSERNRGMQ...LEDLKQRL......
Saimiri_boliviensis             EKRKLAQLQVAYHQLFQEYDNHIKSSVVSSERKRGMQ...LEDLKQQL......
Homo_Sapiens                    EKRKLAQLQVAYHQLFQEYDNHIKSSVVGSERKRGMQ...LEDLKQQL......
Pongo_abelii                    EKRKLAQLQVAYHQLFQEYDNHIKSSVVGSERKRGMQ...LEDLKQQL......
Macaca_mulatta                  EKRKLAQLQVAYHQLFQEYDNHIKSSLVGSERKRGMQ...LEDLKQQL......
Macaca_fascicularis             EKRKLAQLQVAYHQLFQEYDNHIKSSLVGSERKRGMQ...LEDLKQQL......
Chlorocebus_sabaeus             EKRKLAQLQVAYHQLFQEYDNHIKSSLVGSERKRGMQ...LEDLKQQL......
Papio_anubis                    EKRKLAQLQVAYHQLFQEYDNHIKSSLVGSERKRGMQ...LEDLKQQL......
Callithrix_jacchus              EKRKLAQLQVAYHQLFQEYDNHIKSSVVSSERKRGMQ...LEDLKQQL......
Callicebus_moloch               EKRKLAQLQVAYHQLFQEYDNHIKSSVVSGERKRGMQ...LEDLKQQL......
Canis_lupus_familiaris          EKRKLAQLQVAYHQLFQEYDNHIKSSMVSSERNRGMQ...LEDLKQQL......
Equus_caballus                  EKRKLAQLQVAYHQLFQEYDNHIKSSMVSSERNRGMQ...LEDLKQQL......
Felis_catus                     EKRKLAQLQVAYHQLFQEYDSHIKSSVVSSERNRGLQ...LEDLKQQL......
Ailuropoda_melanoleuca          EKRKLAQLQVAYHQLFQEYDSHIKSSVVSSERNRGMQ...LEDLKQQL......
Odobenus_rosmarus_divergens     EKRKLAQLQVAYHQLFQEYDNHIKSSMVSSERNRGMQ...LEDLKQQL......
Leptonychotes_weddellii         EKRKLAQLQVAYHQLFQEYDNHIKSSMVSSERNRGMQ...LEDLKQQL......
Drosophila_melanogaster         .......QLNHSF.EFVPEYAT.....................................
Pelodiscus_sinensis             EKRKLAQLQAAYHQLFQEYDSHMKSSLDQEKRSQGME.LHLEELLQQL......
Anolis_carolinensis             EKRKLAQLQVAYHELFREYDSHIKTSLESEKRSKGLD.LQVAELSQQL......
Xenopus_tropicalis              EKRKLAQLQVAYHTLFQEYDTHIKVSMQQAKHTKGVD.LQIQELKQQL......
Latimeria_chalumnae             EKRKLAQLQAAYHQLFQDYDQHIKTTMESKKRNRGMDREQFEDLKQQL......
Oreochromis_niloticus           EKKKLTQLQHAYTCLFRDYDSKLKNE........GGD......LCSRL......
Gasterosteus_aculeatus          ERKKLSQLQHAYTCLFRDYDNKVKSEFQ......GED......LCSRL......
Oryzias_latipes                 ERKKLTQLQHAYTCLFRDYDAKLKNE........GGD......LSSRL......
Xiphophorus_maculatus           EKKKLSQLQHAYTCLFRDYDSKLKSE........GGD......LSSKL......
Danio_rerio                     ERRKLAQLQHAYTCLFQDYDNKLKSEKQANHR..GGE...ADTLANRL......
Takifugu_rubripes               EKKKLTQLQHAYTCLFKDYDSKLKNELQ.......GGD.....LCSRLXXXXXX
```

```
                                 270       280       290       300       310
Heterocephalus_glaber        ....QQAEEALVAKQEV.IDKLKEEAEQHKMVMETVPVLKAQADIYKADFQAER
Cavia_porcellus              ....QQAEEALVAKQEV.IDKLKEEAEQHKMVIETVPVLKAQADIYKADFQAER
Mesocricetus_auratus         ....QQAEEALVAKQEL.IDKLKEEAEQHKIVMETVPVLKAQADIYKADFQAER
Mus_musculus                 ....QQAEEALVAKQEL.IDKLKEEAEQHKIVMETVPVLKAQADIYKADFQAER
Rattus_norvegicus            ....QQAEEALVAKQEL.IDKLKEEAEQHKIVMETVPVLKAQADIYKADFQAER
Bos_taurus                   ....QQAEEALVAKQEV.IDKLKEEAEQHKIVMETVPVLKAQADIYKADFQAER
Tarsius_syrichta             ....QQAEEALVAKQEV.IDKLKEEAEQHKIVMETVPVLKAQADIYKADFQAER
Oryctolagus_cuniculus        ....RQAEEALVAKQEV.IDKLKEEAEQHKMVMETVPVLKAQADIYKADFQAER
Lipotes_vexillifer           ....KQAEEALVAKQEL.IDKLKEEAEQHKTVMETVPVLKAQADIYKADFQAER
Otolemur_garnettii           ....QQAEEALVAKQEV.IDKLKEEAEQHKIVMETVPVLKAQADIYKADFQAER
Sus_scrofa                   ....QQAEEALVAKQEV.IDKLKEEAEQHKIVMETVPVLKAQADIYKADFQAER
Rhinolophus_ferrumequinum    ....QQAEEALVAKQEV.IDKLKEEAEQHKIVMETVSVLKVQADIYKTDFQAER
Saimiri_boliviensis          ....QQAEEALVAKQEV.IDKLKEEAEQHKMVMETVPVLKAQADIYKADFQAER
Homo_Sapiens                 ....QQAEEALVAKQEV.IDKLKEEAEQHKIVMETVPVLKAQADIYKADFQAER
Pongo_abelii                 ....QQAEEALVAKQEV.IDKLKEEAEQHKIVMETVPVLKAQADIYKADFQAER
Macaca_mulatta               ....QQAEEALVAKQEV.IDKLKEEAEQHKIVMETVPVLKAQADIYKADFQAER
Macaca_fascicularis          ....QQAEEALVAKQEV.IDKLKEEAEQHKIVMETVPVLKAQADIYKADFQAER
Chlorocebus_sabaeus          ....QQAEEALVAKQEV.IDKLKEEAEQHKIVMETVPVLKAQADIYKADFQAER
Papio_anubis                 ....QQAEEALVAKQEV.IDKLKEEAEQHKIVMETVPVLKAQADIYKADFQAER
Callithrix_jacchus           ....QQAEEALVAKQEL.IDKLKEEAEQHKMVMETVPVLKAQADIYKADFQAER
Callicebus_moloch            ....QQAEEALVAKQEV.IDKLKDEAEQHKMVMETVPVLKAQADIYKADFQAER
Canis_lupus_familiaris       ....QQAEEALVAKQEV.IDKLKEEAEQHKIVMETVPVLKAQADIYKADFQAER
Equus_caballus               ....QQAEEALVAKQEA.IDKLKEEAEQHKIVMETVPVLKAQADIYKADFQAER
Felis_catus                  ....QQAEEALVAKQEV.IDKLKEEAEQHKIVMETVPVLKAQADIYKADFQAER
Ailuropoda_melanoleuca       ....QQAEEALVAKQEV.IDKLKEEAEQHKMVMETVPVLKAQADIYKADFQAER
Odobenus_rosmarus_divergens  ....QQAEEALVAKQEV.IDKLKEEAEQHKIVMETVPVLKAQADIYKADFQAER
Leptonychotes_weddellii      ....QQAEEALVAKQEV.IDKLKEEAEQHKIVMETVPVLKAQADIYKADFQAER
Drosophila_melanogaster      ....ESKSQELIKKMQLDINELKARDIQKQ...EVIKGLQIQNDIYRRDFEMER
Pelodiscus_sinensis          ....QQAEEALVAKQEL.IDKLKEETEQHKTLLETIPVLKAQADIYKADFLAER
Anolis_carolinensis          ....QEAEEALVAKQEL.IDKLKEEAEQHKAIMETVPVLKAQADIYKTDFLAER
Xenopus_tropicalis           ....QEAEEALVAKQAL.IDKLKDEAEKQRTELDTVPVLKAQVEIYRADFLAER
Latimeria_chalumnae          ....QQAEEALVSKQEY.IDKLKEEAEQSKMVLEEIPVLKAQAEIFKADFLAER
Oreochromis_niloticus        ....EEAERALALKQDL.IDKLKEEVEQQKGSLETIPVLTAQAEIYKADFLAER
Gasterosteus_aculeatus       ....EEAERALALKQDL.IDKLKEEVEQQKGSLETVPVLTAQAEIYKADFLAER
Oryzias_latipes              ....DEAEQALALKQDL.IDKLKEEVEQLKGSLETVPVLTAQAEIYKADFLAER
Xiphophorus_maculatus        ....EEAERALAIKQDL.IDKLKEEVEQQKGSLETVPVLTAQAEIYKADFLAER
Danio_rerio                  ....GEAEKALALKQEH.IDKLKEEMEQLRAKLETIPVLNHQAEIYKMDFLAER
Takifugu_rubripes            XXXXXXXXXXXXXLKQDL.IDKLKEEVERQKGXLETVPVLTAQAEIYKADFLAER

                             320       330       340       350       360
Heterocephalus_glaber        QAREKLAEKKEVLQEQLDQLQREFGKLKASCQES..ARIEDLRKRHVE..VPQP
Cavia_porcellus              QAREKLAEKKEALQEQLDQLQREFSKLKASCQES..ARMEDLRKRHME..VPQP
Mesocricetus_auratus         HAREKLVEKKELLQEQLEQLQREFSKLKVGCHES..ARIEDMRKRHVE..TSQP
Mus_musculus                 HAREKLVEKKEYLQEQLEQLQREFNKLKVGCHES..ARIEDMRKRHVE..TPQP
Rattus_norvegicus            HAREKLVERKELLQEQLEQLQREFNKLKVGCHES..ARIEDMRKRHVE..TSQP
Bos_taurus                   QAREKLAEKKEFLQEQLEQLQREYSRLKTSCQES..ARIEDMRKRHVE..VSQP
Tarsius_syrichta             QAREKLAEKKELLQEQLEQLQREYSKLKASCQES..ARIEDMRKRHIE..VPQL
Oryctolagus_cuniculus        QAREKLAEKKELLQEQLEQLQREYSKLKASCQES..ARIEDLRKRHVE..VSQP
Lipotes_vexillifer           QAREKLAEKKEFLQAQLEQLQREHNRLKTSCQES..ARIEDMRKRHVE..VSQP
Otolemur_garnettii           QAREKLAEKKELLQEQLEQLQREYSKLKASCQES..ARIEDMRKRHIE..VSQA
Sus_scrofa                   QAREQLAERKELLQEQLEQLQREYSRLKTSCQES..ARIEDMRKRHVE..VSQP
Rhinolophus_ferrumequinum    QAREKLAEKKELLQEQLEQLQRDYSRLKASCQES..ARIEDMRKRHVE..VSQP
Saimiri_boliviensis          QAREKLAEKKELLQEQLEQLQREYSKLKATCQES..ARIEDMRKRHGE..VSQA
Homo_Sapiens                 QAREKLAEKKELLQEQLEQLQREYSKLKASCQES..ARIEDMRKRHVE..VSQA
Pongo_abelii                 QAREKLAEKKELLQEQLEQLQREYSKLKASCQES..ARIEDMRKRHVE..VSQA
Macaca_mulatta               QAREKLAEKKELLQEQLEQLQREYSKLKASCQES..ARIEDMRKRHVE..VSQA
Macaca_fascicularis          QAREKLAEKKELLQEQLEQLQREYSKLKASCQES..ARIEDMRKRHVE..VSQA
Chlorocebus_sabaeus          QAREKLAEKKELLQEQLEQLQREYSKLKASCQES..ARIEDMRKRHVE..VSQA
Papio_anubis                 QAREKLAEKKELLQEQLEQLQREYSKLKASCQES..ARIEDMRKRHVE..VSQA
Callithrix_jacchus           QAREKLAEKKELLQEQLEQLQREYSKLKASCQES..ARIEDMRKRHVE..VSPT
Callicebus_moloch            QAREKLAEKKELLQEQLEQLQREYSKLKASCQES..ARIEDMRKRHGE..VSQA
Canis_lupus_familiaris       QAREKLAEKKEILQDQLEQLQREYSRLKASCQES..ARIEDLRKRHVE..VSQA
Equus_caballus               QAREKLAEKKECLQEQLEQLQREYSRLKASCQES..ARIEDMRKRHVE..VSQP
Felis_catus                  QAREKLAEKKEILQEQLAQLQRDYSRLKASCQES..ARIEDMRKRHVE..ASQA
Ailuropoda_melanoleuca       QAREKLAEKKEFLQEQLEQLQREYSRLKASCQES..ARIEDLRKRHVE..VSQA
Odobenus_rosmarus_divergens  QAREQLAEKKEFLQEQLEQLQREYSRLKASCQES..ARIEDLRKRHVE..VSQA
Leptonychotes_weddellii      QAREQLAEKKEFLQEQLEQLQREYSRLKASCQES..ARIEDLRKRHVE..VSQA
Drosophila_melanogaster      ADREKNAGEKDQYLMDLRSLQRRNQ.........ELIEALAESHKASKACST
Pelodiscus_sinensis          EAREKLHEQREALQEQLEQLRRDYDKLKADTEGATWALMEEMRNRHWG....GP
Anolis_carolinensis          QAREKLHEQREALLEQLAQLQRDYEKLKADSEGASRALMEEMRNRHSD..VR..
Xenopus_tropicalis           KAREELHAEKERLQEQLNVLLQERLSNR........AMIDEMRNRHSD..TLRP
Latimeria_chalumnae          QARENLHEQKERLQEQLQQLRAELDGASR.......ARIEEMQQRHME..PFRA
Oreochromis_niloticus        EAREKLNQKKEELQEQLNQALAENERLKQEATSR..ARMEQMKMRHLEDFSARP
Gasterosteus_aculeatus       EAREKLNQKKEDLQDQLTQAIAEIDRLKVEATSR..VRMEQMKLRHQEDFPTRT
Oryzias_latipes              EAREKLNQKKEELQDQLNQAKTEIDRLNLEATSR..ARMEQMKLRHLDDFSTRT
Xiphophorus_maculatus        EAREKLNQKKEELQEQFTQALAEIERLKHELTAR..ARLEQMKLKHMDDFPARQ
Danio_rerio                  EAREKLNQKKEELQEDLNKALVEIERFKQERTSR..ARIEEMQQRHLEDYRPRP
Takifugu_rubripes            EAREKLNQKKEELQEQLTQALADIDRLKQEATSR..ACMEQMKLRHREEFTPRP
```

```
                                370                 380                         390
Heterocephalus_glaber           ALPPTSVHHS......FHMPN...QRRSP............PEEPPDFCCPKCQ
Cavia_porcellus                 VLPPACSLSPGYRS..FHM..PN.QRRSP............PEEPRDFCCPKCQ
Mesocricetus_auratus            PLLPTPAHHS......FHLALPN.QRRSP............PEEPPDFCCPKCQ
Mus_musculus                    PLLPAPAHHS......FHLALSN.QRRSP............PEEPPDFCCPKCQ
Rattus_norvegicus               PLLPAPAHHS......FHLALSN.QRRSP............PEEPPDFCCPKCQ
Bos_taurus                      PLAPGPAHHS......FHLNPSS.QRRSP............PDEPPKFCCPKCQ
Tarsius_syrichta                PLPPAPAHQS......FHPTLPS.QRRSP............PEEPPDFCCPKCQ
Oryctolagus_cuniculus           PLPPAPAHHS......FYLTLSN.QRRSP............PEEPPDFCCPKCQ
Lipotes_vexillifer              PLAPAPAHHS......FHLALPS.QRRSP............PEEPPNFCCPKCQ
Otolemur_garnettii              PLPPVQAHPS......FHMALPI.QRRSP............PEEPPDFCCPKCQ
Sus_scrofa                      TLPPAPAHHS......FHPALPS.QRRSP............PEEPPNFCCPKCQ
Rhinolophus_ferrumequinum       PLAPAPAHHS......FHLALSS.QRRST............PEEPPDFCCPKCQ
Saimiri_boliviensis             PLPAAPAHHS......FLLAQSN.QRRSP............PEEPPDFCCPKCQ
Homo_Sapiens                    PLPPAPAYLS......SPLALPS.QRRSP............PEEPPDFCCPKCQ
Pongo_abelii                    PLPPAPAYLS......SPLALPS.QRRSP............PEEPPDFCCPKCQ
Macaca_mulatta                  PLPPAPAYLS......SPLALPS.QRRSP............PEEPPDFCCPKCQ
Macaca_fascicularis             PLPPAPAYLS......SPLALPS.QRRSP............PEEPPDFCCPKCQ
Chlorocebus_sabaeus             PLPPAPAYLS......SPLALPS.QRRSP............PEEPPDFCCPKCQ
Papio_anubis                    PLPPAPAYLS......SPLALPS.QRRSP............PEEPPDFCCPKCQ
Callithrix_jacchus              PLPPAPAHHS......FLLAQPN.QRRSP............PEEPPDFCCPKCQ
Callicebus_moloch               PLPPAPAHHS......FLLAQPN.QRRSP............PEEPPDFCCPKCQ
Canis_lupus_familiaris          PLPVTPVHAS......FH.VPVSIQRRSP............PEEPPDFCCPKCQ
Equus_caballus                  PLPPTPAHHS......IHSALPS.QRRSP............PEEPPDFCCPKCQ
Felis_catus                     PVAPAPAHPS......FHLALPN.QRRSP............PEEPPDFCCPKCQ
Ailuropoda_melanoleuca          PLPPTPAHPS......FHLALPS.QRRSP............PEEPPDFCCPKCQ
Odobenus_rosmarus_divergens     PLPPTPAHPS......FHLALPS.QRRSP............PEEPPDFCCPKCQ
Leptonychotes_weddellii         PLPPTPAHPS......FHLALPN.QRRSP............PEEPPDFCCPKCQ
Drosophila_melanogaster         ASPLSSSRSNLREEQRPILDPTGASSRTS...............DTTLRCPICS
Pelodiscus_sinensis             PPVPQPAYNMAPGT..FQPGPAAGRRRSI............PEEQPDFCCPKCQ
Anolis_carolinensis             PPPPLPDYQMGWNG..PGMLMAG.PRQSF............AEEQPNYCCPKCQ
Xenopus_tropicalis              TLPHGPS.........LYPLQPA.MPFQP............EVEPPDFSCPKCF
Latimeria_chalumnae             ALPPQGGFAVGGNTVPFFPAQDAGRRRSI............PEEQPDYCCPKCQ
Oreochromis_niloticus           TRIPPPQGVFPP....FNTVPPAPSFRTPGLGPVGDQGPVGTEELPDLCCPKCQ
Gasterosteus_aculeatus          PHIPPPQA........FNTVPPAASFRVP...GLAAGGAAGAEELPDLCCPKCH
Oryzias_latipes                 PLIPPPQVFPGAG...FNTVPAAPSFRQL...PVSDPGAVGTEDLPDLCCPKCQ
Xiphophorus_maculatus           THIPPQQVVGFPGAG.FNTVPPN...RNHVLAPVIDPAAAGAADLPDLCCPKCN
Danio_rerio                     HPPPPAAPFPGPAM..FNSAQPPSARRRD..........EDQEELPDYRCPKCM
Takifugu_rubripes               PHIPPPQA........FNTVPPASSFRTQGLGPVGDPGAGRAEELPDLCCPKCQ

                                400         410
Heterocephalus_glaber           YQAPDMDTLQIHVMECIE..
Cavia_porcellus                 YQAPDMDTLQIHVMECIE..
Mesocricetus_auratus            YQAPDMDTLQIHVMECIE..
Mus_musculus                    YQAPDMDTLQIHVMECIE..
Rattus_norvegicus               YQAPDMDTLQIHVMECIE..
Bos_taurus                      YQAPDIDTLQIHVMECIE..
Tarsius_syrichta                YQAPDMDTLQIHVMECIE..
Oryctolagus_cuniculus           YQAPDMDTLQIHVMECIE..
Lipotes_vexillifer              YQAPDMDTLQIHVMECIE..
Otolemur_garnettii              YQAPDMDTLQIHVMECIE..
Sus_scrofa                      YQAPDMDTLQIHVMECIE..
Rhinolophus_ferrumequinum       YQAPDMDTLQIHVMECIE..
Saimiri_boliviensis             YQAPDMDTLQIHVMECIE..
Homo_Sapiens                    YQAPDMDTLQIHVMECIE..
Pongo_abelii                    YQAPDMDTLQIHVMECIE..
Macaca_mulatta                  YQAPDMDTLQIHVMECIE..
Macaca_fascicularis             YQAPDMDTLQIHVMECIE..
Chlorocebus_sabaeus             YQAPDMDTLQIHVMECIE..
Papio_anubis                    YQAPDMDTLQIHVMECIE..
Callithrix_jacchus              YQAPDMDTLQIHVMECIE..
Callicebus_moloch               YQAPDMDTLQIHVMECIE..
Canis_lupus_familiaris          YQAPDMDTLQIHVMECIE..
Equus_caballus                  YQAPDMDTLQIHVMECIE..
Felis_catus                     YQAPDMDTLQIHVMECIE..
Ailuropoda_melanoleuca          YQAPDMDTLQIHVMECIE..
Odobenus_rosmarus_divergens     YQAPDMDTLQIHVMECIE..
Leptonychotes_weddellii         YQAPDMDTLQIHVMECIE..
Drosophila_melanogaster         KSFNALSVLQSHVNDCLDKN
Pelodiscus_sinensis             YQAPDMDTLQIHVMDCIK..
Anolis_carolinensis             YRAPDMDTLQIHVMDCIQ..
Xenopus_tropicalis              YKAPDMDTLQIHVMDCIQ..
Latimeria_chalumnae             YQAPDMDTLQIHVMDCIQ..
Oreochromis_niloticus           YLAPDMDTLQIHVMDCIQ..
Gasterosteus_aculeatus          YQAPDMDTLQIHVVDCKG..
Oryzias_latipes                 YLAPDMDTLQIHVMDCIQ..
Xiphophorus_maculatus           YLAPDMDTLQIHVMDCIQ..
Danio_rerio                     YKAPDMDTLQIHVMDCIQ..
Takifugu_rubripes               YQAPDMDTLQIHVMDCIQ..
```

IκBα MSA:

```
                                   1         10                          20
Heterocephalus_glaber      ...........MFQPAERVPEWAM................EGP...RDGLKK
Cavia_porcellus            ...........MFQPAERVQEWAM................EGP...RDVLKK
Mesocricetus_auratus       ...........MFQPAGHGQDWAM................EGP...RDGLKK
Mus_musculus               ...........MFQPAGHGQDWAM................EGP...RDGLKK
Rattus_norvegicus          ...........MFQPAGHGQDWAM................EGP...RDGLKK
Bos_taurus                 ...........MFQPAEPGQDWAM................EGP...RDALKK
Tarsius_syrichta           ..........................................................
Oryctolagus_cuniculus      ...........MFQPAEHAQDWAM................EGP...RDALKK
Lipotes_vexillifer         ...........MFQPAEPGQEWAM................EGP...RDALKK
Otolemur_garnettii         ...........MFQPVEHAPEWAM................EGA...RDGLKK
Sus_scrofa                 ...........MFQPAEPGQEWAM................EGP...RDALKK
Saimiri_boliviensis        ...............MFQAAEWAM................EGP...RDGLKK
Homo_sapiens               ...........MFQAAERPQEWAM................EGP...RDGLKK
Pongo_abelii               ...........MFQAAERPQEWAM................EGP...RDGLKK
Macaca_mulatta             ...........MFQAAERPQEWAM................EGP...RDGLKK
Macaca_fascicularis        ...........MFQAAERPQEWAM................EGP...RDGLKK
Chlorocebus_sabaeus        ...........MFQAAERPQEWAM................EGP...RDGLKK
Papio_anubis               ...........MFQAAERPQEWAM................EGP...RDGLKK
Callithrix_jacchus         ...............MFQAAEWAM................EGL...RDGLKK
Canis_lupus_familiaris     ...........MLQQAEHAQDWAM................EGP...RDALKK
Equus_caballus             LFWSDWLGNSPRLTPPRRNPLPAF................IGR...RGGAAE
Felis_catus                ...........MFQPAEHAQDWAM................EGP...RDALKK
Ailuropoda_melanoleuca     ..........................................................
Odobenus_rosmarus_divergens ..........MFQPAEHAQDWAM................DGP...RDALKK
Leptonychotes_weddellii    ...........MFQPAEHGQDWAM................DGP...RDALKK
Pelodiscus_sinensis        ILAQQYLDSKAELTDHLKRQKLGF................GP...KEVEKK
Anolis_carolinensis        ...........MLSPAVDFAAMEA.......................PKKE
Xenopus_tropicalis         ...........MSVPFHDYQGNMM................EGEA..RDLRKD
Latimeria_chalumnae        ......................M.................DQD...LKNHKD
Oreochromis_niloticus      ..........MDLHRTSILNQMDY................SRD...SKEGKT
Oryzias_latipes            ..........MDLHRNTVLNQMDY................SED...PKEVKS
Xiphophorus_maculatus      HSTTRTARTNMDLHRASILNQMDY................NRE...SKEGKA
Danio_rerio                ..........MELYRGTTANQTDY................NDDGRGPKSGKL
Takifugu_rubripes          ..........MDLHRTSILNQMDY................SRE...SKEGKP
Drosophila_melanogaster    QDQTAAINKQKEFAVPNETSDSGFISGPQSSQIFSEEIVPDSEEQDKDQQES
```

```
                                   30        40        50
Heterocephalus_glaber        ERLLDDRH..DSGLDSMKDEEYEQMVKELRE...................IR
Cavia_porcellus              ERLLDDRH..DSGLDSMKDEEYEQMMKELQE...................IR
Mesocricetus_auratus         ERLVDDRH..DSGLDSMKDEEYEQMVRELQE...................IR
Mus_musculus                 ERLVDDRH..DSGLDSMKDEEYEQMVKELRE...................IR
Rattus_norvegicus            ERLVDDRH..DSGLDSMKDEDYEQMVKELRE...................IR
Bos_taurus                   ERLLDDRH..DSGLDSMKDEEYEQMVKELRE...................IR
Tarsius_syrichta             ..........................PAETPALRN...................
Oryctolagus_cuniculus        ERLLDDRH..DSGLDSMKDEEYEQMVKELRE...................IR
Lipotes_vexillifer           ERLLDDRH..DSGLDSMKDEEYEQMVKELRE...................IR
Otolemur_garnettii           ERLLDDRH..DSGLDSMKDEDYEQMVRELRE...................IR
Sus_scrofa                   ERLLDDRH..DSGLDSMKDEEYEQMVKELRE...................IR
Saimiri_boliviensis          ERLLDDRH..DSGLDSMKDEEYEQMVKELRE...................IR
Homo_sapiens                 ERLLDDRH..DSGLDSMKDEEYEQMVKELQE...................IR
Pongo_abelii                 ERLLDDRH..DSGLDSMKDEEYEQMVKELQE...................IR
Macaca_mulatta               ERLLDDRH..DSGLDSMKDEEYEQMVKELQE...................IR
Macaca_fascicularis          ERLLDDRH..DSGLDSMKDEEYEQMVKELQE...................IR
Chlorocebus_sabaeus          ERLLDDRH..DSGLDSMKDEEYEQMVKELQE...................IR
Papio_anubis                 ERLLDDRH..DSGLDSMKDEEYEQMVKELQE...................IR
Callithrix_jacchus           ERLLDDRH..DSGLDSMKDEEYEQMVKELRE...................IR
Canis_lupus_familiaris       ERLLDDRH..DSGLDSMKDEEYEQLVKELRE...................IR
Equus_caballus               PTTVPSRR..RRHQGRRCQRASEAREQRCSSTHPRGPPPRPRGKHRGRGLPK
Felis_catus                  ERLLDDRH..DSGLDSMKDEEYEQMVKELRE...................IR
Ailuropoda_melanoleuca       ..........................MKDEDYEQLVKELRE...................IR
Odobenus_rosmarus_divergens  ERLLDDRH..DSGLDSMKDEDYEQLVKELRE...................IR
Leptonychotes_weddellii      ERLLDDRH..DSGLDSMKDEDYEQLVKELRE...................IR
Pelodiscus_sinensis          SFNVTNGRVLERGLVSLLKGDQLNEKGQKGS....................K
Anolis_carolinensis          RQLDSDRH..DSGLDSMKDEEYEDLVRELEG...................IR
Xenopus_tropicalis           KLLQDDRI..DSGLDSLKEEEYTAIITDLSN...................MR
Latimeria_chalumnae          QNFAEDRF..DSGVGSLTEEEYQSVQKDLAA...................LR
Oreochromis_niloticus        AQATEDRL..DSGLDSLKEEEYQAVAAEIRR...................LQ
Oryzias_latipes              SQLTEDRL..DSGIDSLKEEEYQAVAAEIHR...................LQ
Xiphophorus_maculatus        AQSTEERL..DSGVDSLKEEEYQAVAEELHR...................LQ
Danio_rerio                  LSNTDERL..DSGLDSLKEDNLPSLEE.......................CR
Takifugu_rubripes            AQATEERL..DSGLDSLREEEYQAVAAEFHR...................LR
Drosophila_melanogaster      APQKEQPVVLDSGIIDEEEDQEEQEKEEEHQDTTTATADS..........MR

Heterocephalus_glaber        LE.................................................
Cavia_porcellus              LE.................................................
Mesocricetus_auratus         LQ.................................................
Mus_musculus                 LQ.................................................
Rattus_norvegicus            LQ.................................................
Bos_taurus                   LE.................................................
Tarsius_syrichta             ..................................................
Oryctolagus_cuniculus        LE.................................................
Lipotes_vexillifer           LE.................................................
Otolemur_garnettii           LE.................................................
Sus_scrofa                   LE.................................................
Saimiri_boliviensis          LE.................................................
Homo_sapiens                 LE.................................................
Pongo_abelii                 LE.................................................
Macaca_mulatta               LE.................................................
Macaca_fascicularis          LE.................................................
Chlorocebus_sabaeus          LE.................................................
Papio_anubis                 LE.................................................
Callithrix_jacchus           LE.................................................
Canis_lupus_familiaris       LE.................................................
Equus_caballus               PR.................................................
Felis_catus                  LE.................................................
Ailuropoda_melanoleuca       LE.................................................
Odobenus_rosmarus_divergens  LQ.................................................
Leptonychotes_weddellii      LE.................................................
Pelodiscus_sinensis          GD.................................................
Anolis_carolinensis          LQ.................................................
Xenopus_tropicalis           ME.................................................
Latimeria_chalumnae          LD.................................................
Oreochromis_niloticus        LE.................................................
Oryzias_latipes              LD.................................................
Xiphophorus_maculatus        LD.................................................
Danio_rerio                  IT.................................................
Takifugu_rubripes            VE.................................................
Drosophila_melanogaster      LKHSADTGIPQWTVESHLVSRGEQLNNLGQSSSTQITGRSKVQSSTASTGNA
```

```
                                                  60                                  70
Heterocephalus_glaber          ...P.....QEAPRG..........AEP...WKQQ..LTEDG......DS.F
Cavia_porcellus                ...P.....HEVLRG..........AEP...WKQQ..LTEDG......DS.F
Mesocricetus_auratus           ...P.....QEAPLA..........AEP...WKQQ..LTEDG......DS.F
Mus_musculus                   ...P.....QEAPLA..........AEP...WKQQ..LTEDG......DS.F
Rattus_norvegicus              ...P.....QEAPLA..........AEP...WKQQ..LTEDG......DS.F
Bos_taurus                     ...P.....QEAPRG..........AEP...WKQQ..LTEDG......DS.F
Tarsius_syrichta               ...........PPQP..........APP...WAPRSALTTPGVFPSRPRR.F
Oryctolagus_cuniculus          ...P.....QEAPRA..........AEP...WRQQ..LTEDG......DS.F
Lipotes_vexillifer             ...P.....QEAPRG.........................AG......LR.F
Otolemur_garnettii             ...P.....QEAPRG..........AEP...WKQQ..LTEDG......DS.F
Sus_scrofa                     ...P.....QEAPRG..........AEP...WKQQ..LTEDG......DS.F
Saimiri_boliviensis            ...P.....QEAPQG..........AEP...WKQQ..LTEDG......DS.F
Homo_sapiens                   ...P.....QEVPRG..........SEP...WKQQ..LTEDG......DS.F
Pongo_abelii                   ...P.....QEVPRG..........AEP...WKQQ..LTEDG......DS.F
Macaca_mulatta                 ...P.....QEVPRG..........AEP...WKQQ..LTEDG......DS.F
Macaca_fascicularis            ...P.....QEVPRG..........AEP...WKQQ..LTEDG......DS.F
Chlorocebus_sabaeus            ...P.....QEVPRG..........AEP...WKQQ..LTEDG......DS.F
Papio_anubis                   ...P.....QEVPRG..........AEP...WKQQ..LTEDG......DS.F
Callithrix_jacchus             ...P.....QEAQHG..........AEP...WKQQ..LTEDG......DS.F
Canis_lupus_familiaris         ...P.....QEAPRG..........AEP...WKQQ..LTEDG......DS.F
Equus_caballus                 ...P.....CAIPRSPRLPGPTHCTHRP...W..G..FPSLP......LR.F
Felis_catus                    ...P.....QEAPRG..........TEP...WKQQ..LTEDG......DS.F
Ailuropoda_melanoleuca         ...P.....QEAPRG..........AEP...WKQQ..LTEDG......DS.F
Odobenus_rosmarus_divergens    ...P.....QEAPRG..........AEP...WKQQ..LTEDG......DS.F
Leptonychotes_weddellii        ...P.....QEAPRG..........AEP...WKQQ..LTEDG......DS.F
Pelodiscus_sinensis            ...TPGQKKHRLPVN.........EKAHVLPWLIVPGPTLRGCFFFPPSCRF
Anolis_carolinensis            .........PVLPDV..........AAPQTAWKQQ..VTEDG......DT.F
Xenopus_tropicalis             ...GPPDTSNYEPEP.........................WKKE..VNEDG......DT.F
Latimeria_chalumnae            ...TK....YELPQE..........ES...WKYQ..VTEDG......DT.L
Oreochromis_niloticus          ...CEAPEHKQLPAP..........TRELYEWQTQ..ITEDG......DT.L
Oryzias_latipes                ...CE....HKQPAA........VTGEPLQEWQTQ..ITEEG......DT.L
Xiphophorus_maculatus          ...SE..RQQAAART..........EEPLQEWQTQ..TTDEG......DT.L
Danio_rerio                    ...D.....FVGPTD..........EP...WKKE..LTEDG......DT.Y
Takifugu_rubripes              ...CEPPQQQPDPAV..........TGELHEWKRQ..ITEDG......DT.L
Drosophila_melanogaster        NPSGSGATSSAPPSS..........INIMNAWEQFYQQNDDG......DT.P

                                 80        90        100       110       120
Heterocephalus_glaber          LHLAIIHEEKALTMEVIRQVKGDLAFLNFQNNLQQTPLHLAVITKQPEITQA
Cavia_porcellus                LHLAIIHEEKVLTMEVIRQVKGDLAFLNFQNNLQQTPLHLAVITKQPEITQA
Mesocricetus_auratus           LHLAIIHEEKTLTMEVIRQVKGDLAFLNFQNTLQQTPLHLAVITNQPGIAEA
Mus_musculus                   LHLAIIHEEKPLTMEVIGQVKGDLAFLNFQNNLQQTPLHLAVITNQPGIAEA
Rattus_norvegicus              LHLAIIHEEKTLTMEVIGQVKGDLAFLNFQNNLQQTPLHLAVITNQPGIAEA
Bos_taurus                     LHLAIIHEEKALTMEVVRQVKGDLAFLNFQNNLQQTPLHLAVITNQPEIAEA
Tarsius_syrichta               LHLAIIHEEKALAMEVIRQVKGDVAFLNFQNNLQQTPLHLAVITNQPEIAKA
Oryctolagus_cuniculus          LHLAIIHEEKALTMEVIRQVKGDLAFLNFQNNLQQTPLHLAVITSQPEIAEA
Lipotes_vexillifer             LHLAIIHEEKVLTMEVVRQVKGDLAFLNFQNNLQQTPLHLAVITNQPEIAEA
Otolemur_garnettii             LHLAIIHEEKTLTMEVIRQVKGDLAFLNFQNNLQQTPLHLAVITKQPEIAEA
Sus_scrofa                     LHLAIIHEEKALTMEVVRQVKGDLAFLNFQNNLQQTPLHLAVITNQPEIAEA
Saimiri_boliviensis            LHLAIIHEEKALTMEVIRQVKGDVAFLNFQNNLQQTPLHLAVITNQPEIAEA
Homo_sapiens                   LHLAIIHEEKALTMEVIRQVKGDLAFLNFQNNLQQTPLHLAVITNQPEIAEA
Pongo_abelii                   LHLAIIHEEKALTMEVIRQVKGDLAFLNFQNNLQQTPLHLAVITNQPEIAEA
Macaca_mulatta                 LHLAIIHEEKALTMEVIRQVKGDLAFLNFQNNLQQTPLHLAVITNQPEIAEA
Macaca_fascicularis            LHLAIIHEEKALTMEVIRQVKGDLAFLNFQNNLQQTPLHLAVITNQPEIAEA
Chlorocebus_sabaeus            LHLAIIHEEKALTMEVIRQVKGDLAFLNFQNNLQQTPLHLAVITNQPEIAEA
Papio_anubis                   LHLAIIHEEKALTMEVIRQVKGDLAFLNFQNNLQQTPLHLAVITNQPEIAEA
Callithrix_jacchus             LHLAIIHEEKALTMEVIRQVKGDVAFLNFQNNLQQTPLHLAVITNQPEIAEA
Canis_lupus_familiaris         LHLAIIHEEKALTMEVVRQVKGDLAFLNFQNNLQQTPLHLAVITNQPEIAEA
Equus_caballus                 LHLAIIHEEKALTMEVVRQVKGDLAFLNFQNNLQQTPLHLAVITNQPEIAKA
Felis_catus                    LHLAIIHEEKALTMEVVRQVKGDLAFLNFQNNLQQTPLHLAVITNQPEIAEA
Ailuropoda_melanoleuca         LHLAIIHEEKALTMEVIRQVKGDLAFLNFQNNLQQTPLHLAVITNQPEIAEA
Odobenus_rosmarus_divergens    LHLAIIHEEKALTMEVIRQVKGDLAFLNFQNNLQQTPLHLAVITNQPEIAEA
Leptonychotes_weddellii        LHLAIIHEEKALTMEVIRQVKGDLAFLNFQNNLQQTPLHLAVITNQPEIAEA
Pelodiscus_sinensis            LHLAIIHEEKALSVEVIRQAAGDPAFLNFQNNLNQTPLHLAVITEQAEIAES
Anolis_carolinensis            LHLAIIHEEKPLSLEIIRQAERDAAFLNFQNNLNQTPLHLAVITDQPEIAET
Xenopus_tropicalis             LHLAIIHEEKTLVKEAIQRSYRDHFYLNKQNNLHQTALHLAVITEQQDISQS
Latimeria_chalumnae            LHLAIIHEEKMVSLNVIKAAG.NPVYLSLQNNLKQTPLHLSVITDQPEIAEC
Oreochromis_niloticus          LHLAIIHEAKEFIKTMIDQSK.NTDFLNRQNDLRQTPLHLAVITKQPEVCLN
Oryzias_latipes                LHLAIIHEAKDFTQKMINMTK.NTDFLNAQNDLRQTPLHLAVITNQPDVCYG
Xiphophorus_maculatus          LHLAIIHEAKDYIKQMIDLSK.NTPFLNAQNDLRQTPLHLAVITNQLNVCSS
Danio_rerio                    LHLAIIHEATDAALKMIALSRRDP.FLNIQNNQRQTALHLAIITDQPLIVEQ
Takifugu_rubripes              LHLAIIHEAKDYIKTMIDLSR.NTDFLDLQNDQRQTPLHLAVITNQANVCLD
Drosophila_melanogaster        LHLACISGSVDVVAALIRMAP.HPCLLNIQNDVAQTPLHLAALTAQPNIMRI
```

```
                                  130       140       150       160       170
Heterocephalus_glaber            LLEAGCDPELRDFRGNTPLHLACEQGCLASVGVLTQTCTAQRLHSI......
Cavia_porcellus                  LLEAGCDPELRDFRGNTPLHLACEQGCLASVAVLTQTCTTQHLHSI......
Mesocricetus_auratus             LLEAGCDPELRDFRGNTPLHLACEQGCLASVGVLTQTCTPQHLHSI......
Mus_musculus                     LLKAGCDPELRDFRGNTPLHLACEQGCLASVAVLTQTCTPQHLHSV......
Rattus_norvegicus                LLKAGCDPELRDFRGNTPLHLACEQGCLASVAVLTQTCTPQHLHSV......
Bos_taurus                       LLEAGCDPELRDFRGNTPLHLACEQGCLASVGVLTQPRGTQHLHSI......
Tarsius_syrichta                 LLAAGCDPELRDFRGNTPLHLACEQGCLASVGVLTQTCTTQHLHSI......
Oryctolagus_cuniculus            LLEAGCDPELRDFRGNTPLHLACEQGCLASVGVLKQTCTAQHLHSI......
Lipotes_vexillifer               LLEAGCDPELRDFRGNTPLHLACEQGCLASVGVLTQPRGTQHLHSI......
Otolemur_garnettii               LLEAGCDPELRDFRGNTPLHLACEQGCLASVGVLTQTCTSQHLHSI......
Sus_scrofa                       LLEAGCDPELRDFRGNTPLHLACEQGCLASVGVLTQPRGTQHLHSI......
Saimiri_boliviensis              LLGAGCDPELRDFRGNTPLHLACEQGCLASVGVLTQACTTPHLHSI......
Homo_sapiens                     LLGAGCDPELRDFRGNTPLHLACEQGCLASVGVLTQSCTTPHLHSI......
Pongo_abelii                     LLGAGCDPELRDFRGNTPLHLACEQGCLASVGVLTQSCTTQHLHSI......
Macaca_mulatta                   LLGAGCDPELRDFRGNTPLHLACEQGCLASVGVLTQSCTTPHLHSI......
Macaca_fascicularis              LLGAGCDPELRDFRGNTPLHLACEQGCLASVGVLTQSCTTPHLHSI......
Chlorocebus_sabaeus              LLGAGCDPELRDFRGNTPLHLACEQGCLASVGVLTQSCATPHLHSI......
Papio_anubis                     LLGAGCDPELRDFRGNTPLHLACEQGCLASVGVLTQSCTTPHLHSI......
Callithrix_jacchus               LLGAGCDPELRDFRGNTPLHLACEQGCLASVGVLTQACTTPHLHSI......
Canis_lupus_familiaris           LLEAGCDPELRDFRGNTPLHLACEQGCLASVGVLTQTCRTQHLYSI......
Equus_caballus                   LLEAGCDPELRDFRGNTPLHLACEQGCLASVGVLTQSYGTPHLHSI......
Felis_catus                      LLEAGCDPELRDFRGNTPLHLACEQGCLASVGVLTQTCRTQHLYSI......
Ailuropoda_melanoleuca           LLEAGCDPELRDFRGNTPLHLACEQGCLASVGVLTQTCRTQPLYSI......
Odobenus_rosmarus_divergens      LLEAGCDPELRDFRGNTPLHLACEQGCLASVGVLTQTCRTQHLYSI......
Leptonychotes_weddellii          LLEAGCDPELRDFRGNTPLHLACEQGCLASVGVLTQTCRTQHLYSI......
Pelodiscus_sinensis              LLKAGCDPEIRDFRGNTPLHIACDQGSLRAVSVLTQYCQQHLCSV......
Anolis_carolinensis              LLKAGCDPEIRDFRGNTPLHIACERGSLSSVGVLTQYC.QKQVCSL......
Xenopus_tropicalis               LLQAGCDPEIQDFCGNTALHIACKQGSLRGVGVIFQYC.EKQLPAL......
Latimeria_chalumnae              LLWAGCDPEIRDLRGNTALHVACEQGSLLSVAVLTQACNKEQIPSL......
Oreochromis_niloticus            LLVSGCDPTLVDNNGDTPLHIACRHGNLHCFSVITQKSRPVHLHTA......
Oryzias_latipes                  LIVSGCNITVVDNNGDTPLHIACRHGNLHCFSAITQNCRPEQLHTA......
Xiphophorus_maculatus            LLASGCDPTLVDNSGDTPLHIACRHGNLYCFSVITQNCRLEHLHTA......
Danio_rerio                      LLKAGCDASLVDDHGNTALHIACRKGSLACFGLLTQGC.SQHLSAI......
Takifugu_rubripes                LLASGCDPTLVDRHGDTPLHIACRHGNLLCFSVITQNCRPEHLSGM......
Drosophila_melanogaster          LLLAGAEPTVRDRHGNTALHLSCIAGEKQCVRALTEKFGATEIHEAHRQYGH

                                                  180       190       200
Heterocephalus_glaber            ..................LQATNYNGHTCLHLASIHNYLGIVELLVSLGADV
Cavia_porcellus                  ..................LQATNYNGHTCLHLASIHGYLAIVERLVSLGADV
Mesocricetus_auratus             ..................LQATNYNGHTCLHLASIHGYLGIVEHLVSLGADV
Mus_musculus                     ..................LQATNYNGHTCLHLASIHGYLAIVEHLVTLGADV
Rattus_norvegicus                ..................LQATNYNGHTCLHLASIHGYLGIVEHLVTLGADV
Bos_taurus                       ..................LQATNYNGHTCLHLASIHGYLGIVELLVSLGADV
Tarsius_syrichta                 ..................LQATNYNGHTCLHLASIHGYLGIVELLVSLGADV
Oryctolagus_cuniculus            ..................LQAINYNGHTCLHLASIHGYLGIVELLVSWGADV
Lipotes_vexillifer               ..................LQATNYNGHTCLHLASIHGYLGIVELLVSLGADV
Otolemur_garnettii               ..................LQATNYNGHTCLHLASIHGYLGIVELLVSLGADV
Sus_scrofa                       ..................LQATNYNGHTCLHLASIHGYLGIVELLVSLGADV
Saimiri_boliviensis              ..................LKATNYNGHTCLHLASIHGYLGIVELLVSLGADV
Homo_sapiens                     ..................LKATNYNGHTCLHLASIHGYLGIVELLVSLGADV
Pongo_abelii                     ..................LKATNYNGHTCLHLASIHGYLGIVELLVSLGADV
Macaca_mulatta                   ..................LKATNYNGHTCLHLASIHGYLGIVELLVSLGADV
Macaca_fascicularis              ..................LKATNYNGHTCLHLASIHGYLGIVELLVSLGADV
Chlorocebus_sabaeus              ..................LKATNYNGHTCLHLASIHGYLGIVELLVSLGADV
Papio_anubis                     ..................LKATNYNGHTCLHLASIHGYLGIVELLVSLGADV
Callithrix_jacchus               ..................LKATNYNGHTCLHLASIHGYLGIVELLVSLGADV
Canis_lupus_familiaris           ..................LQATNYNGHTCLHLASIHGYLGIVELLVSLGADV
Equus_caballus                   ..................LQATNYNGHTCLHLASIHGYLGIVELLVSLGADV
Felis_catus                      ..................LQATNYNGHTCLHLASIHGYLGIVELLVSLGADV
Ailuropoda_melanoleuca           ..................LQATNYNGHTCLHLASIHGYLGIVELLVSLGADV
Odobenus_rosmarus_divergens      ..................LQATNYNGHTCLHLASIHGYLGIVELLVSLGADV
Leptonychotes_weddellii          ..................LQATNYNGHTCLHLASIHGYLGIVELLVSLGADV
Pelodiscus_sinensis              ..................LQSANYNGHTCLHLASIQGYLAIVEYLLSLGADV
Anolis_carolinensis              ..................LQSSNYNGHTCLHLASIQGYLAIVEYLLSLGADV
Xenopus_tropicalis               ..................LQSVNYDGHTCLHLASIHGYLAIVENLINKGADI
Latimeria_chalumnae              ..................LQIKNYSGYTCLHLASIHGYLCLVEYLLSIGADI
Oreochromis_niloticus            ..................MAACNYNGQNCLHLASVQGFLSLVERLVDLGADI
Oryzias_latipes                  ..................MATWNYNGQNCLHLASIYGFLLLVEKMVDLGADI
Xiphophorus_maculatus            ..................MAACNYNGQNCLHLASVHGFLSLVEKMVDLGADI
Danio_rerio                      ..................LQTPNYNGQKCIHVVAIQGYLSLLESLIQLGADI
Takifugu_rubripes                ..................MGACNYQGQNCLHVASVQGFLSLVENLVNLGADI
Drosophila_melanogaster          RSNDKAVSSLSYACLPADLEIRNYDGERCVHLAAEAGHIDILRILVSHGADI
```

```
                                210       220       230       240       250
Heterocephalus_glaber           NAQEPCNGRTALHLAVDLQNPDLVSLLLKCGADVNR..VTYQGYSPYQLTWG
Cavia_porcellus                 NAQEPCNGRTALHLAVDLQNPDLVSLLLKCGADVNR..VTYQGYSPYQLTWG
Mesocricetus_auratus            NAQEPCNGRTALHLAVDLQNPELVSLLLKCGADVNR..VTYQGYSPYQLTWG
Mus_musculus                    NAQEPCNGRTALHLAVDLQNPDLVSLLLKCGADVNR..VTYQGYSPYQLTWG
Rattus_norvegicus               NAQEPCNGRTALHLAVDLQNPDLVSLLLKCGADVNR..VTYQGYSPYQLTWG
Bos_taurus                      NAQEPCNGRTALHLAVDLQNPDLVSLLLKCGADVNR..VTYQGYSPYQLTWG
Tarsius_syrichta                NAQEPCNGRTALHLAVDLQNPDLVSLLLKCGADVNR..VTYQGYSPYQLTWG
Oryctolagus_cuniculus           NAQEPCNGRTALHLAVDLQNPDLVSLLLKCGADVNR..VTYQGYSPYQLTWG
Lipotes_vexillifer              NAQEPCNGRTALHLAVDLQNPDLVSLLLKCGADVNR..VTYQGYSPYQLTWG
Otolemur_garnettii              NAQEPCNGRTALHLAVDLQNPDLVSLLLKCGADVNR..VTYQGYSPYQLTWG
Sus_scrofa                      NAQEPCNGRTALHLAVDLQNPDLVSLLLKCGADVNR..VTYQGYSPYQLTWG
Saimiri_boliviensis             NAQEPCNGRTALHLAVDLQNPDLVSLLLKCGADVNR..VTYQGYSPYQLTWG
Homo_sapiens                    NAQEPCNGRTALHLAVDLQNPDLVSLLLKCGADVNR..VTYQGYSPYQLTWG
Pongo_abelii                    NAQEPCNGRTALHLAVDLQNPDLVSLLLKCGADVNR..VTYQGYSPYQLTWG
Macaca_mulatta                  NAQEPCNGRTALHLAVDLQNPDLVSLLLKCGADVNR..VTYQGYSPYQLTWG
Macaca_fascicularis             NAQEPCNGRTALHLAVDLQNPDLVSLLLKCGADVNR..VTYQGYSPYQLTWG
Chlorocebus_sabaeus             NAQEPCNGRTALHLAVDLQNPDLVSLLLKCGADVNR..VTYQGYSPYQLTWG
Papio_anubis                    NAQEPCNGRTALHLAVDLQNPDLVSLLLKCGADVNR..VTYQGYSPYQLTWG
Callithrix_jacchus              NAQEPCNGRTALHLAVDLQNPDLVSLLLKCGADVNR..VTYQGYSPYQLTWG
Canis_lupus_familiaris          NAQEPCNGRTALHLAVDLQNSDLVSLLLKCGADVNR..VTYQGYSPYQLTWG
Equus_caballus                  NAQEPCNGRTALHLAVDLQNPDLVSLLLKCGADVNR..VTYQGYSPYQLTWG
Felis_catus                     NAQEPCNGRTALHLAVDLQNSDLVSLLLKCGADVNR..VTYQGYSPYQLTWG
Ailuropoda_melanoleuca          NAQEPCNGRTALHLAVDLQNSDLVSLLLKCGADVNR..VTYQGYSPYQLTWG
Odobenus_rosmarus_divergens     NAQEPCNGRTALHLAVDLQNSDLVSLLLKCGADVNR..VTYQGYSPYQLTWG
Leptonychotes_weddellii         NAQEPCNGRTALHLAVDLQNSDLVSLLLKCGADVNR..VTYQGYSPYQLTWG
Pelodiscus_sinensis             NAQEPCNGRTALHLAVDLQNSELVSLLVKHGADVNK..VTYQGYSPYQLTWG
Anolis_carolinensis             NAQEPCNGRTALHLAVDLQNQDLVTLLLNHGADVNR..VTYQGYSPYQLTWG
Xenopus_tropicalis              NAQEPCNGRTVLHMAVDLQNYDLMKLLLKHGADVNR..VTYQGYSPCQLTWG
Latimeria_chalumnae             NAQESCNGRTALHLAVDLQNAGLVSLLVKKEADVNC..VTYEGYSPYQLTWG
Oreochromis_niloticus           NAKEQHNGRSALHLAVDQQNLLLVKLLLKKGANPNL..LSFGGHCPYHLTIG
Oryzias_latipes                 NTREQHNGRGALHLAVDQQNLCLVKLLLKKGADPNL..LTSGGYTPYHLTYG
Xiphophorus_maculatus           NAKEQHNGRSSLHLAVDQQNLALVKLLLRKGADPNL..LSSGGHTPFHLTYG
Danio_rerio                     NAQEQCNGRTALHLAVDLQNFDMVKLLIEKGASVHS..VTYGGHTPYHLTYG
Takifugu_rubripes               NAQEQRNGRGALHLAVDQQNLSLVKLLLSRGADPNL..VSSGGHTPYHLTYG
Drosophila_melanogaster         NAREGKSGRTPLHIAIEGCNEDLANFLLDECEKLNLETATYAGLTAYQFACI

                                260       270       280       290       300
Heterocephalus_glaber           RPSTRIQQQLGQLTLKNLQMLPESEDEESYDTESE.....FTEDELPYD...
Cavia_porcellus                 RPSTQIQQQLGQLTLENLQMLPESEDEESYDTESE.....FTEDELPYD...
Mesocricetus_auratus            RPSTRIQQQLGQLTLENLQMLPESEDEESYDTESE.....FTEDELPYD...
Mus_musculus                    RPSTRIQQQLGQLTLENLQMLPESEDEESYDTESE.....FTEDELPYD...
Rattus_norvegicus               RPSTRIQQQLGQLTLENLQTLPESEDEESYDTESE.....FTEDELPYD...
Bos_taurus                      RPSTRIQQQLGQLTLENLQTLPESEDEESYDTESE.....FTEDELPYD...
Tarsius_syrichta                RPSTRIQQQLGQLTPENLQMLPESEDEESYDTESE.....FTEDELPYD...
Oryctolagus_cuniculus           RPSTRIQQQLGQLTLENLQRLPESEDEESCDTESD.....GTEDELPYD...
Lipotes_vexillifer              RPSTRIQQQLGQLTLENLQMLPESEDEESYDTESE.....FTEDELPYD...
Otolemur_garnettii              RPSTRIQQQLGQLTLENLQMLPESEDEESYDTESE.....FTEDELPYD...
Sus_scrofa                      RPSTRIQQQLGQLTLENLQMLPESEDEESYDTESE.....FTEDELPYD...
Saimiri_boliviensis             RPSTRIQQQLGQLTLENLQMLPESEDEESYDTESE.....FTEDELPYD...
Homo_sapiens                    RPSTRIQQQLGQLTLENLQMLPESEDEESYDTESEFTE..FTEDELPYD...
Pongo_abelii                    RPSTRIQQQLGQLTLENLQMLPESEDEESYDTESEFTE..FTEDELPYD...
Macaca_mulatta                  RPSTRIQQQLGQLTLENLQMLPESEDEESYDTESEFTE..FTEDELPYD...
Macaca_fascicularis             RPSTRIQQQLGQLTLENLQMLPESEDEESYDTESEFTE..FTEDELPYD...
Chlorocebus_sabaeus             RPSTRIQQQLGQLTLENLQMLPESEDEESYDTESEFTE..FTEDELPYD...
Papio_anubis                    RPSTRIQQQLGQLTLENLQMLPESEDEESYDTESEFTE..FTEDELPYD...
Callithrix_jacchus              RPSTRIQQQLGQLTLENLQMLPESEDEESYDTESE.....FTEDELPYD...
Canis_lupus_familiaris          RPSTRIQQQLGQLTLENLQMLPESEDEESYDTESE.....FTEDELPYD...
Equus_caballus                  RPSTRIQQQLGQLTLENLQMLPESEDEESYDTESE.....FTEDELPYD...
Felis_catus                     RPSTRIQQQLGQLTLENLQMLPESEDEESYDTESE.....FTEDELPYD...
Ailuropoda_melanoleuca          RPSTRIQQQLGQLTLENLQMLPESEDEESYDTESE.....FTEDELPYD...
Odobenus_rosmarus_divergens     RPSTRIQQQLGQLTLENLQLLPESEDEESYDTESE.....FTEDELPYD...
Leptonychotes_weddellii         RPSTRIQQQLGQLTLENLQMLPESEDEESYDTESE.....FTEDELPYD...
Pelodiscus_sinensis             RESCRIQEQLKHLTMADLQMLPESEDEESCESESE.....FMEDEIMYD...
Anolis_carolinensis             RSNSSIQEKLKQFTTMDLQMLPESEDEESCESDSE.....FTEDELLYD...
Xenopus_tropicalis              RNNMLIQQQLVEVTHKNLQYLPESEEEDSSDSEYE.....YNDDELMYD...
Latimeria_chalumnae             RENFEIQKELGCLTDPCLQLLPEGDESDISDSEA........EEEQMYD...
Oreochromis_niloticus           LDNWEINKELYSVTHPDLRELPDSESDDSDEEEHM.....DSDDEVNYD...
Oryzias_latipes                 LDNCDIRKELHPLTHPDLRELPDSDSENSEEDSDE.....EFDEGVMYD...
Xiphophorus_maculatus           LDNCDIQKELFPVTHPDLRDLSESENSGEESSEEE......SDEEGMYD...
Danio_rerio                     RSNADIQKVLYELTSPHLRELPESDSEDSEDSDEDYEERCQSEVEDLYD...
Takifugu_rubripes               RHDDDIRKELYATTNPDLRELPDSESDDSEGEEDE.....ASDDEVGYD...
Drosophila_melanogaster         MNKSRMQNILEKRGAETVT..PPDSDYDSSDIED......LDDTKMYDRFG
```

```
                                          310
                                           .
Heterocephalus_glaber          DCVF.....GGQRLTL.
Cavia_porcellus                DCVF.....GGQRLTL.
Mesocricetus_auratus           DCVF.....GGQRLTL.
Mus_musculus                   DCVF.....GGQRLTL.
Rattus_norvegicus              DCVF.....GGQRLTL.
Bos_taurus                     DCVL.....GGQRLTL.
Tarsius_syrichta               DCVF.....GGQRLTL.
Oryctolagus_cuniculus          DCVF.....GGQRLTL.
Lipotes_vexillifer             DCVL.....GGQRLTL.
Otolemur_garnettii             DCVF.....GGQRLKL.
Sus_scrofa                     DCVL.....GGQRLTL.
Saimiri_boliviensis            DCVF.....AGQRLTL.
Homo_sapiens                   DCVF.....GGQRLTL.
Pongo_abelii                   DCVF.....GGQRLML.
Macaca_mulatta                 DCVF.....GGQRLTL.
Macaca_fascicularis            DCVF.....GGQRLTL.
Chlorocebus_sabaeus            DCVF.....GGQRLTL.
Papio_anubis                   DCVF.....GGQRLTL.
Callithrix_jacchus             DCVF.....AGQRLTL.
Canis_lupus_familiaris         DCVL.....GGQRLTL.
Equus_caballus                 DCVL.....GGQRLTL.
Felis_catus                    DCVL.....GGQRLTL.
Ailuropoda_melanoleuca         DCVL.....GGQRLTL.
Odobenus_rosmarus_divergens    DCVL.....GGQRLTL.
Leptonychotes_weddellii        DCVL.....GGQRLTL.
Pelodiscus_sinensis            DCVI.....GGRQLVS.
Anolis_carolinensis            DCVI.....GGRHVPC.
Xenopus_tropicalis             DCII.....GGRPLH..
Latimeria_chalumnae            DCVM.....GGFLVSL.
Oreochromis_niloticus          DIHW.....NGH.....
Oryzias_latipes                DIKL.....NGH.....
Xiphophorus_maculatus          DIQW.....NGH.....
Danio_rerio                    DIKV.....MGQ.....
Takifugu_rubripes              DIQW.....NGH.....
Drosophila_melanogaster        DPRYFVSYNGGNPMTVA
```

Appendix VI) Structures of NEMO-IKKβ Interaction Inhibitor Hits

CMLD10190	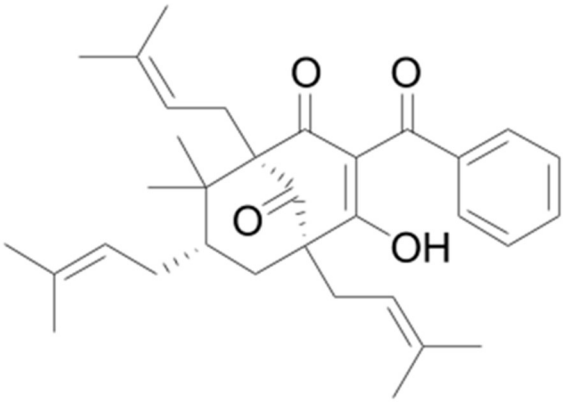
CMLD10487	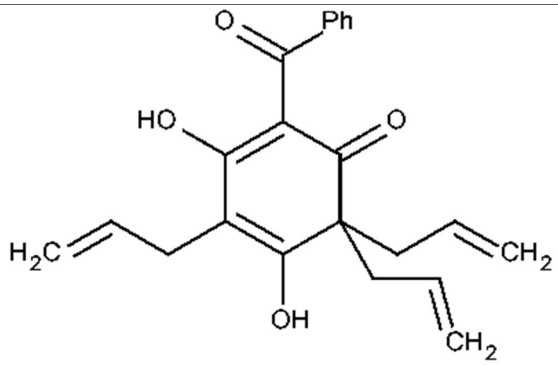
CMLD10557	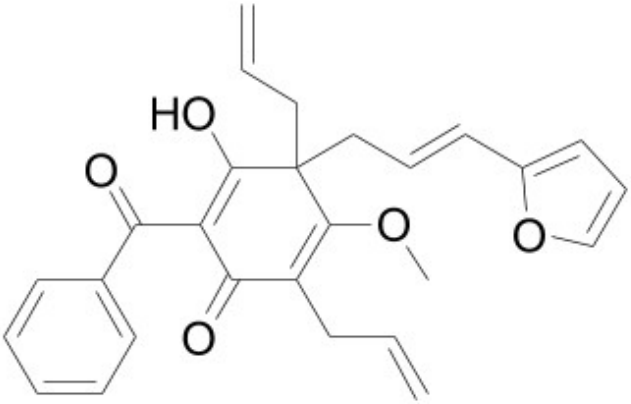

Appendix VII) Flow synthesis of IκBα 13mer Peptide

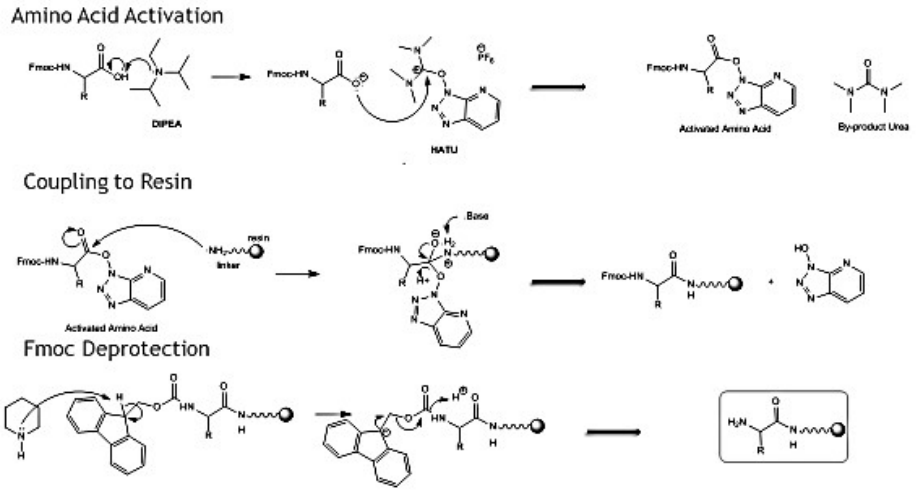

Appendix Figure 5: Synthesis schematic for base-activating amino acids, amide coupling to the resin or growing polypeptide chain on resin, and deprotecting the coupled amino acid by removing Fmoc (Simon 2014).

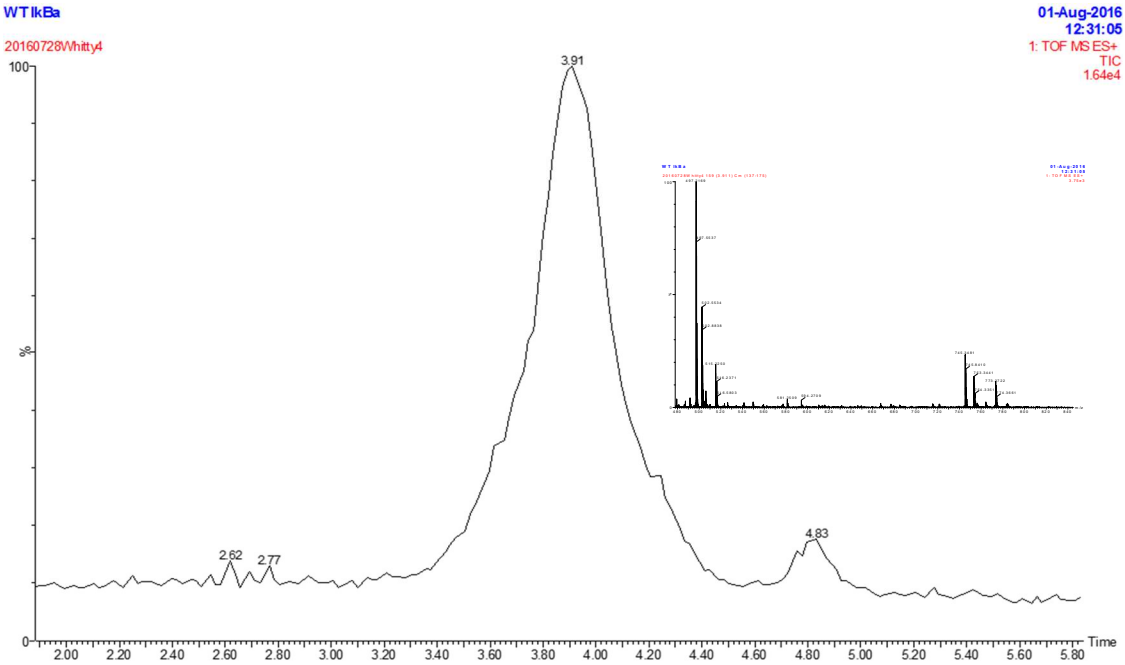

Appendix Figure 6: liquid chromatography result for WT IκBα(27-DDRHDSGLDSMKD-39). Major peak shows purity of desired peptide. Inset: ESI-MS confirmation of peptide mass (daughter ion peaks at 497 [3^+] and 745 [2^+]). LC-MS performed on Waters qTOF Premier instrument using reverse phase column.

References

(1) Shaw, A. S., and Filbert, E. L. (2009) Scaffold proteins and immune-cell signalling. *Nature Reviews Immunology 9*, 47–56.

(2) Cortese, M. S., Uversky, V. N., and Keith Dunker, A. (2008) Intrinsic disorder in scaffold proteins: Getting more from less. *Progress in Biophysics and Molecular Biology 98*, 85–106.

(3) Dhanasekaran, D. N., Kashef, K., Lee, C. M., Xu, H., and Reddy, E. P. (2007) Scaffold proteins of MAP-kinase modules. *Oncogene 26*, 3185–3202.

(4) Pan, C. Q., Sudol, M., Sheetz, M., and Low, B. C. (2012) Modularity and functional plasticity of scaffold proteins as p(l)acemakers in cell signaling. *Cellular Signalling 24*, 2143–2165.

(5) Vaquero, J., Nguyen Ho-Bouldoires, T. H., Clapéron, A., and Fouassier, L. (2017) Role of the PDZ-scaffold protein NHERF1/EBP50 in cancer biology: from signaling regulation to clinical relevance. *Oncogene* 3067–3079.

(6) Pawson, T. (1995) Protein modules and signalling networks. *Nature 373*, 573–580.

(7) Good, M. C., Zalatan, J. G., and Lim, W. A. (2011) Scaffold Proteins: Hubs for Controlling the Flow of Cellular Information. *Science 332*, 680–686.

(8) Adams, D. R., Ron, D., and Kiely, P. A. (2011) RACK1, A multifaceted scaffolding protein: Structure and function. *Cell Communication and Signaling 9*, 22.

(9) Evdokimov, A. G., Anderson, D. E., Routzahn, K. M., and Waugh, D. S. (2001) Unusual molecular architecture of the Yersinia pestis cytotoxin YopM: a leucine-rich repeat protein with the shortest repeating unit 1 1Edited by R. Huber. *Journal of Molecular Biology 312*, 807–821.

(10) Brown, M. D., and Sacks, D. B. (2009) Protein scaffolds in MAP kinase signalling. *Cellular Signalling 21*, 462–469.

(11) Robert, H. S., Quint, A., Brand, D., Vivian-Smith, A., and Offringa, R. (2009) BTB and TAZ domain scaffold proteins perform a crucial function in Arabidopsis

development: Arabidopsis BT proteins and gametophyte development. *The Plant Journal 58*, 109–121.

(12) Zeke, A., Lukács, M., Lim, W. A., and Reményi, A. (2009) Scaffolds: interaction platforms for cellular signalling circuits. *Trends in Cell Biology 19*, 364–374.

(13) Nourry, C., Grant, S. G. N., and Borg, J.-P. (2003) PDZ Domain Proteins: Plug and Play! *Science Signaling 2003*, RE7.

(14) Goldberg, J. M., Manning, G., Liu, A., Fey, P., Pilcher, K. E., Xu, Y., and Smith, J. L. (2006) The Dictyostelium Kinome—Analysis of the Protein Kinases from a Simple Model Organism. *PLoS Genetics 2*, e38.

(15) Pincus, D., Letunic, I., Bork, P., and Lim, W. A. (2008) Evolution of the phospho-tyrosine signaling machinery in premetazoan lineages. *Proceedings of the National Academy of Sciences 105*, 9680–9684.

(16) Clapéron, A., and Therrien, M. (2007) KSR and CNK: two scaffolds regulating RAS-mediated RAF activation. *Oncogene 26*, 3143–3158.

(17) Whitmarsh, A. J. (2006) The JIP family of MAPK scaffold proteins. Portland Press Limited.

(18) McDonald, P. H., Chow, C.-W., Miller, W. E., Laporte, S. A., Field, M. E., Lin, F.-T., Davis, R. J., and Lefkowitz, R. J. (2000) beta-Arrestin 2: A Receptor-Regulated MAPK Scaffold for the Activation of JNK3. *Science 290*, 1574–1577.

(19) Malleshaiah, M. K., Shahrezaei, V., Swain, P. S., and Michnick, S. W. (2010) The scaffold protein Ste5 directly controls a switch-like mating decision in yeast. *Nature 465*, 101–105.

(20) Deakin, N. O., and Turner, C. E. (2008) Paxillin comes of age. *Journal of Cell Science 121*, 2435–2444.

(21) Sármay, G., Angyal, A., Kertész, Á., Maus, M., and Medgyesi, D. (2006) The multiple function of Grb2 associated binder (Gab) adaptor/scaffolding protein in immune cell signaling. *Immunology Letters 104*, 76–82.

(22) Zhu, J., Shang, Y., Xia, C., Wang, W., Wen, W., and Zhang, M. (2011) Guanylate kinase domains of the MAGUK family scaffold proteins as specific phospho-protein-binding modules. *The EMBO Journal 30*, 4986–4997.

(23) Shiraishi-Yamaguchi, Y., and Furuichi, T. (2007) The Homer family proteins. *Genome Biology 8*, 1–12.

(24) Langeberg, L. K. (2005) A-kinase-anchoring proteins. *Journal of Cell Science 118*, 3217–3220.

(25) Li, D., and Roberts, R. (2001) WD-repeat proteins: structure characteristics, biological function, and their involvement in human diseases. *Cell and Molecular Life Sciences 58*, 2085–2097.

(26) Ramamurthy, V., Krystek, S. R., Bush, A., Wei, A., Emanuel, S. L., Das Gupta, R., Janjua, A., Cheng, L., Murdock, M., Abramczyk, B., Cohen, D., Lin, Z., Morin, P., Davis, J. H., Dabritz, M., McLaughlin, D. C., Russo, K. A., Chao, G., Wright, M. C., Jenny, V. A., Engle, L. J., Furfine, E., and Sheriff, S. (2012) Structures of Adnectin/Protein Complexes Reveal an Expanded Binding Footprint. *Structure 20*, 259–269.

(27) Weidle, U. H., Auer, J., Brinkmann, U., Georges, G., and Tiefenthaler, G. (2013) The emerging role of new protein scaffold-based agents for treatment of cancer. *Cancer Genomics-Proteomics 10*, 155–168.

(28) Rushe, M., Silvian, L., Bixler, S., Chen, L. L., Cheung, A., Bowes, S., Cuervo, H., Berkowitz, S., Zheng, T., Guckian, K., Pellegrini, M., and Lugovskoy, A. (2008) Structure of a NEMO/IKK-Associating Domain Reveals Architecture of the Interaction Site. *Structure 16*, 798–808.

(29) Watkins, A. M., Wuo, M. G., and Arora, P. S. (2015) Protein–Protein Interactions Mediated by Helical Tertiary Structure Motifs. *Journal of the American Chemical Society 137*, 11622–11630.

(30) Nussinov, R., Ma, B., and Tsai, C.-J. (2013) A broad view of scaffolding suggests that scaffolding proteins can actively control regulation and signaling of multienzyme complexes through allostery. *Biochimica et Biophysica Acta - Proteins and Proteomics 1834*, 820–829.

(31) Liu, W., Rui, H., Wang, J., Lin, S., He, Y., Chen, M., Li, Q., Ye, Z., Zhang, S., Chan, S. C., and others. (2006) Axin is a scaffold protein in TGF-β signaling that promotes degradation of Smad7 by Arkadia. *The EMBO Journal 25*, 1646–1658.

(32) Han, H., and Kursula, P. (2014) Periaxin and AHNAK Nucleoprotein 2 Form Intertwined Homodimers through Domain Swapping. *Journal of Biological Chemistry 289*, 14121–14131.

(33) Cautain, B., Hill, R., de Pedro, N., and Link, W. (2015) Components and regulation of nuclear transport processes. *FEBS Journal 282*, 445–462.

(34) Huxford, T., Huang, D.-B., Malek, S., and Ghosh, G. (1998) The Crystal Structure of the IkBa/NF-kB Complex Reveals Mechanisms of NF-kB Inactivation. *Cell 95*, 759–770.

(35) Brennan, D. F., Dar, A. C., Hertz, N. T., Chao, W. C. H., Burlingame, A. L., Shokat, K. M., and Barford, D. (2011) A Raf-induced allosteric transition of KSR stimulates phosphorylation of MEK. *Nature 472*, 366–369.

(36) Brenman, J. E., Chao, D. S., Gee, S. H., McGee, A. W., Craven, S. E., Santillano, D. R., Wu, Z., Huang, F., Xia, H., Peters, M. F., and others. (1996) Interaction of nitric oxide synthase with the postsynaptic density protein PSD-95 and α1-syntrophin mediated by PDZ domains. *Cell 84*, 757–767.

(37) Dai, Z., Kim, J. H., Tonelli, M., Ali, I. K., and Markley, J. L. (2014) pH-Induced Conformational Change of IscU at Low pH Correlates with Protonation/Deprotonation of Two Conserved Histidine Residues. *Biochemistry* 5290–5297.

(38) Huang, W. Y. C., Ditlev, J. A., Chiang, H.-K., Rosen, M. K., and Groves, J. T. (2017) Allosteric Modulation of Grb2 Recruitment to the Intrinsically Disordered Scaffold Protein, LAT, by Remote Site Phosphorylation. *Journal of the American Chemical Society 139*, 18009–18015.

(39) Morales, F. C., Takahashi, Y., Momin, S., Adams, H., Chen, X., and Georgescu, M.-M. (2007) NHERF1/EBP50 Head-to-Tail Intramolecular Interaction Masks Association with PDZ Domain Ligands. *Molecular and Cellular Biology 27*, 2527–2537.

(40) Zalatan, J. G., Coyle, S. M., Rajan, S., Sidhu, S., and Lim, W. A. (2012) Conformational Control of the Ste5 Scaffold Protein Insulates Against MAP Kinase Misactivation. *Science 337*, 1218–1222.

(41) Walczak, M. J., Samatanga, B., van Drogen, F., Peter, M., Jelesarov, I., and Wider, G. (2014) The RING Domain of the Scaffold Protein Ste5 Adopts a Molten Globular Character with High Thermal and Chemical Stability. *Angewandte Chemie International Edition 53*, 1320–1323.

(42) Courtois, G., and Gilmore, T. D. (2006) Mutations in the NF-κB signaling pathway: implications for human disease. *Oncogene 25*, 6831–6843.

(43) Gilmore, T. D. (2006) Introduction to NF-κB: players, pathways, perspectives. *Oncogene 25*, 6680–6684.

(44) Ghosh, G., Wang, V. Y.-F., Huang, D.-B., and Fusco, A. (2012) NF-κB regulation: lessons from structures. *Immunological Reviews 246*, 36–58.

(45) Hayden, M. S., and Ghosh, S. (2008) Shared Principles in NF-κB Signaling. *Cell 132*, 344–362.

(46) Zandi, E., Rothwarf, D. M., Delhase, M., Hayakawa, M., and Karin, M. (1997) The IkB Kinase Complex (IKK) Contains Two Kinase Subunits, IKKa and IKKb, Necessary for IkB Phosphorylation and NF-kB Activation. *Cell 91*, 243–252.

(47) Shih, V. F.-S., Tsui, R., Caldwell, A., and Hoffmann, A. (2011) A single NFκB system for both canonical and non-canonical signaling. *Cell Research 21*, 86–102.

(48) Xu, M., Skaug, B., Zeng, W., and Chen, Z. J. (2009) A Ubiquitin Replacement Strategy in Human Cells Reveals Distinct Mechanisms of IKK Activation by TNFα and IL-1β. *Molecular Cell 36*, 302–314.

(49) Poyet, J.-L. (2000) Activation of the Ikappa B Kinases by RIP via IKKgamma /NEMO-mediated Oligomerization. *Journal of Biological Chemistry 275*, 37966–37977.

(50) Fujita, H., Rahighi, S., Akita, M., Kato, R., Sasaki, Y., Wakatsuki, S., and Iwai, K. (2014) Mechanism Underlying I B Kinase Activation Mediated by the Linear Ubiquitin Chain Assembly Complex. *Molecular and Cellular Biology 34*, 1322–1335.

(51) Haas, T. L., Emmerich, C. H., Gerlach, B., Schmukle, A. C., Cordier, S. M., Rieser, E., Feltham, R., Vince, J., Warnken, U., Wenger, T., Koschny, R., Komander, D., Silke, J., and Walczak, H. (2009) Recruitment of the Linear Ubiquitin Chain Assembly Complex Stabilizes the TNF-R1 Signaling Complex and Is Required for TNF-Mediated Gene Induction. *Molecular Cell 36*, 831–844.

(52) Tokunaga, F., and Iwai, K. (2012) LUBAC, a novel ubiquitin ligase for linear ubiquitination, is crucial for inflammation and immune responses. *Microbes and Infection 14*, 563–572.

(53) Tokunaga, F., Sakata, S., Saeki, Y., Satomi, Y., Kirisako, T., Kamei, K., Nakagawa, T., Kato, M., Murata, S., Yamaoka, S., Yamamoto, M., Akira, S., Takao, T., Tanaka, K., and Iwai, K. (2009) Involvement of linear polyubiquitylation of NEMO in NF-κB activation. *Nature Cell Biology 11*, 123–132.

(54) Deng, L., Wang, C., Spencer, E., Yang, L., Braun, A., You, J., Slaughter, C., Pickart, C., and Chen, Z. J. (2000) Activation of the IκB kinase complex by TRAF6 requires a dimeric ubiquitin-conjugating enzyme complex and a unique polyubiquitin chain. *Cell 103*, 351–361.

(55) Zhao-Hui Wu, Yuling Shi, Randal S. Tibbetts, and Shigeki Miyamoto. (2006) Molecular Linkage Between the Kinase ATM and NF-kB Signaling in Response to Genotoxic Stimuli. *Science 311*, 1141–1146.

(56) Palkowitsch, L., Leidner, J., Ghosh, S., and Marienfeld, R. B. (2008) Phosphorylation of Serine 68 in the I B Kinase (IKK)-binding Domain of NEMO Interferes with the Structure of the IKK Complex and Tumor Necrosis Factor- -induced NF- B Activity. *Journal of Biological Chemistry 283*, 76–86.

(57) Medunjanin, S., Schleithoff, L., Fiegehenn, C., Weinert, S., Zuschratter, W., and Braun-Dullaeus, R. C. (2016) GSK-3β controls NF-kappaB activity via IKKγ/NEMO. *Scientific Reports 6*, 38553.

(58) Schröfelbauer, B., Polley, S., Behar, M., Ghosh, G., and Hoffmann, A. (2012) NEMO Ensures Signaling Specificity of the Pleiotropic IKKβ by Directing Its Kinase Activity toward IκBα. *Molecular Cell 47*, 111–121.

(59) Israël, A. (2010) The IKK Complex, a Central Regulator of NF- B Activation. *Cold Spring Harbor Perspectives in Biology 2*, a000158–a000158.

(60) Luedde, T., Heinrichsdorff, J., de Lorenzi, R., De Vos, R., Roskams, T., and Pasparakis, M. (2008) IKK1 and IKK2 cooperate to maintain bile duct integrity in the liver. *Proceedings of the National Academy of Sciences USA 105*, 9733–9738.

(61) May, M. J. (2002) Characterization of the Ikappa B-kinase NEMO Binding Domain. *Journal of Biological Chemistry 277*, 45992–46000.

(62) Marienfeld, R. B., Palkowitsch, L., and Ghosh, S. (2006) Dimerization of the I B Kinase-Binding Domain of NEMO Is Required for Tumor Necrosis Factor Alpha-Induced NF- B Activity. *Molecular and Cellular Biology 26*, 9209–9219.

(63) Hauenstein, A. V., Xu, G., Kabaleeswaran, V., and Wu, H. (2017) Evidence for M1-Linked Polyubiquitin-Mediated Conformational Change in NEMO. *Journal of Molecular Biology 429*, 3793–3800.

(64) Chen, Z. J., Parent, L., and Maniatis, T. (1996) Site-Specific Phosphorylation of IkBa by a Novel Ubiquitination-Dependent Protein Kinase Activity. *Cell 84*, 853–862.

(65) Stilmann, M., Hinz, M., Arslan, S. Ç., Zimmer, A., Schreiber, V., and Scheidereit, C. (2009) A Nuclear Poly(ADP-Ribose)-Dependent Signalosome Confers DNA Damage-Induced IκB Kinase Activation. *Molecular Cell 36*, 365–378.

(66) Huang, T. T., Wuerzberger-Davis, S. M., Wu, Z.-H., and Miyamoto, S. (2003) Sequential modification of NEMO/IKKγ by SUMO-1 and ubiquitin mediates NF-κB activation by genotoxic stress. *Cell 115*, 565–576.

(67) Janssens, S., Tinel, A., Lippens, S., and Tschopp, J. (2005) PIDD Mediates NF-κB Activation in Response to DNA Damage. *Cell 123*, 1079–1092.

(68) Field, N. (2003) KSHV vFLIP binds to IKK- to activate IKK. *Journal of Cell Science 116*, 3721–3728.

(69) Shifera, A. S. (2010) Protein-protein interactions involving IKKγ (NEMO) that promote the activation of NF-κB. *Journal of Cellular Physiology* 558–561.

(70) Rudolph, D., Yeh, W.-C., Wakeham, A., Rudolph, B., Nallainathan, D., Potter, J., Elia, A. J., and Mak, T. W. (2000) Severe liver degeneration and lack of NF-kB activation in NEMO/IKKg-deficient mice. *Genes & Development 14*, 854–862.

(71) Reale, C., Iervolino, A., Scudiero, I., Ferravante, A., D'Andrea, L. E., Mazzone, P., Zotti, T., Leonardi, A., Roberto, L., Zannini, M., De Cristofaro, T., Shanmugakonar, M., Capasso, G., Pasparakis, M., Vito, P., and Stilo, R. (2016) NF-kB Essential MOdulator (NEMO) Is Critical for Thyroid Function. *Journal of Biological Chemistry 291*, 5765–5773.

(72) Swarnkar, G., Shim, K., Nasir, A. M., Seehra, K., Chen, H.-P. (Tim), Mbalaviele, G., and Abu-Amer, Y. (2016) Myeloid Deletion of Nemo Causes Osteopetrosis in Mice Owing to Upregulation of Transcriptional Repressors. *Scientific Reports 6*, 29896.

(73) Chan, L. K., Gerstenlauer, M., Konukiewitz, B., Steiger, K., Weichert, W., Wirth, T., and Maier, H. J. (2016) Epithelial NEMO/IKKγ limits fibrosis and promotes regeneration during pancreatitis. *Gut 66*, 1995–2007.

(74) Gilmore, T. D. (1999) Multiple mutations contribute to the oncogenicity of the retroviral oncoprotein v-Rel. *Oncogene 18*, 6925–6937.

(75) Xiao, G., Cvijic, M. E., Fong, A., Harhaj, E. W., Uhlik, M. T., Waterfield, M., and Sun, S.-C. (2001) Retroviral oncoprotein Tax induces processing of NF-kB2/p100 in T cells: evidence for the involvement of IKKa. *The EMBO Journal 20*, 6805–6815.

(76) Mosialos, G. (1997) The role of Rel/NF-κB proteins in viral oncogenesis and the regulation of viral transcription, in *Seminars in Cancer Biology*, pp 121–129. Elsevier.

(77) Karin, M., Cao, Y., Greten, F. R., and Li, Z.-W. (2002) NF-κB in cancer: from innocent bystander to major culprit. *Nature Reviews Cancer 2*, 301–310.

(78) Agou, F., Traincard, F., Vinolo, E., Courtois, G., Yamaoka, S., Israel, A., and Veron, M. (2004) The Trimerization Domain of Nemo Is Composed of the Interacting C-terminal CC2 and LZ Coiled-coil Subdomains. *Journal of Biological Chemistry 279*, 27861–27869.

(79) Tegethoff, S., Behlke, J., and Scheidereit, C. (2003) Tetrameric Oligomerization of I B Kinase (IKK) Is Obligatory for IKK Complex Activity and NF- B Activation. *Molecular and Cellular Biology 23*, 2029–2041.

(80) Bal, E., Laplantine, E., Hamel, Y., Dubosclard, V., Boisson, B., Pescatore, A., Picard, C., Hadj-Rabia, S., Royer, G., Steffann, J., Bonnefont, J.-P., Ursini, V. M., Vabres, P., Munnich, A., Casanova, J.-L., Bodemer, C., Weil, R., Agou, F., and Smahi, A. (2017) Lack of interaction between NEMO and SHARPIN impairs linear ubiquitination and NF-κB activation and leads to incontinentia pigmenti. *Journal of Allergy and Clinical Immunology 140*, 1671–1682.

(81) Zilberman-Rudenko, J., Shawver, L. M., Wessel, A. W., Luo, Y., Pelletier, M., Tsai, W. L., Lee, Y., Vonortas, S., Cheng, L., Ashwell, J. D., Orange, J. S., Siegel, R. M., and Hanson, E. P. (2016) Recruitment of A20 by the C-terminal domain of NEMO suppresses NF-κB activation and autoinflammatory disease. *Proceedings of the National Academy of Sciences USA 113*, 1612–1617.

(82) Senegas, A., Gautheron, J., Maurin, A. G. D., and Courtois, G. (2015) IKK-related genetic diseases: probing NF-κB functions in humans and other matters. *Cellular and Molecular Life Sciences 72*, 1275–1287.

(83) Vincendeau, M., Hadian, K., Messias, A. C., Brenke, J. K., Halander, J., Griesbach, R., Greczmiel, U., Bertossi, A., Stehle, R., Nagel, D., Demski, K., Velvarska, H., Niessing, D., Geerlof, A., Sattler, M., and Krappmann, D. (2016) Inhibition of Canonical NF-κB Signaling by a Small Molecule Targeting NEMO-Ubiquitin Interaction. *Scientific Reports 6*, 18934.

(84) De Falco, F., Di Giovanni, C., Cerchia, C., De Stefano, D., Capuozzo, A., Irace, C., Iuvone, T., Santamaria, R., Carnuccio, R., and Lavecchia, A. (2016) Novel non-peptide small molecules preventing IKKβ/NEMO association inhibit NF-κB activation in LPS-stimulated J774 macrophages. *Biochemical Pharmacology* 83–94.

(85) May, M. J., D'Acquisto, F., Madge, L. A., Glockner, J., Pober, J. S., and Ghosh, S. (2000) Selective Inhibition of NF-kB Activation by a Peptide That Blocks the Interaction of NEMO with the IkB Kinase Complex. *Science 289*, 1550–1554.

(86) Baima, E. T., Guzova, J. A., Mathialagan, S., Nagiec, E. E., Hardy, M. M., Song, L. R., Bonar, S. L., Weinberg, R. A., Selness, S. R., Woodard, S. S., Chrencik, J., Hood, W. F., Schindler, J. F., Kishore, N., and Mbalaviele, G. (2010) Novel Insights into the Cellular Mechanisms of the Anti-inflammatory Effects of NF- B Essential Modulator Binding Domain Peptides. *Journal of Biological Chemistry 285*, 13498–13506.

(87) Rangasamy, S. B., Corbett, G. T., Roy, A., Modi, K. K., Bennett, D. A., Mufson, E. J., Ghosh, S., and Pahan, K. (2015) Intranasal Delivery of NEMO-Binding Domain Peptide Prevents Memory Loss in a Mouse Model of Alzheimer's Disease. *Journal of Alzheimer's Disease 47*, 385–402.

(88) Friedmann-Morvinski, D., Narasimamurthy, R., Xia, Y., Myskiw, C., Soda, Y., and Verma, I. M. (2016) Targeting NF- B in glioblastoma: A therapeutic approach. *Science Advances 2*, e1501292–e1501292.

(89) Bruno, P. A., Morriss-Andrews, A., Henderson, A. R., Brooks, C. L., and Mapp, A. K. (2016) A Synthetic Loop Replacement Peptide That Blocks Canonical NF-κB Signaling. *Angewandte Chemie 128*, 15221–15225.

(90) Li, Q., Van Antwerp, D., Mercurio, F., Lee, K.-F., and Verma, I. M. (1999) Severe liver degeneration in mice lacking the IκB kinase 2 gene. *Science 284*, 321–325.

(91) McCarty, M. F. (2010) Salsalate may have broad utility in the prevention and treatment of vascular disorders and the metabolic syndrome. *Medical Hypotheses 75*, 276–281.

(92) Lan, X., Liu, R., Sun, L., Zhang, T., and Du, G. (2011) Methyl salicylate 2-O–D-lactoside, a novel salicylic acid analogue, acts as an anti-inflammatory agent on microglia and astrocytes. *Journal of Neuroinflammation 8*.

(93) Liou, J.-T., Huang, H.-S., Chiang, M.-L., Lin, C.-S., Yang, S.-P., Ho, L.-J., and Lai, J.-H. (2014) A salicylate-based small molecule HS-Cm exhibits immunomodulatory effects and inhibits dipeptidyl peptidase-IV activity in human T cells. *European Journal of Pharmacology 726*, 124–132.

(94) Bagnéris, C., Ageichik, A. V., Cronin, N., Wallace, B., Collins, M., Boshoff, C., Waksman, G., and Barrett, T. (2008) Crystal Structure of a vFlip-IKKγ Complex: Insights into Viral Activation of the IKK Signalosome. *Molecular Cell 30*, 620–631.

(95) Grubisha, O., Kaminska, M., Duquerroy, S., Fontan, E., Cordier, F., Haouz, A., Raynal, B., Chiaravalli, J., Delepierre, M., Israël, A., Véron, M., and Agou, F. (2010) DARPin-Assisted Crystallography of the CC2-LZ Domain of NEMO Reveals a Coupling between Dimerization and Ubiquitin Binding. *Journal of Molecular Biology 395*, 89–104.

(96) Lo, Y.-C., Lin, S.-C., Rospigliosi, C. C., Conze, D. B., Wu, C.-J., Ashwell, J. D., Eliezer, D., and Wu, H. (2009) Structural Basis for Recognition of Diubiquitins by NEMO. *Molecular Cell 33*, 602–615.

(97) Yoshikawa, A., Sato, Y., Yamashita, M., Mimura, H., Yamagata, A., and Fukai, S. (2009) Crystal structure of the NEMO ubiquitin-binding domain in complex with Lys 63-linked di-ubiquitin. *FEBS Letters 583*, 3317–3322.

(98) Cordier, F., Vinolo, E., Véron, M., Delepierre, M., and Agou, F. (2008) Solution Structure of NEMO Zinc Finger and Impact of an Anhidrotic Ectodermal Dysplasia with Immunodeficiency-related Point Mutation. *Journal of Molecular Biology 377*, 1419–1432.

(99) Rothwarf, D. M., Zandi, E., Natoli, G., and Karin, M. (1998) IKKγ is an essential regulatory subunit of the IκB kinase complex. *Nature 395*, 297–300.

(100) Agou, F., Ye, F., Goffinont, S., Courtois, G., Yamaoka, S., Israel, A., and Veron, M. (2002) NEMO Trimerizes through Its Coiled-coil C-terminal Domain. *Journal of Biological Chemistry 277*, 17464–17475.

(101) Huang, G.-J., Zhang, Z.-Q., and Jin, D.-Y. (2002) Stimulation of IKK-y oligomerization by the human T-cell leukemia virus oncoprotein Tax. *FEBS 531*, 494–498.

(102) Lo, Y.-C., Maddineni, U., Chung, J. Y., Rich, R. L., Myszka, D. G., and Wu, H. (2008) High-Affinity Interaction between IKKβ and NEMO. *Biochemistry 47*, 3109–3116.

(103) Cote, S. M., Gilmore, T. D., Shaffer, R., Weber, U., Bollam, R., Golden, M. S., Glover, K., Herscovitch, M., Ennis, T., Allen, K. N., and Whitty, A. (2013) Mutation of Nonessential Cysteines Shows That the NF-κB Essential Modulator Forms a Constitutive Noncovalent Dimer That Binds IκB Kinase-β with High Affinity. *Biochemistry 52*, 9141–9154.

(104) Ivins, F. J., Montgomery, M. G., Smith, S. J. M., Morris-Davies, A. C., Taylor, I. A., and Rittinger, K. (2009) NEMO oligomerization and its ubiquitin-binding properties. *Biochemical Journal 421*, 243–251.

(105) Rahighi, S., Ikeda, F., Kawasaki, M., Akutsu, M., Suzuki, N., Kato, R., Kensche, T., Uejima, T., Bloor, S., Komander, D., Randow, F., Wakatsuki, S., and

Dikic, I. (2009) Specific Recognition of Linear Ubiquitin Chains by NEMO Is Important for NF-κB Activation. *Cell 136*, 1098–1109.

(106) Catici, D. A. M., Horne, J. E., Cooper, G. E., and Pudney, C. R. (2015) Poly-ubiquitin drives the molecular interactions of NF-κB essential modulator by allosteric regulation. *Journal of Biological Chemistry* jbc.M115.640417.

(107) Drew, D., Shimada, E., Huynh, K., Bergqvist, S., Talwar, R., Karin, M., and Ghosh, G. (2007) Inhibitor κB Kinase β Binding by Inhibitor κB Kinase γ. *Biochemistry 46*, 12482–12490.

(108) Golden, M. S., Cote, S. M., Sayeg, M., Zerbe, B. S., Villar, E. A., Beglov, D., Sazinsky, S. L., Georgiadis, R. M., Vajda, S., Kozakov, D., and Whitty, A. (2013) Comprehensive Experimental and Computational Analysis of Binding Energy Hot Spots at the NF-κB Essential Modulator/IKKβ Protein–Protein Interface. *Journal of the American Chemical Society 135*, 6242–6256.

(109) Kozakov, D., Hall, D. R., Napoleon, R. L., Yueh, C., Whitty, A., and Vajda, S. (2015) New Frontiers in Druggability. *Journal of Medicinal Chemistry* 150811124427009.

(110) Gapuzan, M.-E. R., Pitoc, G. A., and Gilmore, T. D. (2003) Mutations within a conserved protein kinase A recognition sequence confer temperature-sensitive and partially defective activities onto mouse c-Rel. *Biochemical and Biophysical Research Communications 307*, 92–99.

(111) Malay, A. D., Allen, K. N., and Tolan, D. R. (2005) Structure of the Thermolabile Mutant Aldolase B, A149P: Molecular Basis of Hereditary Fructose Intolerance. *Journal of Molecular Biology 347*, 135–144.

(112) Krishnan, N., Koveal, D., Miller, D. H., Xue, B., Akshinthala, S. D., Kragelj, J., Jensen, M. R., Gauss, C.-M., Page, R., Blackledge, M., Muthuswamy, S. K., Peti, W., and Tonks, N. K. (2014) Targeting the disordered C terminus of PTP1B with an allosteric inhibitor. *Nature Chemical Biology 10*, 558–566.

(113) Francis, D. M., Koveal, D., Tortajada, A., Page, R., and Peti, W. (2014) Interaction of Kinase-Interaction-Motif Protein Tyrosine Phosphatases with the Mitogen-Activated Protein Kinase ERK2. *PLoS ONE* (Massiah, M., Ed.) *9*, e91934.

(114) Jain, A., Ma, C. A., Liu, S., Brown, M., Cohen, J., and Strober, W. (2001) Specific missense mutations in NEMO result in hyper-IgM syndrome with hypohydrotic ectodermal dysplasia. *Nature Immunology 2*, 223–228.

(115) Smahi, A., Courtois, G., Vabres, P., Yamaoka, S., Heuertz, S., Munnich, A., Israël, A., Heiss, N. S., Klauck, S. M., Kioschis, P., Wiemann, S., Poustka, A., Esposito, T., Bardaro, T., Gianfrancesco, F., Ciccodicola, A., D'Urso, M., Woffendin, H., Jakins, T., Donnai, D., Stewart, H., Kenwrick, S. J., Aradhya, S., Yamagata, T., Levy, M., Lewis, R. A., and Nelson, D. L. (2000) Genomic rearrangement in NEMO impairs NF-kappaB activation and is a cause of incontinentia pigmenti. The International Incontinentia Pigmenti (IP) Consortium. *Nature 405*, 466–472.

(116) Zhou, L., Yeo, A. T., Ballarano, C., Weber, U., Allen, K. N., Gilmore, T. D., and Whitty, A. (2014) Disulfide-Mediated Stabilization of the IκB Kinase Binding Domain of NF-κB Essential Modulator (NEMO). *Biochemistry 53*, 7929–7944.

(117) Okonechnikov, K., Golosova, O., Fursov, M., and the UGENE team. (2012) Unipro UGENE: a unified bioinformatics toolkit. *Bioinformatics 28*, 1166–1167.

(118) Edgar, R. C. (2004) MUSCLE: multiple sequence alignment with high accuracy and high throughput. *Nucleic Acids Research 32*, 1792–1797.

(119) Gasteiger, E., Hoogland, C., Gattiker, A., Duvaud, S., Wilkins, M. R., Appel, R. D., and Bairoch, A. (2005) Protein Identification and Analysis Tools on the ExPASy Server; (In) John M. Walker (ed): The Proteomics Protocols Handbook. Humana Press.

(120) Greenfield, N. J. (2007) Using circular dichroism spectra to estimate protein secondary structure. *Nature Protocols 1*, 2876–2890.

(121) Greenfield, N. J. (2007) Using circular dichroism collected as a function of temperature to determine the thermodynamics of protein unfolding and binding interactions. *Nature Protocols 1*, 2527–2535.

(122) Allaire, M., and Yang, L. (2011) Biomolecular solution X-ray scattering at the National Synchrotron Light Source. *Journal of Synchrotron Radiation 18*, 41–44.

(123) Petoukhov, M. V., Franke, D., Shkumatov, A. V., Tria, G., Kikhney, A. G., Gajda, M., Gorba, C., Mertens, H. D., Konarev, P. V., and Svergun, D. I. (2012)

New developments in the ATSAS program package for small-angle scattering data analysis. *Journal of Applied Crystallography 45*, 342–350.

(124) Svergun, D. I. (1992) Determination of the regularization parameter in indirect-transform methods using perceptual criteria. *Journal of Applied Crystallography 25*, 493–503.

(125) Svergun, D. I. (1999) Restoring low resolution structure of biological macromolecules from solution scattering using simulated annealing. *Biophysical Journal* 2879–2886.

(126) Volkov, V. V., and Svergun, D. I. (2003) Uniqueness of ab-initio shape determination in small-angle scattering. *Journal of Applied Crystallography 36*, 860–864.

(127) Schneidman-Duhovny, D., Hammel, M., Tainer, J. A., and Sali, A. (2013) Accurate SAXS Profile Computation and its Assessment by Contrast Variation Experiments. *Biophysical Journal 105*, 962–974.

(128) Schneidman-Duhovny, D., Hammel, M., Tainer, J. A., and Sali, A. (2016) FoXS, FoXSDock and MultiFoXS: Single-state and multi-state structural modeling of proteins and their complexes based on SAXS profiles. *Nucleic Acids Research 44*, W424–W429.

(129) Pettersen, E. F., Goddard, T. D., Huang, C. C., Couch, G. S., Greenblatt, D. M., Meng, E. C., and Ferrin, T. E. (2004) UCSF Chimera?A visualization system for exploratory research and analysis. *Journal of Computational Chemistry 25*, 1605–1612.

(130) Petoukhov, M. V., and Svergun, D. I. (2005) Global Rigid Body Modeling of Macromolecular Complexes against Small-Angle Scattering Data. *Biophysical Journal 89*, 1237–1250.

(131) Cole, J. L., Lary, J. W., P. Moody, T., and Laue, T. M. (2008) Analytical Ultracentrifugation: Sedimentation Velocity and Sedimentation Equilibrium, in *Methods in Cell Biology*, pp 143–179. Elsevier.

(132) Stafford, W. F. (1998) Time difference sedimentation velocity analysis of rapidly reversible interacting systems: Determination of equilibrium constants by global non-linear curve fitting procedures. *Biophysical Journal 74*, A301.

(133) Doublie, Sylvie. (1997) Preparation of selenomethionyl proteins for phase determination. *Methods in Enzymology 276*, 523–530.

(134) Otwinowski, Z., and Minor, W. (1997) Processing of X-ray diffraction data collected in oscillation mode. *In Methods in Enzymology, Macromolecular Crystallography Part A* 307–326.

(135) Terwilliger, T. C., Adams, P. D., Read, R. J., McCoy, A. J., Moriarty, N. W., Grosse-Kunstleve, R. W., Afonine, P. V., Zwart, P. H., and Hung, L.-W. (2009) Decision-making in structure solution using Bayesian estimates of map quality: the PHENIX AutoSol wizard. *Acta Crystallographica Section D Biological Crystallography 65*, 582–601.

(136) Terwilliger, T. C., Grosse-Kunstleve, R. W., Afonine, P. V., Moriarty, N. W., Zwart, P. H., Hung, L.-W., Read, R. J., and Adams, P. D. (2008) Iterative model building, structure refinement and density modification with the PHENIX AutoBuild wizard. *Acta Crystallographica Section D Biological Crystallography 64*, 61–69.

(137) Sheldrick, G. M. (2010) Experimental phasing with SHELXC/D/E: combining chain tracing with density modification. *Acta Crystallographica Section D Biological Crystallography 66*, 479–485.

(138) Kunkel, T. A. (2004) DNA Replication Fidelity. *Journal of Biological Chemistry 279*, 16895–16898.

(139) Shih, J., Hodge, R., and Andrade-Navarro, M. A. (2015) Comparison of inter- and intraspecies variation in humans and fruit flies. *Genomics Data 3*, 49–54.

(140) Fusco, F. (2004) Molecular analysis of the genetic defect in a large cohort of IP patients and identification of novel NEMO mutations interfering with NF- B activation. *Human Molecular Genetics 13*, 1763–1773.

(141) Hanson, E. P., Monaco-Shawver, L., Solt, L. A., Madge, L. A., Banerjee, P. P., May, M. J., and Orange, J. S. (2008) Hypomorphic nuclear factor-κB essential modulator mutation database and reconstitution system identifies phenotypic and immunologic diversity. *Journal of Allergy and Clinical Immunology 122*, 1169-1177.e16.

(142) Hsiao, P.-F., Lin, S.-P., Chiang, S.-S., Wu, Y.-H., Chen, H.-C., and Lin, Y.-C. (2010) NEMO gene mutations in Chinese patients with incontinentia pigmenti. *Journal of the Formosan Medical Association 109*, 192–200.

(143) Ku, C.-L., Picard, C., Erdos, M., Jeurissen, A., Bustamante, J., Puel, A., von Bernuth, H., Filipe-Santos, O., Chang, H.-H., Lawrence, T., Raes, M., Marodi, L., Bossuyt, X., and Casanova, J.-L. (2006) IRAK4 and NEMO mutations in otherwise healthy children with recurrent invasive pneumococcal disease. *Journal of Medical Genetics 44*, 16–23.

(144) Salt, B. H., Niemela, J. E., Pandey, R., Hanson, E. P., Deering, R. P., Quinones, R., Jain, A., Orange, J. S., and Gelfand, E. W. (2008) IKBKG (nuclear factor-κB essential modulator) mutation can be associated with opportunistic infection without impairing Toll-like receptor function. *Journal of Allergy and Clinical Immunology 121*, 976–982.

(145) Luo, P., and Baldwin, R. L. (1997) Mechanism of helix induction by trifluoroethanol: a framework for extrapolating the helix-forming properties of peptides from trifluoroethanol/water mixtures back to water. *Biochemistry 36*, 8413–8421.

(146) Mary Koeppe Luidens, James Figge, Kimberly Breese, and Sandor Vajda. (1995) Predicted and Trifluoroethanol-Induced a-Helicity of Polypeptides. *Biopolymers 39*, 367–376.

(147) Putnam, C. D., Hammel, M., Hura, G. L., and Tainer, J. A. (2007) X-ray solution scattering (SAXS) combined with crystallography and computation: defining accurate macromolecular structures, conformations and assemblies in solution. *Quarterly Reviews of Biophysics 40*, 191–285.

(148) McCoy, A. J., Grosse-Kunstleve, R. W., Adams, P. D., Winn, M. D., Storoni, L. C., and Read, R. J. (2007) Phaser crystallographic software. *Journal of Applied Crystallography 40*, 658–674.

(149) Emsley, P., Lohkamp, B., Scott, W. G., and Cowtan, K. (2010) Features and development of Coot. *Acta Crystallographica Section D Biological Crystallography 66*, 486–501.

(150) Strnad, J., McDonnell, P., Riexinger, D., Mapelli, C., Cheng, L., Gray, H., Ryseck, R., and Burke, J. (2006) NEMO binding domain of IKK-2 encompasses amino acids 735-745. *Journal of Molecular Recognition 19*, 227–233.

(151) Shults, M. D., and Imperiali, B. (2003) Versatile Fluorescence Probes of Protein Kinase Activity. *Journal of the American Chemical Society 125*, 14248–14249.

(152) Seidel, S. A. I., Dijkman, P. M., Lea, W. A., van den Bogaart, G., Jerabek-Willemsen, M., Lazic, A., Joseph, J. S., Srinivasan, P., Baaske, P., Simeonov, A., Katritch, I., Melo, F. A., Ladbury, J. E., Schreiber, G., Watts, A., Braun, D., and Duhr, S. (2013) Microscale thermophoresis quantifies biomolecular interactions under previously challenging conditions. *Methods 59*, 301–315.

(153) Herscovitch, M., Comb, W., Ennis, T., Coleman, K., Yong, S., Armstead, B., Kalaitzidis, D., Chandani, S., and Gilmore, T. D. (2008) Intermolecular disulfide bond formation in the NEMO dimer requires Cys54 and Cys347. *Biochemical and Biophysical Research Communications 367*, 103–108.

(154) Liang, M.-C., Bardhan, S., Pace, E. A., Rosman, D., Beutler, J. A., Porco, J. A., and Gilmore, T. D. (2006) Inhibition of transcription factor NF-κB signaling proteins IKKβ and p65 through specific cysteine residues by epoxyquinone A monomer: Correlation with its anti-cancer cell growth activity. *Biochemical Pharmacology 71*, 634–645.

(155) Cote, S. M. (2014) Characterization of the Structure and Function of NF-KAPPA B Essential Modulator and its Interactionwith Inhibitor KAPPA B Kinase BETA and Development of a Screening Protocol to Discover and Validate Inhibitors of the Interaction. Boston University.

(156) Lakowicz, J. R. (2006) Principles of fluorescence spectroscopy. Springer, New York.

(157) Sénèque, O., and Latour, J.-M. (2010) Coordination Properties of Zinc Finger Peptides Revisited: Ligand Competition Studies Reveal Higher Affinities for Zinc and Cobalt. *Journal of the American Chemical Society 132*, 17760–17774.

(158) Kishore, N., Huynh, Q. K., Mathialagan, S., Hall, T., Rouw, S., Creely, D., Lange, G., Caroll, J., Reitz, B., Donnelly, A., Boddupalli, H., Combs, R. G., Kretzmer, K., and Tripp, C. S. (2002) IKK-i and TBK-1 are Enzymatically Distinct

from the Homologous Enzyme IKK-2: COMPARATIVE ANALYSIS OF RECOMBINANT HUMAN IKK-i, TBK-1, AND IKK-2. *Journal of Biological Chemistry 277*, 13840–13847.

(159) Liu, S., Misquitta, Y. R., Olland, A., Johnson, M. A., Kelleher, K. S., Kriz, R., Lin, L. L., Stahl, M., and Mosyak, L. (2013) Crystal Structure of a Human I B Kinase Asymmetric Dimer. *Journal of Biological Chemistry 288*, 22758–22767.

(160) Guo, B., Audu, C. O., Cochran, J. C., Mierke, D. F., and Pellegrini, M. (2014) Protein Engineering of the N-Terminus of NEMO: Structure Stabilization and Rescue of IKK? Binding. *Biochemistry 53*, 6776–6785.

(161) Huang, T. T., Feinberg, S. L., Suryanarayanan, S., and Miyamoto, S. (2002) The Zinc Finger Domain of NEMO Is Selectively Required for NF- B Activation by UV Radiation and Topoisomerase Inhibitors. *Molecular and Cellular Biology 22*, 5813–5825.

(162) Day, E. S., Wen, D., Garber, E. A., Hong, J., Avedissian, L. S., Rayhorn, P., Shen, W., Zeng, C., Bailey, V. R., Reilly, J. O., Roden, J. A., Moore, C. B., Williams, K. P., Galdes, A., Whitty, A., and Baker, D. P. (1999) Zinc-Dependent Structural Stability of Human Sonic Hedgehog. *Biochemistry 38*, 14868–14880.

(163) Haverkamp, M. H., Marciano, B. E., Frucht, D. M., Jain, A., van de Vosse, E., and Holland, S. M. (2014) Correlating Interleukin-12 Stimulated Interferon-γ Production and the Absence of Ectodermal Dysplasia and Anhidrosis (EDA) in Patients with Mutations in NF-κB Essential Modulator (NEMO). *Journal of Clinical Immunology* 436–443.

(164) Tarantino, N., Tinevez, J.-Y., Crowell, E. F., Boisson, B., Henriques, R., Mhlanga, M., Agou, F., Israël, A., and Laplantine, E. (2014) TNF and IL-1 exhibit distinct ubiquitin requirements for inducing NEMO–IKK supramolecular structures. *The Journal of Cell Biology 204*, 231–245.

(165) Sebban-Benin, H., Pescatore, A., Fusco, F., Pascuale, V., Gautheron, J., Yamaoka, S., Moncla, A., Ursini, M. V., and Courtois, G. (2007) Identification of TRAF6-dependent NEMO polyubiquitination sites through analysis of a new NEMO mutation causing incontinentia pigmenti. *Human Molecular Genetics 16*, 2805–2815.

(166) Lipinski, C. A. (2000) Drug-like properties and the causes of poor solubility and poor permeability. *Journal of Pharmacological and Toxicological Methods 44*, 235–249.

(167) Ryan, D., and Matthews, J. (2005) Protein–protein interactions in human disease. *Current Opinion in Structural Biology 15*, 441–446.

(168) Hopkins, Andrew L., and Groom, Colin R. (2002) The Druggable Genome. *Nature Reviews Drug Discovery 1*, 727–730.

(169) Bork, P., Jensen, L. J., von Mering, C., Ramani, A. K., Lee, I., and Marcotte, E. M. (2004) Protein interaction networks from yeast to human. *Current Opinion in Structural Biology 14*, 292–299.

(170) Bohnuud, T., Kozakov, D., and Vajda, S. (2014) Evidence of Conformational Selection Driving the Formation of Ligand Binding Sites in Protein-Protein Interfaces. *PLoS Computational Biology* (Briggs, J. M., Ed.) *10*, e1003872.

(171) Mani, T., Wang, F., Knabe, W. E., Sinn, A. L., Khanna, M., Jo, I., Sandusky, G. E., Sledge, G. W., Jones, D. R., Khanna, R., Pollok, K. E., and Meroueh, S. O. (2013) Small-molecule inhibition of the uPAR·uPA interaction: Synthesis, biochemical, cellular, in vivo pharmacokinetics and efficacy studies in breast cancer metastasis. *Bioorganic & Medicinal Chemistry 21*, 2145–2155.

(172) Rechfeld, F., Gruber, P., Kirchmair, J., Boehler, M., Hauser, N., Hechenberger, G., Garczarczyk, D., Lapa, G. B., Preobrazhenskaya, M. N., Goekjian, P., Langer, T., and Hofmann, J. (2014) Thienoquinolines as Novel Disruptors of the PKCε/RACK2 Protein–Protein Interaction. *Journal of Medicinal Chemistry 57*, 3235–3246.

(173) Li, L., Liu, Y., Chen, H., Li, F., Wu, J., Zhang, H., He, J., Xing, Y., Chen, Y., Wang, W., Tian, X., Li, A., Zhang, Q., Huang, P., Han, J., Lin, T., and Wu, Q. (2015) Impeding the interaction between Nur77 and p38 reduces LPS-induced inflammation. *Nature Chemical Biology 11*, 339–346.

(174) Arkin, M. R., Tang, Y., and Wells, J. A. (2014) Small-Molecule Inhibitors of Protein-Protein Interactions: Progressing toward the Reality. *Chemistry & Biology 21*, 1102–1114.

(175) Pettersson, M., Quant, M., Min, J., Iconaru, L., Kriwacki, R. W., Waddell, M. B., Guy, R. K., Luthman, K., and Grøtli, M. (2015) Design, Synthesis and Evaluation of 2,5-Diketopiperazines as Inhibitors of the MDM2-p53 Interaction. *PLOS ONE* (Ganesan, A., Ed.) *10*, e0137867.

(176) Nariai, Y., Mizuguchi, H., Ogasawara, T., Nagai, H., Sasaki, Y., Okamoto, Y., Yoshimura, Y., Kitamura, Y., Nemoto, H., Takeda, N., and Fukui, H. (2015) Disruption of Heat Shock Protein 90 (Hsp90)-Protein Kinase Cδ (PKCδ) Interaction by (-)-Maackiain Suppresses Histamine H_1 Receptor Gene Transcription in HeLa Cells. *Journal of Biological Chemistry 290*, 27393–27402.

(177) Zak, K. M., Grudnik, P., Guzik, K., Zieba, B. J., Musielak, B., Dömling, A., Dubin, G., and Holak, T. A. (2016) Structural basis for small molecule targeting of the programmed death ligand 1 (PD-L1). *Oncotarget 7*, 30323–30335.

(178) Sail, V., Rizzo, A. A., Chatterjee, N., Dash, R. C., Ozen, Z., Walker, G. C., Korzhnev, D. M., and Hadden, M. K. (2017) Identification of Small Molecule Translesion Synthesis Inhibitors That Target the Rev1-CT/RIR Protein−Protein Interaction. *ACS Chemical Biology 12*, 1903–1912.

(179) Zarzycka, B., Kuenemann, M. A., Miteva, M. A., Nicolaes, G. A. F., Vriend, G., and Sperandio, O. (2016) Stabilization of protein–protein interaction complexes through small molecules. *Drug Discovery Today 21*, 48–57.

(180) Kozakov, D., Grove, L. E., Hall, D. R., Bohnuud, T., Mottarella, S. E., Luo, L., Xia, B., Beglov, D., and Vajda, S. (2015) The FTMap family of web servers for determining and characterizing ligand-binding hot spots of proteins. *Nature Protocols 10*, 733–755.

(181) Kozakov, D., Hall, D. R., Chuang, G.-Y., Cencic, R., Brenke, R., Grove, L. E., Beglov, D., Pelletier, J., Whitty, A., and Vajda, S. (2011) Structural conservation of druggable hot spots in protein–protein interfaces. *Proceedings of the National Academy of Sciences USA 108*, 13528–13533.

(182) Rincón, V., Bocanegra, R., Rodríguez-Huete, A., Rivas, G., and Mateu, M. G. (2011) Effects of Macromolecular Crowding on the Inhibition of Virus Assembly and Virus-Cell Receptor Recognition. *Biophysical Journal 100*, 738–746.

(183) Minton, A. P. (2006) How can biochemical reactions within cells differ from those in test tubes? *Journal of Cell Science 119*, 2863–2869.

(184) Driggers, E. M., Hale, S. P., Lee, J., and Terrett, N. K. (2008) The exploration of macrocycles for drug discovery — an underexploited structural class. *Nature Reviews Drug Discovery 7*, 608–624.

(185) Dougherty, P. G., Qian, Z., and Pei, D. (2017) Macrocycles as protein–protein interaction inhibitors. *Biochemical Journal 474*, 1109–1125.

(186) Mallinson, J., and Collins, I. (2012) Macrocycles in new drug discovery. *Future Medicinal Chemistry 4*, 1409–1438.

(187) Kwitkowski, V. E., Prowell, T. M., Ibrahim, A., Farrell, A. T., Justice, R., Mitchell, S. S., Sridhara, R., and Pazdur, R. (2010) FDA Approval Summary: Temsirolimus as Treatment for Advanced Renal Cell Carcinoma. *The Oncologist 15*, 428–435.

(188) Conlin, A., Fornier, M., Hudis, C., Kar, S., and Kirkpatrick, P. (2007) Ixabepilone. *Nature Reviews Drug Discovery 6*, 953–954.

(189) McDonald, E., Workman, P., and Jones, K. (2006) Inhibitors of the HSP90 Molecular Chaperone: Attacking the Master Regulator in Cancer. *Current Topics in Medicinal Chemistry 6*, 1091–1107.

(190) Shoichet, B. K. (2006) Screening in a spirit haunted world. *Drug Discovery Today 11*, 607–615.

(191) Gribbon, P., and Sewing, A. (2003) Fluorescence readouts in HTS: no gain without pain? *Drug Discovery Today 8*, 1035–1043.

(192) Trott, O., and Olson, A. J. (2010) AutoDock Vina: Improving the speed and accuracy of docking with a new scoring function, efficient optimization, and multithreading. *Journal of Computational Chemistry* 455–461.

(193) Lipinski, C. A., Lombardo, F., Dominy, B. W., and Feeney, P. J. (1997) Experimental and computational approaches to estimate solubility and permeability in drug discovery and development settings. *Advanced Drug Delivery Reviews 23*, 3–25.

(194) Ghose, A. K., Viswanadhan, V. N., and Wendoloski, J. J. (1999) A knowledge-based approach in designing combinatorial or medicinal chemistry libraries for drug discovery. *Journal of Combinatorial Chemistry 1*, 55–68.

(195) Veber, D. F., Johnson, S. R., Cheng, H.-Y., Smith, B. R., Ward, K. W., and Kopple, K. D. (2002) Molecular Properties That Influence the Oral Bioavailability of Drug Candidates. *Journal of Medicinal Chemistry 45*, 2615–2623.

(196) Congreve, M., Carr, R., Murray, C., and Jhoti, H. (2003) A 'rule of three' for fragment-based lead discovery? *Drug Discovery Today 8*, 876–877.

(197) Ertl, P., Rohde, B., and Selzer, P. (2000) Fast Calculation of Molecular Polar Surface Area as a Sum of Fragment-Based Contributions and Its Application to the Prediction of Drug Transport Properties. *Journal of Medicinal Chemistry 43*, 3714–3717.

(198) Avdeef, A. (2005) The Rise of PAMPA. *Expert Opinion on Drug Metabolism & Toxicology 1*, 325–342.

(199) Madgula, V., Avula, B., Reddy, N., Khan, I., and Khan, S. (2007) Transport of Decursin and Decursinol Angelate across Caco-2 and MDR-MDCK Cell Monolayers: *In vitro* Models for Intestinal and Blood-Brain Barrier Permeability. *Planta Medica 73*, 330–335.

Curriculum Vitae

[redacted]

[redacted]

[redacted]